

THE LEACHING OF CHALCOPYRITE

by

DAVID L. JONES

B.Sc. University of British Columbia, 1965

M.Sc. University of British Columbia, 1970

A THESIS SUBMITTED IN PARTIAL FULFILMENT
OF THE REQUIREMENTS FOR THE DEGREE OF
DOCTOR OF PHILOSOPHY

in the Department

of

Metallurgy

We accept this thesis as conforming to the
required standard

THE UNIVERSITY OF BRITISH COLUMBIA

May, 1974

In presenting this thesis in partial fulfilment of the requirements for an advanced degree at the University of British Columbia, I agree that the Library shall make it freely available for reference and study.

I further agree that permission for extensive copying of this thesis for scholarly purposes may be granted by the Head of my Department or by his representatives. It is understood that copying or publication of this thesis for financial gain shall not be allowed without my written permission.

Department of Metallurgy

The University of British Columbia
Vancouver 8, Canada

Date July 29, 1974

ABSTRACT

The anodic dissolution of chalcopyrite has been examined in chloride and sulphate solutions from 20°C to 175°C. In chloride the yield of elemental sulphur is nearly 100%, whereas in sulphate solutions it is 75% or less, the remainder being oxidized.

It is postulated that in sulphate solutions the copper dissolves as a thiosulphate complex, which can decompose either to a soluble form, or to cupric sulphide and another sulphur species, probably dithionate.

The anodic polarization of chalcopyrite displays two important regions: first a diffusion region in which the current is highly time-dependent, but potential independent and second a higher current region, attributed to the build up of a space-charge in the mineral. This space-charge current is largely time independent but is linearly dependent on potential.

At low temperatures chloride solutions and sulphate solutions give similar polarization curves but at 90°C and above, the space-charge region in chloride solutions starts at much lower potentials (500 mV) whereas in sulphate solutions it does not. Sulphuric acid solutions passivate the mineral at high temperatures and potentials.

The electrochemical results correlate well with leaching experiments using ferric sulphate and ferric chloride, and there is every reason to believe that for chalcopyrite an electrochemical mechanism is operative during leaching.

Ferric chloride is an equal or more effective oxidizing agent than ferric sulphate; its (ferric chloride) effectiveness is increased by fine particle size, high $[\text{Fe}^{+++}]$. Ferric sulphate leaching is relatively

unaffected by these factors, but decreased by $[\text{Fe}^{++}]$. Linear kinetics are normally observed with both reagents, but under optimum conditions with ferric chloride a rapid initial dissolution precedes the linear stage.

Ferric sulphate appears to selectively attack the mineral along grain boundaries, whereas ferric chloride does not.

Mixed potential measurements indicate that in ferric sulphate the reaction is under mixed control, and that both anodic and cathodic reactions are quite irreversible. In cupric chloride the leaching reaction is under anodic control, and the cathodic reaction is highly reversible. Ferric chloride leaching appears to be cupric chloride leaching in reality; the ferric ions serve the purpose of depressing the $[\text{Cu}^+]$, thus raising the potential of the $\text{Cu}^{++}/\text{Cu}^+$ couple. Thus, ferric chloride leaching is also under anodic control.

LIST OF CONTENTS

	<u>Page</u>
A. INTRODUCTION	1
I. General	1
II. Some Properties of Chalcopyrite	4
(a) Phase Relations	4
(b) Thermodynamics	7
(c) Crystal Structure and Bonding	10
III. The Leaching of Copper Sulphides	14
(a) An Overview	14
(b) Leaching of Simple Copper Sulphides	15
(c) Electrochemical Studies of Simple Copper Sulphides	18
(d) A Note on the Leaching of Bornite, Cubanite, Idaite	22
(e) Leaching of Chalcopyrite	23
(i) Ferric Sulphate	23
(ii) Ferric Chloride	25
(iii) Other Oxidants	31
(f) Electrochemical Studies on Chalcopyrite	32
IV. Electrochemical Experiments in Aqueous Solutions Above 100°C	35
(a) State of the Art	36
(b) Application to Sulphide Minerals	38
B. EXPERIMENTAL	39
I. Apparatus	39
(a) Pressure Vessel Design	42
(b) Electrode Design (for Sulphide Minerals) ...	48
(c) Reference Electrode	49

	<u>Page</u>
II. Chemicals	50
III. Instrumentation	50
IV. Analysis	50
V. Source of Chalcopyrite Used	51
C. RESULTS	53
I. Preliminary Experiments	53
(a) The Meaning of Current Efficiency	53
(b) Potentiostatic Scans	54
(c) Constant Potential Experiments	59
(d) Surface of Chalcopyrite After Anodizing	66
(e) Summary	66
II. Anodic Polarizations	72
(a) Fast Scans	72
(b) Summary	74
(c) Slow Scans	86
(d) Summary	88
III. Constant Potential Experiments	102
(a) Without Solution Analysis	102
(b) With Solution Analysis	111
(i) Dilute Chloride Solutions (90°C) ...	112
(ii) Strong Chloride Solutions (90°C) ...	113
(iii) Sulphate Chloride Solutions (90°C) .	114
(iv) Sulphate/Bisulphate Solutions (125°C)	122
(v) Sulphate/Bisulphate Solutions (125- 175°C)	132
(vi) Chloride/Bisulphate Solutions - A Comparison	133
(vii) Sundry Effects	134
(viii) Summary	135

	<u>Page</u>
IV. Leaching Experiments	147
(a) The Motive	147
(b) Leaching Experiments on Massive CuFeS_2	148
(i) Preliminary Experiments	148
(ii) Morphology	149
(iii) A Comparison of Chemical and Electro- chemical Dissolution	157
(iv) Chemistry of Dissolution	159
(c) Powder Leaching	160
(i) Shape of Leaching Curve	166
(ii) Effect of Particle Size	166
(iii) $\text{Fe}^{++}/\text{Cu}^{++}$ Ratio Produced During Leaching	172
(iv) Effect of Ferric Concentration	172
(v) Effect of Added Chloride	172
(vi) Effect of Ferrous Concentration	172
(vii) Effect of Acid	176
(viii) Effect of Stirring Mode	176
(ix) Effect of Temperature	176
(x) Effect of Grain Size in Ferric Sulphate Leaching	176
(xi) Comparison of Ferric Chloride and Ferric Sulphate Leaching	177
(d) Concentrate Leaching	181
(e) Summary	184
V. Mixed Potential Experiments	189
(a) Motive	189
(b) Results	190
(i) Ferric Sulphate Leaching	190
(ii) Cupric Chloride Leaching	195
(iii) Ferric Chloride Leaching	196
(iv) Summary	205

	<u>Page</u>
(c) Discussion	205
(i) Calculated Potentials	206
(ii) Ferric Sulphate Leaching	209
(iii) Cupric Chloride Leaching	211
(iv) Ferric Chloride Leaching	214
(v) Summary	216
D. DISCUSSION	217
I. The Chemistry of the Anodic Dissolution of Chalcopyrite	217
(a) Chloride System	217
(b) Sulphate System	218
(i) Thiosulphate Mechanism	222
(ii) Sulphur Disproportionation Mechanism .	228
(iii) Hydrogen Sulphide Mechanism	229
II. The Anodic Polarization Curve of Chalcopyrite ...	230
(a) The Diffusional Process in Chalcopyrite	231
(b) The Effect of Solution	235
E. CONCLUSION	238
REFERENCES	239
APPENDIX A	249
APPENDIX B	263

LIST OF TABLES

		<u>Page</u>
I	Dissolution of Covellite in Ferric Sulphate Solutions at 35°C; Effect of Particle Size [from Sullivan (106)].	17
II	Rest Potentials of Copper Sulphides vs. Cu Metal at 25°C Measured by Various Authors.	19
III	Data on Mechanism of Dissolution of Chalcopyrite in Ferric Sulphate (at 35°C) [from Sullivan (130)].	23
IVA	Analysis of Solutions After Constant Potential Experiments on CuFeS ₂ in 0.1M HClO ₄ .	63
IVB	Analysis of Solutions After Constant Potential Experiments on CuFeS ₂ in 0.1M H ₂ SO ₄ .	64
V	Analysis of Solutions After Heating Experiments on CuFeS ₂ in 0.1M HClO ₄ .	64
VI	Successive Anodic Scans at Rapid Scanning Rates; Specimen #200.	84,85
VII	Successive Anodic Scans at Slow Scanning Rates; Specimen #202 and #207.	100,101

FIGURE CAPTIONS

- Fig. 1 Cu-Fe-S system at 200°C (from Yund and Kullerud⁽¹⁰⁾).
- Fig. 2 Crystal structure of CuFeS₂.
- Fig. 3 Leaching of chalcopyrite concentrate in ferric chloride, effect of temperature (from Haver and Wong⁽¹³⁷⁾).
- Fig. 4 Leaching of chalcopyrite concentrate in ferric chloride, effect of particle size (as grinding time). (From Haver and Wong⁽¹³⁷⁾).
- Fig. 5 Anodic dissolution of chalcopyrite. Solution analysis from Zevgolis⁽⁸⁹⁾.
- Fig. 6 Apparatus for leaching powdered chalcopyrite.
- Fig. 7 Apparatus for leaching massive specimens.
- Fig. 8 Pressure vessel
- Fig. 9 Pressure vessel
- Fig. 10 Electrochemical cell
- Fig. 11 Electrode mounting
- Fig. 12 Potentiostatic scans in perchloric acid at various temperatures.
- Fig. 13 Potentiostatic scans in sulphuric acid at various temperatures.
- Fig. 14 Effect of scanning rate on potentiostatic scan.
- Fig. 15 The linear current/potential relationship in potentiostatic scans.
- Fig. 16 Potentiostatic scans in perchloric acid.
- Fig. 17 Current decay during constant potential experiments at 125°C.
- Fig. 18 Current decay during constant potential experiments at 150°C.

- Fig. 19 Scanning electron micrograph of chalcopyrite anodized at 1500 mV for 3 hours in 0.1M HClO₄, 175°C.
- Fig. 20 Scanning electron micrograph of chalcopyrite after anodizing (16 hours, 700 mV, 0.1M HClO₄, 150°C).
- Fig. 21 Scanning electron micrograph of CuFeS₂ specimen after anodizing (7 hours, 615 mV, 0.1M HClO₄, 175°C).
- Fig. 22 Scanning electron micrographs of CuFeS₂ specimen after anodizing (11 hours, 615 mV, 0.1M HClO₄, 175°C).
- Fig. 23 Scanning electron micrographs of CuFeS₂ specimen after anodizing (3½ hours, 690 mV, 0.1M HClO₄, 175°C).
- Fig. 24 Potentiostatic scans on CuFeS₂ in various solutions at 300 mV/min., 20°C.
- Fig. 25 Potentiostatic scans in chloride solutions at 300 mV/min., 20°C.
- Fig. 26 Potentiostatic scans in 0.1M HCl, 20°C at various scanning rates.
- Fig. 27 Potentiostatic scans in sulphate solution, 20°C, at various scanning rates.
- Fig. 28 Potentiostatic scans in 1M HCl, 20°C.
- Fig. 29 Successive potentiostatic scans in 0.1M HCl at 20°C, 300 mV/min.
- Fig. 30 Potentiostatic scans at 20°C.
- Fig. 31 Potentiostatic scans in sulphate solution at 300 mV, and various temperatures.
- Fig. 32 Potentiostatic scans in 0.1M HCl at 95°C, and various scanning rates.
- Fig. 33, 34 Slow scans at 20°C in various solutions.
- Fig. 35 Slow scans at 20°C in sulphate solutions.
- Fig. 36 Slow scans at 20°C in chloride solutions.
- Fig. 37 Slow scans in 0.1M HClO₄ at various temperatures.
- Fig. 38 Slow scans at 90°C in various solutions.

- Fig. 39 Slow scans at 90°C in 1M HCl and 1M H₂SO₄.
- Fig. 40 Slow scans at 90°C in sodium sulphate solutions.
- Fig. 41 Slow scans at 90°C in chloride solutions.
- Fig. 42 Slow scans at 90°C in 4M HCl at pH 1 and pH 3.5.
- Fig. 43 Current decay at 700 mV, 20°C in various solutions.
- Fig. 44 Current decay at 700 mV, 60°C in various solutions.
- Fig. 45 Current decay at 700 mV, 60°C in various solutions.
- Fig. 46 Current decay at 700 mV, 90°C in various solutions.
- Fig. 47 Effect of temperature on current at 700 mV, in 0.1M H₂SO₄.
- Fig. 48 Arrhenius diagram for current at 700 mV in 0.1M HClO₄.
- Fig. 49 Arrhenius diagram for current at 700 mV in 0.1M KCl and 1M KCl.
- Fig. 50 Constant potential experiments in 0.3M NaCl, 0.2M HCl at 90°C, and various potentials.
- Fig. 51 Constant potential experiments in 3.0M NaCl, 0.2M HCl at 90°C, and various potentials.
- Fig. 52 Current oscillations produced after several hours at 900 mV, 90°C in 3M NaCl, 0.2M HCl. Effect of temperature and potential.
- Fig. 53 Constant potential experiments in 0.4M Na₂SO₄, 0.1M H₂SO₄ at 90°C, and various potentials.
- Fig. 54 Constant potential experiments in 0.3M Na₂SO₄, 0.2M H₂SO₄ at 90°C and 735 mV.
- Fig. 55 Constant potential experiments in sulphate and bisulphate solutions at 125°C, 735 mV.
- Fig. 56 Constant potential experiments in sulphate and bisulphate solutions at 125°C → 175°C, 735 mV.
- Fig. 57 Constant potential experiments at 735 mV in 0.4M NaCl, 0.1M HCl at 175°C, 150°C and 125°C.

- Fig. 58 Constant potential experiments at 735 mV in 0.4M NaHSO₄, 0.1M H₂SO₄ at 125°C and 175°C.
- Fig. 59 Arrhenius diagram for current at 735 mV in 0.4M NaCl, 0.1M HCl.
- Fig. 60 Successive constant potential experiments at 90°C, 735 mV in bisulphate and chloride solutions.
- Fig. 61 Effect of decreased acid on constant potential experiment in dilute chloride solution at 735 mV, 90°C.
- Fig. 62 Effect of no acid on constant potential experiment in strong chloride solution at 535 mV, 90°C.
- Fig. 63 Scanning electron micrographs of chalcopyrite after leaching (5 days, 95°C).
- Fig. 64 Scanning electron micrographs of chalcopyrite after leaching (11 hours, 95°C, 1M FeCl₃).
- Fig. 65 Scanning electron micrograph of chalcopyrite after leaching in 1M Fe(SO₄)_{1.5} at 95°C.
- Fig. 66 Scanning electron micrographs of chalcopyrite after leaching in 1M Fe(SO₄)_{1.5} at 95°C.
- Fig. 67 Theoretical relationship between percent sulphur as S⁰ and Fe⁺⁺/Cu⁺⁺ ratio in equation (20).
- Fig. 68 Leaching of massive chalcopyrite in 1M Fe(SO₄)_{1.5}, 90°C.
- Fig. 69 Comparison of leaching in 0.1M and 1M Fe(SO₄)_{1.5}.
- Fig. 70 Comparison of leaching in sulphate, perchlorate and chloride solutions.
- Fig. 71 Effect of surface preparation on FeCl₃ leaching.
- Fig. 72 The leaching of powdered chalcopyrite with ferric sulphate.
- Fig. 73 Comparison of linear and parabolic kinetics in the leaching of powdered chalcopyrite with ferric sulphate.
- Fig. 74 Leaching of powdered chalcopyrite with ferric chloride.
- Fig. 75 Effect of particle size in ferric sulphate leaching.
- Fig. 76 Effect of [Fe⁺⁺⁺] in ferric sulphate leaching.

- Fig. 77 Effect of $[\text{Fe}^{+++}]$ in ferric chloride leaching.
- Fig. 78 Effect of $[\text{Fe}^{++}]$ in ferric sulphate and chloride leaching.
- Fig. 79 Effect of stirring mode in ferric sulphate and chloride leaching.
- Fig. 80 Effect of temperature on ferric chloride leaching.
- Fig. 81 Effect of grain size on ferric sulphate leaching.
- Fig. 82 Leaching of various concentrates with ferric chloride.
- Fig. 83 Effect of particle size on concentrate leaching.
- Fig. 84 Optimum leaching of various concentrates.
- Fig. 85 Mixed potential of chalcopyrite in ferric sulphate. Effect of $[\text{Fe}^{+++}]$.
- Fig. 86 Mixed potential of chalcopyrite in ferric sulphate. Effect of $[\text{Fe}^{++}]$.
- Fig. 87 Mixed potential of chalcopyrite in dilute ferric sulphate. Effect of $[\text{Fe}^{++}]$.
- Fig. 88 Mixed potential of chalcopyrite in cupric chloride. Effect of $[\text{Cu}^{++}]$.
- Fig. 89 Mixed potential of chalcopyrite in cupric chloride. Effect of $[\text{Cu}^+]$.
- Fig. 90 Mixed potential of chalcopyrite in cupric chloride. Effect of $[\text{Cl}]$.
- Fig. 91 Mixed potential of chalcopyrite in cupric chloride. Effect of $[\text{Cl}]$ in absence of cuprous chloride.
- Fig. 92 Mixed potential of chalcopyrite in ferric chloride. Effect of $[\text{Fe}^{+++}]$.
- Fig. 93 Mixed potential of chalcopyrite in ferric chloride. Effect of $[\text{Fe}^{++}]$.
- Fig. 94 Mixed potential of chalcopyrite in ferric chloride. Effect of $[\text{Fe}^{++}]$ when $[\text{Fe}^{+++}]$ is low.
- Fig. 95 Mixed potential of chalcopyrite in ferric chloride. Effect of $[\text{Cl}^-]$.
- Fig. 96 Mixed potential of chalcopyrite in ferric chloride. Effect of $[\text{Cu}^{++}]$.

ACKNOWLEDGEMENTS

The author wishes to express his sincere thanks to Dr. E. Peters for his support and encouragement during this project. The numerous critical discussions that he has provoked have been a most welcome source of stimulation.

The interaction with other graduate students has also been very rewarding; particular thanks are due to Dr. K. Jibiki for his help with the preparation of the final manuscript.

The technical staff of the Department of Metallurgy have given invaluable help in overcoming a series of experimental difficulties.

The author is also keenly appreciative of the open door policy of the Department of Metallurgy, and its Head, Dr. E. Teghtsoonian, which has greatly facilitated access to materials and equipment.

Finally, the author would like to thank his wife, Susan, and other family members for their exceptional patience and support, which enabled this work to be carried to completion.

A. INTRODUCTION

I. General

Copper is the twenty-fifth most abundant element in the earth's crust, with an average concentration of only 70 ppm (1). In useful ore bodies the concentration is typically 1% (10,000 ppm) present as sulphide minerals or their oxidation products. The most important sulphide mineral of copper is chalcopyrite, CuFeS_2 .

Sulphide ores can readily be upgraded by flotation methods to eliminate most of the associated gangue minerals, and achieve a typically 30% copper concentrate. The extraction of the copper from the sulphide mineral has traditionally been carried out by melting and converting: the concentrate is slowly melted and partly oxidized in a large reverberatory furnace, to remove remaining gangue and some of the iron and sulphur; the resulting liquid copper-iron sulphide, or matte, is then blown with air to oxidize the remaining iron and sulphur, which are respectively slagged off and vented as SO_2 gas.

This process, which is now nearly 100 years old (4), was an outstanding achievement of the early metallurgists. It depends for its success on the remarkable nobility of liquid copper at converting temperatures (1100°C), such that air may be blown through the liquid metal, oxidizing the iron and sulphur selectively. This situation may be compared to that existing in a nickel or tin smelter, where the affinity for oxygen is much greater, and separation from iron is consequently not achieved.

The main drawback to the copper smelting process is the production of large quantities of SO_2 -containing gas, which can cause serious pollution

problems when it is vented to the atmosphere. The economical conversion of this gas into sulphuric acid may be achieved if the SO₂ content of the gas is high enough, but lack of nearby markets for the sulphuric acid produced can present a problem.

It has long been recognized that an alternative method of extracting copper from its ores might be found in hydrometallurgy; some types of ore, particularly oxides, have been processed by aqueous methods for years, but no generally applicable process for sulphide concentrates has yet been proven on a plant scale. However, this problem has recently been the subject of intensive research by numerous organizations and individuals; it seems very likely that at least one economic process will be demonstrated in the near future.

The variety of processes that have been or are being investigated is quite large, and a number of excellent review articles have recently appeared (2-5). The various processes can be classified according to the nature of the leaching step (in which the copper is dissolved), for it is usually the most difficult and furthermore, it determines the possible choices in subsequent steps. The most inert mineral to treat is almost invariably chalcopyrite, which is also the most common. Therefore the problem is one of extracting copper from chalcopyrite. This may be achieved with a number of reagents, but economics dictates that only a few are practicable - these are all oxidizing agents:

Ferric Sulphate	}	in acid solutions
Ferric Chloride		
Oxygen in sulphuric acid		
Oxygen in ammoniacal solutions		
Nitric Acid		

There are other technically feasible oxidants, but they do not seem to be receiving much attention recently. In addition, considerable effort has been directed towards the possibility of 'activating' the chalcopryrite before the leach, i.e. subjecting it to some form of pre-treatment such as heating which will enhance its reactivity. These processes, which usually involve substantial chemical change, show much promise, but do not fall within the scope of this work, which is directed only at the dissolution of chalcopryrite in its natural form.

Although there are several publications dealing with the leaching of chalcopryrite with each of these oxidants, there is little published information on the fundamental behaviour of chalcopryrite under oxidizing aqueous conditions. A unified understanding of the various leaching conditions might be gained through considering such reactions as being electrochemical in nature; then the (anodic) dissolution of the mineral can be studied independently of the chemistry of reduction of the oxidant.

The theory that chalcopryrite, like other sulphides, leaches electrochemically, is frequently mentioned in the literature (5); however, in spite of the logic and consistency of such a mechanism there appears to be little direct experimental evidence to support it.

The aim of this work is to further our understanding of the leaching of chalcopryrite under oxidizing conditions, and to demonstrate that such leaching may indeed be electrochemical. To achieve this, both electrochemical and chemical experiments have been carried out; in particular, leaching with ferric sulphate and ferric chloride has been studied, for these are two of the most important oxidants industrially available.

An additional incentive for examining the electrochemical dissolution of chalcopryrite lies in the possibility of direct electrolytic refining of copper concentrates. Such a process has been operated commercially on

nickel sulphide mattes for some years (183,4) and several investigators have studied the comparable process on copper matte. There is, however, little known about the anodic behaviour of chalcopyrite.

II Some Properties of Chalcopyrite

a) Phase Relations

The Cu-Fe-S system has probably received more attention than any other ternary mineral system (6-44) and yet there are still some important features which are unclear. Yund and Kullerud (10), using pure materials annealed together for long periods to form synthetic mineral assemblages, constructed phase diagrams for temperatures from 700°C down to 200°C. At 200°C, many reactions in this system are already very slow, requiring up to 500 days for equilibration, and below this temperature, results are unreliable. This has been a major hurdle to investigators in this field.

It appears from Figure 1 that there is only a single phase with the CuFeS_2 composition, and that the stoichiometric variation of this phase is very small, and decreasing with temperature. Further, the possible two phase assemblages involving chalcopyrite are:

- 1) Chalcopyrite - bornite
- 2) Chalcopyrite - pyrite
- 3) Chalcopyrite - pyrrhotite (and/or cubanite)

These associations are the same as those found in nature: the first two are typical of a porphyry copper deposit in British Columbia, whereas the last is found with nickel minerals in the Sudbury Basin.

Yund and Kullerud also showed that at high temperatures the ' CuFeS_2 ' phase actually contained less sulphur than required by the stoichiometric formula. At 500°C, this might be written as $\text{CuFeS}_{1.8}$. This implies that chalcopyrite formed at high temperatures will be deficient in sulphur, if not annealed for sufficiently long times, in the presence of sulphur.

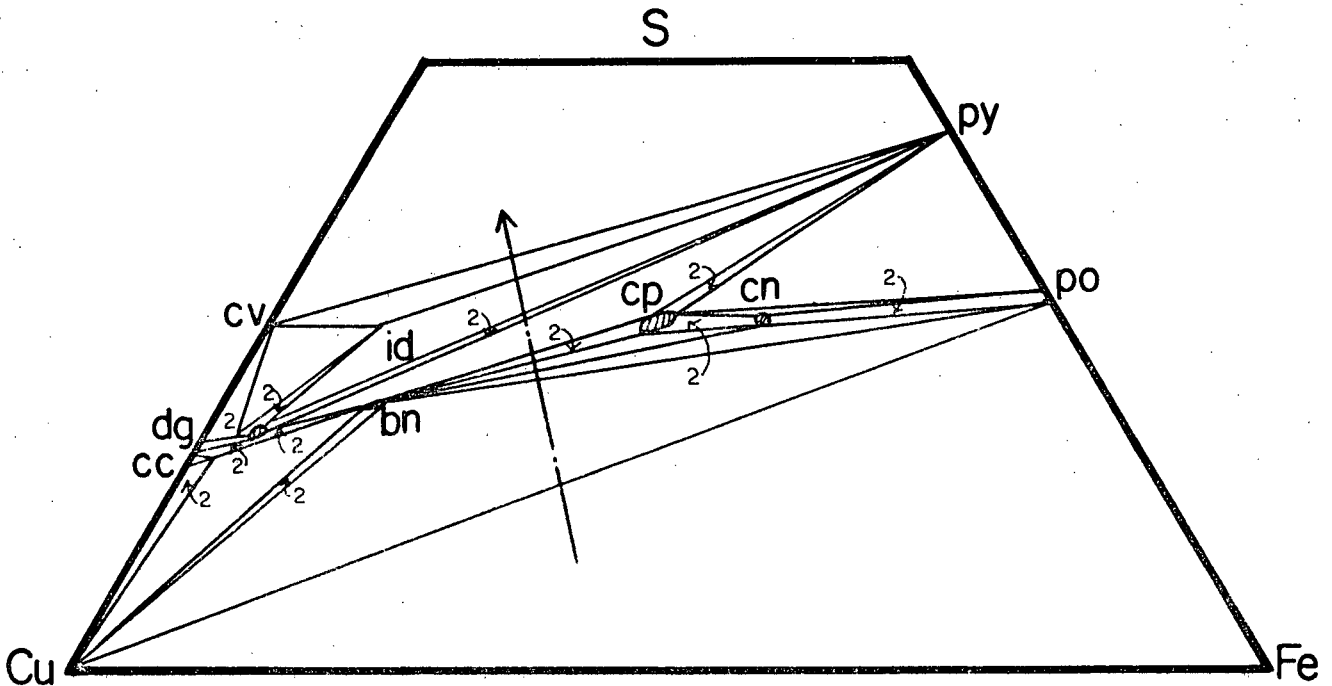


Fig.1 Cu-Fe-S system at 200°C.

Fig. 1 Cu-Fe-S system at 200°C (from Yund and Kullerud⁽¹⁰⁾).

bn	bornite	Cu_5FeS_4
cc	chalcocite	Cu_2S
cn	carbonite	$CuFe_2S_3$
cp	chalcopyrite	$CuFeS_2$
cv	covellite	CuS
dg	digenite	$Cu_{1.8}S$
id	idaite	$Cu_{5.5}FeS_{6.5}$
po	pyrrhotite	$Fe_{1-x}S$
py	pyrite	FeS_2

In the main, Yund and Kullerud's results were in agreement with the earlier study by Merwin and Lombard (6) although the latter postulated a new phase $\text{Cu}_3\text{Fe}_4\text{S}_6$ (which was not observed by Yund and Kullerud), and a low temperature composition of $\text{CuFeS}_{1.97}$ for chalcopyrite, (as opposed to stoichiometric CuFeS_2 proposed by Yund and Kullerud). Perhaps the most important conclusion from the point of view of the extractive metallurgist, was that a large solid solution field (iss) existed at high temperatures (but did not include the CuFeS_2 stoichiometric composition) and gradually shrank to the stoichiometric CuFeS_2 composition at ambient temperatures, where the range was very small. Although low temperature (<200°C) equilibria could not be observed, it was inferred that the same pattern would continue to ambient temperatures.

These conclusions have been placed in doubt by recent results of other workers (20-29), and it now appears that the Cu-Fe-S phase diagram is far more complicated at 25-100°C than as indicated above. Shortly after the publication of Yund and Kullerud's work a new copper-iron sulphide, talnakhite, was discovered in the Soviet Union(21), and this was soon followed by two others (26). Thus four phases in the ' CuFeS_2 ' region are now known as well as cubanite, which is also included in the 'iss' at high temperatures:

CuFeS_2	chalcopyrite
$\text{Cu}_9\text{Fe}_8\text{S}_{16}$	talnakhite
$\text{Cu}_9\text{Fe}_9\text{S}_{16}$	mooihoekite
$\text{Cu}_4\text{Fe}_5\text{S}_{16}$	haycockite
CuFe_2S_3	cubanite

The situation is summarized by Cabri (27):

... the central area of the Cu-Fe-S system is characterized by a large solid solution field at elevated temperatures which breaks up into five distant phases at low temperatures.

The picture is complicated by numerous phase transformations, unquenchable phases and phases with closely related crystal chemistry, resulting in their having similar physical appearance and X-ray diffraction powder patterns. The slow rate of most of the reactions at low temperatures also makes it difficult (in some cases impossible) to achieve equilibrium in the laboratory.

Chalcopyrite, talnakhite and mooihoekite were synthesized, while attempts to synthesize cubanite and haycockite were unsuccessful.

In addition to the new data on the central portion of the Cu-Fe-S system, there have been several other recent developments:

Idaite, long a subject of controversy, was given the formula $\text{Cu}_{5.5}\text{FeS}_{6.5}$ by Yund and Kullerud (10) and Cu_7FeS_4 by Cabri. (27)

Digenite, $\text{Cu}_{1.8}\text{S}$, an 'accepted' mineral for several years in the Cu-S system (36), has recently been considered as an iron-containing mineral (30-32), and a new mineral anilite Cu_7S_4 proposed, which unlike its predecessor has a very limited range of composition. Furthermore anilite may be converted into a metastable digenite phase by grinding.

Although Yund and Kullerud (10) showed no copper-containing phase that was more sulphur-rich than covellite, CuS , a copper disulphide phase has been synthesized under high pressure (33), and a new mineral, fukuchilite Cu_3FeS_8 discovered (34) and synthesized (35). The importance of these discoveries to hydrometallurgy is that oxidation of covellite or chalcopyrite could conceivably result in the formation of such a phase, even if metastable, instead of elemental sulphur.

b) Thermodynamics

The most useful thermodynamic quantities pertaining to chalcopyrite are naturally the free energy ΔF_T° and entropy, S_T° . Unfortunately, at the present time there appear to be no reliable experimental values published for the quantities (nor for any other ternary Cu-Fe-S mineral). This deficiency, which will hopefully be remedied soon, has in part been overcome

by calculation based on mineral assemblages, and decomposition pressures (37-44). Kelley (39), published some calculations of Maier (which were based on Joly's observation (41) that the decomposition temperature of chalcopyrite was 743°K) and gave $\Delta F_{248}^{\circ} = -41.3$ kcal./mole.

Golomzik (38) however, measured the sulphur vapour pressures at three temperatures (500, 600 and 700°C) and calculated $\Delta F_{298}^{\circ} = -51.5$ kcal./mole.

Young made a more detailed study of the problem (42,43) and evaluated the little-known work of Bartholomé (40), who calculated the equilibrium partial pressures of sulphur vapour over the various ternary associations. This method depends on having a reliable phase diagram, from which one can predict reactions. Bartholomé, with less experimental data than was available to Young, calculated $\Delta F_{298}^{\circ} = -45.0$ kcal/mole. Young used McKinstry's (44) and Yund and Kullerud's (10) data and calculated $\Delta F = -45.5$ kcal/mole. Young also utilized Merwin and Lombard's data for the decomposition pressure of chalcopyrite (6) and calculated $\Delta F_{298}^{\circ} = -41.8$ kcal./mole. These calculations are discussed in more detail in Appendix A.

Experimentally one may determine the free energy of a mineral in several ways, for instance:

- 1) Rest Potential Measurements in a Cell
- 2) Bomb Calorimetry (enthalpy only)
- 3) Solution Calorimetry (enthalpy only)
- 4) Low temperature heat capacity measurements
- 5) Sulphur activity measurements.

The first of these methods depends on having a reversible electrode reaction, involving the mineral, in which the free energies of the other products and reagents are known and their activities measurable. This is quite possible with simple copper sulphides, as discussed later, but does

not appear to have been attempted with a ternary mineral. This was attempted unsuccessfully in the present work.

Bomb calorimetry can yield a value for the enthalpy of a mineral if it can be combusted to products (oxides) whose heat contents are accurately known. This method has been used extensively in some fields and some of the oft quoted values for sulphides were obtained in this way. Thus von Wartenberg (45) measured ΔH_{298}° of Cu_2S and CuS , Zeumer and Roth (46) measured ΔH_{298}° of FeS , and Lipin et al. (47) measured ΔH_{298}° of pyrite and marcasite. This method was also attempted in the present work (Appendix A); no previous attempt appears in the literature.

Solution calorimetry can also yield a value for ΔH_{298}° if the mineral can dissolve reasonably rapidly (about an hour, maximum) in a solution where the product has a known heat content. This method also has been applied to binary sulphides (48,49) but not ternary sulphides as far as can be determined. The difficulty of dissolving chalcopyrite rapidly, except in hot solutions, has probably not encouraged work in this direction.

Heat capacity measurements appear to offer the best chance of obtaining reliable ΔF_{298}° values. Kelley (50) has given a useful summary of the restrictions on this method, which depends chiefly on the applicability of the third law of thermodynamics. Numerous binary sulphides and oxides have been studied by this method (51-61) but not ternary minerals. Pankratz and King (62) measured the high temperature (298 \rightarrow 1050°K) enthalpies of bornite and chalcopyrite in 1970 and low temperature measurements were said to be in progress. A recent compilation by the same authors (63) does give standard free energy and enthalpy values for bornite and chalcopyrite ($\Delta H_{298}^{\circ} = -45.50$ kcal/mole; $\Delta F_{298}^{\circ} = -45.55$ kcal./mole) based on low temperature measurements. However the source of the data is a private communication

(Stuves, U.S. Bureau of Mines, 1971) which so far (1974) does not appear to have been published.

By measurement of the partial pressure ratio $P_{\text{H}_2\text{S}}/P_{\text{H}_2}$ in equilibrium with a sulphide at a temperature T, one may measure the standard free energy of formation of the sulphide at that temperature. However, such measurements can only be carried out at high temperatures, and values at 298°K can only be obtained by extrapolation, using reliable values for the specific heat. Although this method has been used extensively for binary sulphides (64-66), extrapolation to low temperatures is unreliable (67). High temperature studies have been made on the Cu-Fe-S system (68) and other ternary systems (69).

c) Crystal Structure and Bonding

Chalcopyrite has the zinblende structure (70-72), in which alternate Zn atoms are replaced by Cu and Fe Atoms. The zinblende structure itself is derived from the diamond structure; each Zn atom is tetrahedrally coordinated to four S atoms, and vice versa. The S lattice has the fcc structure with the metal atoms in alternate tetrahedral holes. Due to the slight asymmetry caused by alternating Cu and Fe, the unit cell in chalcopyrite is twice as large as in zinblende, and is tetragonal ($a = 5.24 \text{ \AA}$, $c = 10.30 \text{ \AA}$), rather than cubic. However, at 547°C, chalcopyrite undergoes a transformation to a cubic form, presumably due to disordering of the Cu and Fe atoms.

The magnetic structure of chalcopyrite was determined by Donnay et al. (73) using neutron diffraction, in a pioneering experiment (75). The two Fe atoms connected to a common S atom were found to be anti-parallel, resulting in antiferro-magnetism.

Mössbauer spectra of chalcopyrite have been reported many times, but with varying results.

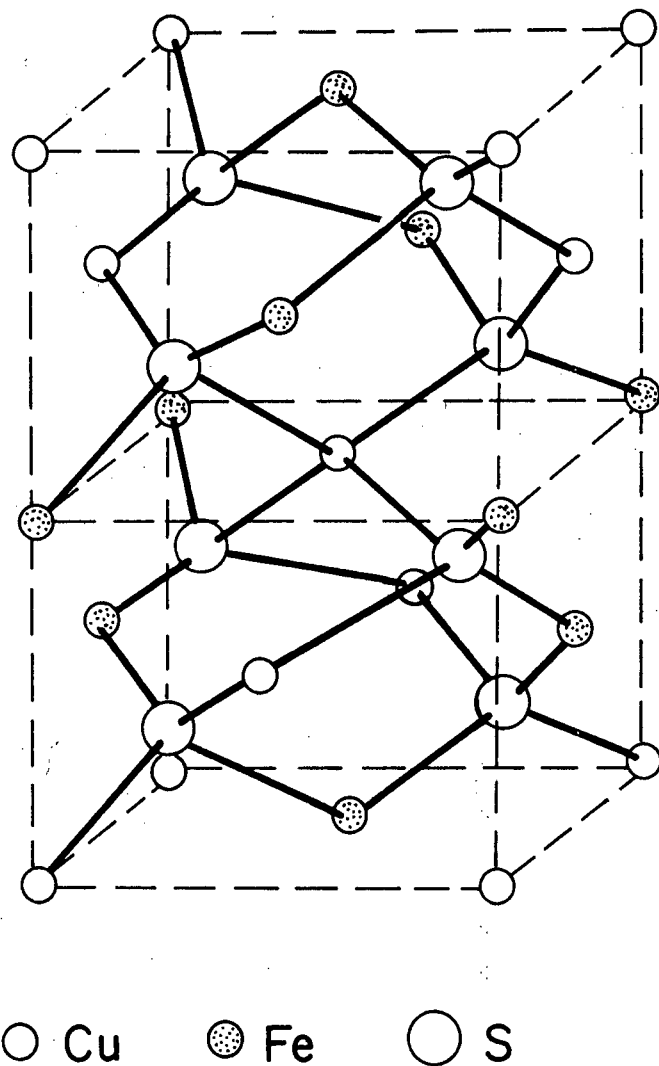
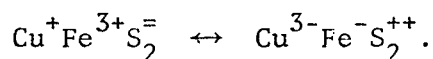


Fig. 2 Crystal structure of CuFeS_2 .

Vaughan (74) reported a six-line hyperfine magnetic spectrum, which was interpreted as originating from magnetically ordered iron in one type of site. The observed values in the spectrum suggested magnetically coupled high spin Fe^{3+} in tetrahedral sites. This conclusion is supported by other work in the literature (76-79), but in disagreement with that of Cabri and Goodman (80) and particularly that of Aramu (81), who reported a two-line spectrum which was interpreted as originating from the resonant configuration:



This work has been discussed by Herzenberg (82) and Frank (83) who suggest that there may be two forms of chalcopyrite, one of which is paramagnetic.

The bonding in chalcopyrite has been discussed by Vaughan (74); it may be considered in ionic, covalent or molecular orbital terms. In the ionic model, the fcc lattice of $\text{S}^=$ anions has alternate tetrahedral holes filled with either Fe^{3+} or Cu^+ atoms. In covalent terms, the S and metal atoms may be viewed as forming sp^3 bonds, which are tetrahedrally directed. The bond lengths which are sometimes used as a criterion of degree of covalency are (7):

Cu-S 2.34 Å

Fe-S 2.22 Å

whereas the sum of the ionic radii are (1):

$\text{Cu}^+ + \text{S}^=$ 2.80 Å

$\text{Cu}^{++} + \text{S}^=$ 2.56 Å

$\text{Fe}^{++} + \text{S}^=$ 2.58 Å

$\text{Fe}^{3+} + \text{S}^=$ 2.48 Å

In the molecular orbital approach, there is a filled set of valence bonds formed by overlapping s and p orbitals from metal and sulphur atoms, and a higher energy set of empty antibonding orbitals (the conduction band).

The d levels of Cu and Fe may contribute to sd^3 hybridization and create new energy levels between the filled valence and empty conduction bands, thus reducing the band gap.

Frueh (84-86), considered that the semi-metallic characteristics of the sulphide minerals justified a limited application of zone theory, and determined the important Brillouin zones of digenite, bornite and chalcopyrite. These three minerals have the same basic structure, i.e. cubic close-packed sulphur atoms with the interstitial tetrahedral holes being in part occupied by the metal atoms. Assuming that all the outer shell electrons of each element can contribute free electrons, (Cu one, Fe three, and S six electrons) then the electron/atom ratio of the minerals would be:

chalcopyrite	4
bornite	3.2
digenite	2.8
chalcocite	2.7
covellite	3.5.

The principal Brillouin zones of these minerals were then calculated and the electron/atom ratios necessary to fill these zones. The electrons of the first three minerals just filled one of the important Brillouin zones, and in each instance, the Brillouin zone just filled was that constructed from the same basic reflections. However chalcocite and covellite did not fit in any zone. Frueh concluded that in the field from digenite to chalcopyrite the structural type is maintained, despite the increase in the Fe/Cu ratio by the omission of sufficient metal atoms to avoid increasing the e^- /atom ratio beyond the capacity of the filled zone.

Vaughan (74) has noted the high stability of the zincblende structure is to be expected from such a network of tetrahedrally directed covalent bonds

similar to those in diamond, and that such a structure is favoured by transition metal cations with the symmetrical d^5 (Fe^{+++}) and d^{10} (Cu^+) electron configurations.

Chalcopyrite is a semiconductor and is reported always to be n-type (74,86-88), due to a stoichiometric excess of cations (86). Frueh (86) studied the resistivity of chalcopyrite, and found that it increased slowly with temperature, up to $310^{\circ}C$, at which point it fell rapidly. This behaviour is contrary to the usual semiconductor pattern, in which resistivity declines with temperature as more electrons are excited across the band gap. In this case, the conductivity evidently arises from an extra band of electrons, which are derived from the excess cations; they lie just below the conduction band and can be excited into it with little or no activation energy. The mineral thus behaves like a metal with a vastly reduced number of electrons in the conduction band, whose conductivity is inversely affected by temperature, due to increased thermal vibrations of the lattice. The rapid decrease in resistivity at $310^{\circ}C$ is due to decomposition with sulphur loss; thus Frueh concluded that it is impossible to reach the intrinsic region before the mineral decomposes.

The use of 'chalcopyrite-like' compounds is very widespread in the electronics industry, and a considerable literature exists on the subject, particularly in the Soviet sector, due to the work of Poplavnoi (e.g. (87)).

III The Leaching of Copper Sulphides

a) An Overview

Despite the impressive array of proposed processes for extracting copper from chalcopyrite (over forty may be counted in a recent review (4)), there is comparatively little published literature on the fundamental behaviour of the mineral under oxidizing aqueous conditions. However, there is consider-

ably more information on the corresponding processes with the binary copper sulphides - chalcocite (Cu_2S), digenite ($\text{Cu}_{1.8}\text{S}$) and covellite (CuS). Furthermore, there is far more known about the electrochemical behaviour of these minerals, and it is useful to consider this information first. All of the copper sulphide minerals are semiconductors with conductivities ranging from $10^{-1}\Omega^{-1}\text{cm}^{-1}$ to $10^2\Omega^{-1}\text{cm}^{-1}$, and their dissolution reactions are often considered to be electrochemical in nature. However, evidence to support this proposition is invariably indirect, and usually consists of demonstrating that the anodic reaction driven by an appropriate external emf will give the same results as the leaching reaction (90). This evidence can, however, be quite convincing: thus Needes and Nicol (91) showed that the dissolution rate of UO_2 in a variety of oxidants corresponded closely with the rate of the anodic reaction resulting from imposing an external emf appropriate to each oxidant.

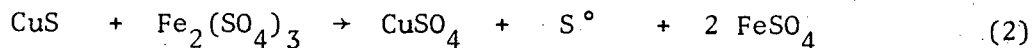
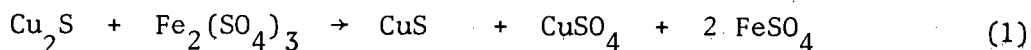
Some other evidence for electrochemical reactions on sulphides has come from studies of the leaching of pyrite (92-94), which is attacked at certain sites, causing pitting. These are interpreted as anodic sites. Other workers (95) have demonstrated that the leaching of sphalerite is catalyzed by certain metal cations which was accounted for by an electrochemical mechanism. However, Peters and Majima (96) demonstrated that the anodic dissolution of pyrite produced 100% sulphate whereas pressure leaching can produce up to 50% elemental sulphur (185).

Several reviews of this subject have been published (92,98-101,186).

b) Leaching of Simple Copper Sulphides

Sullivan (102) studied the leaching of natural chalcocite in powdered form, with acidified ferric sulphate solutions. The dissolution occurred in two stages: the first, which was rapid, involved dissolution of copper to

form a CuS phase, and the second, much slower, resulted in elemental sulphur formation:



The reaction rate was found to be independent of $[\text{Fe}^{+++}]$ above 0.01M and also largely independent of pH and $[\text{Fe}^{++}]$.

Sullivan also examined the effect of particle size, and concluded that the dissolution rate was virtually the same for sizes (-10+28) to (-150+200). For particles larger than this, the dissolution was much slower, although this fact seems to have been overlooked. In fact, the much slower leaching rates of Thomas et al (103) (approx. 2%/hour, compared to 30%/hr.) can only be explained this way.

Later studies on the dissolution of chalcocite and digenite have agreed with the results of Sullivan; the mechanism has been refined to include digenite, $\text{Cu}_{1.8}\text{S}$, as an intermediate phase. Thomas et al (103), using rotating sintered disks of synthetic chalcocite, found that the dissolution rate was linearly dependent on $[\text{Fe}^{+++}]$ up to about 0.1M (at 95 rpm and 25°C), and then appeared to level off somewhat. A similar dependence of dissolution rate upon rotation speed was found. These findings, together with an activation energy of 5 kcal/mole, were taken as an indication of a process controlled by mass transport of reagents across the boundary layer.

Sullivan (102) also examined the leaching of natural chalcocite powder with ferric chloride solutions, and reported similar dissolution rates (as with ferric sulphate) at 35°C, but very rapid dissolution at boiling temperatures. King (104) and Burkin (105) also studied this reaction and found that the first stage (50% Cu extracted) was complete in 3-4 minutes at 40°C, but the second required two hours at 70°C. They found an activation energy

of 0.8 kcal for the first stage and proposed that solid state diffusion of Cu^+ ions was rate limiting.

Sullivan (106) and Thomas et al (107) also studied the leaching of covellite with ferric sulphate. The stoichiometry of the reaction was found to be the same as the second stage of chalcocite leaching (equation (2)), i.e. 100% elemental sulphur formation. The rate, however, was considerably slower. An activation energy of 22-25 kcal./mole was found, implying that the process was controlled by a surface reaction. Sullivan found the rate was unaffected by pH or $[\text{Fe}^{+++}]$, but was dependent on particle size, though not proportionately (see Table 1).

TABLE 1 [from Sullivan (106)]

Dissolution of Covellite in Ferric Sulphate Solutions at 35°C
-Effect of Particle Size

Mineral	Calculated Area (cm^2/g)	% Dissolved After	
		5 days	24 days
Butte			
- 3+ 10	26	6	9
- 10+ 28	65	10	13
-100+200	385	16	25
-200	4,575	40	56
Kennecott			
- 3+ 10	26	14	25
- 10+ 28	65	20	31
-100+200	385	27	41
-200	3,867	42	62

Sullivan also compared the rates of covellite leaching in ferric chloride and ferric sulphate. At 35°C, leaching was faster in ferric sulphate than in ferric chloride, but at 98°C, the leaching rates were identical. In all cases the $[\text{Fe}^{+++}]$ was unimportant in the range covered.

This situation is to be compared with that of chalcocite, where the rate is faster in ferric chloride (102).

Jackson and Strickland (108) studied the leaching of chalcocite and covellite by chlorine in acid chloride solutions; they found exclusive elemental sulphur formation and a reaction controlled by diffusion of chlorine in the solution.

Oxygen pressure leaching of copper sulphides produces some sulphate, depending inversely on the acidity (109-111). Tkachenko and Tseft (112) studied the ferric chloride leaching of massive chalcocite and found an activation energy of 4 kcal./mole, indicative of a diffusion process. The reaction slowed down with time, but was unaffected by changing the stirring speed from 100 to 500 rpm. The authors concluded that the rate controlling step was diffusion of reagent through the sulphur film.

c) Electrochemical Studies of Simple Copper Sulphides

(i) Thermodynamic measurements

Several authors have measured the rest potentials of the various copper sulphides (90,113-118). Most of the early work was done at ambient temperature on natural minerals, but there is surprisingly little scatter in the results. There have been several studies recently using synthetic minerals, which nevertheless give as much scatter as the former experiments. Etienne (90), using synthetic stoichiometric mineral mixtures, sintered into disks at 400°C, obtained quite reversible electrodes above 45°C, with covellite - digenite and digenite - djurleite mixtures. Precise rest potentials

(± 0.35 mV) were obtained from these electrodes, but chalcocite - djurleite and covellite - sulphur mixtures did not give such reliable results. Rickert and Matheu (117) using vacuum deposited thin films and a coulometric titration method arrived at significantly lower values. Cole (118), on the other hand, using synthetic minerals fused into disks at 950°C for 30 minutes, and the coulometric titration method, obtained values that were significantly higher than Etienne's. The reason for these differences is not apparent.

TABLE II

Rest Potentials of Copper Sulphides vs. Cu Metal at 25°C
Measured by Various Authors

Phases	*Etienne (90) (45-90°C)	Rickert (117) (15-90°C)	Cole (118) (25°C)	Others (25°C)
Chalcocite + Djurleite	Metastability Problem	127 mV	+145 mV (± 5)	47 (116) 166 (115) 134 (113)
Djurleite + Digenite	+163($\pm .35$)mV	144 150 mV	+180(± 5)mV	
Digenite + Covellite	+178($\pm .45$)mV	165 mV	+200(± 5)mV	
Covellite + Sulphur	Irreversible Electrode	251 mV	--	340 (113)

*Extrapolated to 25°C

(ii) Stoichiometry

Several workers have studied the anodic dissolution of Cu_2S and CuS , using either synthetic material (90,116,118,119), natural minerals or matte anodes (120-126). Most are agreed that the anodic reactions are the same as found in leaching (equations (1) and (2)). However, Venkatachalam et al and Loshkarev (120,121) indicated that a significant amount (up to 55%) of sulphur was oxidized to sulphate. Other workers generally found 3% or less. Another important feature observed by several authors is the high CuS content in the anode slime, which would be a severe drawback to any process utilizing direct electrolytic refining of copper matte anodes.

(iii) Leaching Mechanism

Kuxmann and Biallass (116) studied the anodic dissolution of fused synthetic chalcocite in acidified copper sulphate solutions, under galvanostatic conditions. They found the dissolution behaviour similar to that in the leaching experiments described above, but the polarization underwent a sharp increase of about one volt after a certain time, which depended inversely on the current density. Etienne (90) obtained similar results with synthetic digenite and covellite anodes, and showed the transition time, τ , was related to the current density, I .

$$I^2 \tau = 2.5 \text{ amp}^2 \text{ cm}^{-4} \text{ sec}^{-1}$$

At the transition, the normal anodic dissolution of CuS is no longer capable of maintaining the imposed current. A second, higher potential reaction, probably oxygen evolution or sulphate formation, then takes over. Kuxmann and Biallass attributed this to the surpassing of the maximum diffusion rate of Cu^+ ions in the solid, because the internal diffusion layer is too deep. This assumes that the Cu^+ ions move through the covellite layer by solid state diffusion as proposed by King and Burkin (104,105).

Etienne (90), however, considered that the solid state diffusion of Cu^+ in covellite is too slow to account for the observed dissolution rate, and therefore proposed that there must be aqueous diffusion through the shrinkage pores of the partially reacted covellite, which are filled with solution. At high current densities, or after sufficiently long times, these pores would saturate with and precipitate CuSO_4 , thus stopping the reaction, and causing a rise in potential.

The aqueous pore diffusion model resulted from another experiment of Etienne's, in which a copper sulphide scale was 'grown' on a copper anode in an H_2S saturated solution, and the ionic conductivity of Cu^+ ion measured. In digenite, at 55°C , this was $7.5 \times 10^{-5} \Omega^{-1} \text{cm}^{-1}$, and in chalcocite $3.5 \times 10^{-5} \Omega^{-1} \text{cm}^{-1}$. In comparison, the observed dissolution rate of a digenite anode resulted in a flux of Cu^+ ions through the covellite (product) layer equivalent to an ionic conductivity of $8 \times 10^{-4} \Omega^{-1} \text{cm}^{-1}$. Since there was no reason to believe that covellite would have such a high ionic conductivity, it was concluded that some other mechanism must account for the high flux of Cu^+ ions: due to the decrease in molar volume in passing from digenite to covellite, there is 19.7% of the cross-sectional area occupied by aqueous electrolyte.

This view of the diffusional processes in the copper sulphides has been contested by Cole (118), who subjected synthetic chalcocite anodes to coulometric titrations, and estimated diffusion coefficients of Cu^+ ion ($1.8 \times 10^{-8} \text{ cm}^2/\text{sec}$ at 25°C) that are 1000 times larger than those calculated by Etienne ($2.5 \times 10^{-11} \text{ cm}^2/\text{sec}$ at 25°C). He therefore concluded that the solid state diffusion of Cu^+ ions is capable of generating a sufficient flux to account for the observed diffusion rate.

d) A Note on the Leaching of Bornite, Cubanite and Idaite

Although bornite is an important copper mineral, especially in B.C., it will not be considered here, for it apparently leaches rapidly compared with chalcopyrite (127,128) and will not therefore be a limiting factor in a process. Furthermore, its dissolution behaviour is different from that of chalcopyrite, in that copper dissolves preferentially. There appears to be no electrochemical work on bornite, published in the literature.

Cubanite (CuFe_2S_3) is reported to leach even slower than chalcopyrite (129); fortunately it is a comparatively rare mineral.

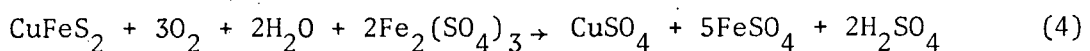
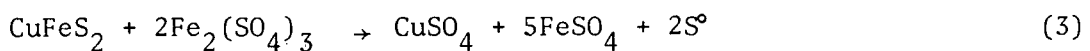
Nothing is known about the leaching of idaite (Cu_5FeS_6) and the very formula of this rare mineral is still under controversy. However, it is reportedly the product of bornite leaching (127).

e) Leaching of Chalcopyrite

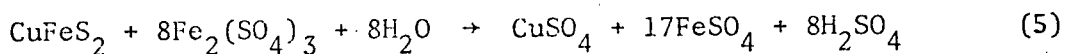
This reaction is best treated by covering each reagent separately.

(i) Ferric Sulphate

This reagent has great importance as the active agent in dump leaching, as is practised in the South Western United States and elsewhere. It was first investigated by Sullivan (130), who showed that hot solutions dissolved appreciable amounts of copper from finely divided material, but the rate appeared to decrease rapidly with time. A significant amount of sulphur was oxidized to sulphate, and two equations for the leaching reaction were given:



This observation, that sulphate is formed, appears to have been missed by later workers, possibly because of the inclusion of oxygen in the second equation, instead of:



From Sullivan's data, (Table III), it can be seen that the ratio of Cu:Fe:S in the residue remained nearly constant, in that there was no selective dissolution; since more copper was extracted than pure sulphur liberated some sulphur was undoubtedly oxidized (about 25-35%). The possibility that oxygen can contribute to the reaction cannot of course be ruled out, but appears unlikely from the general experience that oxygen reacts extremely slowly under such conditions.

Table III [from Sullivan (130)]

Data on Mechanism of Dissolution of Chalcopyrite
in Ferric Sulphate (at 35°C)

Time (days)	Copper Dissolved (%)	Total Sulphur in Original Sample Existing in Residue in a form Soluble in CS ₂ (%) (Free Sulphur)	Atomic Ratio of Cu:Fe:S in Residue after CS ₂ Treatment ²
0	-	-	1.00:1.18:2.20
1	8.2	5.4	1.00:1.17:2.27
7	14.8	10.4	1.00:1.16:2.23
14	21.8	15.8	1.00:1.17:2.25
21	25.5	19.1	1.00:1.17:2.25
42	30.1	22.6	1.00:1.17:2.17

Dutrizac et al. (131) also studied the reaction of chalcopyrite with ferric sulphate. To avoid the complications of impurities and an indefinite surface area, they used synthetic chalcopyrite which was pressed into disks. The dissolution reaction found was equation (3), i.e. no sulphate formation. The basis for this conclusion was a statement that the ratio Fe^{+++}/Cu^{++} produced was close to 5 (as required by equation (3)), rather than 17 (equation (5)), and S°/Cu^{++} was approximately 2:1. However, no other experimental data were given.

Dutrizac et al. found the leaching rate to decrease with time, t , according to a parabolic rate law:

$$Cu \text{ dissolved} = K\sqrt{t} \quad \text{or} \quad \text{Rate} = K_1/\sqrt{t} \quad (6)$$

This result was attributed to a thickening film of elemental sulphur on the surface, which retarded the reaction. The reaction was found to be independent of pH, rotation speed and $[Fe^{+++}]$ above a very low level (0.005 M) but sharply dependent on $[Fe^{++}]$. It was concluded that the rate determining step was the diffusion of Fe^{++} ions away from the surface through the S° film. An activation energy of 17.3 kcal./mole was determined. This interpretation has been criticized by Roman and Brenner (3) who concluded that such a high activation energy must be due to chemical control, and Peters (132) who suggested that the parabolic dissolution rate could be due to the diffusion of solid state defects out to the surface of the mineral.

Dutrizac et al. also found that natural massive chalcopyrite leached about 15 times slower than synthetic material. They claimed that the same parabolic rate law applied however, but the data appear to be insufficient to verify this. The slower leaching rate was attributed to the reduced porosity of the natural material.

This postulate has been affirmed in another publication by the same

authors (133) in which natural chalcopyrite was crushed and then pressed into a disk like the synthetic mineral. The results showed that the pressed disk of natural mineral also reacted rapidly. This same paper also showed that impurities can significantly affect the rate presumably due to galvanic effects. More noble sulphides (or rather more passive) such as pyrite and molybdenite accelerated the rate, whereas less noble ones (galena) decreased it.

Lowe (134) also examined the kinetics of ferric sulphate leaching of chalcopyrite and found the reaction to be independent of pH and $[Fe^{+++}]$, and therefore concluded that the rate-controlling step was a surface electrode reaction involving chemisorbed ferric ions. An activation energy of 17.8 Kcal was calculated. The experimental data for these calculations consisted only of Fe^{+++} ion consumption; the stoichiometry was assumed to be that of equation (3).

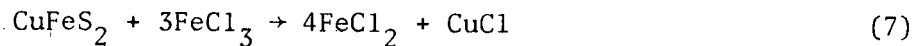
(ii) Ferric Chloride

Ferric chloride has been utilized for leaching chalcopyrite for many years, for it was recognized that it was a far stronger reagent than ferric sulphate. Forward and Warren (135) have summarized the early work. However, there is little in the way of published data comparing the two reagents except for a few results of Sullivan (130), and Pike et al. (136). Most of the investigators seemed satisfied with the ability of ferric chloride to extract the copper from chalcopyrite and concentrated on the difficult problems of the rest of the process, such as reagent regeneration and copper recovery.

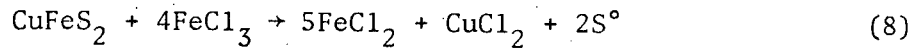
Sullivan (130) reported that stronger solutions (i.e. more concentrated in $[Fe^{+++}]$) were beneficial, which was not true in ferric sulphate leaching. Fine grinding and high temperatures also increased the

rate of extraction, as expected.

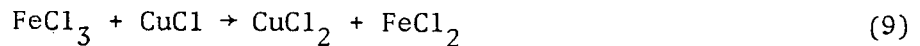
A more complete examination of the leaching reaction was undertaken by Haver and Wong (137); they reported excellent dissolution rates (essentially 100% extraction in one hour) on finely ground material with strong ($[\text{Fe}^{+++}]$) solutions at reflux temperatures (106°C). The stoichiometry of the reaction was found to be



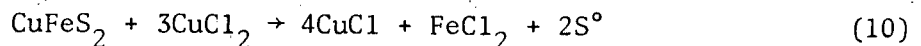
rather than



By using a constant volume of solution (212 g/l Fe^{+++}) the stoichiometry was revealed by varying the quantity of concentrate. Thus it was found that 2.7 pounds of FeCl_3 were needed per pound of concentrate (equation (7)) rather than 3.5 pounds (equation (8)). Since the reaction



goes readily it is apparent that the actual leaching agent in the latter part of the leach (when FeCl_3 is used up), must be CuCl_2 , i.e.:



Haver and Wong reported that agitation slightly decreased the dissolution rate; Roman (3) commenting on this unexpected result, suggested that a reaction product such as CuCl_2 might have a catalytic effect. This had been reported on work on chalcocite (138,139). This suggestion is supported by the results described herein.

A large temperature dependence was demonstrated by Haver and Wong, but appreciable dissolution did not take place below 80°C .

The leaching curves (Figure 3) also show that for all temperatures a very high proportion of the total copper that is extracted (within 2 hours) actually dissolves by the time of the first sample (fifteen

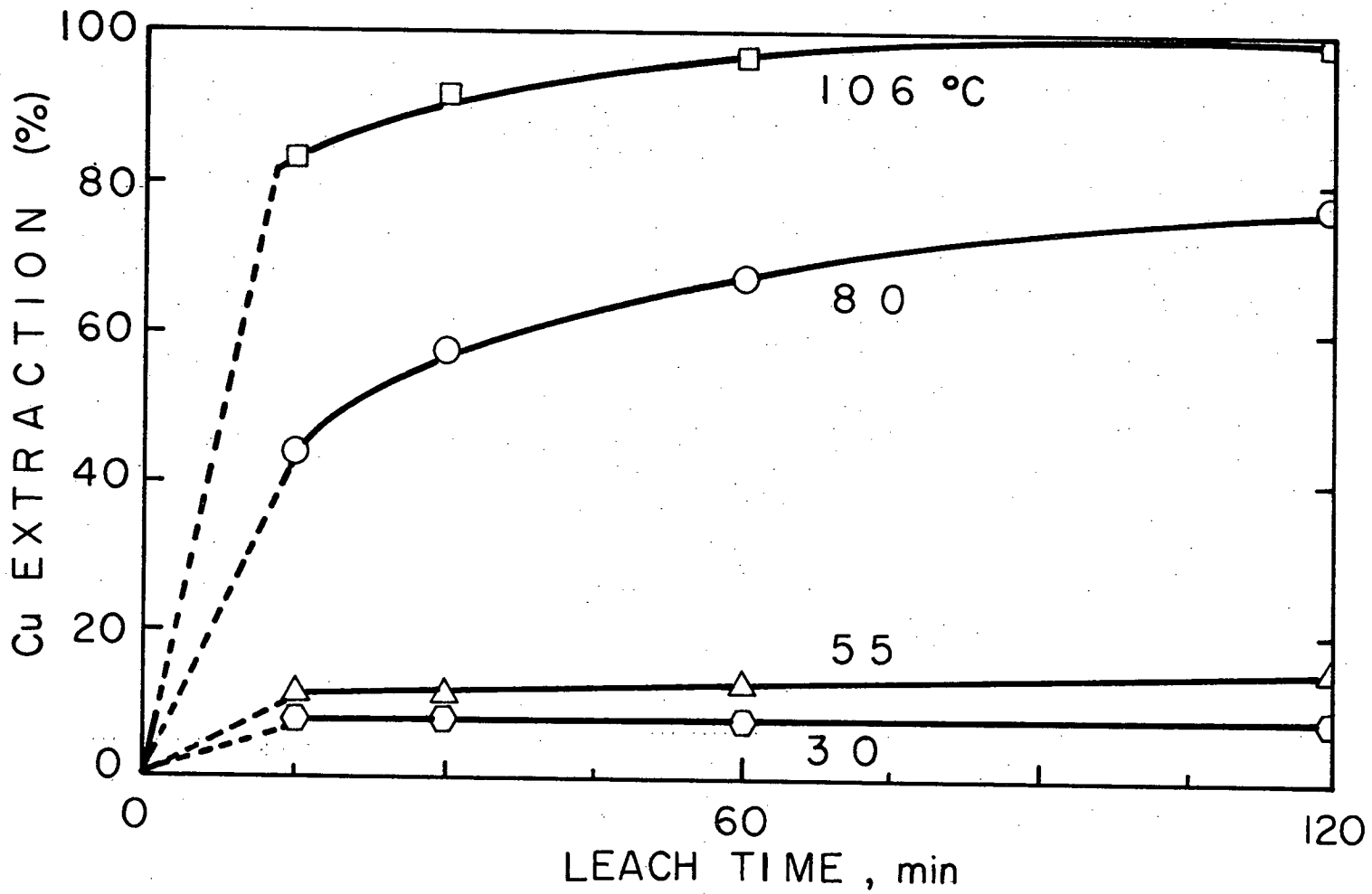


Fig. 3 Leaching of chalcopyrite concentrate in ferric chloride; effect of temperature, showing the change in rate after 15 minutes (from Haver and Wong⁽¹³⁷⁾).

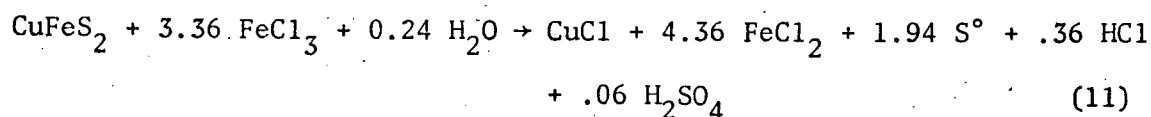
minutes).*

Thus the dissolution is extremely rapid initially, and then slows down by an order of magnitude. Practical leaching therefore must aim at extracting the copper almost entirely in the first period. The reason for this slower rate may be the buildup of a sulphur film.

Ermilov (140) investigated the leaching of massive specimens in ferric chloride and reported that the dissolution rate depended linearly on $[\text{Fe}^{+++}]$ in the range 50 → 150 g/l. This is contrary to the findings of Klets and Serikov (141), who reported that the $[\text{Fe}^{+++}]$ was not important in the dissolution of Ni-Cu concentrates. Ermilov also found that the sulphur film produced during the reaction did not slow down the dissolution which was linear with time. This result is not necessarily in conflict with the above interpretation of Haver and Wong's two-part leaching curve. In the latter case the particles were ground to an average size of only 3 μ ; and larger particles exhibited a much reduced initial dissolution.

Hence the initial dissolution on a massive specimen might well be negligible and the actual dissolution measured by Ermilov would then correspond to the slow second part of Haver and Wong's leaching curves.

The production of sulphate in ferric chloride leaching is reported to be small (137) (2-4%) but significant when one considers that 3% sulphate results in a 12% higher consumption of ferric chloride:



* This phenomenon is masked somewhat by the authors' decision to draw the dissolution curve from 15 minutes instead of zero time.

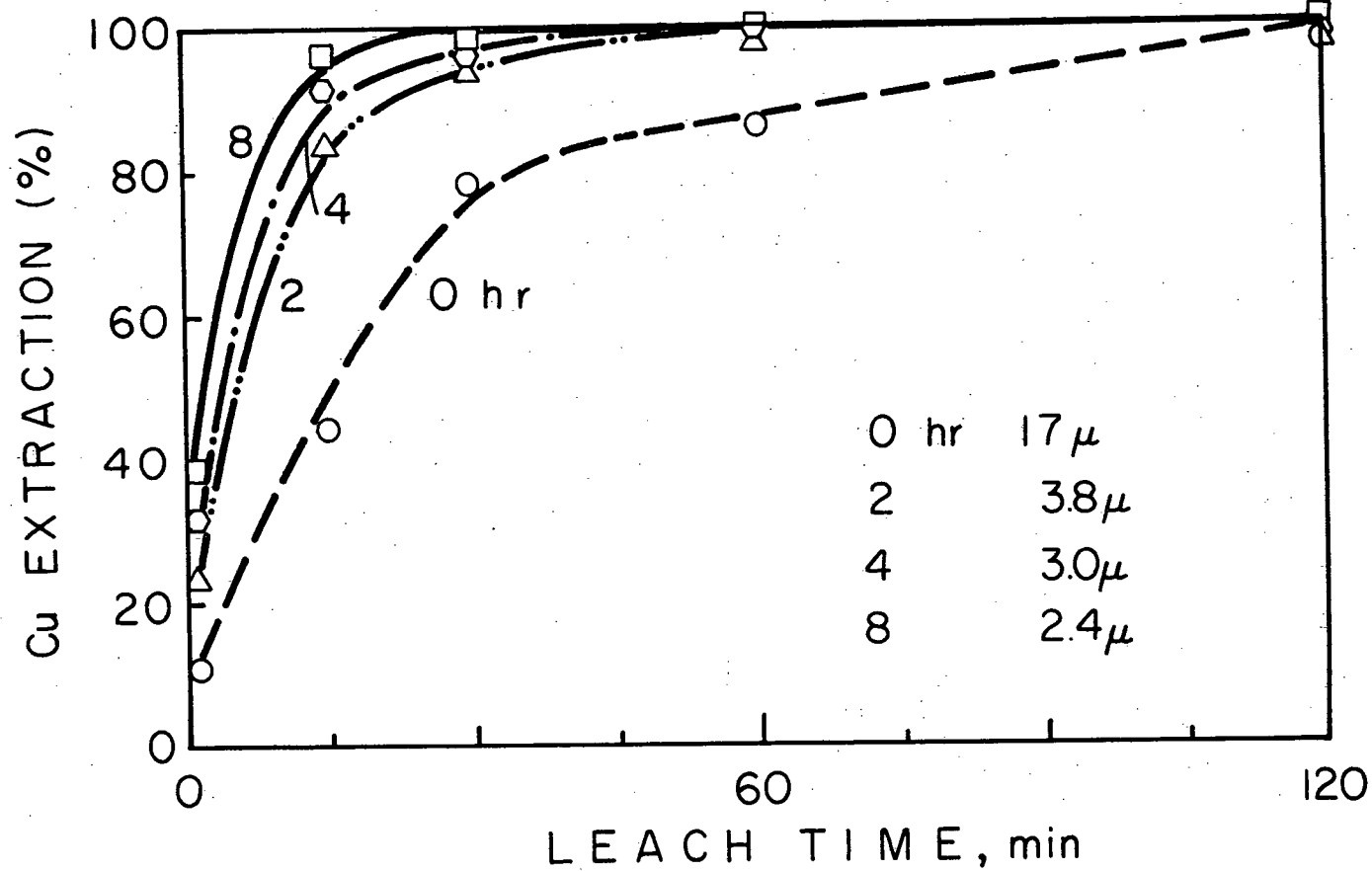
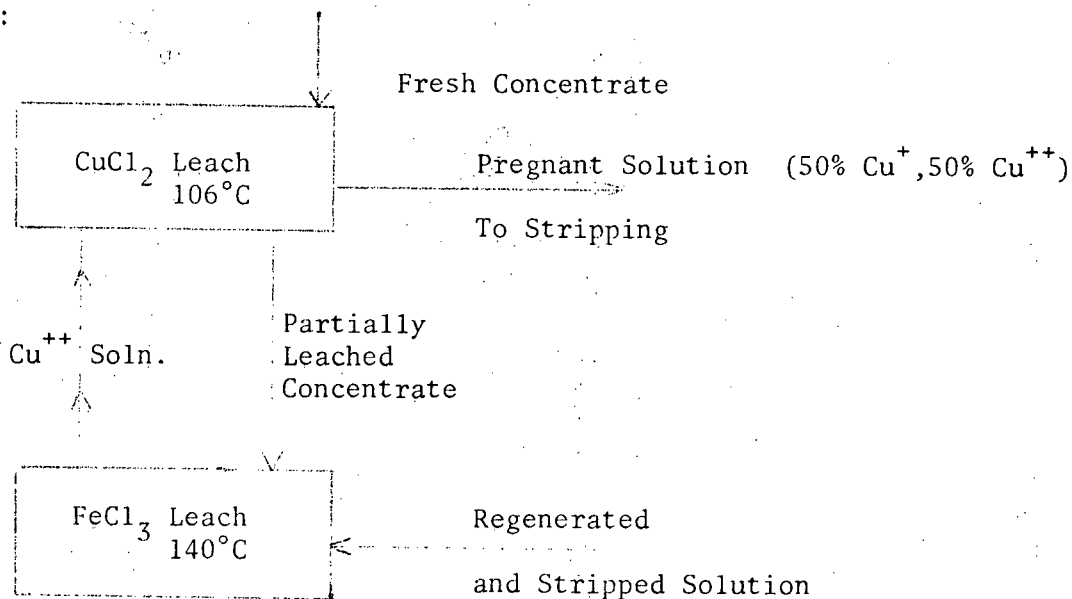


Fig. 4 Leaching of chalcopyrite concentrate in ferric chloride, effect of particle size (as grinding time). (From Haver and Wong⁽¹³⁷⁾).

However, it is possible that the sulphate arises from prior oxidation of the concentrate, during grinding, flotation, shipping or storage.

In addition to many early industrial attempts to use ferric chloride (135), two recent patents have been issued which utilize the reagent (142, 143). In the Cominco process (142) a single leach at atmospheric pressure (106°C) is used, and complete extraction is obtained in only 9-12 hours, using strong solutions (200 g./l.) and reground concentrates. In agreement with the work of Haver and Wong, less FeCl_3 is required than needed by equation (8), thus finishing up with some cuprous (approximately 50% of total Cu) in the final solution; beyond this point leaching with CuCl_2 apparently became too slow.

The process proposed by Duval (143), is also in agreement on this point. However the extractions obtained by them at atmospheric pressures (106°C) were considerably lower than those of Cominco (142) or Haver and Wong (137). Because of this, Duval chose a two-stage counter-current leach:



The strong FeCl_3 leach, which strips the remaining Cu values out of the partially leached concentrates, is conducted at 140°C , because the 106°C leach required 12 hours. The CuCl_2 leach has two purposes:

- 1) Reduces the quantity of FeCl_3 required
- 2) Partially reduces the cupric solution to cuprous in preparation for electrolysis.

The requirement that the FeCl_3 leach (Duval) be conducted in a pressure vessel is a significant escalation in cost, which the Cominco process indicates is not required. The reason for this conflicting result lies probably in the type of concentrate leached and its particle size. At any rate the extremely fast reactions obtained by Haver and Wong (on a Nevada concentrate) may not be obtainable on all chalcopyrite concentrates.

(iii) Other Oxidants

Several other oxidizing agents have been extensively studied, but will not be considered in detail here except as they contribute to a general understanding of the anodic dissolution of chalcopyrite. This does not reflect a preference for ferric solutions as reagents; however, the emphasis of the present work has been on understanding the leaching by ferric solutions as a matter of convenience, in linking electrochemical results with practical leaching conditions.

At sufficiently high temperatures and pressures, oxygen will dissolve chalcopyrite at practical rates. In strongly acid solutions, iron and copper both go into solution, and the yield of elemental sulphur is high (144). At higher pH, iron is hydrolyzed and sulphur is largely oxidized to sulphate (145). In ammoniacal solutions, intermediate sulphur species, particularly thiosulphate, $\text{S}_2\text{O}_3^{=}$, are formed. Sherritt-Gordon utilizes the $\text{NH}_3\text{-O}_2$ system to dissolve chalcopyrite-pentlandite concentrates (146) and the new

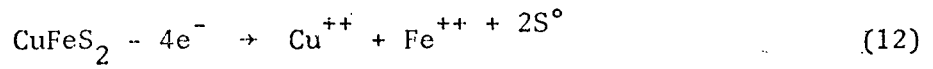
Arbiter process (147) also uses $\text{NH}_3\text{-O}_2$.

Nitric acid is an effective oxidizing agent for chalcopyrite (148-150) but the chemistry of the dissolution reaction is complex. In addition to the possibility of sulphate formation, there is a complicated dependence on nitric acid concentration. Both NO_2 and NO may be produced in the reaction, but NO_2 can further react with the sulphide, or react with water to form more nitric acid and NO . At high acid strengths, NO_2 is lost by evolution and elemental sulphur is oxidized to sulphate; thus the efficiency of the reaction, in terms of copper extracted, is decreased although the rate of reaction is increased. In dilute acid the NO and NO_2 may be trapped within the solution, and re-oxidized by O_2 , the nitric acid thus acting as a catalyst.

f) Electrochemical Studies on Chalcopyrite

Springer (151) examined the semiconducting properties of chalcopyrite by measuring the anodic polarization up to 10 mA/cm^2 and found no saturation current, as expected for an n-type semiconductor (152). Zevgolis (89) also measured anodic polarizations, at much higher voltages, and found a saturation current at about 50 mA/cm^2 above 3 volts (vs. S.C.E.). He concluded that the hole density in chalcopyrite determines the value of the limiting anodic current. This conclusion was supported by an illumination experiment which increased the current, presumably due to the increased concentration of holes (152). However, the 200 watt illuminator used shone directly on the mineral specimen, and raised the bath temperature by 4°C . The resulting heat effect was not corrected for.

Zevgolis also examined the stoichiometry of the anodic dissolution reaction (in $1.5\text{M H}_2\text{SO}_4$ at 30°C) and claimed 100% current efficiency for the reaction:



However, the author apparently made an error in calculating current efficiency, for only 50% of the current is actually accounted for by reaction (12). This may be seen by examining Figure 5, reproduced from reference (89).

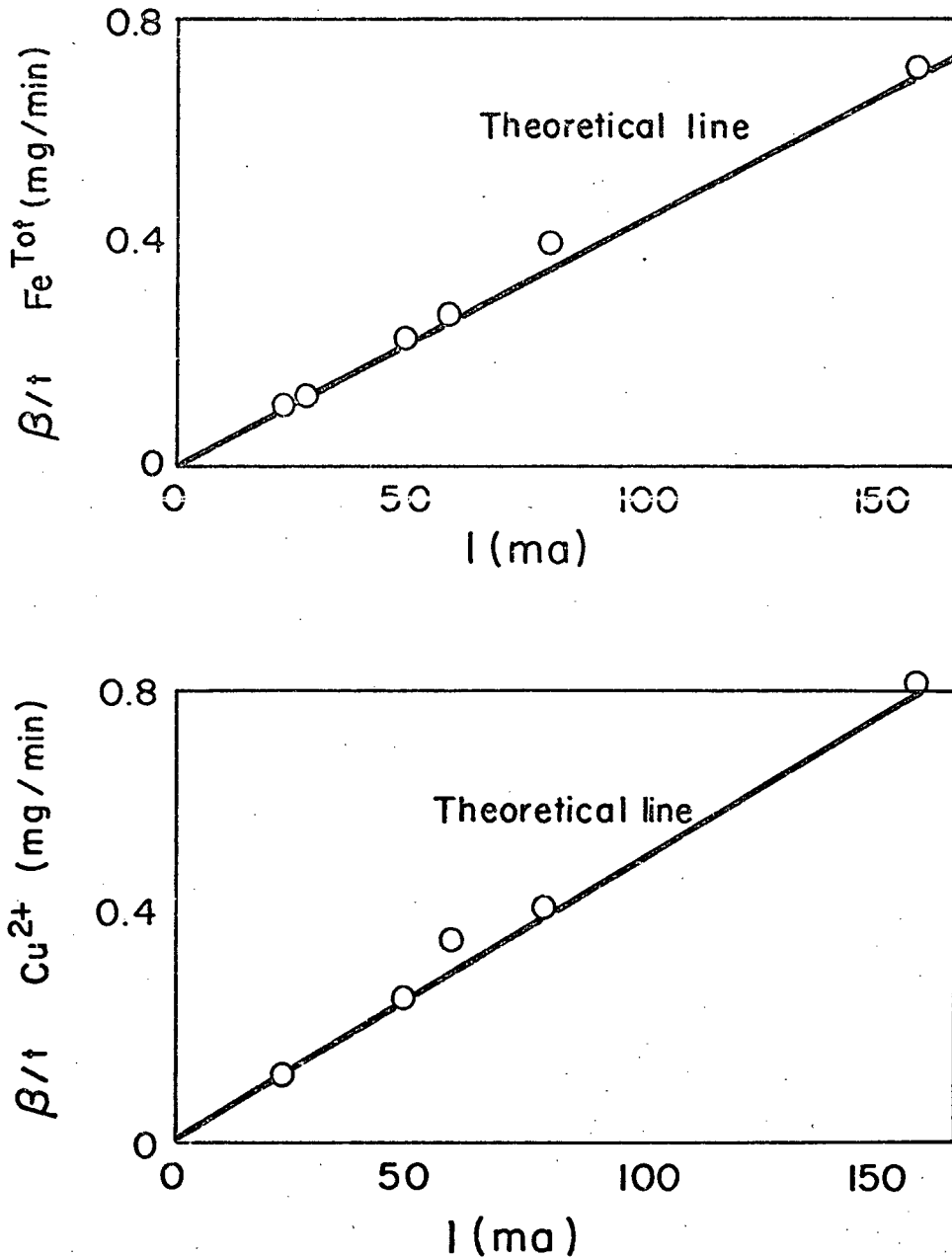


Fig. 5 Anodic dissolution of chalcopyrite. Solution analysis from Zevgolts⁽⁸⁹⁾.

The solid lines are theoretical lines generated from Faraday's Laws:

$$\beta_i = \frac{A_i}{F} I \tau$$

β_i = Electrochemical conversion at an electrode of substance i (grams)

A_i = Equivalent weight of substance i

= Molecular weight/number of electrons in reaction

= M_i/n

F = Faraday's constant (96,500 coulombs/equivalent)

I = Current (amps)

τ = Time (seconds)

$$\frac{\beta_i}{\tau} = \left(\frac{M_i}{nF} \right) I$$

If the reaction is equation (12), then $n = 4$. For Cu:

$$\frac{\beta_i}{\tau} = \left(\frac{63.54}{4 \times 96,500} \right) \times I = 1.53 \times 10^{-4} \frac{\text{grams}}{\text{sec}} / \text{amp} = 9.2 \times 10^{-3} \frac{\text{milligrams}}{\text{minute} - \text{mA}}$$

Thus the expected slope will be :

0.0092 mg/min-mA for Cu

0.0081 mg/min-mA for Fe

if $n = 4$.

In Zevgolis' figures the actual slopes are: 0.0050 (Cu)

0.0042 (Fe).

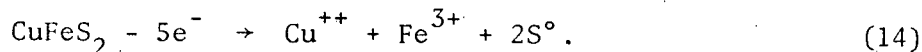
Therefore n must be approximately 8, instead of 4, and half of the electrons are unaccounted for. This may also be seen from other data in Zevgolis' work, e.g. 3 hours at 160 mAmps produced 148 mg of Cu (Figure 26 (89)). From this, $n = 7.8$.

Oki and co-workers (126,154,155) have studied the anodic reactions of CuS and CuFeS₂ at high current densities. The CuS electrode suffered a very large potential (40 volts!) increase after a certain time, which was attributed to CuSO₄ precipitation in agreement with Etienne (90). However, up to this point the reaction went smoothly, producing elemental sulphur:



as noted before. The CuFeS₂ electrode potential (in 1M H₂SO₄, 25°C) was shown to be dependent on [Fe⁺⁺], [Cu⁺⁺] and [Fe⁺⁺⁺] in dilute solutions of these ions (10⁻³ → 10⁻² M).

Anodic polarizations of CuFeS₂ were carried out at 10 → 100mA/cm², resulting mainly in the reaction



Seventy-five percent current efficiency was reported for this reaction, independent of current density. [Fe⁺⁺] was low compared to [Fe⁺⁺⁺].

IV Electrochemical Experiments in Aqueous Solutions above 100°C

In the existing literature on the electrochemical behaviour of sulphides, there is an evident distinction between those minerals which equilibrate under normal laboratory conditions and those which do not. Thus in the binary copper sulphide system investigated by Etienne (90), Cole (118), and others, useful thermodynamic data can be obtained from rest potentials in the range 25 - 85°C, while in the iron sulphide system only mixed potentials are obtained (153) and passivity is present (96). The copper-iron sulphur system, as investigated here, unfortunately falls rather within the latter class of minerals and it is partly for this reason that high temperature studies have been carried out, in hope that diffusion

processes can be speeded up and equilibrium more nearly attained.

a) State of the Art

High temperature electrochemistry is a rapidly developing sub-field with its own specialized technology. A recent conference (156) and review article (157) have summarized the state of the art. Three particular experimental difficulties arise when attempting to make electrochemical measurements at high temperature:

- 1) The pressure vessel design and the nature of the liner, to prevent contamination.
- 2) The design of the insulated electrical connections.
- 3) The reference electrode.

Pressure vessels have sometimes been used for electrochemical experiments without liners, but the applications are generally limited to non-chloride solutions, for the high nickel alloys are known to be subject to stress corrosion cracking in chloride solutions.

Liners are generally made of metallic, ceramic or plastic (fluorocarbon) materials. The precious metals have high corrosion resistance and are commonly used (161,162) but place economic limits on the size of the autoclave. Silicate materials are significantly soluble in many high temperature solutions and can give misleading results (163). Teflon and other fluorocarbons appear to give off fluorides above 200°C (158,159) but this problem can be reduced by pre-heating (160).

Electrode leads can be sealed into pressure vessel walls by several methods but mainly the choice lies between a metallized ceramic seal, such as a spark plug, and a compression seal. Compression seals, which are the most widely used and are commercially available, form a pressure-tight connection by compressing an insulating material around the electrode lead.

Teflon or soapstone are generally used for the insulating material. The Aminco seal (164), the Conax seal (165) which can carry multiple leads, the Bridgeman seal (166) and mineral insulated cable (167) have all been used. Teflon tends to extrude under high pressure and temperature (about 250°C) and specialized designs (160) or air cooling (164) may be necessary to exceed this limit.

Reference electrodes may be used internally or externally, with respect to the autoclave. The disadvantage of an internal electrode is that it must be calibrated for high temperatures; external electrodes require either a pressure-reducing device (168) to connect them to the cell or a method of containing the pressure externally (165).

Internal reference electrodes can either be primary (hydrogen electrode) or secondary. The use of a platinum/hydrogen electrode does not seem to have serious drawbacks (169,170), other than the inconvenience of maintaining a given partial pressure of hydrogen, and a slight solubility of platinum in high temperature aqueous solutions (157).

Lietzke and coworkers have carried out an extensive series of reference electrode evaluations, some of which have been summarized (171).

The following electrodes have been used :

Ag/AgCl

Ag/AgBr

Ag/AgI

Ag/Ag₂SO₄

Hg/Hg₂Cl₂

Hg/Hg₂SO₄

PbO₂/PbSO₄

The AgCl electrode has been widely used and calibrated up to 275°C (160,170); it has the disadvantage of significant solubility above 100°C. To overcome this the AgBr (172) and AgI (173) electrodes have been used. The former is reported to be less reliable than AgCl (174). Ag₂SO₄ electrodes appear to be suitable for use in sulfuric acid up to 200°C (175). Hg₂Cl₂ (calomel) and Hg₂SO₄ electrodes are reported to be unstable at high temperature (175,176).

A comprehensive review of this subject has been published by Ives and Janz (177), and also by Jones and Masterson (157).

b) Application to Sulphide Minerals

Electrochemical studies on sulphide minerals appear to have been limited to solutions below the boiling point. The particular problem that arises when studying sulphides is that of the connecting leads to the mineral. Due to the semiconducting properties, care must be exercised to avoid a rectifying junction; this can be done by having a low current density at the connection interface, or by using two leads, one for current and one for potential. Primarily, previous workers have used the first alternative (90,153) and this may be accomplished by a mercury contact, silver solder, graphite-impregnated glue or other means. Mercury contacts were found to be unsuitable, for the mercury penetrates the pores of the mineral at high temperatures, whereas silver solder is liable to contaminate the electrode with Ag⁺ ions. Epoxy cement remained insufficiently conductive despite liberal doses of graphite. The problem was solved using pressed Pt wires in holes drilled carefully to a press-fit size.

B. EXPERIMENTAL

Four types of experiments were carried out on chalcopyrite:

- 1) Leaching experiments - on powder and massive specimens
- 2) Anodic Polarizations - current/voltage scans
- 3) Constant Potential experiments
- 4) Mixed Potential experiments.

The leaching experiments were carried out in ferric sulphate and ferric chloride solutions, primarily at 90°C, to determine reaction rates, stoichiometry and possible mechanisms. Mainly high grade chalcopyrite was used, but some experiments were done with a variety of commercial copper concentrates, from various mines.

The anodic polarizations were done in order to determine the shape of the current/voltage curve for chalcopyrite and its dependence on the major variables such as scanning speed, temperature and solution.

The constant potential experiments were of two kinds: One in which the current/time relationship for chalcopyrite at a given potential was determined, and the second, more involved, in which the chemistry of dissolution of chalcopyrite was determined.

Mixed potential experiments simply consisted of measuring the electrode potential of chalcopyrite while under leaching conditions. These experiments provide the link between the leaching and electrochemical experiments.

I Apparatus

Leaching experiments on powder were carried out in an apparatus as shown in Figure 6, using either mechanical or magnetic stirring.

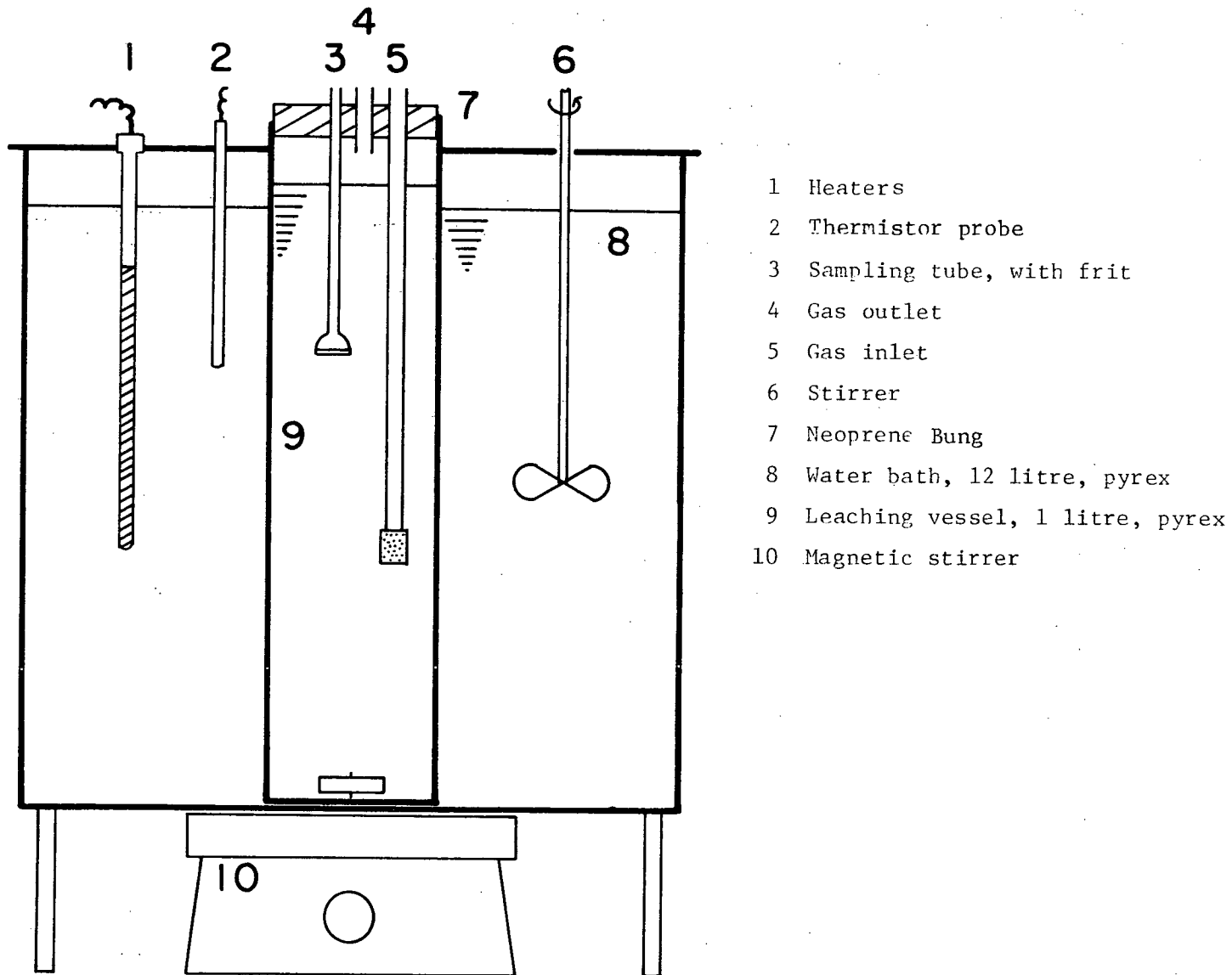


Fig. 6 Apparatus for leaching powdered chalcopyrite.

Leaching with mechanical stirring was performed with a similar apparatus except that the sample tube was removed and a mechanical stirrer (glass rod) installed above the leaching vessel.

Leaching experiments on massive chalcopyrite were performed in apparatus as shown in Figure 7.

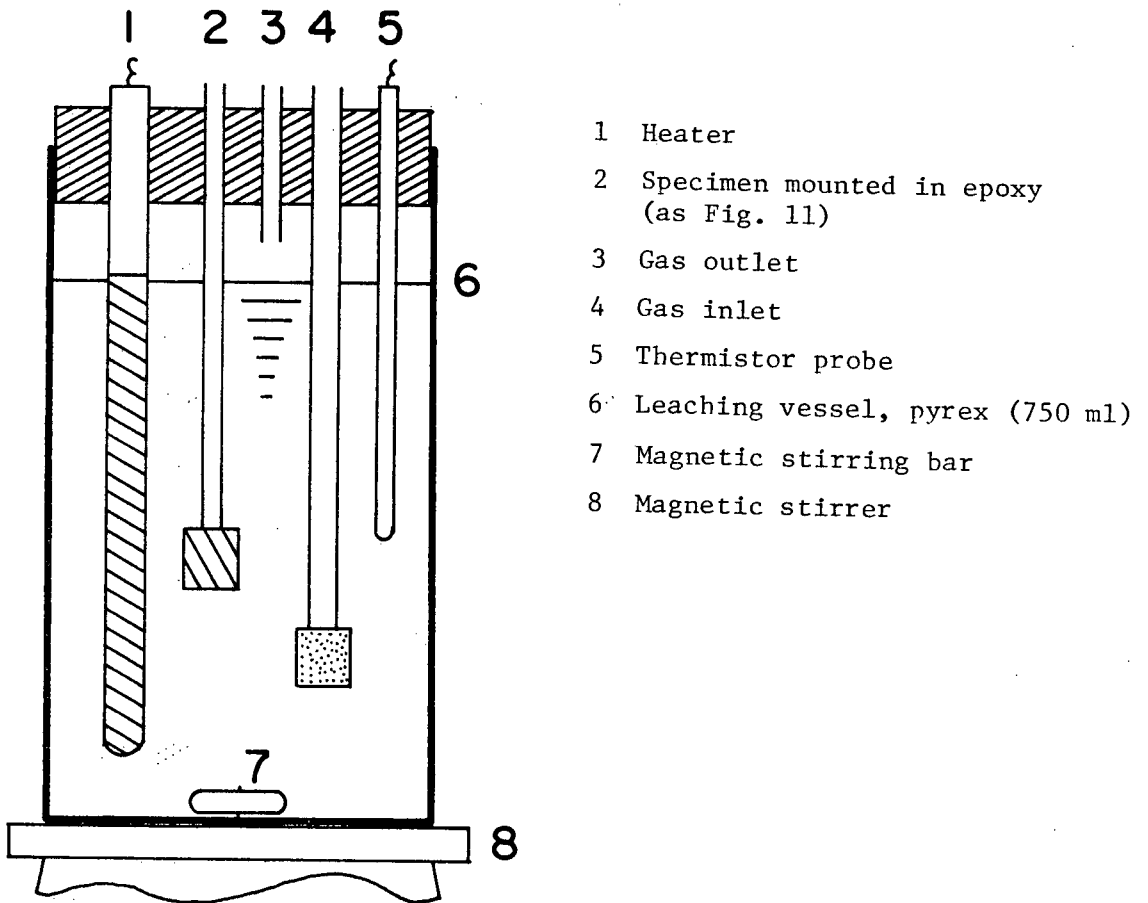


Fig. 7 Apparatus for leaching massive specimens.

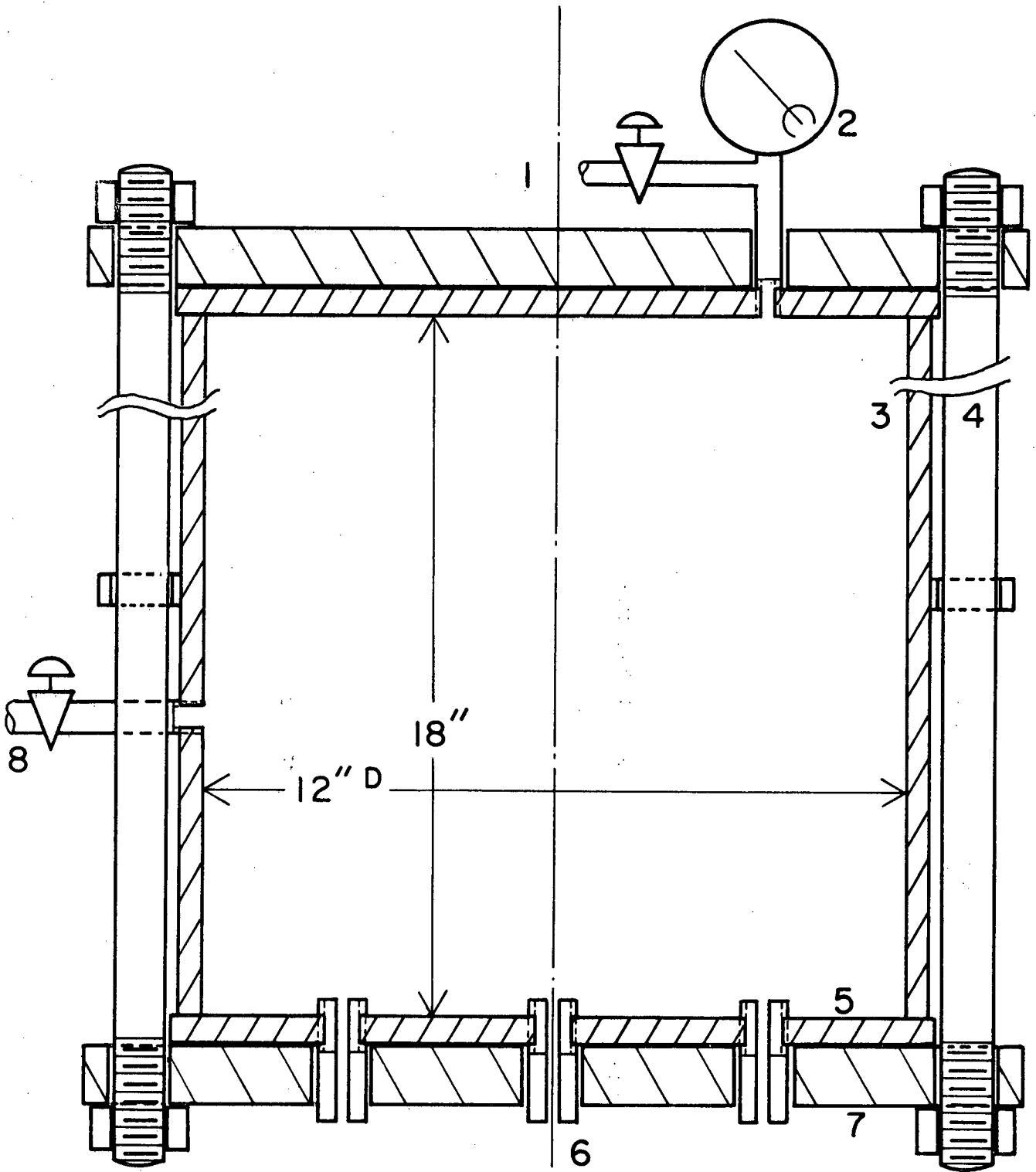
All electrochemical experiments were done in large H-cells, constructed of two 1-litre Berzelius beakers joined by a short tube containing a fitted disk, 30 mm O.D. Magnetic stirring was used for both compartments, but temperature and atmospheric control was maintained only in the anode cell. Two such cells were used, one exclusively for low temperature (<100°C) experiments and one for all temperatures -6°C → 190°C. In the low temperature cell neoprene bungs served as cell lids; in the high temperature cell silicone rubber was used in the (unheated) cathode cell, whereas a solid Teflon bung was used in the anode compartment. A thin (3/8") plate of silicone rubber on top of the Teflon served to hold the various electrodes, etc.

For experiments at atmospheric pressures only one heater was employed, and a gas bubbler installed (not shown). For high temperature experiments, (inside a pressure vessel) two heaters were used and the inert atmosphere supplied by the pressure vessel atmosphere.

Mixed potential experiments (measurement of electrode potential under leaching conditions) were carried out in the large H-cell (Figure 10).

a) Pressure Vessel Design

A large pressure vessel (Figures 8, 9) was designed and built to do the electrochemical experiments at high temperatures, using the duplex system, i.e. with an internal pyrex cell (shown in Figure 10). A cylindrical shape was used with the inside dimensions, 12" (diameter) x 18" (high). The walls were constructed of a single welded shell of type 304 stainless steel, (3/8" thick x 12" I.D. x 18"). The base-plate and top-plate were similarly constructed of 304 stainless steel (1/2" thick x 14" ϕ). Steel backing plates (1" thick) were added for extra rigidity. The



- 1 Gas inlet
- 2 Pressure Gauge
- 3 Cylindrical shell
- 4 Bolts (8) 7/8" O.D.

- 5 Base (and top) plate
- 6 Conax pressure seals (3)
- 7 Backing plates
- 8 Gas outlet

Fig. 8 Pressure vessel

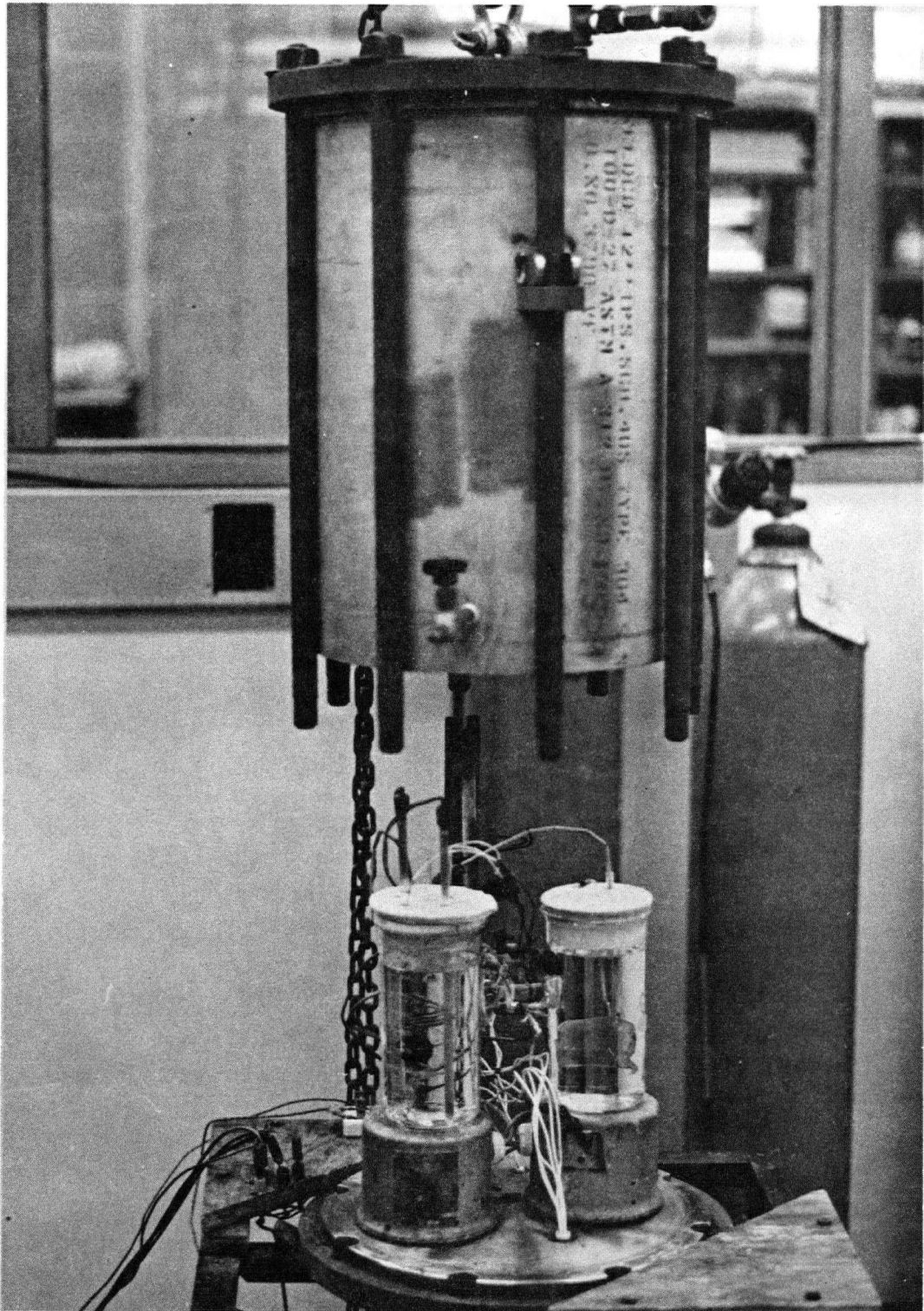


Fig. 9 Pressure vessel

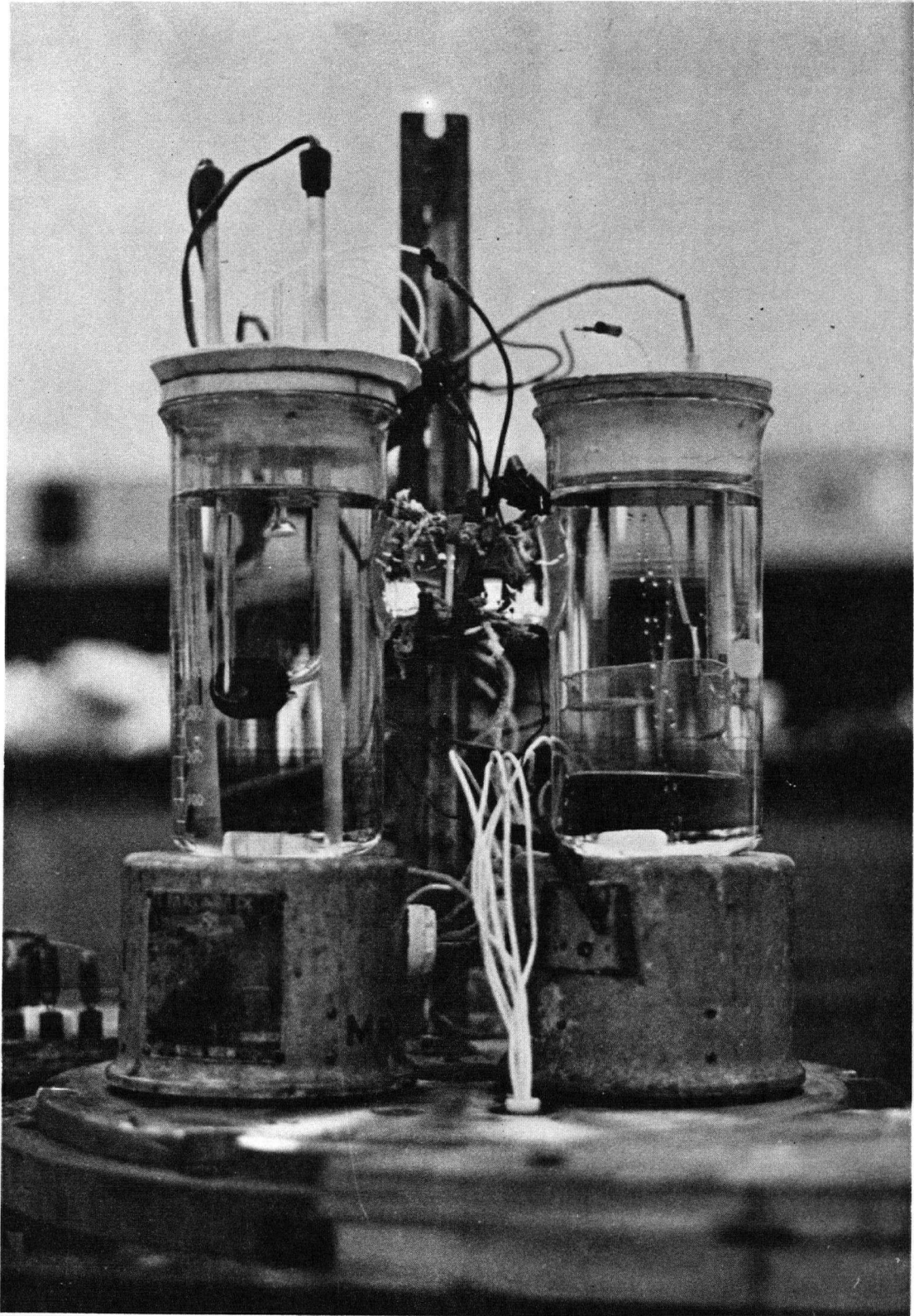


Fig. 10 Electrochemical cell

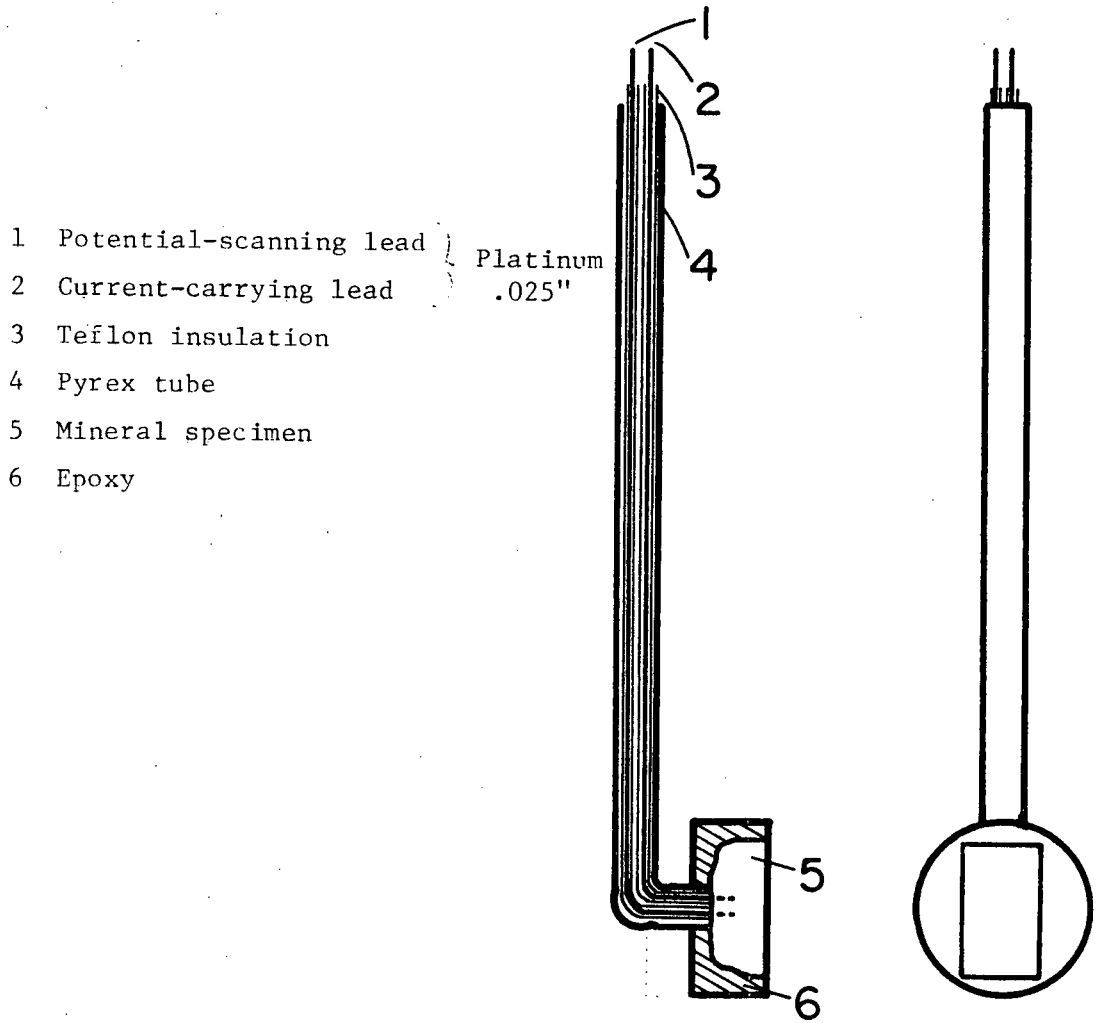


Fig. 11 Electrode mounting

whole pressure vessel was bolted together by long bolts (7/8" ϕ) passing through both backing plates. The pressure seal was maintained by rubber O-rings set in grooves at the top and bottom of the shell.

The pressure vessel was designed to be used up to 250 psi, with a safety factor of five. The main limitation to the pressure is the bending of the end-plates, causing leakage around the O-rings. So far this was never encountered.

The pressure vessel was bolted together in such a way that, when the bottom nuts were unscrewed, the top-plates could be lifted clear of the base, together with the bolts and shell, leaving the bottom plates free and clear.

This facilitated adjustments to the cell and electrical connections.

The H-cell sat on the magnetic stirrers on the base plate and was held in place by a clamp and a small structural piece lightly screwed into the base.

All electrical connections were made through three Conax seals which were screwed into the base plate, (holes were cut into the backing plate). This enabled the top assembly to be lifted clear, with no electrical leads attached. One Conax seal (PL-16-6) carried the power leads (two heaters and two stirrers), another (PL-16-2) carried the two potential sensing leads to the potentiostat (working and reference electrodes). The last (P1-16-6) carried two current-carrying leads to the potentiostat (working and auxiliary electrodes) two thermocouple leads, and two thermistor leads.

All these leads were 16 gauge copper wires encased in Teflon for insulation and pressure sealing, (as supplied by the manufacturer), with the exception of the thermocouple leads which were chromel and alumel. These were encased in "Heat-Shrink" (teflon) and substituted for the

copper leads in the Conax seal, which was modified slightly to accept the slightly larger diameter of these wires.

Purified nitrogen (Canadian Liquid Air L-grade, 20 ppm O₂) was admitted through a one-way valve in the top plate and released through a one-way valve in the shell. A pressure gauge was attached to the inlet pipe. An inert atmosphere was achieved by flushing the autoclave at least six times with L-grade N₂, i.e. pressurizing to 50 psig and releasing. This expensive method was adopted after abandoning attempts to evacuate the autoclave with an oil-pump, which frequently and unpredictably resulted in flushing of the cell solution. The work described in preliminary experiments was, however, carried out in this way.

b) Electrode Design (For Sulphide Minerals)

Small pieces of chalcopyrite, cut to approximately 1/2 x 1 x 1 cm., were used as specimens. Two holes, each 0.025" in diameter and 3/32" deep were drilled into the back and 0.025" Pt wires (10" long) pressed into them. Teflon spaghetti tubing was slid over each wire and the specimen placed face down in a 1" ϕ silicone rubber mold. An epoxy cement, consisting of 100:20 Epon 828: Shell Curing Agent Z, was poured in to a depth of at least 1/2" and cured at 80°C for at least four hours. A fresh surface of chalcopyrite was obtained by cutting a thin slice off the front of the specimen with a thin blade (0.020") diamond saw. To prevent excess wear on the diamond saw blade, unnecessary epoxy on the sides of the specimen was removed with the belt sander.

In earlier work a fresh surface was obtained by grinding off the epoxy with a polishing wheel, but polishing appeared to affect the properties of the specimen.

Other electrode designs were tried. A two-part Teflon assembly that

screwed together was desirable because it would allow ready examination of the specimen, but at 200°C no design could be found which would reliably prevent leakage of the solution into the interior of the holder. Silicone cement was tried, but it dissolved at 200°C in dilute HCl. 'Sauereisen' cement lost its adhesive properties under these conditions. Mercury contacts were tried, but the mercury rapidly leaked through the fissures in the specimen.

The epoxy used was capable of withstanding 1M HCl at 200°C for several hours; a normal epoxy using DETA as curing agent did not stand up. No chemical dissolution or wear of the epoxy electrodes as used was observed.

c) Reference Electrode

The Ag/AgCl electrode was used as a reference electrode; it has the advantages of ease of construction, wide range of temperature application and well established properties. The major disadvantages were that in strong chloride solutions it dissolved at high temperatures, and in cathodic experiments it acted as an oxidizing agent. For the latter application, the AgI electrode was calibrated but more complete work was later discovered in the literature (173).

The work of Greeley (178) carefully documents the properties of the AgCl electrode, and his methods of preparation were followed. A mixture of silver oxide, (Ag₂O) with silver chlorate (AgClO₃) (20%) was made into a paste with water, and a platinum spiral (0.015" thick, and approximately 1/8" φ) coated with it. This was fired at 650°C for five minutes. The procedure was repeated twice more. Several such electrodes gave identical potentials, within the precision required in this work (± 0.5 mV), and the predicted potential versus a freshly prepared calomel electrode.

II Chemicals

Double-distilled water was used in all cases. All chemicals (reagent grade) were used as received from the manufacturer with the exception of barium chloranilate, (used in the sulphate analysis) which was freshly prepared, as described by Agterdenbos and Martinius (181).

III Instrumentation

Two potentiostats were used: Wenking 68TS10 and Wenking 70HV1/90. For scanning experiments, a Wenking SMP 66 scanning motor potentiometer was used. Working electrode potentials were measured with a Wenking Potentiometer PPT 69. Total coulombs passed in an experiment were monitored by a Varitech Coulometer; Sargent SR recorders were used to record potential or current as a function of time.

Heating of the electrochemical cell was achieved by internal 'Glo-quartz' heaters (410 watt), and controlled by thermistors set in a pyrex well connected to a Yellow Springs Temperature Controller. The temperature of the cell was independently monitored by a Chromel-Alumel thermocouple set in another pyrex well. The thermistor leads (thermistor itself + guard wire) were cut in order to pass through the Conax seal, and joined up on the other side. This did not appear to have a detrimental effect.

IV Analysis

Copper in solution was originally measured by the Cuproin method (179) (Section I) but this was soon abandoned in favour of atomic absorption. However the Cuproin method was used for simultaneous $[\text{Cu}^+]$ and $[\text{Cu}^{++}]$

determination. The O-Phenanthroline method (179) was used to determine $[\text{Fe}^{++}]$ and $[\text{Fe}^{+++}]$, (with or without hydroxylamine hydrochloride). Sulphate concentrations were measured by the Barium Chloranilate method, using the UV band at 332 m μ (180) and modifications suggested in reference (181); Dowex 50-W resin, in a vertical column, was used to remove cations.

Spectrophotometric measurements were made on a Beckman DV instrument, equipped with a photomultiplier and voltage stabilizer.

Atomic absorption measurements were made on a Unicam SP90 instrument. Corrections were made for iron, chloride and sulphate contained in the solution. The quantity of ferrous ions produced during ferric sulphate/chloride leaching was measured by the ceric sulphate titration method (182) using Ferroin (1,10 O-phenanthroline ferrous sulphate) as indicator.

V Source of Chalcopyrite used

All electrochemical experiments and most of the leaching experiments were done using specimens of chalcopyrite cut from the same rock, a high grade lump about 4" in diameter obtained from the Craigmont Mine, through the courtesy of G. Bacon. The purity of this specimen was exceptionally good: X-ray, microprobe, chemical and microscopic analysis revealed no sulphides other than chalcopyrite which had the stoichiometric composition (34.9% S, 34.6% Cu, 30.5% Fe). Occasionally small quantities of three other minerals were evident, which were identified by x-ray and microscopic analysis as calcium carbonate, hematite and an insoluble Ca, Mg, Fe silicate probably actinolite. These impurities occurred in well defined veins, generally together, which could be easily avoided in most cases when cutting a specimen. However, small quantities of hematite did occasionally find their way into a specimen and thereby cause high iron extractions.

Powder samples for leaching were either crushed (in a mortar) from above specimens, or commercial concentrates, used as received or, as noted, further crushed. A few experiments were done on single crystals from Baxter Springs, Kansas obtained through Ward's Museum.

C. RESULTS

I Preliminary Experiments

Two types of anodic experiments were carried out, potentiostatic scans and constant potential experiments; in the former the relative rates of dissolution at each potential were measured, and in the latter the chemistry of dissolution at each potential was determined.

All potentials quoted in this work are on the standard hydrogen electrode (S.H.E.) scale.

a) The Meaning of Current Efficiency

Current efficiency as used in relatively simple electrochemical processes, such as metal refining, is usually defined as the percentage of the total current which is used in the dissolution (or plating out) of the metal concerned. In a complex process such as the dissolution of chalcopyrite, where each of three elements has more than one possible valence state in solution, and not all of the elements go into solution, the meaning of the term is not obvious. There is considerable confusion on this simple point in the literature; usually authors first postulate a particular reaction and then state the current efficiency for each element, as if that reaction were the only one involved in the anodic process. Here the current efficiency for each element is defined as the

$$\begin{aligned} \text{C.E. (i)} &= 100 \times \frac{\text{Total equivalents (i) dissolved}}{\text{Total faradays passed}} \\ &= 100 \times \frac{\text{Moles (i)}}{\text{Coulombs/F}} \times n \end{aligned}$$

where n = valence state of (i) in solution.

The procedure then is to calculate the current efficiency of each element, and then postulate a reaction.

The current efficiency of sulphate was not always determined experimentally, (as in sulphate solutions); however, as a first approximation the quantity $(100 - \text{C.E.}_{\text{Cu} + \text{Fe}})$ can be used as a measure of $\text{C.E.}_{\text{SO}_4}$.

b) Potentiostatic Scans

Anodic behaviour was studied in 0.1M HClO_4 and 0.1M H_2SO_4 , at temperatures from 7°C to 175°C. At low temperatures (up to 85°C) polarization curves in the two acids are very similar, but at higher temperatures the reactivity of chalcopyrite suddenly drops in H_2SO_4 , whereas in HClO_4 it continues to increase steadily with temperature (Figures 12, 13). At 95°C and above, in H_2SO_4 , the current density at low potentials continues to increase with temperature, but at higher potentials (above 1 volt) it 'passivates' - that is the current fails to increase in the usual way.

It is evident that there are two regions on the polarization curves, the first being quite flat and the second, starting around 800 mV, exhibiting a sharp increase of current with potential. The boundary between the two regions is not always clear from a graph, but experimentally, it can be seen because the current in the first region falls back between each increment of potential but not in the second region.

This can be also seen from Figure 14, where the scanning rate affects the current in the first region, but not in the second; these regions may be characterized as time-dependent and time-independent respectively.

A specimen whose potential was raised well into the second region exhibited a linear dependence of current on voltage (Figure 15); thus the current appeared to be controlled by an ohmic resistance.

Some specimens were prepared with the potential-scanning lead pressed

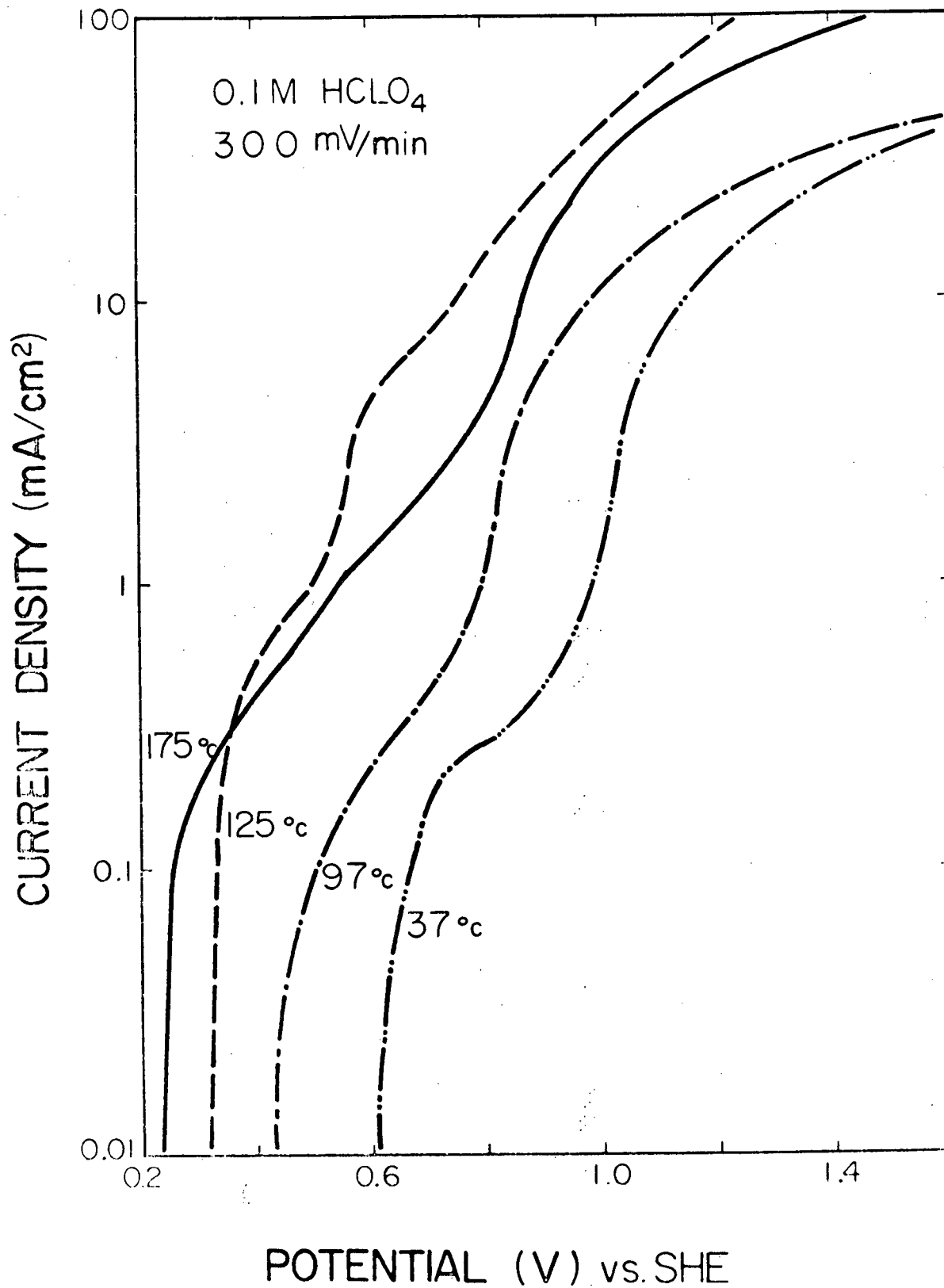


Fig. 12 Potentiostatic scans in perchloric acid at various temperatures.

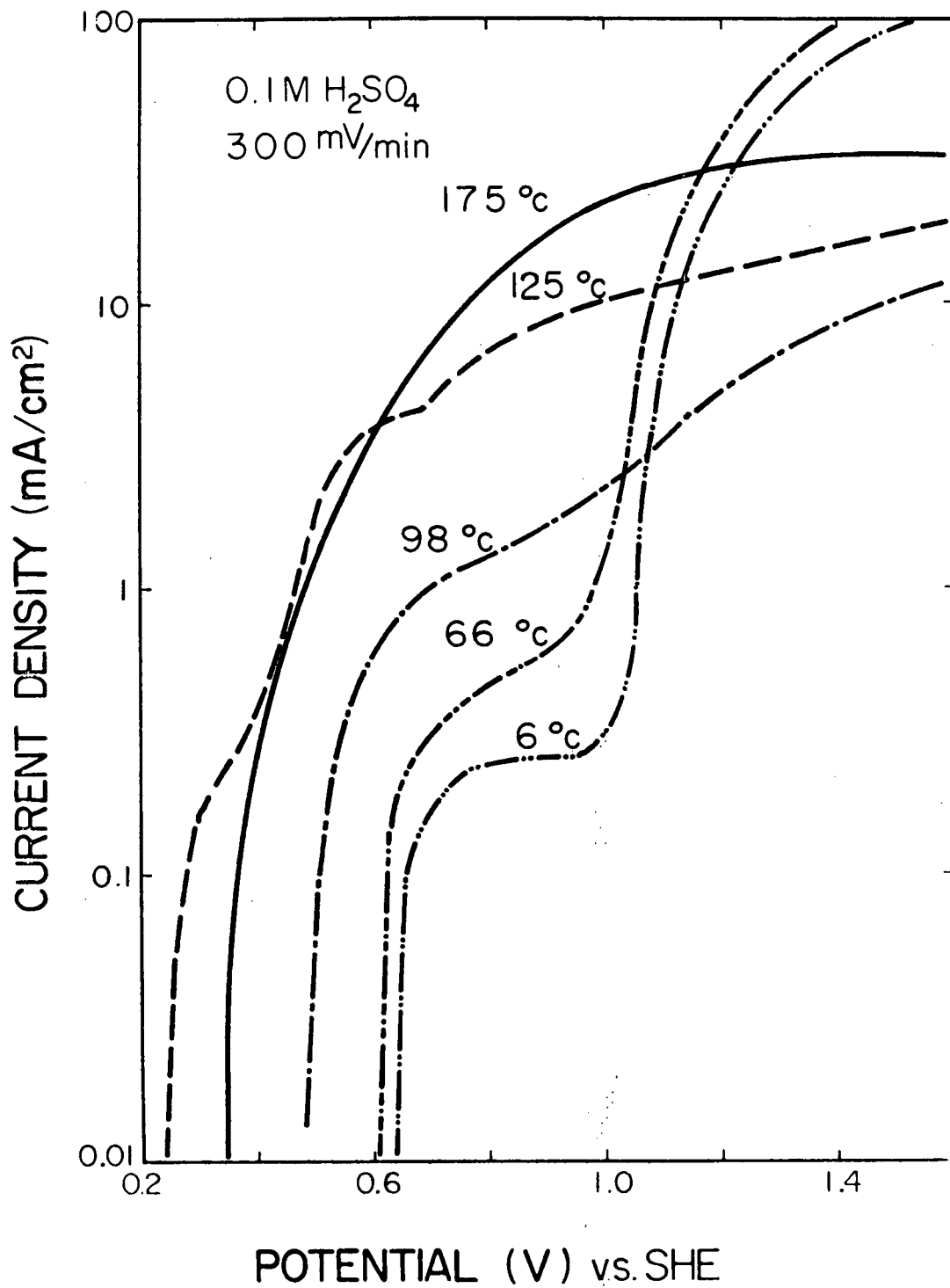


Fig. 13 Potentiostatic scans in sulphuric acid at various temperatures.

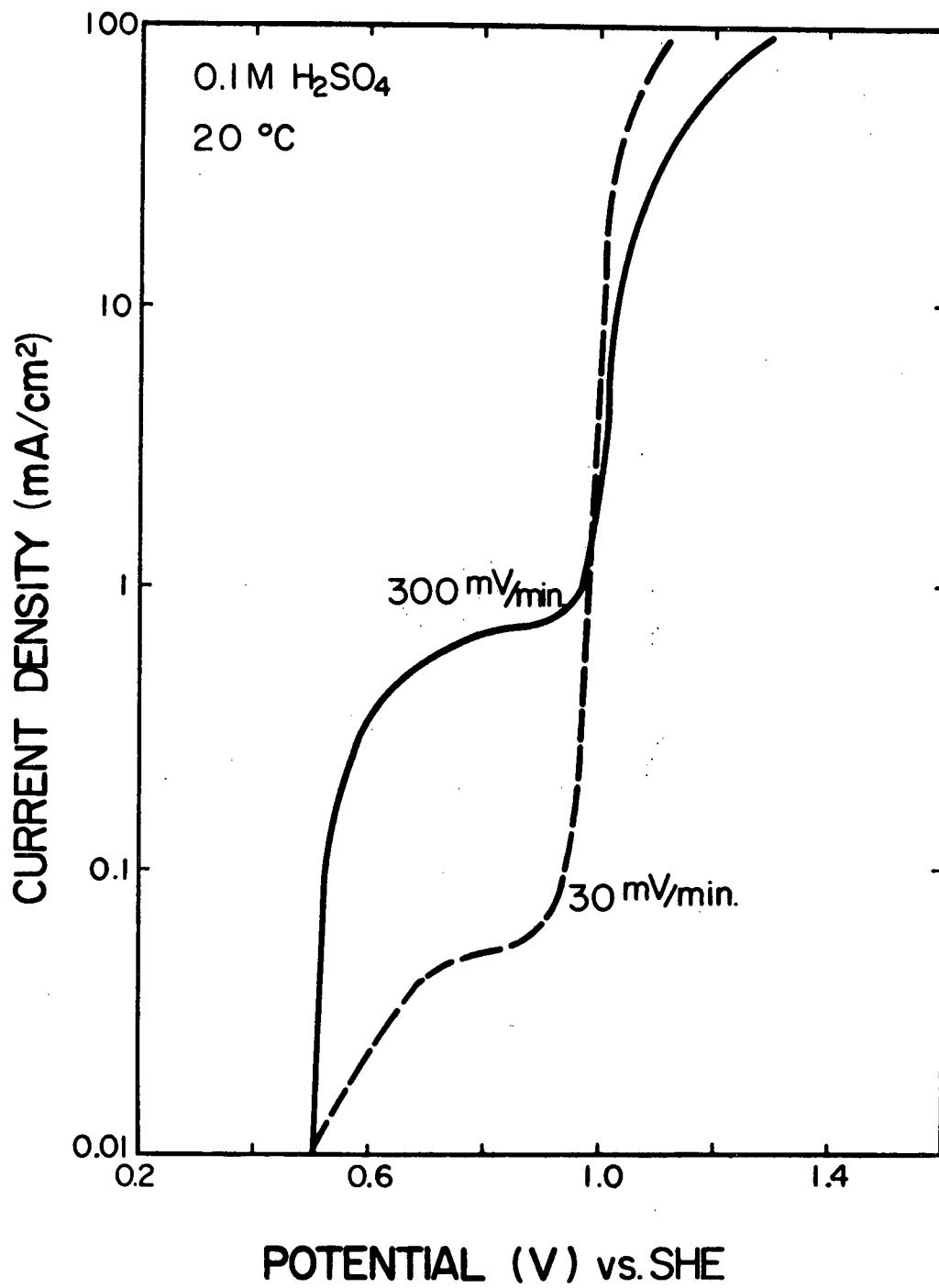


Fig. 14 Effect of scanning rate on potentiostatic scan.

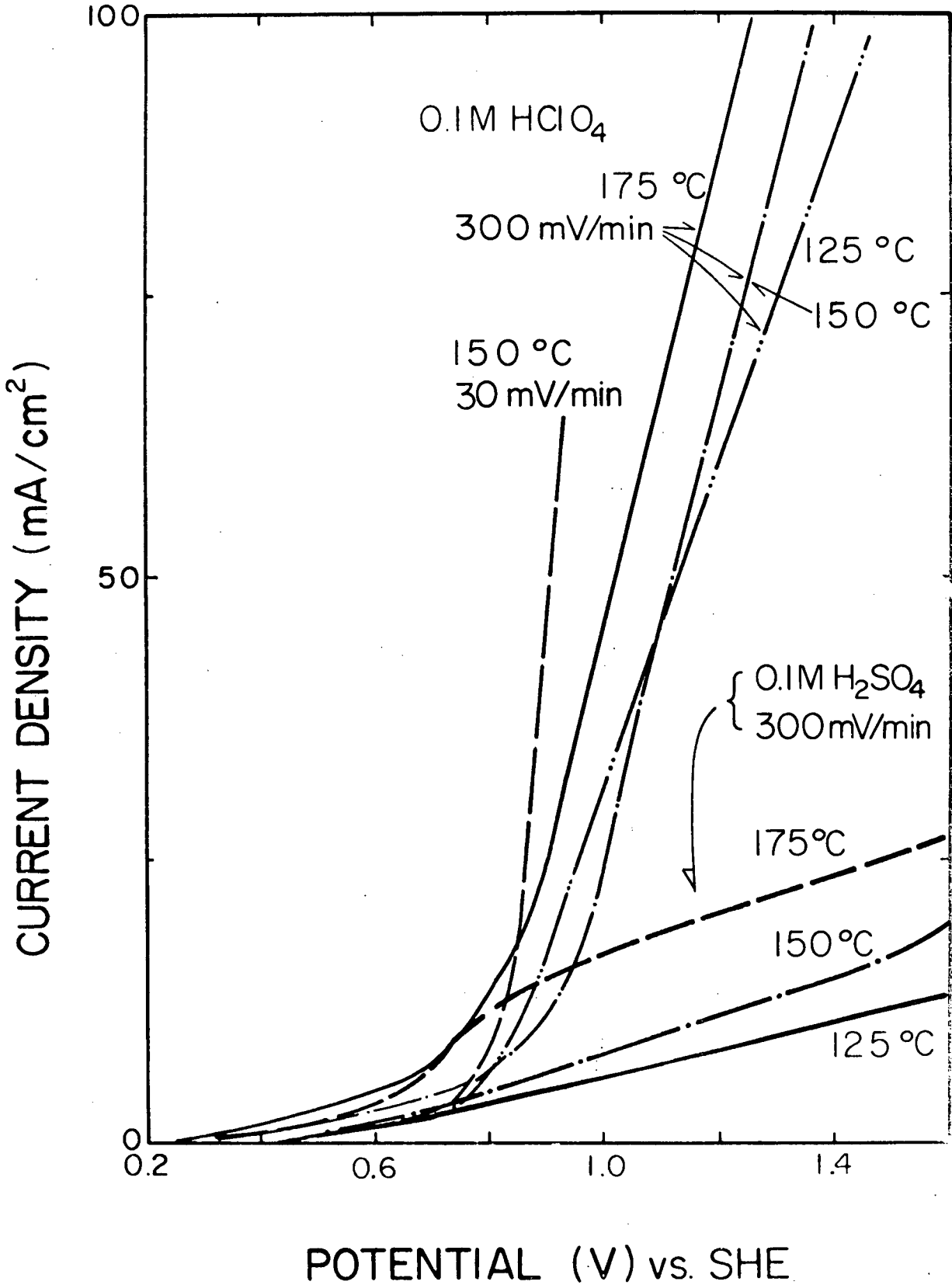


Fig. 15 The linear current/potential relationship in potentiostatic scans.

in very close to the surface, whilst the current-carrying lead was put in at the back as before. However, no difference was observed in the polarization behaviour of a given specimen, using this side lead, and in fact reversing the leads made no difference either. Evidently the ohmic drop through the bulk of the specimen was not important.

The exposure of a specimen to hot sulphuric acid for prolonged periods appeared to adversely affect the reactivity; the conditions required varied, but generally a few hours at 150°C lowered the reactivity. The loss in reactivity was also accompanied by a reduction in conductivity, which sometimes dropped to 10^{-3} Ω - cm. or less. Perchloric acid never had this effect, and it seems more than coincidental that hot sulphuric acid has a depressant effect on the current achieved at high potentials.

c) Constant Potential Experiments

After performing the polarizations shown in Figure 16, the specimen was held at constant potential, as indicated by the circles on the curve, to determine the time dependence and stoichiometry of the dissolution. The time dependence is seen most clearly in comparing current-decay curves (for constant potential). In Figure 17 there is a drop of 35% in current at 710 mV (in the flat region) but at 785 mV at the beginning of the high current region, the current stays nearly constant, after an initial rise. The effect of stirring was studied in 0.1 M HClO₄ at 20°C and was observed to have no appreciable effect even on the high-current region, where the current appears to be limited by some ohmic drop (see above). Similarly the acidity was varied up to 1M HClO₄ without effect.

After these constant potential experiments (in 0.1 M HClO₄), solution analysis was carried out; this data are listed in Table Iya, along with some

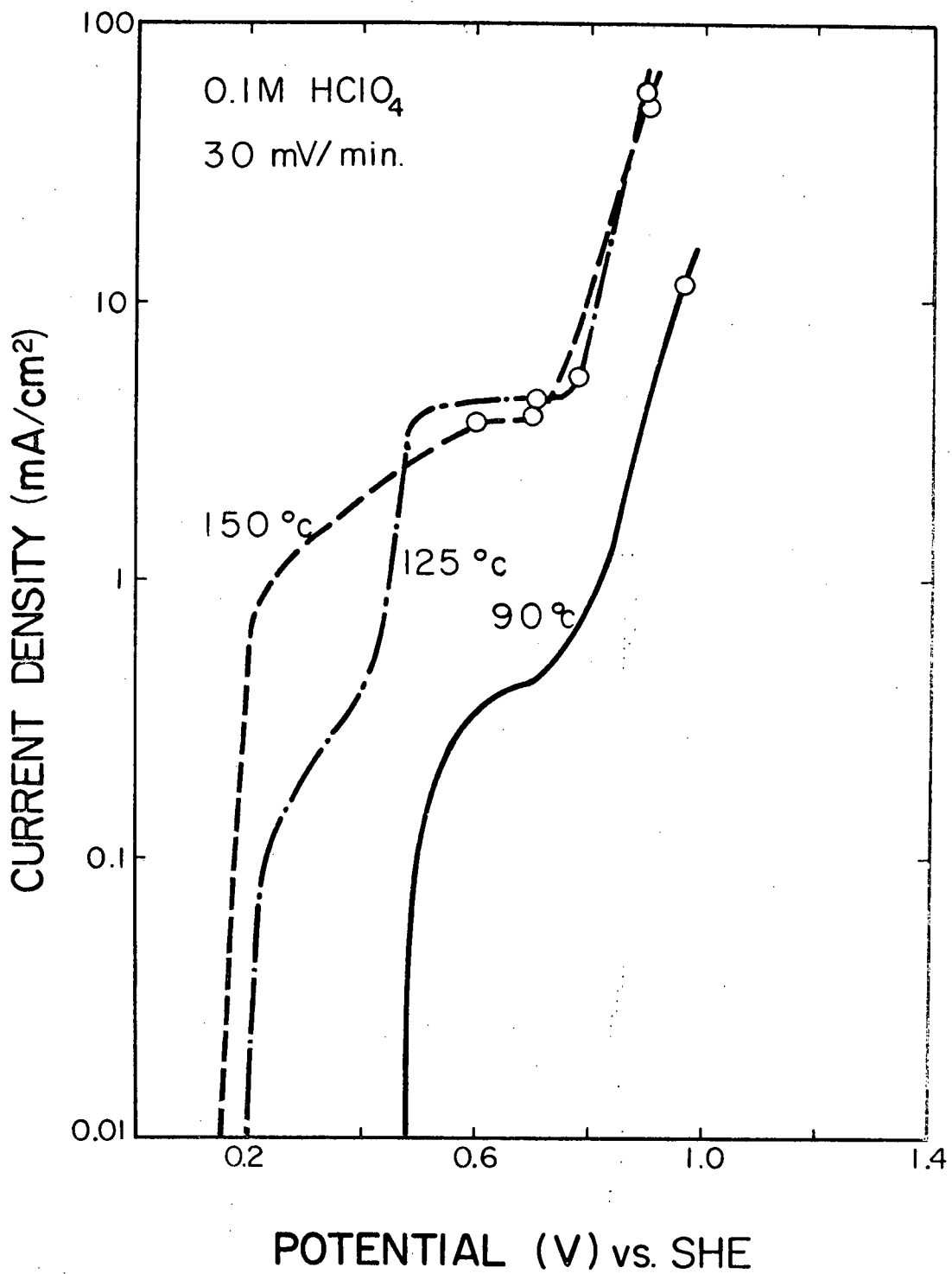


Fig. 16 Potentiostatic scans in perchloric acid, showing potentials of constant potential experiments.

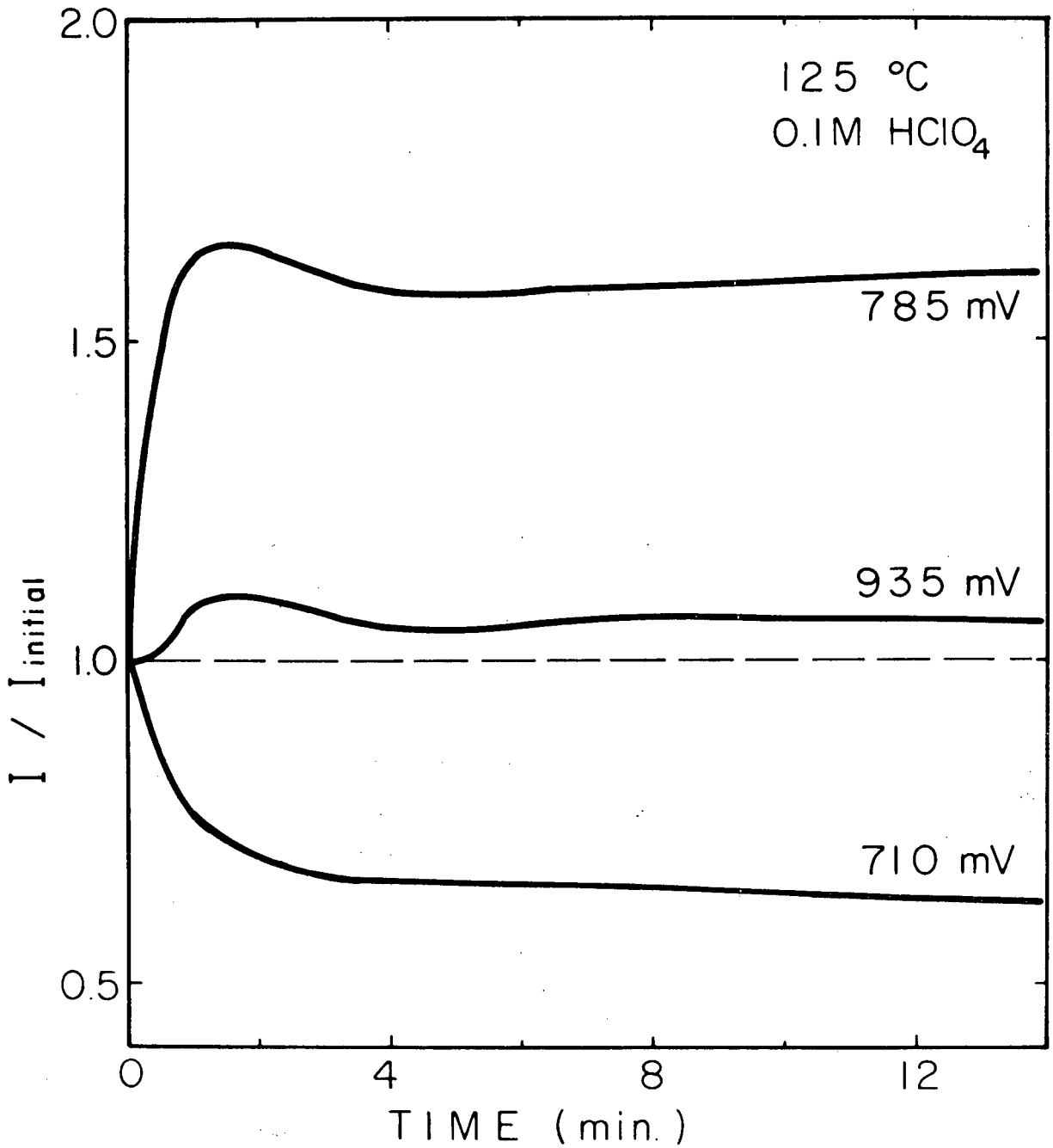


Fig. 17 Current decay during constant potential experiments at 125°C.

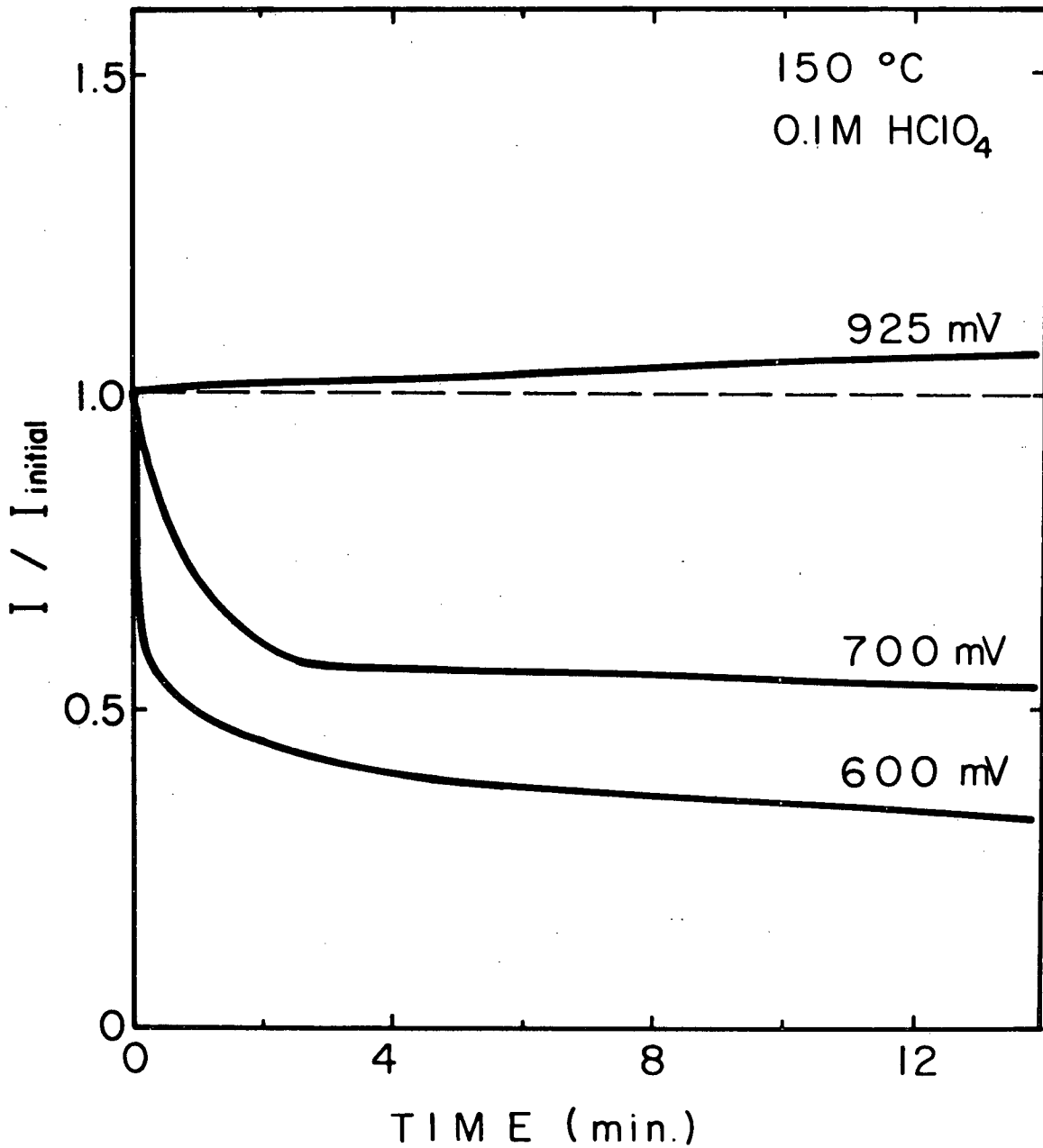


Fig. 18 Current decay during constant potential experiments at 150°C.

TABLE IVA

ANALYSIS OF SOLUTIONS AFTER CONSTANT POTENTIAL EXPERIMENTS
ON CuFeS_2 IN 0.1M HClO_4

Coulombs Passed/ (cm^2)	Temp ($^{\circ}\text{C}$)	Potential (mV)	Time (hrs)	Current Efficiency (%)				% S as SO_4
				Cu	Fe	SO_4	Total	
234	85	970	16	30.0	30.0	44.8	105	25
215	125	710	42	23.0	35	52.1	110	30
125	125	785	6	32.2	40.8	47.4	120	22
300	125	935	2	34.3	34.0	49.8	118	24
145	150	700	16	17.4	38.9	67.8	123	40
295	150	935	3	34.6	36	46.1	116	22
93	175	615	7	29	77.6	189	295	59
115	175	690	6	338	62.8	232	328	80
125	175	765	16	32	46.6	202	280	86
680	175	1500	24	30.5	33.8	-	-	-

TABLE IVB

ANALYSIS OF SOLUTIONS AFTER CONSTANT POTENTIAL
EXPERIMENTS ON CuFeS_2 IN $0.1\text{M H}_2\text{SO}_4$

Coulombs Passed/cm ²	Temp (°C)	Potential (mV)	Time (hrs)	Current Efficiency	
				Cu	Fe
440	85	1100	47	28.3	28.8
335	7	1500	6	29.4	-
1240	37	1500	10	30.0	-
240	67	1500	5	7.7*	-
455	97	1500	25	32.0	-
320	125	1500	18	33.8	-
180	175	1500	3	32.2	-

* There was a significant amount of pyrite in the specimen.

TABLE V

ANALYSIS OF SOLUTIONS AFTER HEATING EXPERIMENTS
ON CuFeS_2 IN 0.1M HClO_4

Temp (°C)	Hours	Area of Specimen (cm ²)	Moles Dissolved x 10 ⁻⁴		
			Cu ⁺⁺	Fe ⁺⁺	SO ₄ ⁼
125	12	1.0	Undetectable	0.56	0.08
150	12	1.95	"	2.9	2.9
175	6	2.7	"	3.8	3.8

other experiments at 85°C and 175°C.

The current efficiency for copper was fairly constant, for potentials in the second region, at about 32%. At lower potentials (125°C, 710 mV and 150°C, 700 mV), lower values were found.

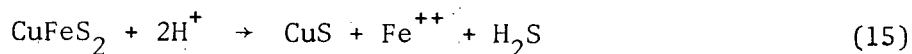
Iron current efficiencies were also fairly constant at about 35%, up to 150°C; but at 175°C very high values were recorded except at high potentials.

The current efficiency for sulphate was approximately 47% up to 150°C, except for the two experiments in the low potential region where higher values were observed. At 175°C, unreasonably high values indicated that some chemical oxidation of sulphur was taking place, possibly by perchlorate.

The total current efficiencies are seen to be in the 110-120% range, except for 175°C experiments.

Similar experiments were also carried out in 0.1 M H₂SO₄ (Table IVb). At high potentials (1.5 v), the copper current efficiency seems quite constant, over a large temperature range, at about 31% ± 3%. The presence of pyrite in the specimen severely lowered the copper current efficiency.

The anomalously large quantities of iron and sulphate produced at 175°C, can be attributed to a direct dissolution of chalcopyrite in acid:



To test this hypothesis, blank runs were carried out on fresh specimens at 125°C, 150°C and 175°C in 0.1 M HClO₄ (Table V), and it was found that while copper did not dissolve at all, iron and sulphur did, and in some manner the sulphur was completely oxidized to sulphate at 150°C and 175°C. The oxidizing agent for this reaction is unknown, but the familiar inertness of perchloric acid is known to disappear at high temperature. There

is also the possibility that not all the oxygen was removed from the pressure vessel by the evacuation procedure.

d) Surface of Chalcopyrite After Anodizing

Various solid products were observed on the surface of the mineral, depending on conditions. At low temperatures, it was possible to produce a 'clean' chalcopyrite surface with only a loosely adherent sulphur film.

Increasing the temperature caused the deposition of hematite, Fe_2O_3 , and depending on the potential it may occur in pits and cracks (low potential) or it may cover the surface (high potential). Removal of the Fe_2O_3 with a brief oxalate leach (190) revealed the deeply pitted chalcopyrite matrix, (Figure 19). This hematite may be a secondary oxidation product, due to the action of perchlorate.

At low potentials, i.e. in the first region of the polarization curve another solid phase, covellite, CuS , appeared, corresponding to the preferential dissolution of iron. At low temperatures (125°C) the covellite appeared as a finely crystalline material, but at high temperatures (175°C), large well-defined crystals were visible, Figures 21-23, and in the cracks of the specimens especially large plates of CuS were formed.

e) Summary

In 0.1 M HClO_4 and $0.1 \text{ M H}_2\text{SO}_4$ the anodic polarization curve of CuFeS_2 is composed of two regions, the first (up to $\sim 800 \text{ mV}$) being time-dependent and the second time-independent. Furthermore the second region is characterized by a linear dependence of current upon potential. The anodic behaviour in the two acids is similar up to 85°C , but beyond

that sulfuric acid has a passivating effect in the second region, whereas perchloric acid does not.

Up to 150°C, the current efficiencies for copper and iron are about 30-35% in both acids independent of potential, except that in the lower potential region (<700 mV), copper current efficiency is lower. About 25-30% of the sulphur is oxidized to sulphate, independent of potential, and temperature (up to 150°C).

At 175°C, chemical dissolution of iron becomes important, with excessively high current efficiency for iron at low potentials. Copper current efficiency remains constant, however.

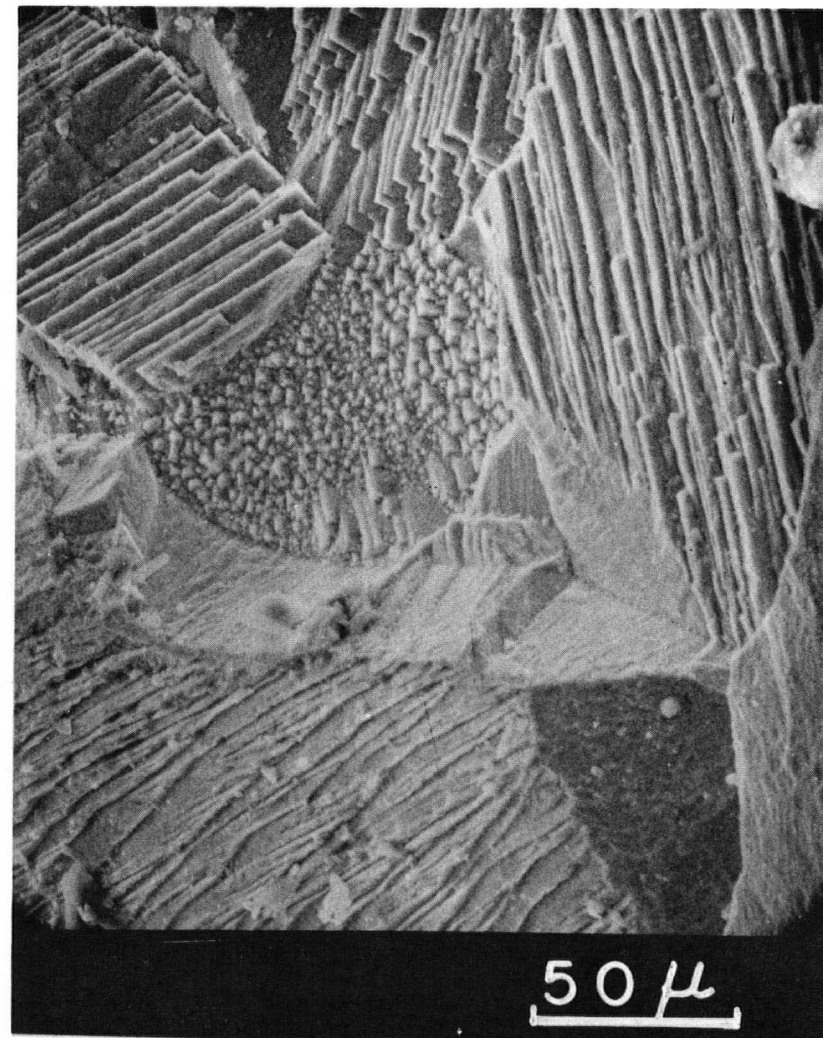
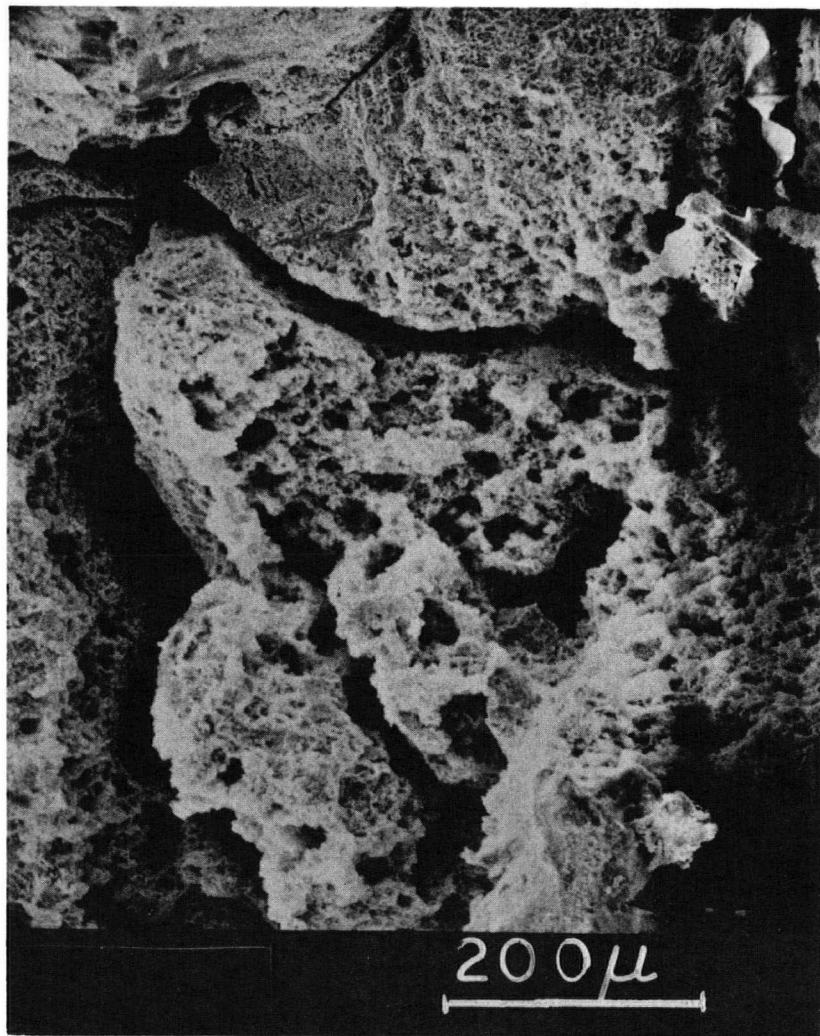


Fig. 19 Scanning electron micrograph of chalcopyrite anodized at 1500 mV for 3 hours in 0.1M HClO_4 , 175°C ; showing deep pitting attack. Surface films of sulphur and Fe_2O_3 were previously removed with CS_2 and an oxalate solution (190), respectively.

Fig. 20 Scanning electron micrograph of chalcopyrite after anodizing (16 hours, 700 mV, 0.1M HClO_4 , 150°C). 'Clean' CuFeS_2 surface showing crystal structure. Other solid phases have presumably been swept away by stirring action.

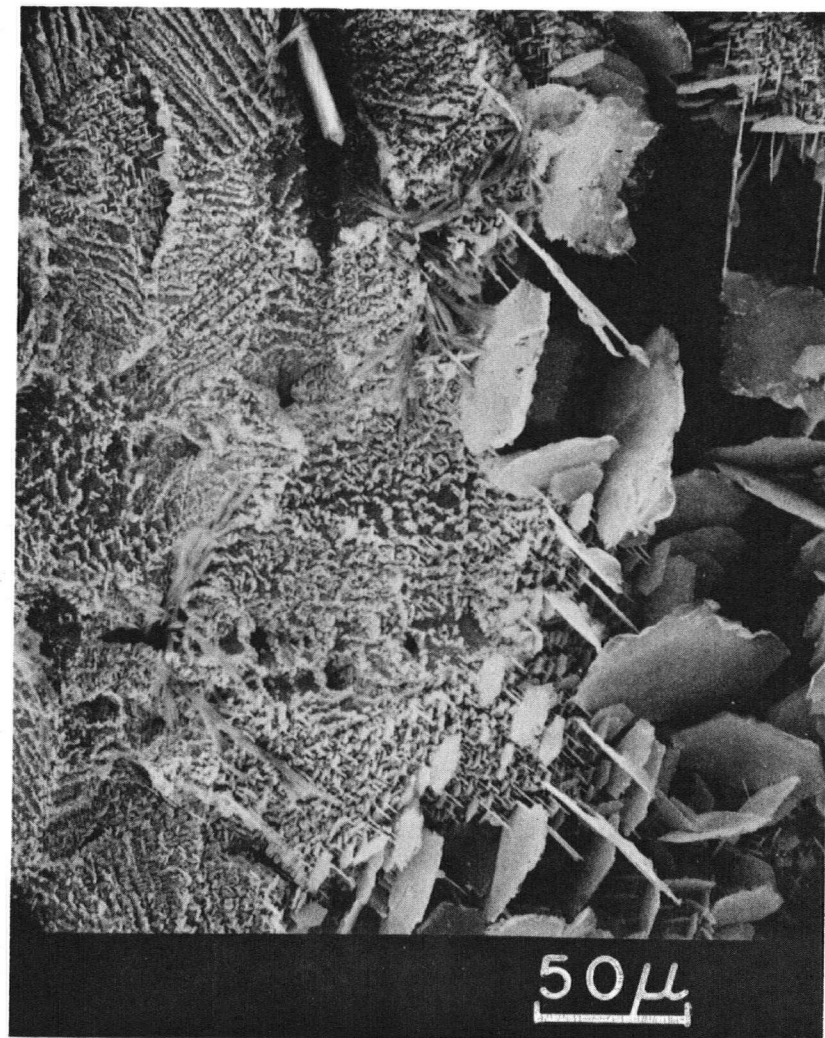
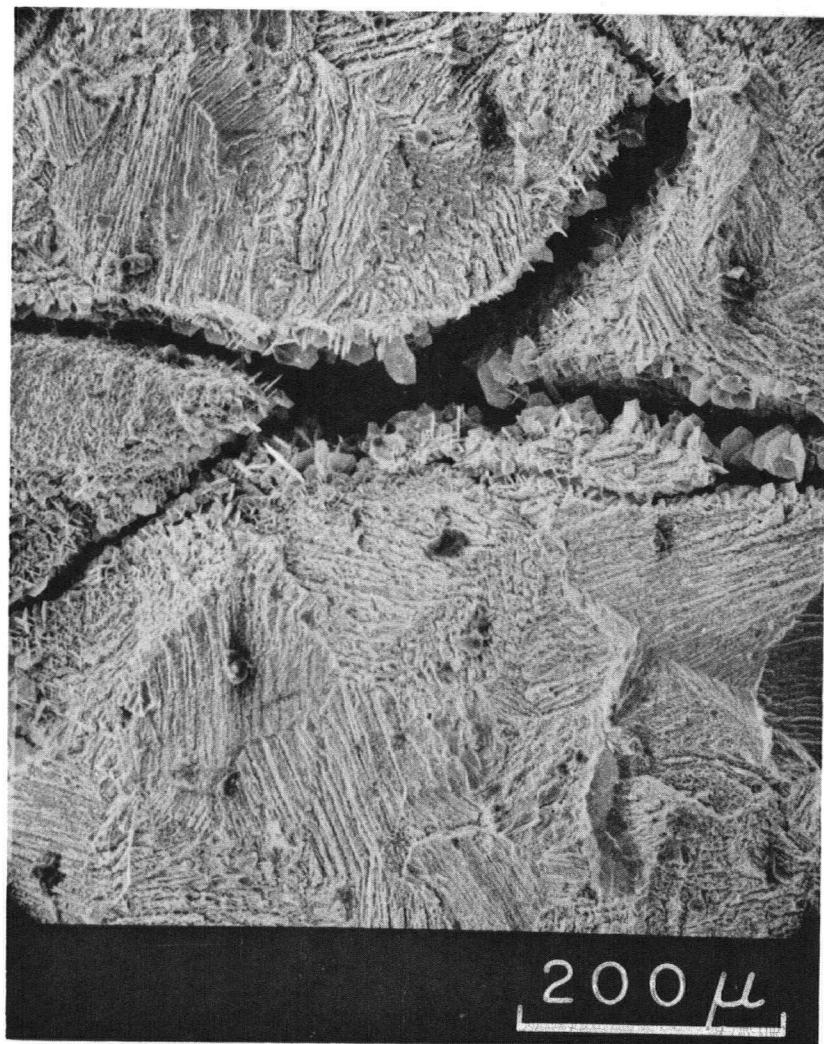


Fig. 21 Scanning electron micrograph of CuFeS_2 specimen after anodizing (7 hours, 615 mV, 0.1M HClO_4 , 175°C). Fine crystals and large plates of CuS .

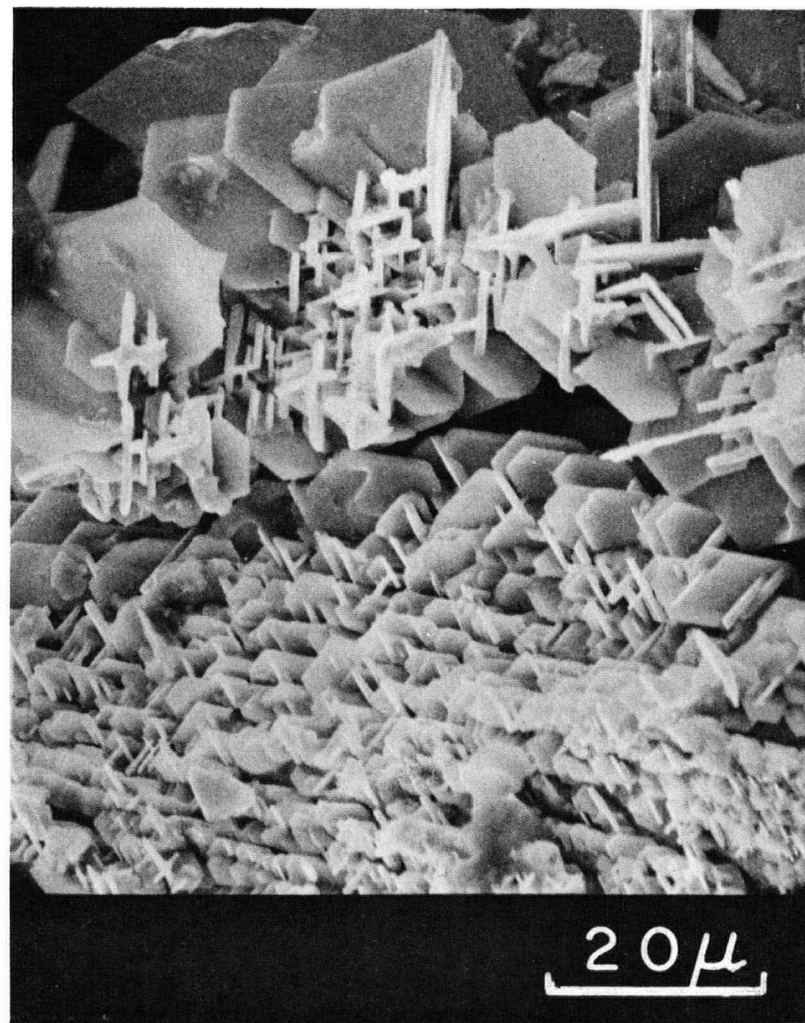
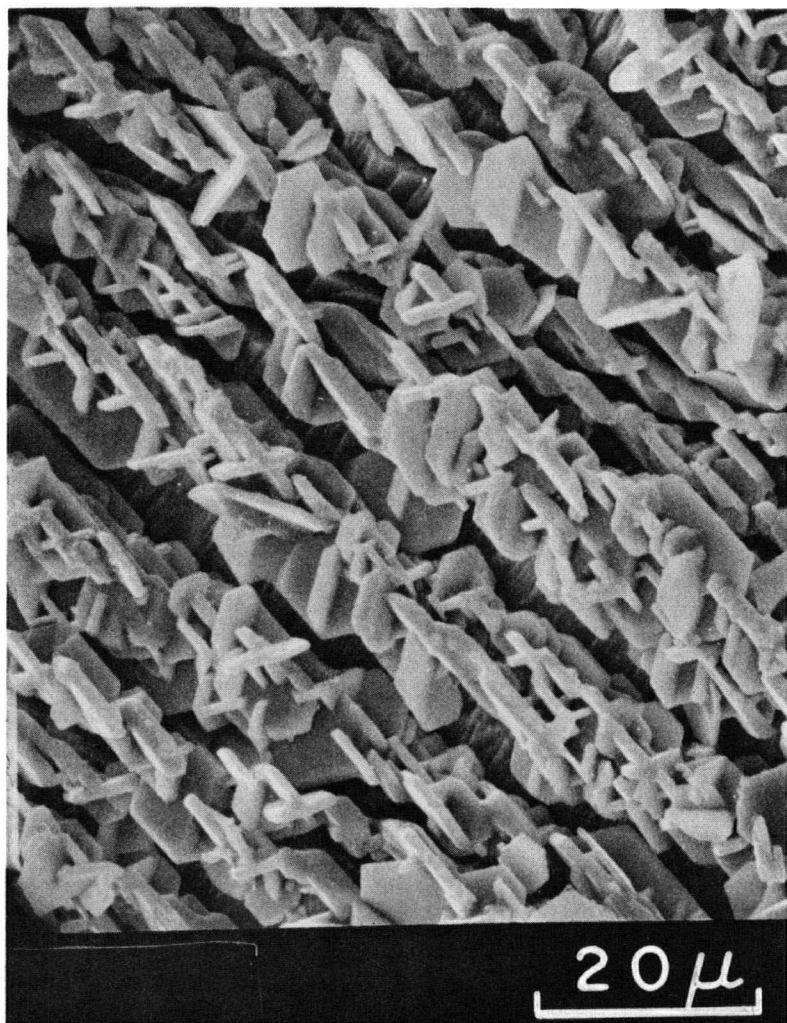


Fig. 22 Scanning electron micrographs of CuFeS_2 specimen after anodizing (11 hours, 615 mV, 0.1M HClO_4 , 175°C). Ordered matrix of CuS crystals overlaying unreacted CuFeS_2 lattice.

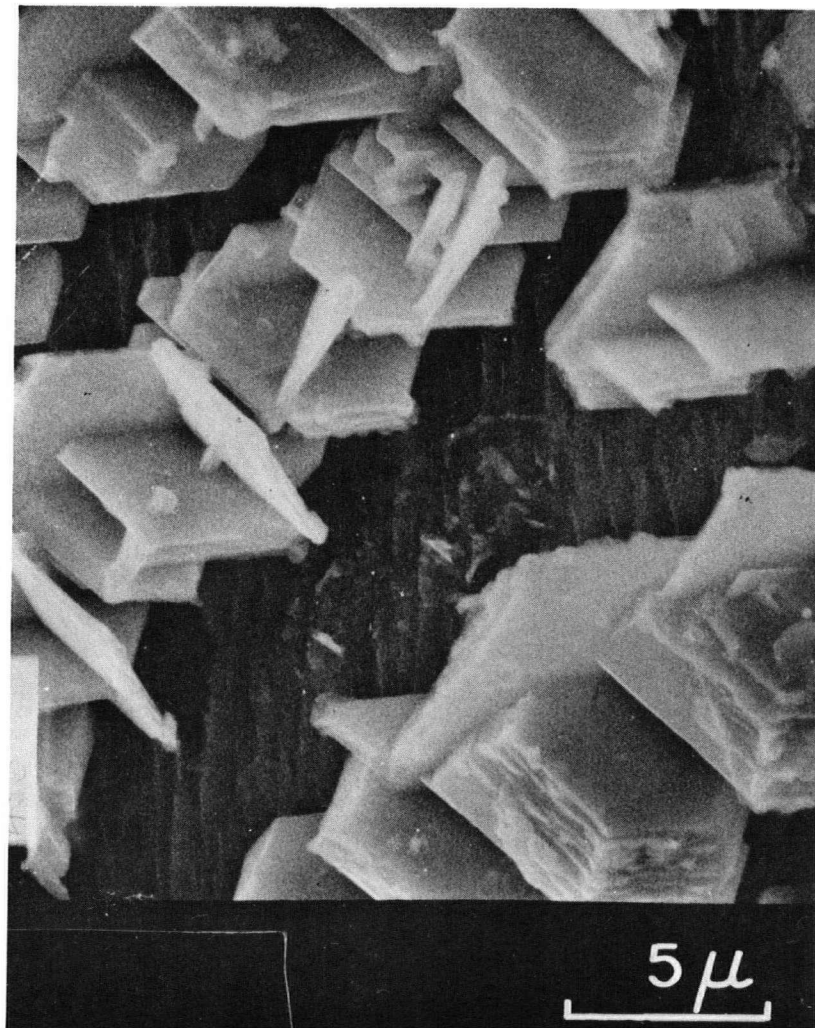
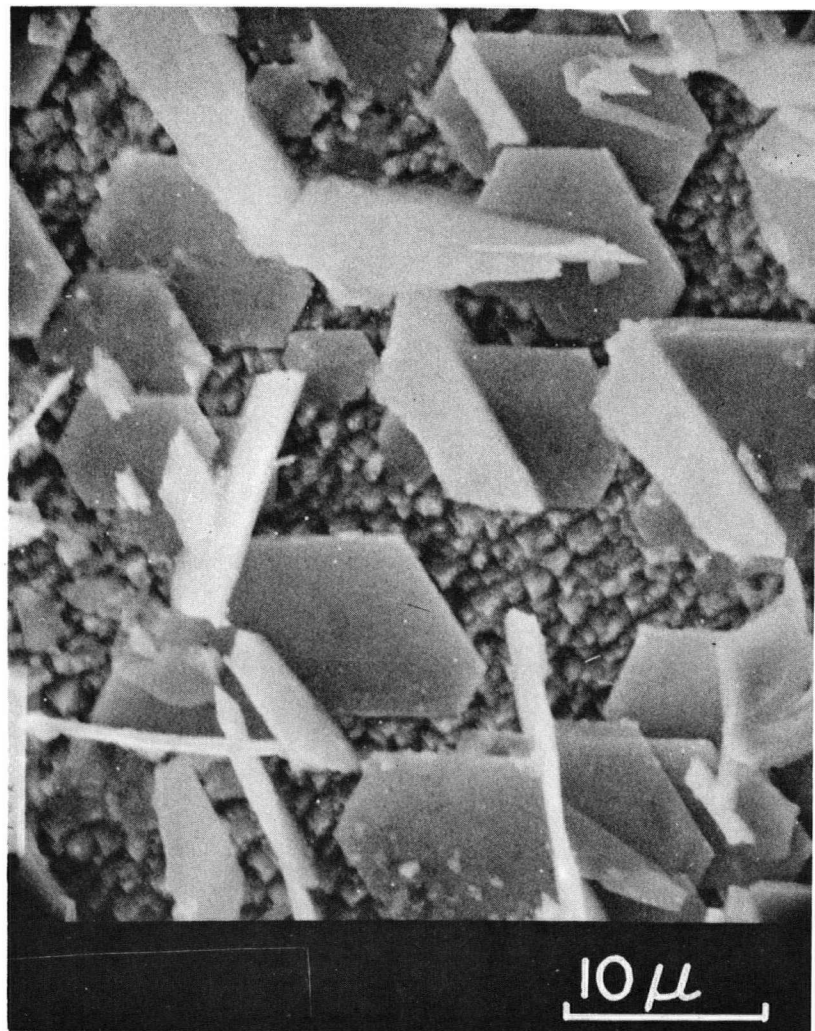


Fig. 23 Scanning electron micrographs of CuFeS_2 specimen after anodizing ($3\frac{1}{2}$ hours, 690 mV, 0.1M HClO_4 , 175°C). Large crystals of CuS on top of CuFeS_2 .

II Anodic Polarizations

The polarizations shown in Section I were conducted only in 0.1 M H_2SO_4 and 0.1 M $HClO_4$, primarily as a function of temperature, with only two scanning speeds, 300 and 30 mV/min., both of which are 'fast' compared with steady state. The object of the experiments in this section is to investigate more thoroughly the effect of solution composition and slower scan rates. The temperature range for these experiments is 20-95°C. Such experiments are more useful in interpreting leaching reactions, which may be considered steady state anodizations, in which the main variables are oxidant strength (potential) temperature (generally near 100°C) and solution composition.

Four variables we examined here were:

1. [Chloride]
2. [Sulphate]
3. pH
4. Scan Rate.

a) Fast Scans

It was shown in the previous section that at low temperatures (<80°C), similar polarization curves were obtained in 0.1 M $HClO_4$ and 0.1 M H_2SO_4 . However, at high temperatures, the electrode 'passivated' in the high potential region in sulphate solutions, but not in perchlorate.

The term 'passivation' normally implies a decrease in current (with an increase in potential), whereas 'inhibition' refers to a constant current, which does not increase with potential. In this work, however, passivation will be used to describe a polarization in which the current either decreases with potential or stays constant.

It can be seen from Figure 24 that polarizations at low temperature in 0.1 M HCl are also similar to those in 0.1 M H₂SO₄; furthermore additions of Na₂SO₄ have little effect. However, additions of KCl passivate the mineral at high potential (Figure 25).

The two regions of the polarization curves are clearly seen in comparing the log I and linear I plots. The first region which extends from 500-1000 mV (at 20°C) is time-dependent, and represents some kind of limiting current. Variation of scanning rate (Figures 26-28) demonstrates this time-dependence.

The second region (1000 mV →) clearly is less time-dependent, and the current is proportional to the potential, but largely independent of solution composition. Except in strong KCl solutions, the slope of the I/V plot was approximately constant, independent of solution or scanning rate. Furthermore the onset of this region is clearly marked and reproducible at 1000 mV (20°C) (Table VI).

The actual slope of this region decreased about 50% or less, in passing from 300 to 3 mV/min. (scan rates) as seen in Table VI.

Polarizations in strong KCl solutions affect subsequent polarizations in solutions not containing high [KCl]. This effect can be partly removed by polishing or completely by heating to 95°C (Figure 29).

A brown deposit was noticed on the surface of the mineral after polarizations in strong chloride. This was not further investigated but is possibly cuprous chloride or basic cupric chloride, Cu(OH)_{1.5}Cl_{0.5}.

Polarizations in 1 M HCl do not passivate the mineral in the same way as those in (1 M KCl, 0.1 M HCl). The transition point is shifted to higher potential (1150 mV), but the slope of the second region is

approximately the same, or higher, (Figure 30) (in contrast to the reduced slope produced in strong KCl solutions). This supports the idea of a basic salt precipitating out, for it would be more soluble in HCl than KCl.

There does appear to be a small difference between polarizations in 0.1 M H₂SO₄ and in 0.1 M HCl; although the slopes of the second region are indistinguishable, the transition point is 50 mV lower in the case of 0.1 M H₂SO₄ (Figures 24, 30).

The effect of increasing the temperature on polarization in a sulphate solution is again illustrated in Figure 31 - an increased current in the first region and a passivating effect in the second region. The transition point however remains fairly constant. No such effects are seen at 95°C in 0.1 M HCl (Figure 32).

b) Summary

At low temperatures, a two-stage anodic polarization curve is obtained for chalcopyrite. The first region, extending from the rest potential (500 mV) to about 1000 mV, appears to have a limiting current, which is markedly dependent upon scanning rate, and to some extent solution composition. This region will be referred as the diffusion region. The current in the second region beginning at 1000 mV is largely independent of scanning rate, and solution composition and is proportional to potential. It will be referred to as the space-charge region.

Sulphate, perchlorate and chloride solutions all give similar polarization curves except for strong KCl solutions which at high potential appears to form a precipitate on the surface, possibly Cu(OH)_{1.5}Cl_{0.5}, and passivate.

At higher temperatures this feature is absent, but sulphate solutions passivate instead.

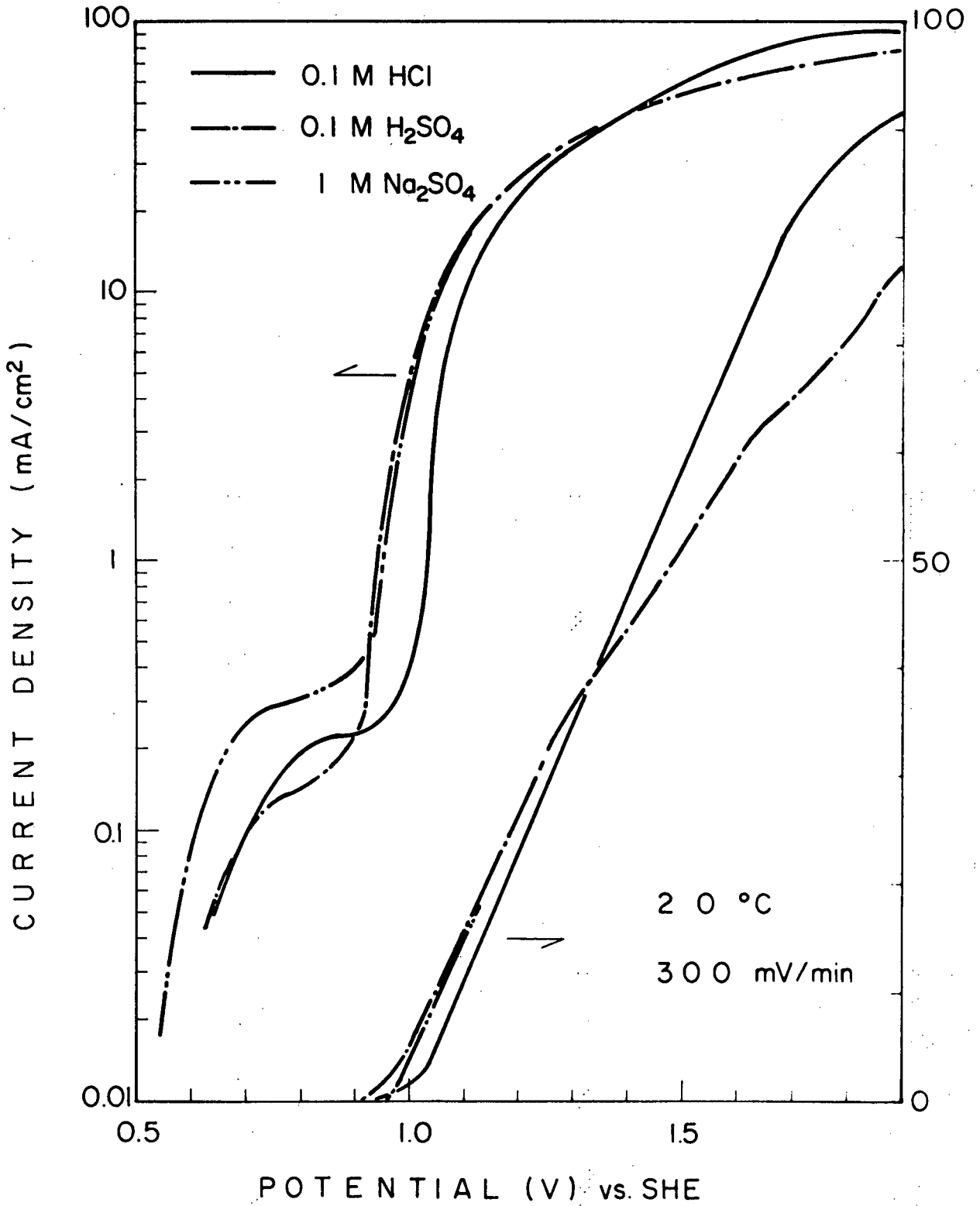


Fig. 24 Potentiostatic scans on CuFeS₂ in various solutions at 300 mV/min., 20°C.

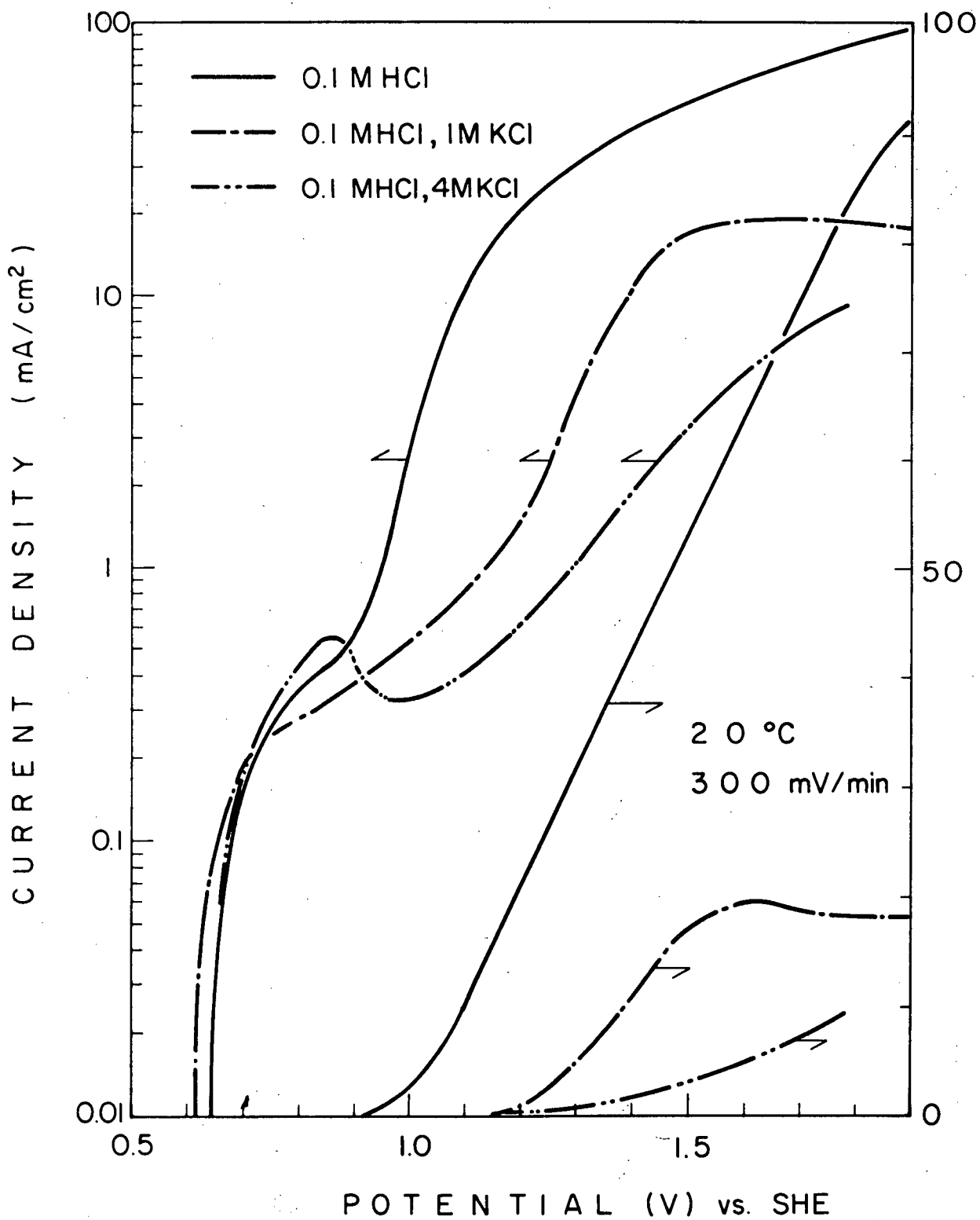


Fig. 25 Potentiostatic scans in chloride solutions at 300 mV/min., 20°C.

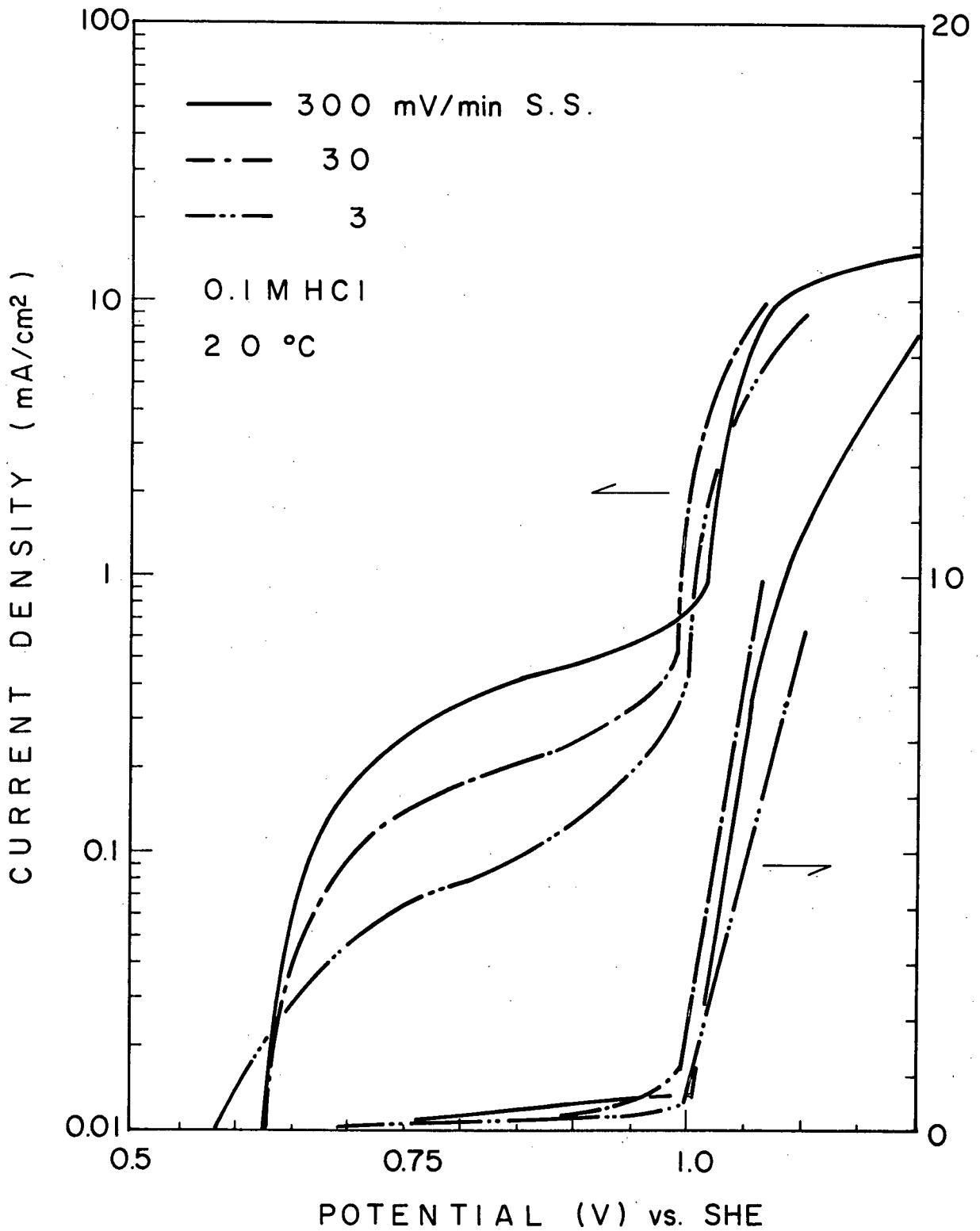


Fig. 26 Potentiostatic scans in 0.1M HCl, 20°C at various scanning rates.

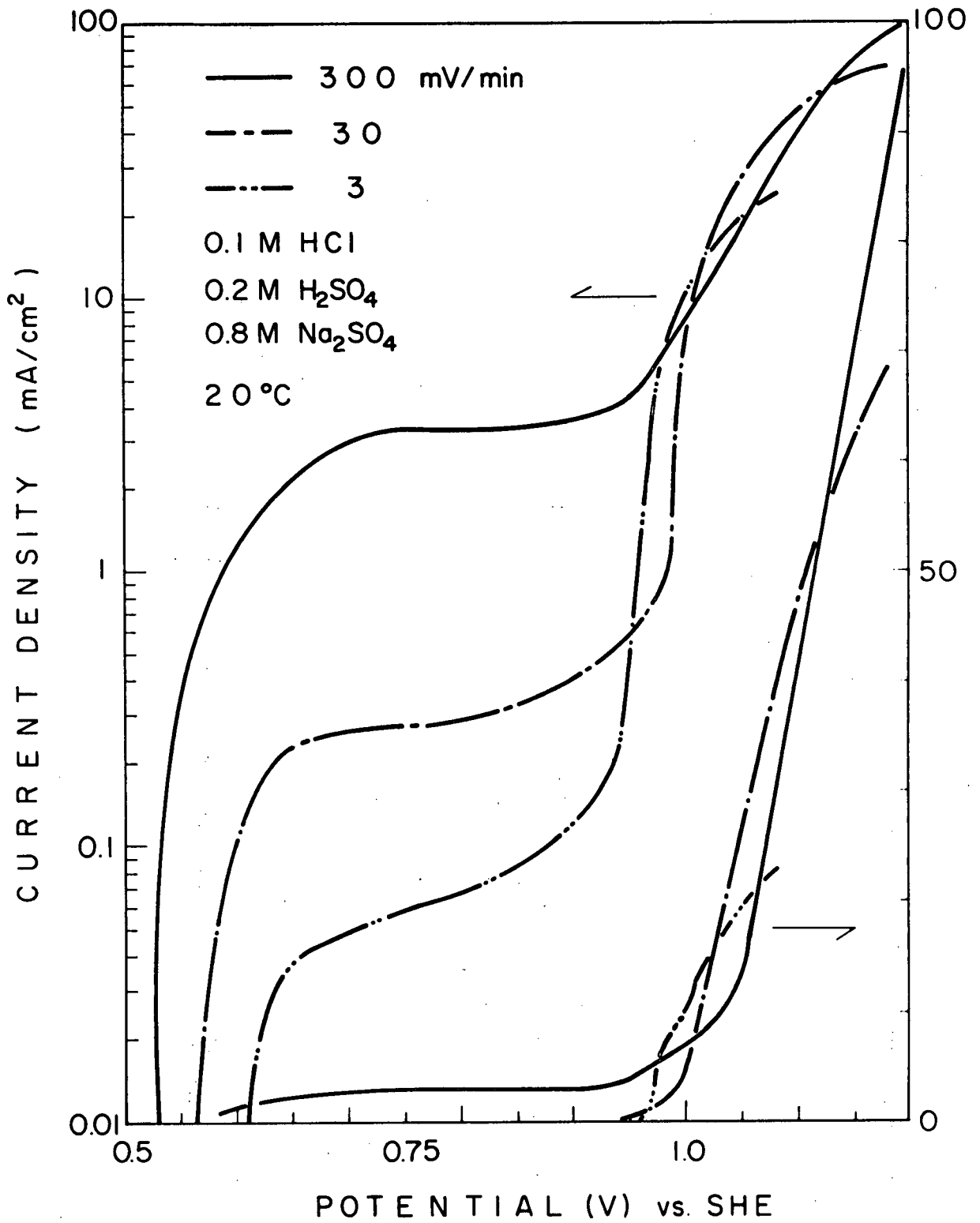


Fig. 27 Potentiostatic scans in sulphate solution, 20°C, at various scanning rates.

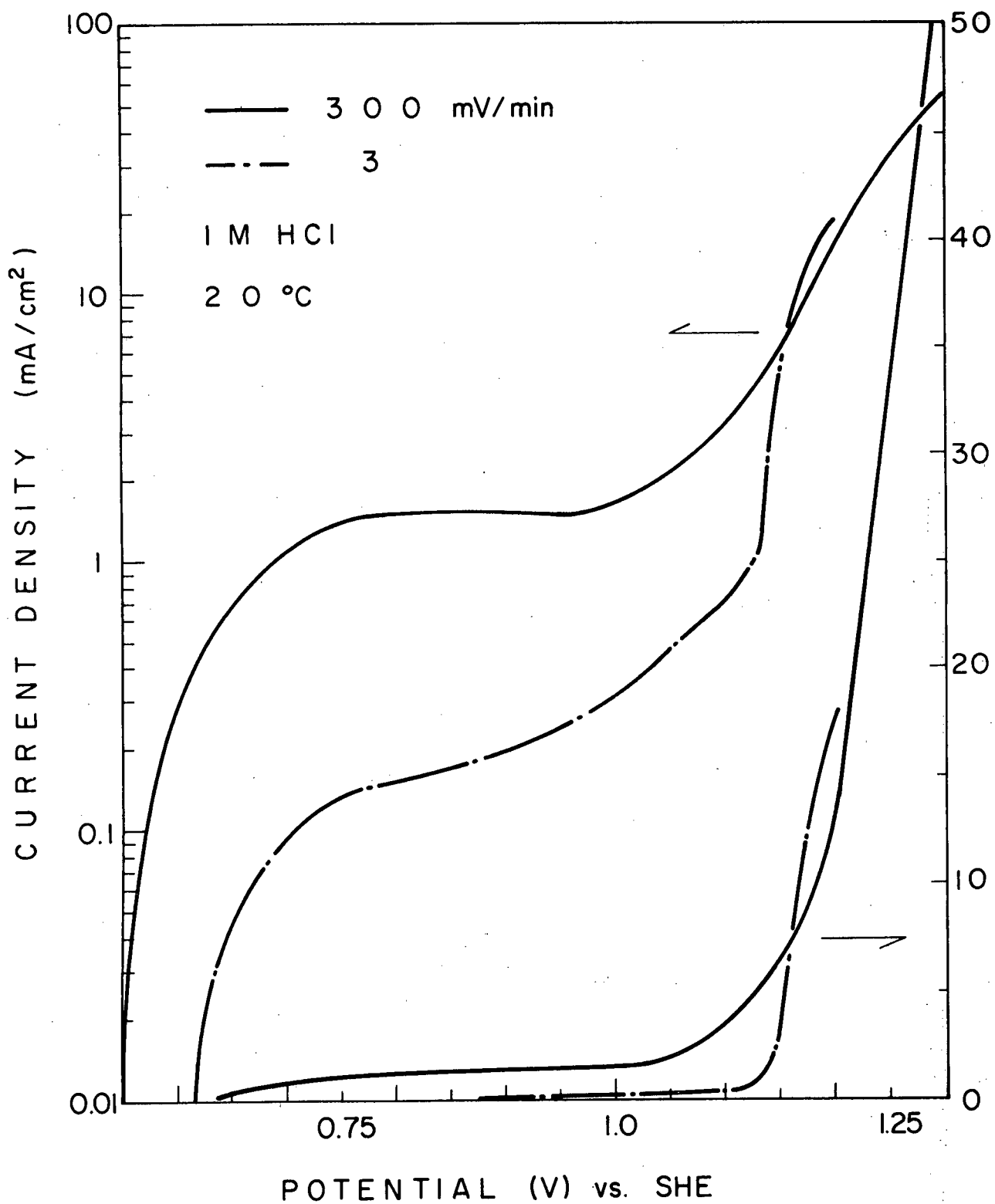


Fig. 28 Potentiostatic scans in 1M HCl, 20°C.

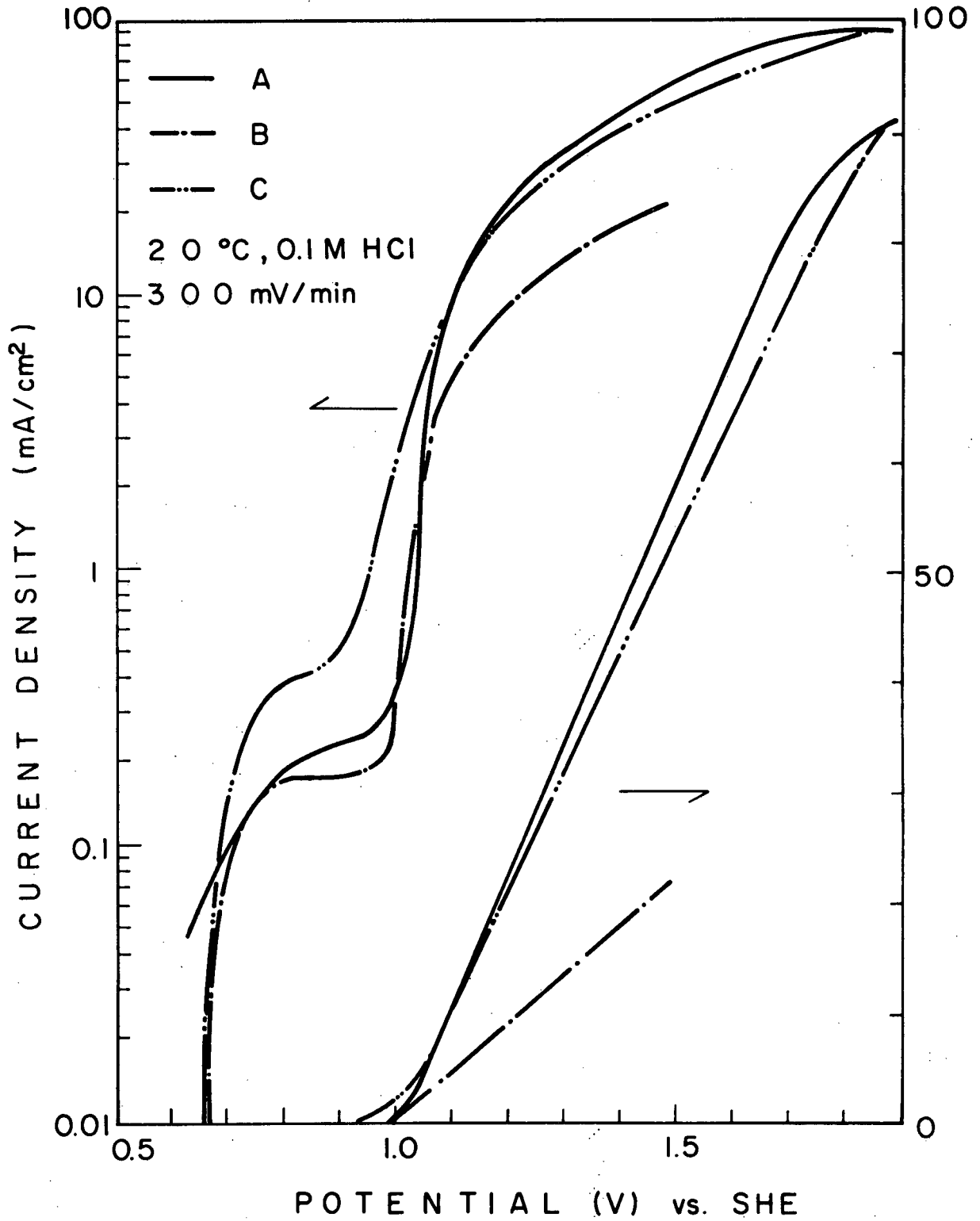


Fig. 29 Successive potentiostatic scans in 0.1M HCl at 20°C, 300 mV/min., showing passivating effect of KCl on subsequent experiments.

- (A) Initial scan
- (B) After a scan in 1M KCl
- (C) After polishing specimen.

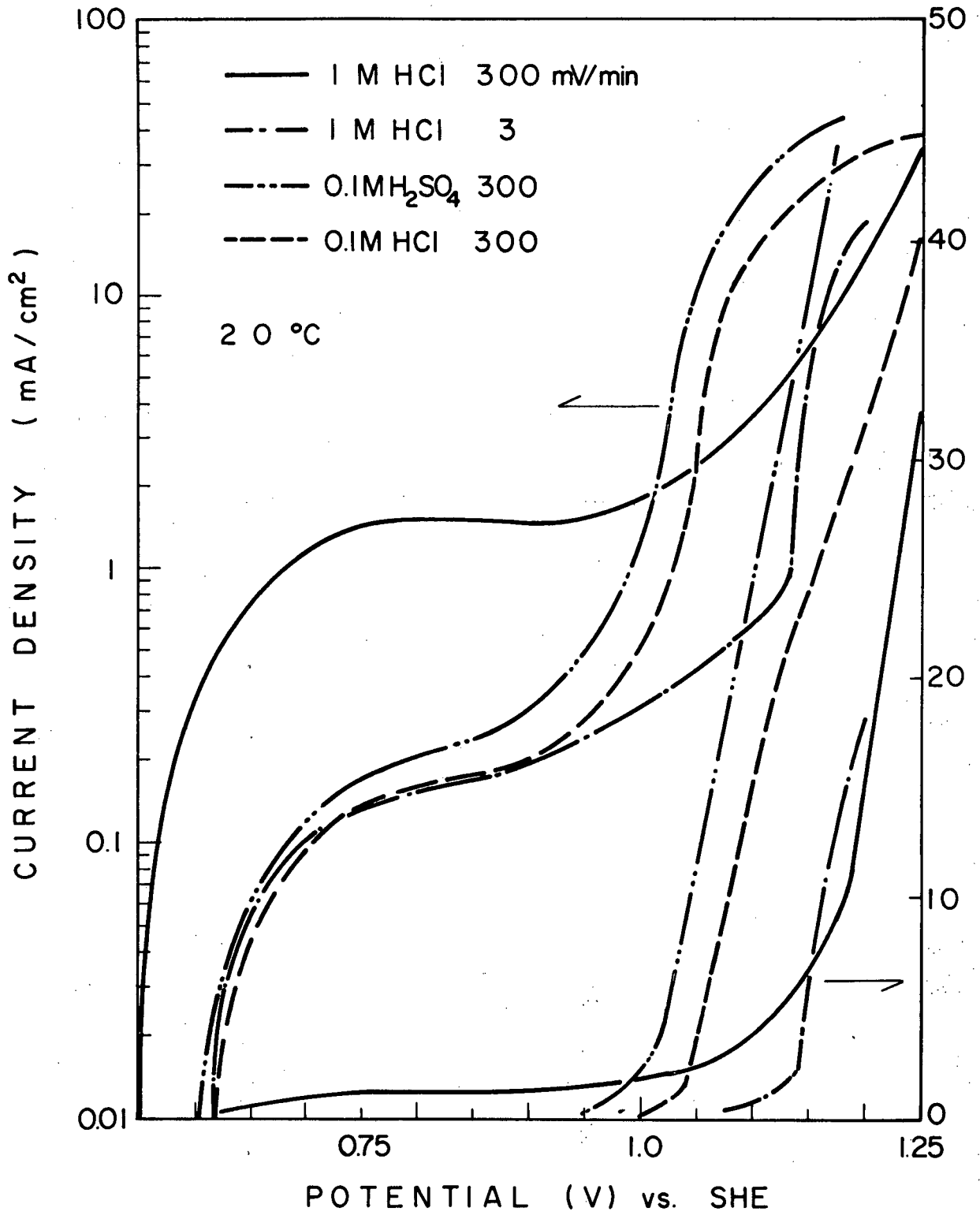


Fig. 30 Potentiostatic scans at 20°C, showing effect of chloride and sulphate solutions on transition potential.

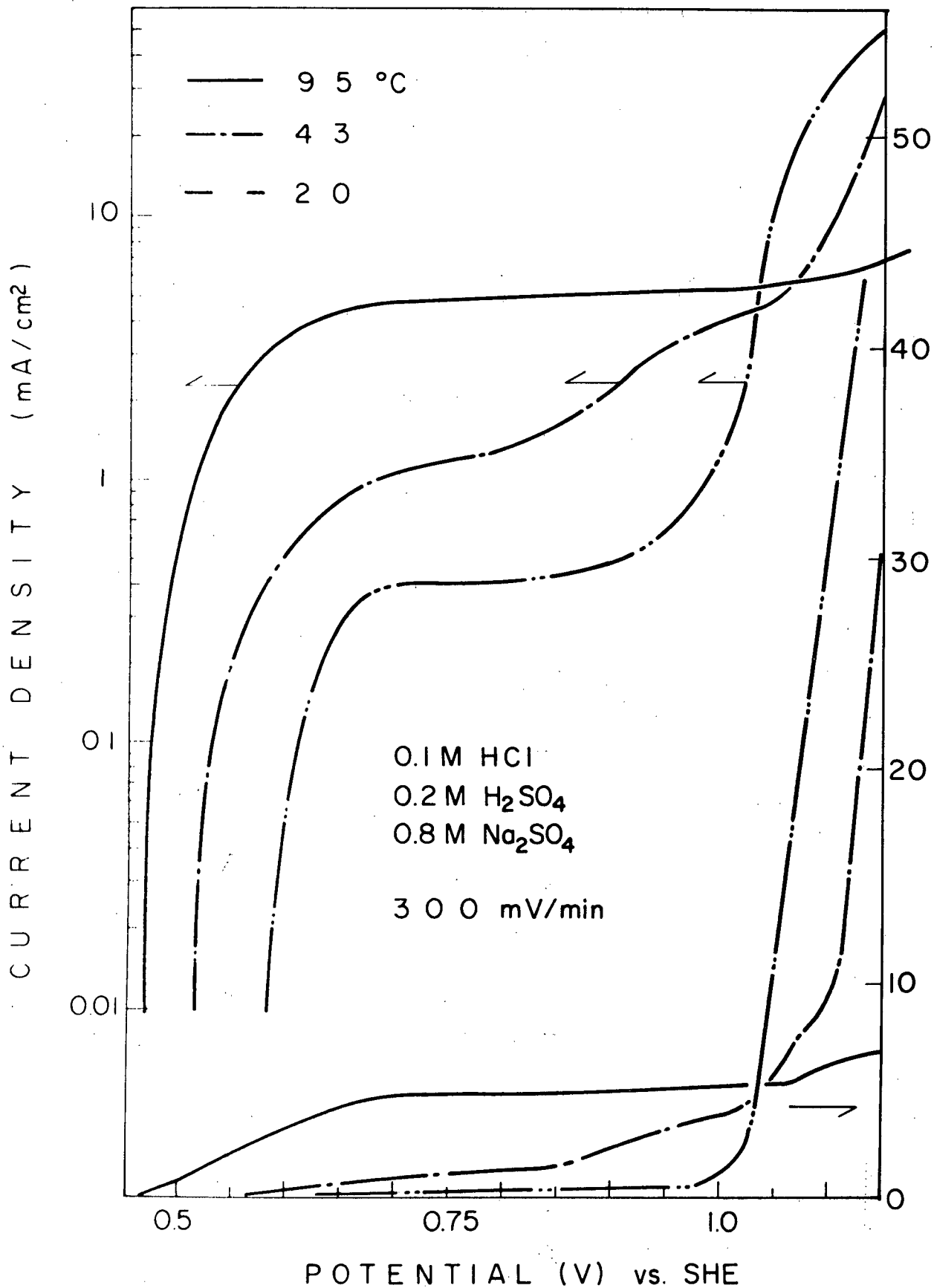


Fig. 31 Potentiostatic scans in sulphate solution at 300 mV, and various temperatures; showing passivating effect of sulphate at 95°C.

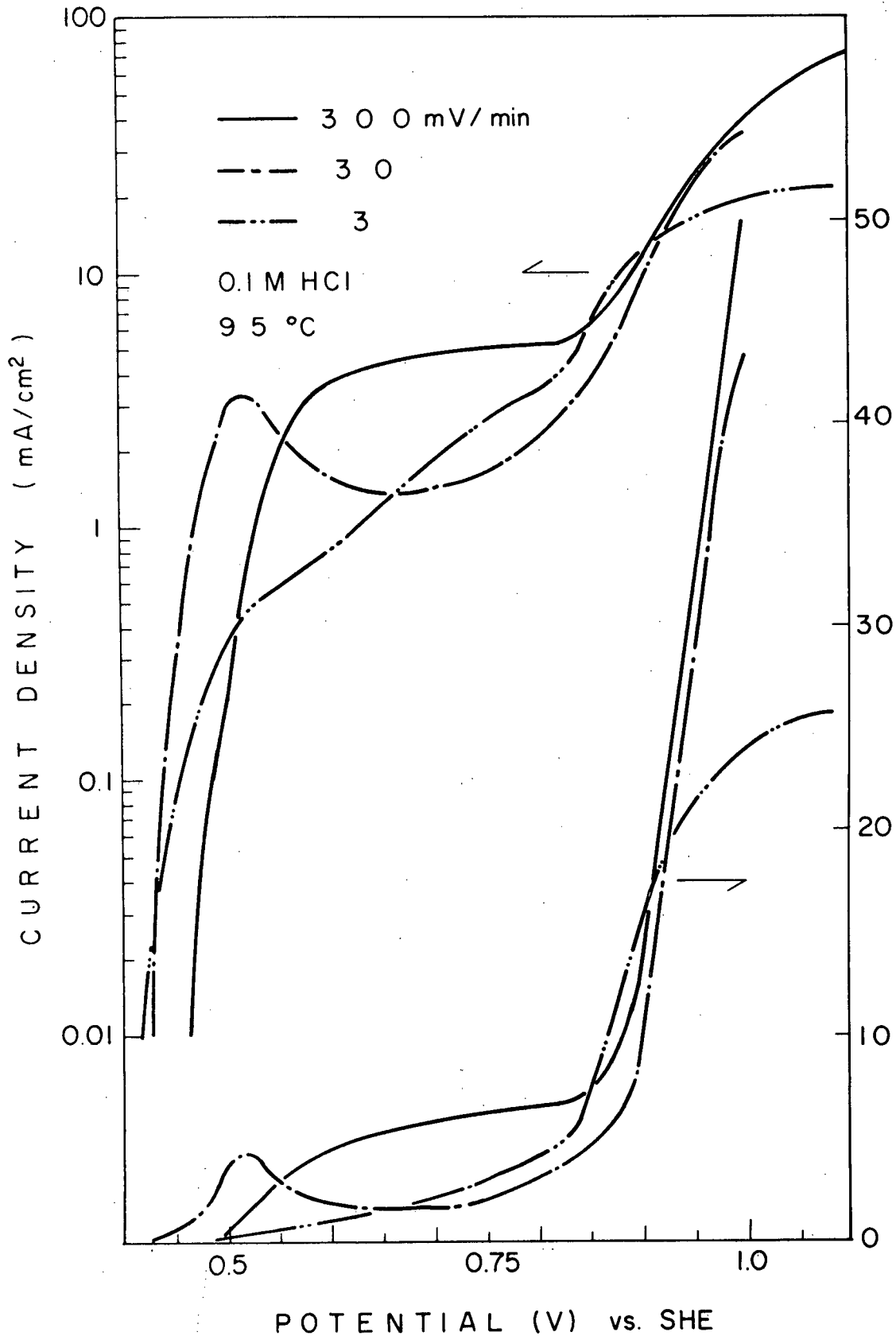


Fig. 32 Potentiostatic scans in 0.1M HCl at 95°C, and various scanning rates; an unreactive specimen.

TABLE VI

Successive Anodic Scans At Rapid Scanning Rates

Specimen #200

Number	Temp. (°C)	Scan Rate (mV/min.)	Solution	1st Slope ($\frac{\mu\text{A}}{\text{mV}^2 \cdot \text{cm}}$)	Transition (mV)	2nd Slope ($\frac{\mu\text{A}}{\text{mV}^2 \cdot \text{cm}}$)	Other
201-1,2	20	300	0.1M HCl	0	1000	116	
201-3	220	300	0.1M H ₂ SO ₄	0	950	116	
201-4,5	20	300	0.1M H ₂ SO ₄ + 1M Na ₂ SO ₄	0	970	92	
201-6	20	300	0.1M H ₂ SO ₄ } 1.0M Na ₂ SO ₄ } + 1M KCl	0	1060	87	
201-7	20	300	0.1M H ₂ SO ₄ } 1.0M Na ₂ SO ₄ } + 1M KCl	0	1160	45	
201-8	20	300	0.1M HCl	0	990	45	
201-9	20	300	0.1M HCl	0	1000	108	Repolished
201-11	20	300	1M KCl + 0.1M HCl	0	1230	53	Repolished
201-12	20	300	4M KCl + 0.1M HCl		~1350	22	Repolished
201-13	20	300	4M KCl + 0.1M HCl		Indefinite		Repolished
201-17	20	300	0.1M HCl		1000	150	
201-18	20	30	0.1M HCl		1000	125	
201-20	20	3	0.1M HCl		1000	85	

TABLE VI (Cont.)

Specimen #201

Number	Temp. (°C)	Scan Rate (mV/min.)	Solution	1st Slope ($\frac{\mu\text{A}/\text{mV}^2}{\text{cm}}$)	Transition (mV)	2nd Slope ($\frac{\mu\text{A}/\text{mV}^2}{\text{cm}}$)	Plateau
201-1	95	300	0.1M HCl	~ 5	890	300	
201-2	95	30	0.1M HCl	0	880	300	
201-3	95	3	0.1M HCl	~14	835	120	
201-6	20	300	0.1M HCl 0.2M H ₂ SO ₄ 0.8M Na ₂ SO ₄		1040	600	
201-7	20	30			990	410	
201-9	20	3			960	~200	
201-8	20	300	0.1M HCl 0.2M H ₂ SO ₄ 0.8M Na ₂ SO ₄	0	1025	420	
201-11	43	300		0	1090	540	1.5 mV/cm ²
201-10	95	3000		25	1070	15.5	5 mV/cm ²
201-12	95	3		~10		~7.5	1.5 mV/cm ²
201-13	20	300	1M HCl		1175	390	1.5 mV/cm ²
201-14	20	3	1M HCl		1135	360	
201-15	20	300	0.1M HCl		1050	220	
201-17	20	300	0.1M H ₂ SO ₄		1000	250	

The transition point between diffusion and space-charge region is remarkably constant (1000 mV) decreasing somewhat for sulphate solutions, and increasing with [Cl].

The slope of the line in the space-charge region is typically 100-300 $\mu\text{A}/\text{cm}^2\text{-mV}$ at 20°C for fast scans; this value varies considerably from one specimen to another, but is relatively independent of solution and scan rates in the range 3 - 300 mV/min.

c) Slow Scans

Slow scanning in this context is defined as 0.3 mV/minute. This figure was used, because it is a reasonable approximation to steady state, and slower rates are impractical.

At 0.3 mV/min., a typical 600 mV scan takes over 30 hours. Lower scan rates would reduce the number of experiments possible, and lead to such extensive mineral decomposition as to destroy the specimen before the scan is complete in many cases.

(i) Low Temperature (20°C)

At 20°C, slow polarizations in 0.1 M and 1 M HCl, H₂SO₄ and HClO₄ are very similar (Figures 33,34) except as noted above; the transition point moves to higher potential with increasing [Cl], and in the diffusion region the current increases with increasing strength of solution. However the relationship in the space-charge region is still linear, and the slopes similar ($7.5 \pm 2.5 \frac{\mu\text{Amp}}{\text{cm}^2\text{-mV}}$) for each of these six solutions. These slopes are much smaller than those obtained with fast scan rates. A relationship between transition point and diffusion region current may be noted, i.e. the higher the diffusion current, the higher the potential needed to start the space-charge region, but the sharper the slope in the space-charge region.

Increasing the pH (at 20°C) has little effect on polarizations in sulphate solutions, but a more severe effect on those in chloride solutions, as noted in the previous section (Figure 35,36), although the diffusion current is lower in each case.

Increasing the temperature has a drastic effect on the diffusion current, as shown in Figure 37 for 0.1 M HClO₄ solutions. However, the space-charge region current is remarkably constant over the range 20, 40, 60°C but is about six times higher at 90°C.

(ii) High Temperature (90°C)

Shown in Figure 38 is the effect of solution composition on 90°C scans. There is such a large change in passing from 0.1 M HClO₄ to 0.1 M HCl that it is not obvious that the same features are present. The transition point in HCl has shifted about 500 mV towards lower potentials, and the diffusion current region is 'lost', due to the high rest potential. Furthermore, the slope of the line in the space-charge region is nearly doubled ($17.5 \rightarrow 32 \frac{\mu\text{A}}{\text{cm}^2} / \text{mV}$) in passing from 0.1 M HCl to 1 M HCl.

The actual values of the space-charge slopes (at 90°C) are (Table VII) in the range $17.5 \rightarrow 75 \frac{\mu\text{A}}{\text{cm}^2} / \text{mV}$, an order of magnitude higher than at 20°C.

The variation in these values is due not only to solution, but also to the differing behaviour of individual specimens.

The passivating effect of H₂SO₄ noted above is again seen in Figure 38; evidently the space-charge region is not accessible in this solution at reasonable potentials.

The maxima in the HCl polarizations appear to be the cumulative effect of the slow scan rate and high dissolution rates.

Additional confirmation of the differing behaviour in HCl, H₂SO₄

is provided by Figure 39, in which the H_2SO_4 scan was performed first, on a fresh mineral. The potential of the transition point, from diffusion to space-charge region, is lowered by the addition of KCl, although the slope of the line in the space-charge region is little affected (Figure 40).

Approximately 100 mV less potential is needed for the onset of the space-charge region in 4M KCl than in 0.1M KCl.

It is possible to consider the first part of the diffusion region as an activation-controlled process, for in some experiments there is an approximate Tafel relationship at the start of the polarization (a linear relationship on the log I plots). Thus, in the experiments shown in Figure 41 (variation of [KCl]) a Tafel slope of 85 mV/current decade is evident from the first 200 mV. In most experiments (e.g. Figure 38) the rest potential is too high to observe this feature.

Anodizations (at 90°C) in 1M Na_2SO_4 solutions do not appear to passivate as readily as those in 1M H_2SO_4 (Figure 41). It is interesting to compare the log I and linear I plots in this figure. The log I plot appears to indicate a linear (Tafel) relationship with slope 95 mV. whereas the linear I plot indicates two stages, i.e. diffusion - space charge regions. The same comments apply to the following figure.

Lowering the pH from 3.5 to 1.05 in a 4M KCl solution had virtually no effect on the polarization (Figure 42).

d) Summary

At 20°C, steady state currents are relatively independent of solution composition; and the boundary between the diffusion region and the space-charge region is clearly marked, at about 1000 mV.

Increasing the temperature to 60°C has little effect except to increase

the diffusion current, which is still very low.

At 90°C the diffusion current in HClO_4 and H_2SO_4 is greatly increased; and adding chloride to a perchlorate solution allows the space-charge region to start 500 mV lower. Thus the current is strongly potential-dependent in the region 500-800 mV, for chloride solutions.

The steady-state space-charge slope is increased by an order of magnitude from 20°C to 90°C ($5 \rightarrow 50 \frac{\mu\text{A}}{\text{cm}^2} / \text{mV}$) in chloride solutions.

In H_2SO_4 (1M), the electrode passivates at 90°C, and the space-charge region is not achieved; thus the current in this solution is largely potential-independent. This passivating effect disappears at higher pH.

pH has no effect on polarizations in 4M KCl (from pH 1 \rightarrow 3), at 90°C.

The polarization curve may be considered as a three-part curve:

- 1) An activation controlled region
- 2) A diffusion-controlled region
- 3) A space-charge region.

The first region is often obscured by high rest potentials.

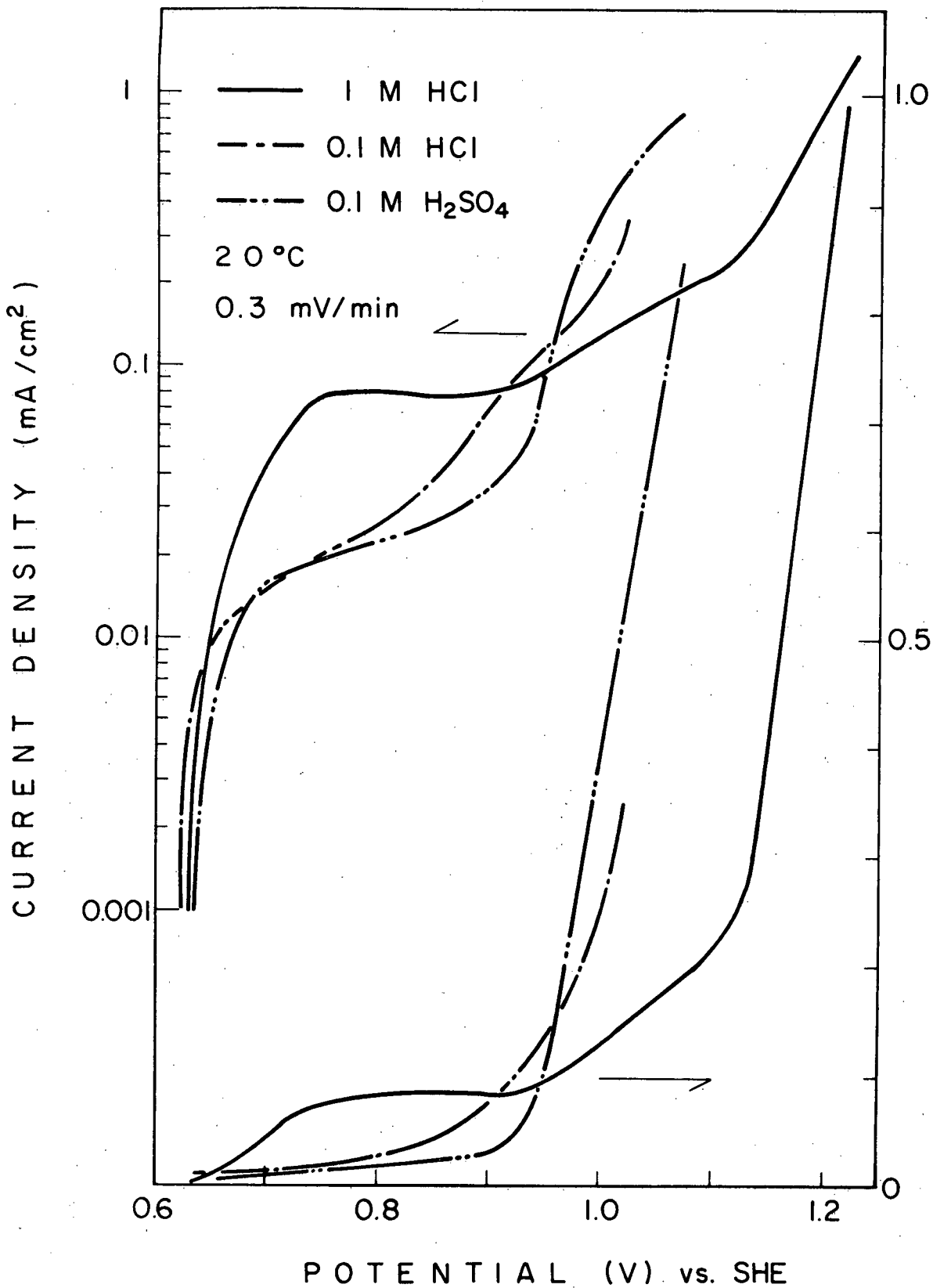


Fig. 33 Slow scans at 20°C in various solutions.

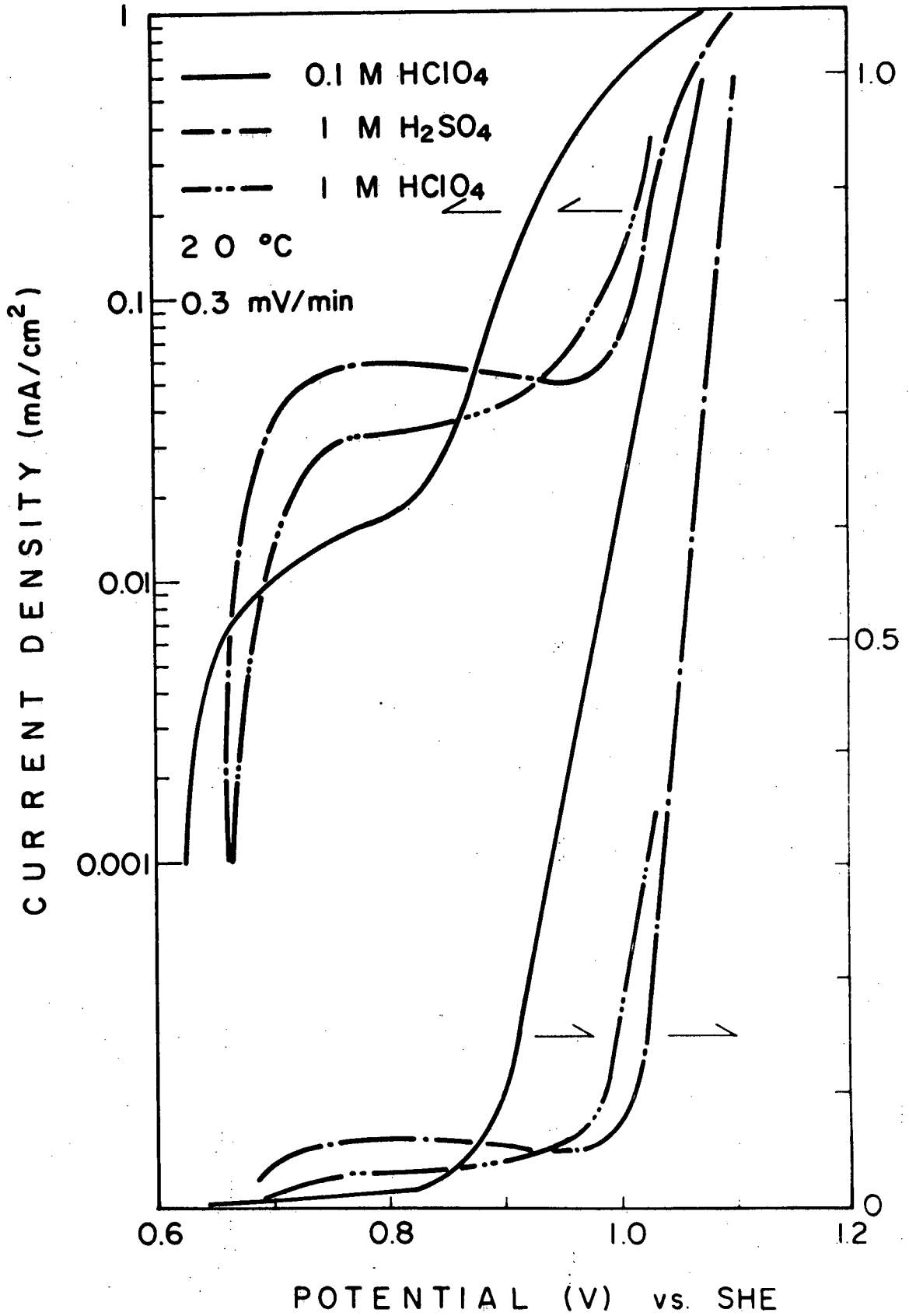


Fig. 34 Slow scans at 20°C in various solutions.

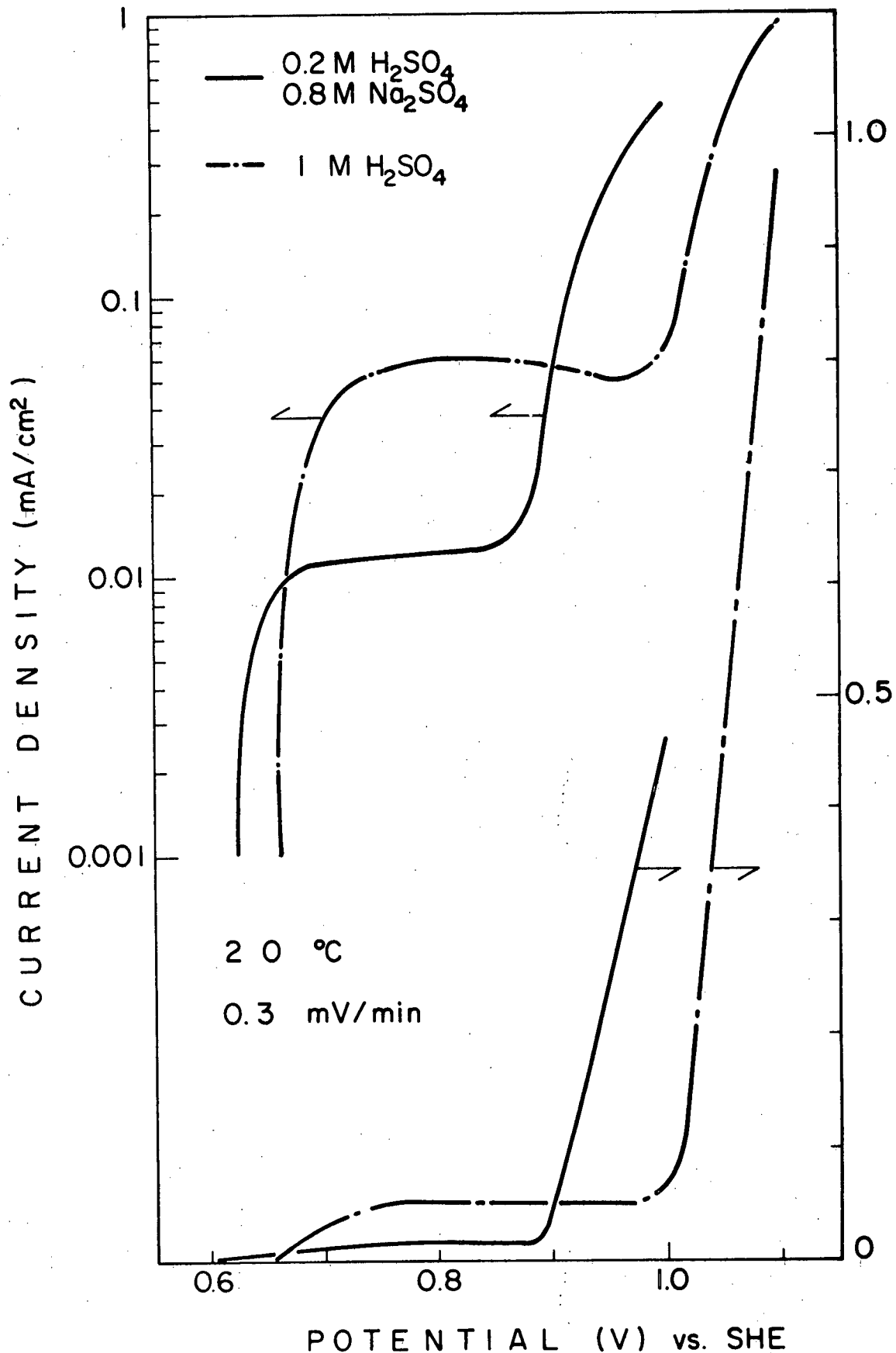


Fig. 35 Slow scans at 20°C in sulphate solutions, showing effect of pH.

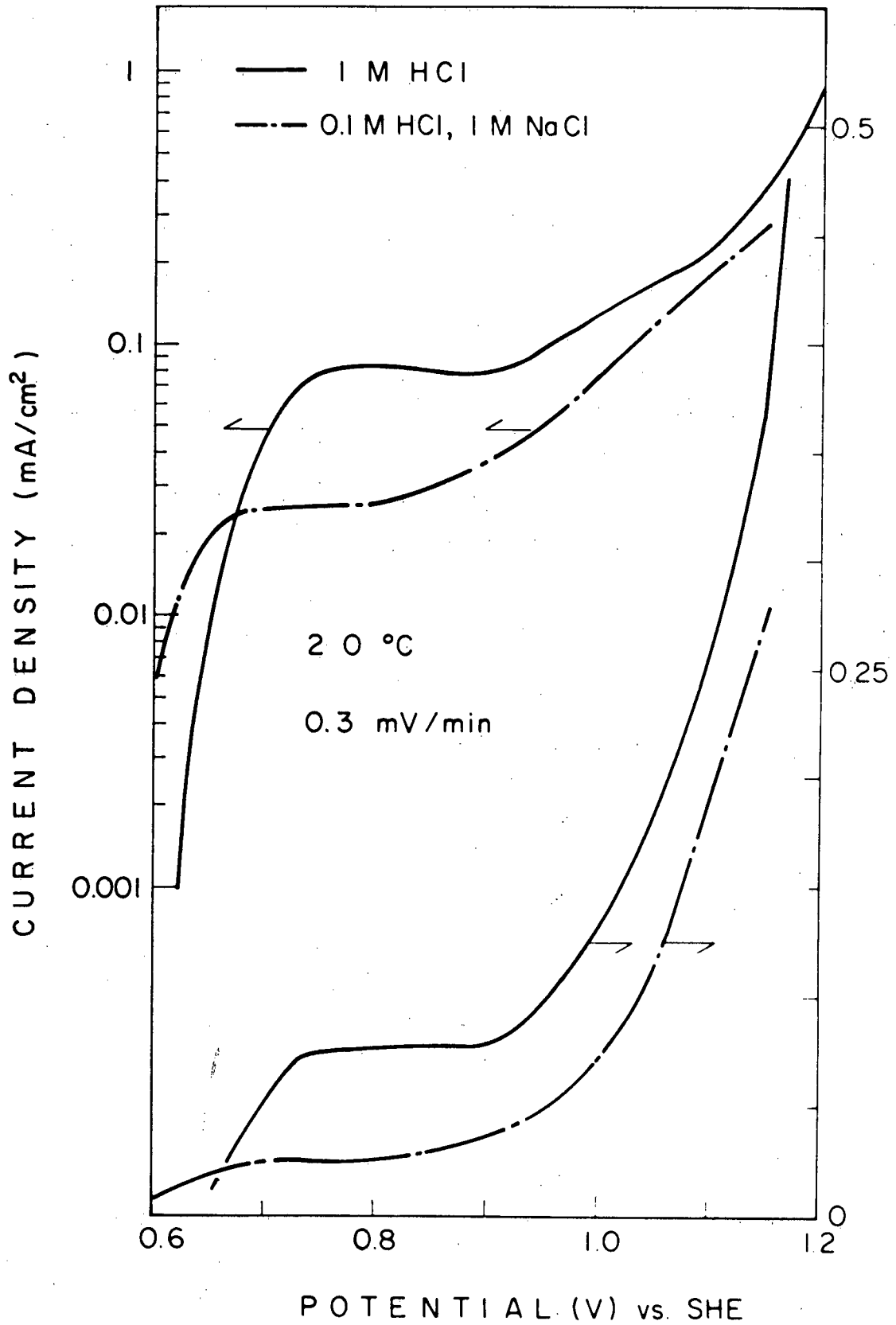


Fig. 36 Slow scans at 20°C in chloride solutions, showing effect of pH.

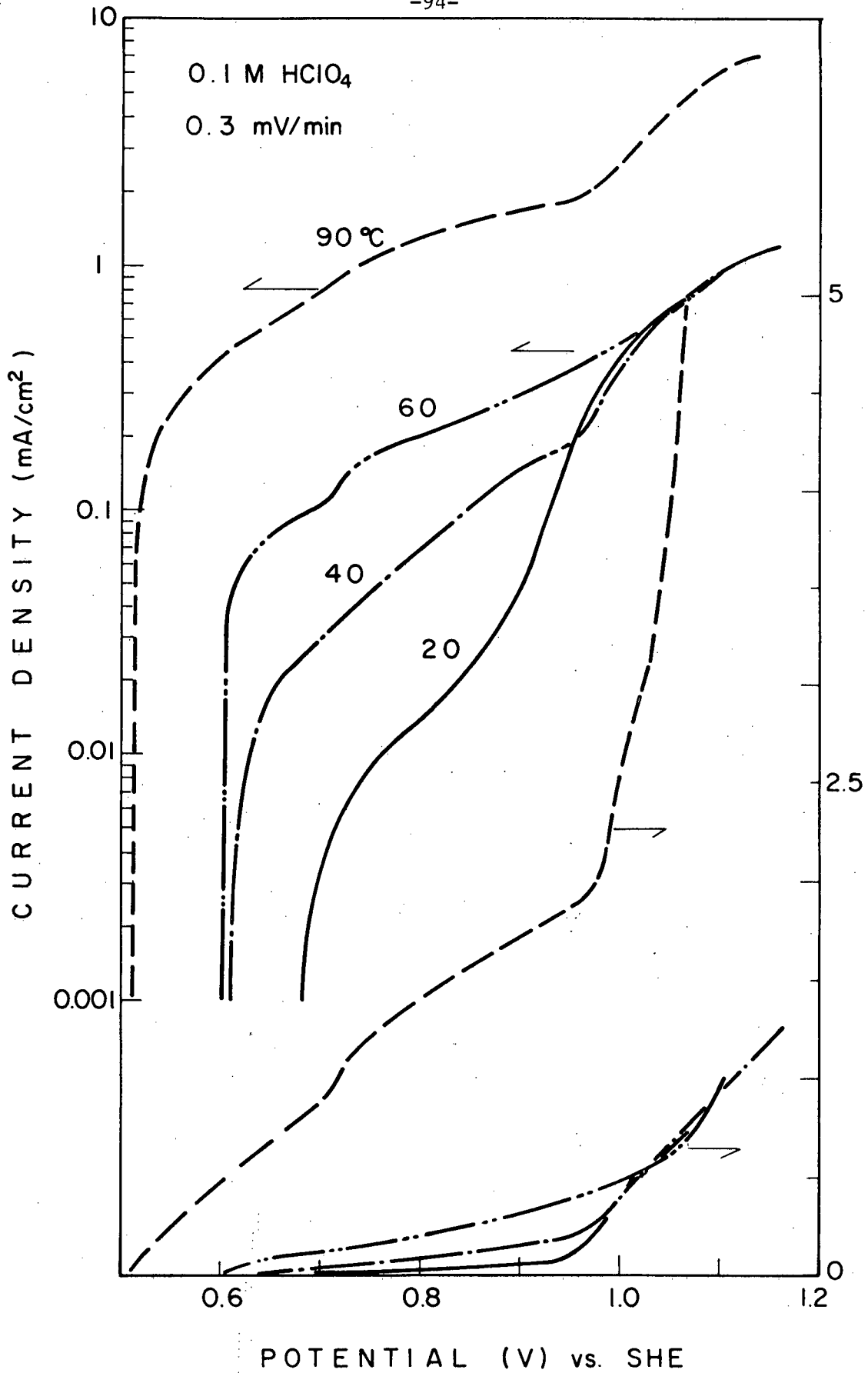


Fig. 37 Slow scans in 0.1M HClO₄ at various temperatures.

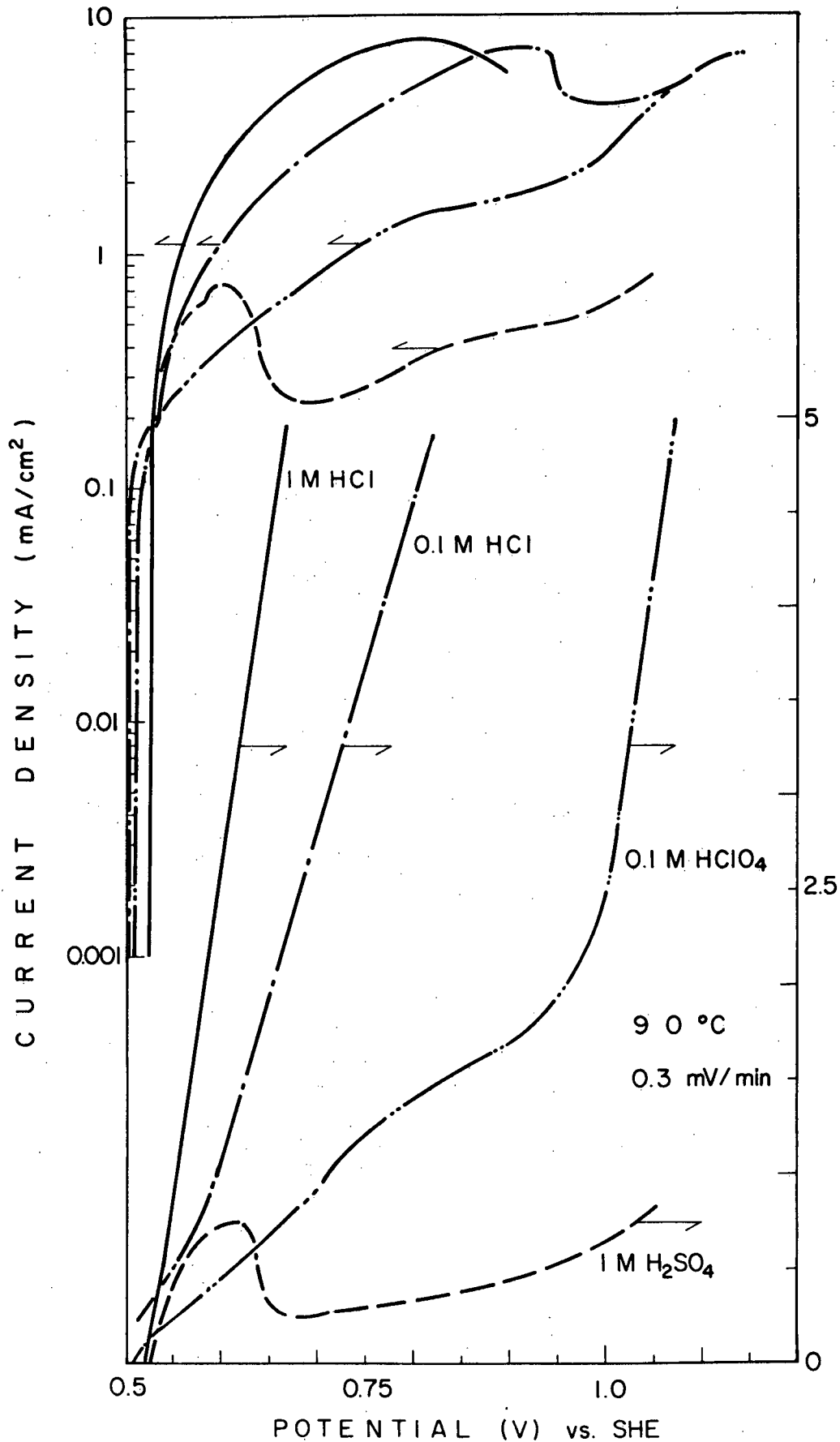


Fig. 38 Slow scans at 90°C in various solutions.

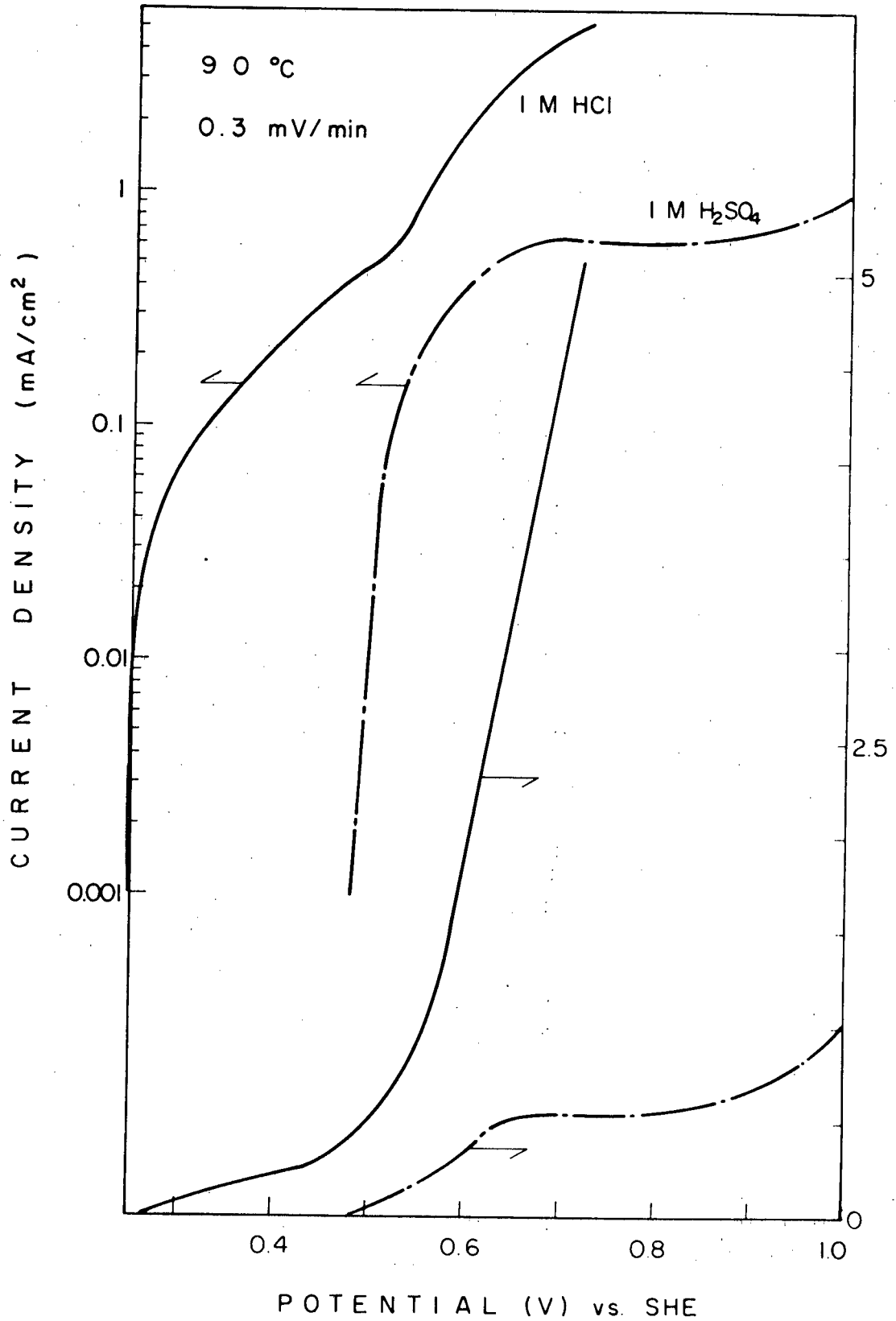


Fig. 39 Slow scans at 90°C in 1M HCl and 1M H₂SO₄.

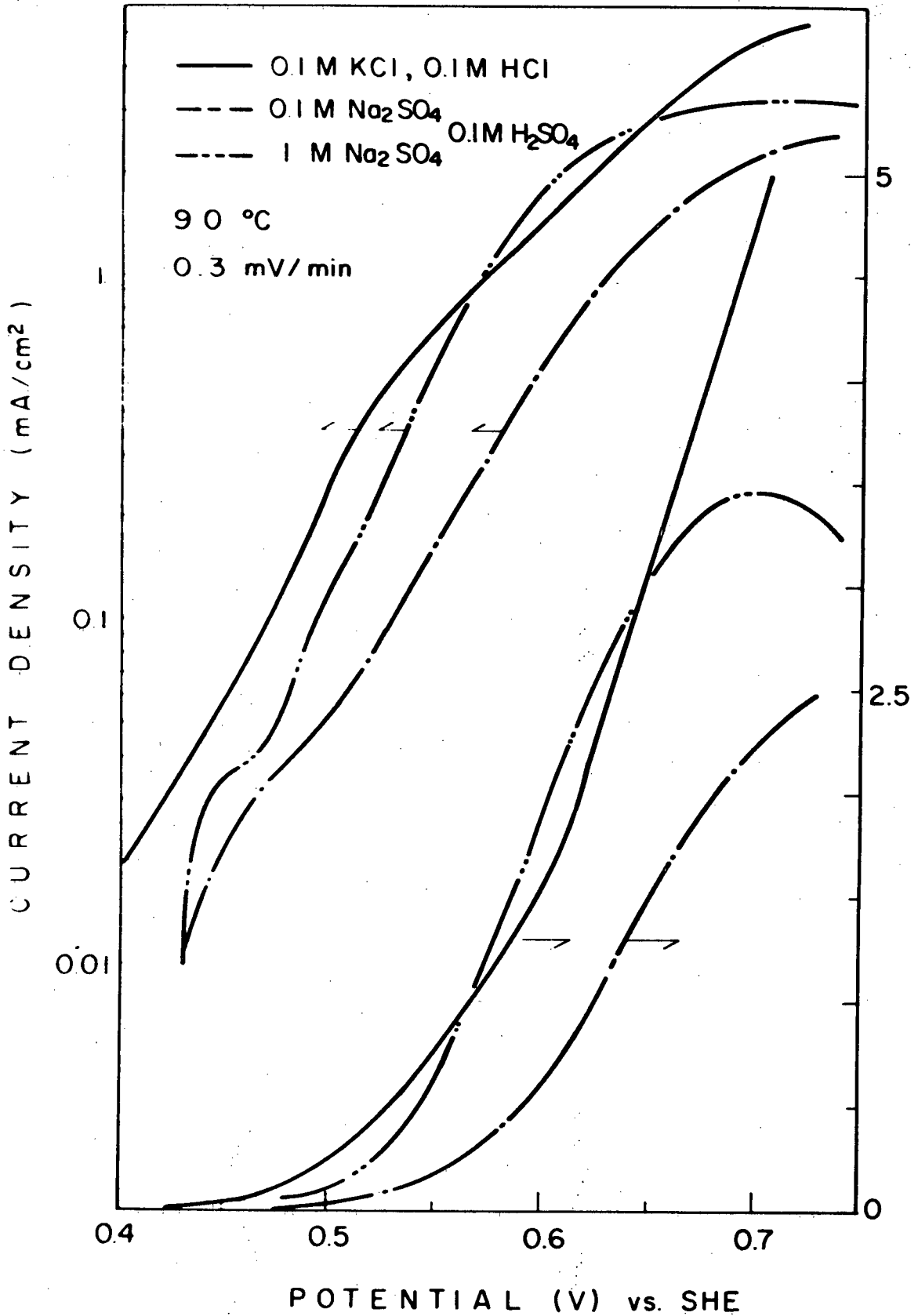


Fig. 40 Slow scans at 90°C in sodium sulphate solutions.

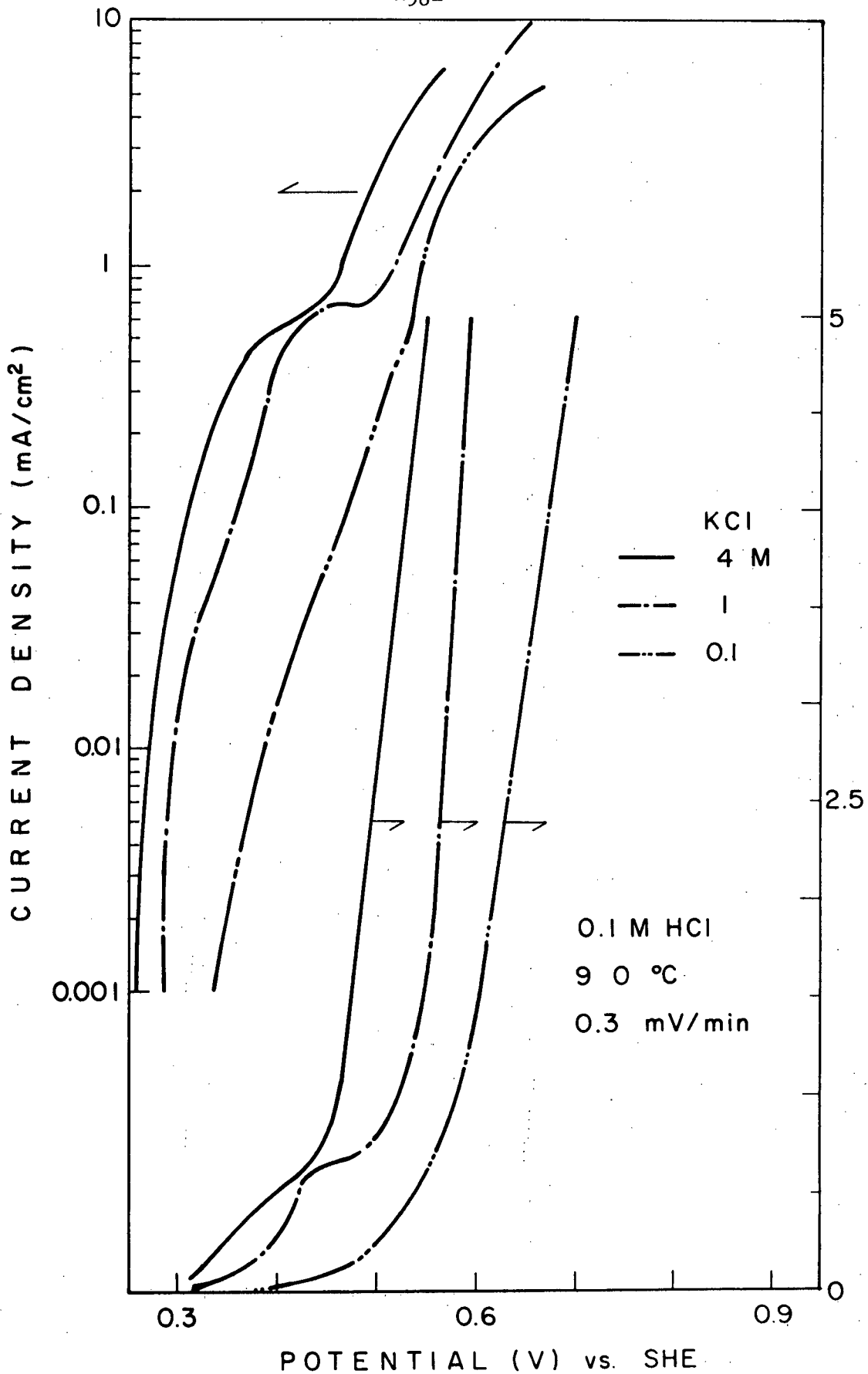


Fig. 41 Slow scans at 90°C in chloride solutions.

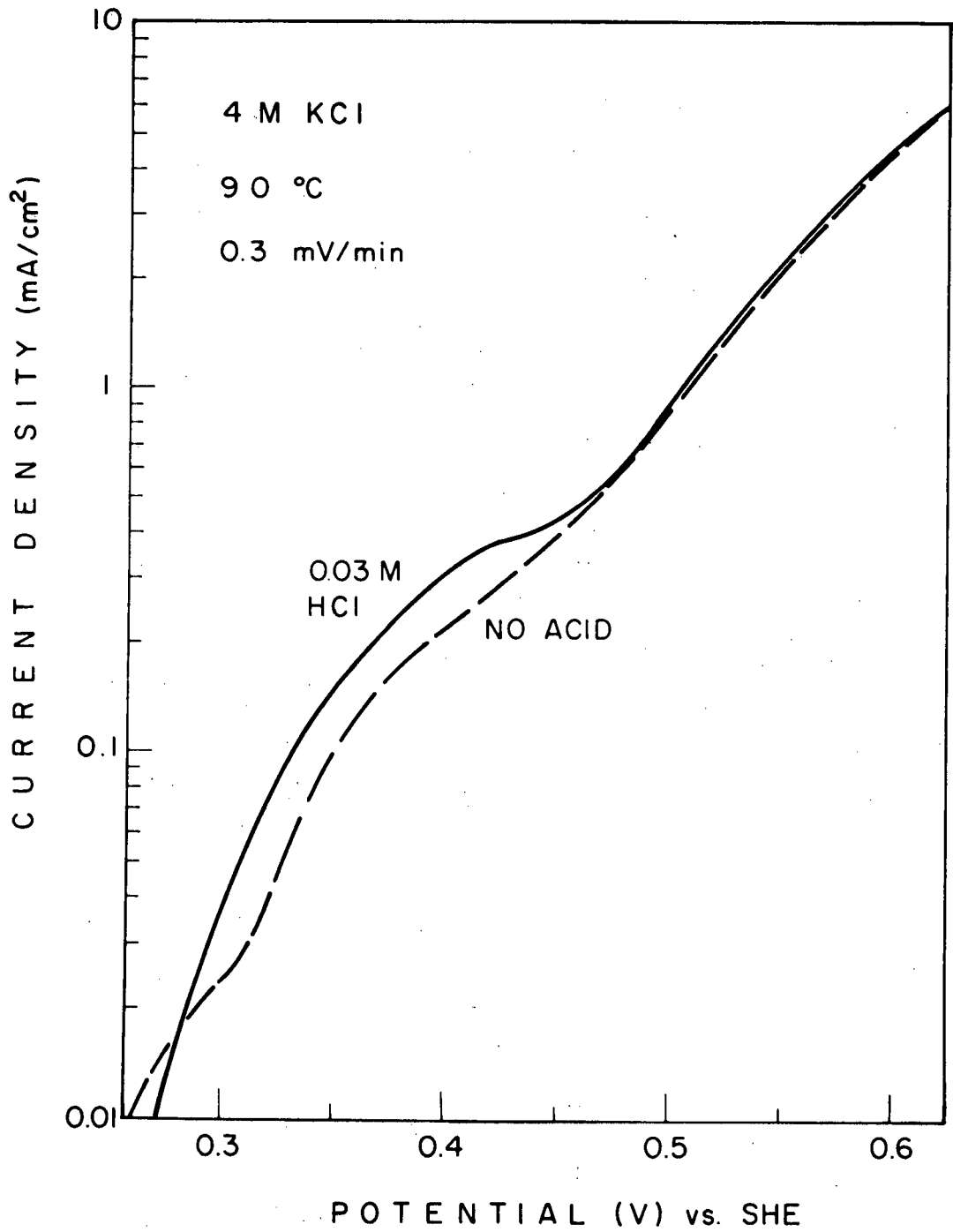


Fig. 42 Slow scans at 90°C in 4M HCl at pH 1 and pH 3.5.

TABLE VII

Successive Anodic Scans At Slow Scanning Rates

Specimen #202 & #207

Number	Temp. (°C)	Scan Rate (mV/min.)	Solution	1st Slope ($\frac{\mu\text{A}}{\text{mV}} \cdot \frac{\text{cm}^2}{\text{cm}^2}$)	Trans-ition (mV)	2nd Slope ($\frac{\mu\text{A}}{\text{mV}} \cdot \frac{\text{cm}^2}{\text{cm}^2}$)	Plateau
202-1	20°	0.3	1M HCl	0	1110	9.2	0.08 mA/cm ²
202-2	20°	0.3	0.1M HCl	0.1	985	5.7	0.02 mA/cm ²
202-3	20°	0.3	0.1M H ₂ SO ₄	0.1	935	6.4	0.02 mA/cm ²
202-4	20°	0.3	0.1M HClO ₄		885	5.2	0.015 mA/cm ²
202-5	20°	0.3	1M H ₂ SO ₄		1015	10.8	0.05 mA/cm ²
202-6	20°	0.3	1M HClO ₄		980	6.4	0.035 mA/cm ²
202-7	20°	0.3	0.2M H ₂ SO ₄ 0.8M Na ₂ SO ₄		915	5.9	0.01 mA/cm ²
202-8	20°	0.3	0.1M HCl 1.0M NaCl	0	1000	1.7	0.025 mA/cm ²
202-9	20°	0.3	0.1M HClO ₄	0	890	5.0	0.025 mA/cm ²
207-3	20	0.3	0.1M HClO ₄	0.03	920	5.9	
207-2	43	0.3	0.1M HClO ₄	0.68	965	5.9	
207-4	60	0.3	0.1M HClO ₄	1.10	1040	8.55	
207-6	90	0.3	0.1M HClO ₄	16.3	520	3.73	
					1057	48.7	
207-7	90	0.3	0.1M HCl	10.3	580	17.5	
207-8	90	0.3	1M HCl		525	32	
207-9	90	0.3	1M H ₂ SO ₄	17.3	542	decreasing	0.73 mA/cm ²

TABLE VII (Cont.)

Specimen #208 & #210

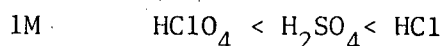
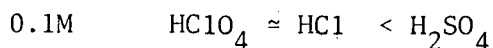
Number	Temp. (°C)	Scan Rate (mV/min.)	Solution	1st Slope ($\frac{\mu A}{mV \cdot cm^2}$)	Transition (mV)	2nd Slope ($\frac{\mu A}{mV \cdot cm^2}$)	Tafel Slope
208-1	90	0.3	1M H ₂ SO ₄	~ 3.4	650 900	0 4.0	
208-2	90	0.3	1M HCl	1.2	535	25.4	
210-1	90	0.3	1M KCl 0.1M HCl	2.4	385 510	12.0 56	~85
210-2	90	0.3	4M KCl 0.1M HCl	4.8	488	68	~85
210-3	90	0.3	1M KCl 0.1M HCl	4.8	510	74	~85
210-4	90	0.3	4M KCl 0.1M HCl	~2.5	460	45	88
210-5	90	0.3	0.1M KCl 0.1M HCl	< 1	560	34.3	88
210-6	90	0.3	0.1M Na ₂ SO ₄ 0.1M H ₂ SO ₄	.50	570	16	95
210-7	90	0.3	1M Na ₂ SO ₄ 0.1M H ₂ SO ₄	0.36	525 625 → 700 → 725	24 decreasing 0 negative	95
210-8	90	0.3	4M KCl (No acid) (pH 3.5)	0.06	525	58	~130
210-9	90	0.3	4M KCl + 0.03 HCl (pH 1.0)	0.05	528	58	~130

III Constant Potential Experiments

The main object of these experiments is to examine the chemistry of the anodic dissolution of the mineral, CuFeS_2 , as a function of potential, temperature and solution. However, a secondary aim is to observe the current/time relationship at a fixed potential; such experiments are quickly performed, if not encumbered with solution analysis.

a) Without Solution Analysis

Current decay curves at 20°C , (700 mV) in (0.1M and 1M) HCl , H_2SO_4 and HClO_4 solutions are shown in Figure 43. Amongst the 0.1M solutions, H_2SO_4 clearly gives a higher current, whereas HCl and HClO_4 are similar. Adding H_2SO_4 to the HClO_4 solution confirms this. However, for the 1M solutions, HCl gives the highest current, although in H_2SO_4 it is also increased, i.e.



In the case of HClO_4 and H_2SO_4 , the current approximately doubles from 0.1M to 1M, but for HCl it quadruples.

At 60°C (and 700 mV) the distinction between HCl and $\text{HClO}_4/\text{H}_2\text{SO}_4$ (1M) is much greater (Figure 44); the current is three times higher after three hours, and five times higher after twelve hours. This figure also shows that in HCl the current increases with time, after an initial decline, (while in HClO_4 or H_2SO_4 it continues to decline). This behaviour indicates that in HCl , the mineral is in the space-charge region under these conditions, while in HClO_4 or H_2SO_4 it is still in the diffusion region. Additions of KCl further increase the current, and again demonstrate the time-independence.

In (0.2M H₂SO₄ + 0.8M Na₂SO₄) the behaviour under the above conditions (60°C, 700 mV) is very similar to that in 1M H₂SO₄ (Figure 45).

At 90°C and 700 mV, similar differences are observed (Figure 46), between chloride and sulphate, though not as pronounced.

In Figure 47 is shown the effect of temperature on the current at 700 mV in 0.1M H₂SO₄. There is a marked difference between the increasing temperature curve and the decreasing temperature curve. Although the values are close at 20°, 30°, 60° and 90°C, there is an order of magnitude difference at 40°C. Other current/temperature curves are shown in Figures 48, 49 and activation energies were calculated:

16.9 kcal/mole	0.1M HClO ₄	
<hr/>		
14.1 kcal/mole	0.1M HClO ₄	
	0.1M KCl	700 mV
<hr/>		
14.1 kcal/mole	0.1M HClO ₄	
	1M KCl	
<hr/>		

b) Summary

At 700 mV, which is a typical potential (vs S.H.E.) one might expect in ferric leaching (E° = 770 mV), current densities (at 20°C) are similar in chloride and sulphate solutions. At 60°C, current densities are much higher in chloride than in sulphate and time independent; additions of KCl accentuate this. At 90°C, this difference is lessened, but still appreciable. An activation energy of 14.1 kcal was calculated for the current in chloride solutions at 700 mV.

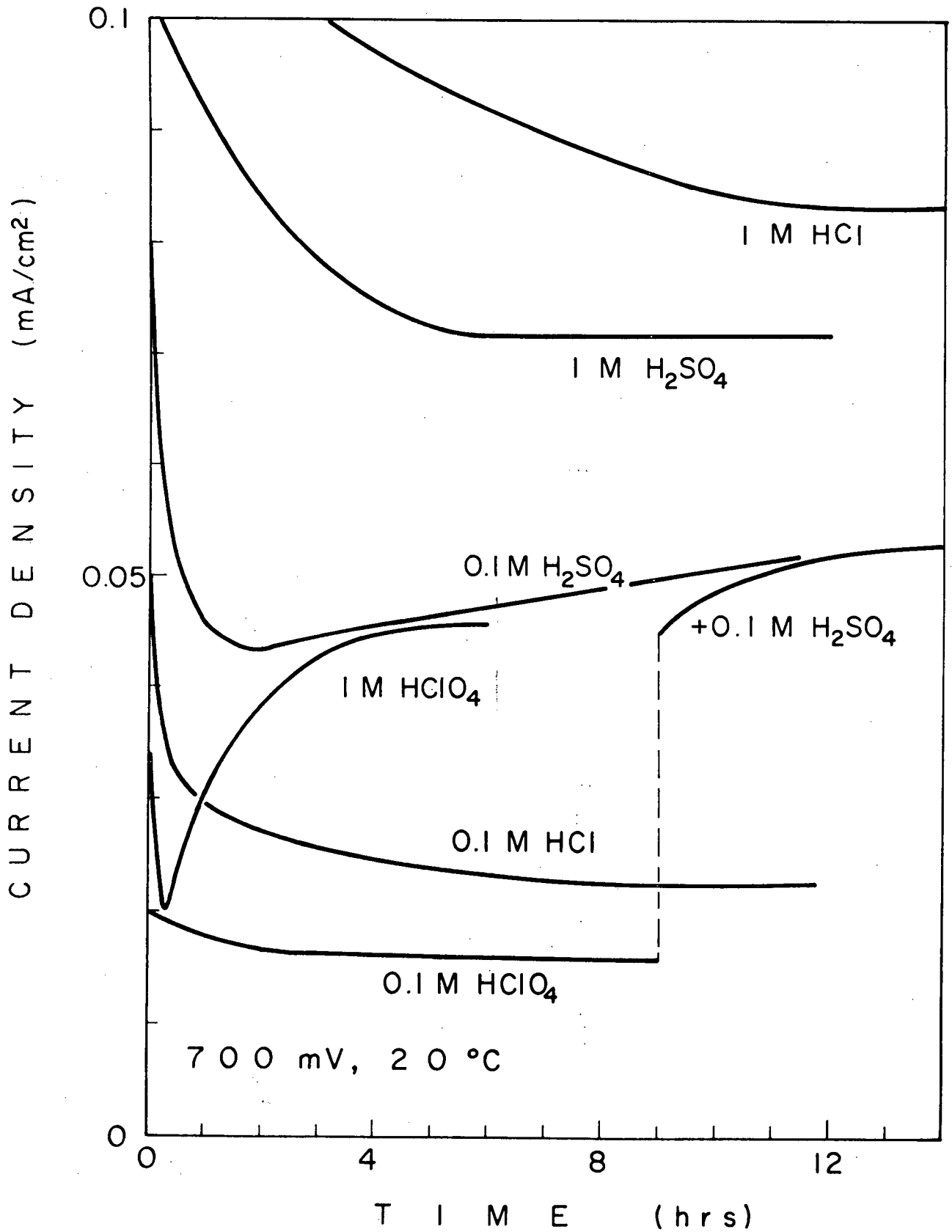


Fig. 43 Current decay at 700 mV, 20°C in various solutions.

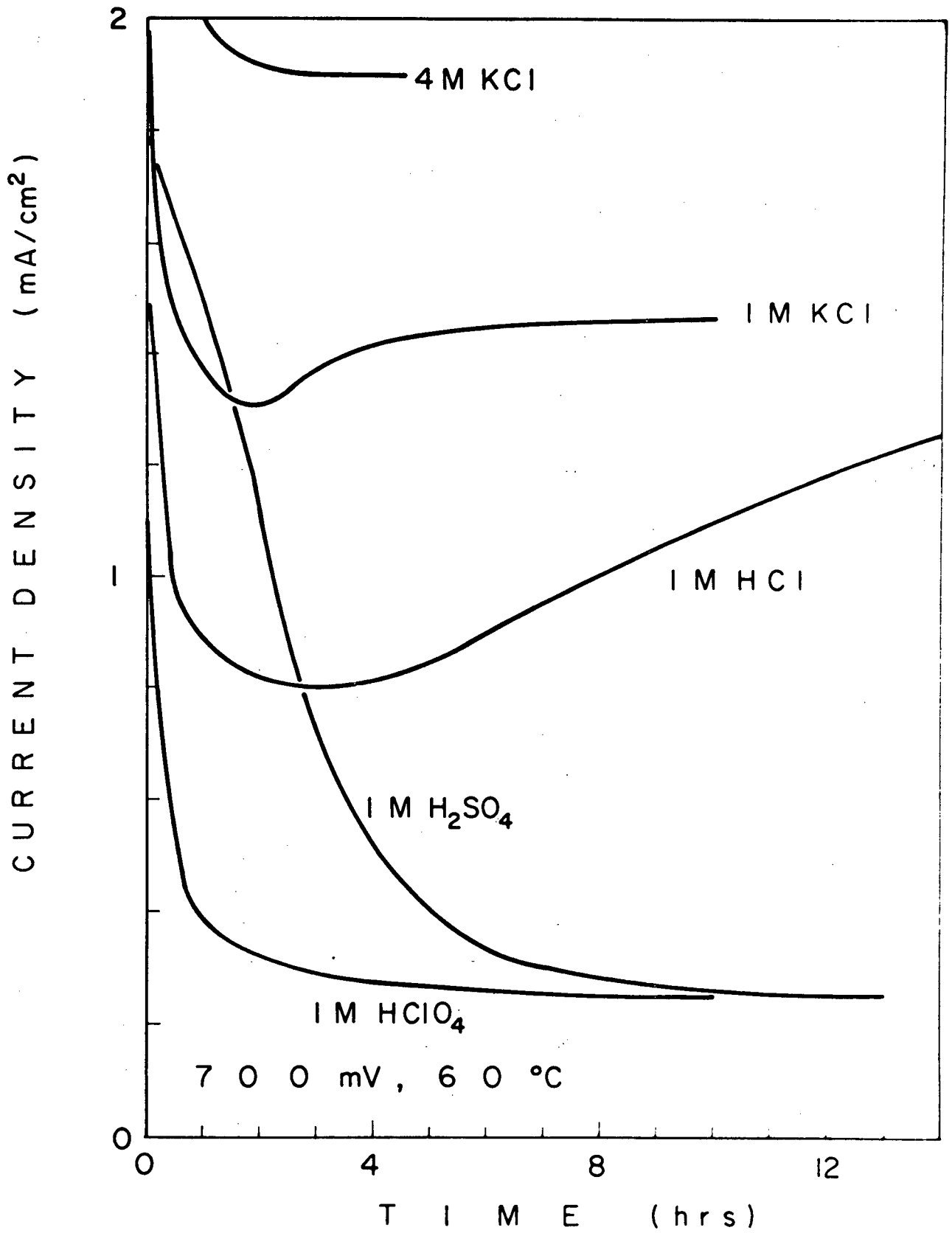


Fig. 44 Current decay at 700 mV, 60°C in various solutions.

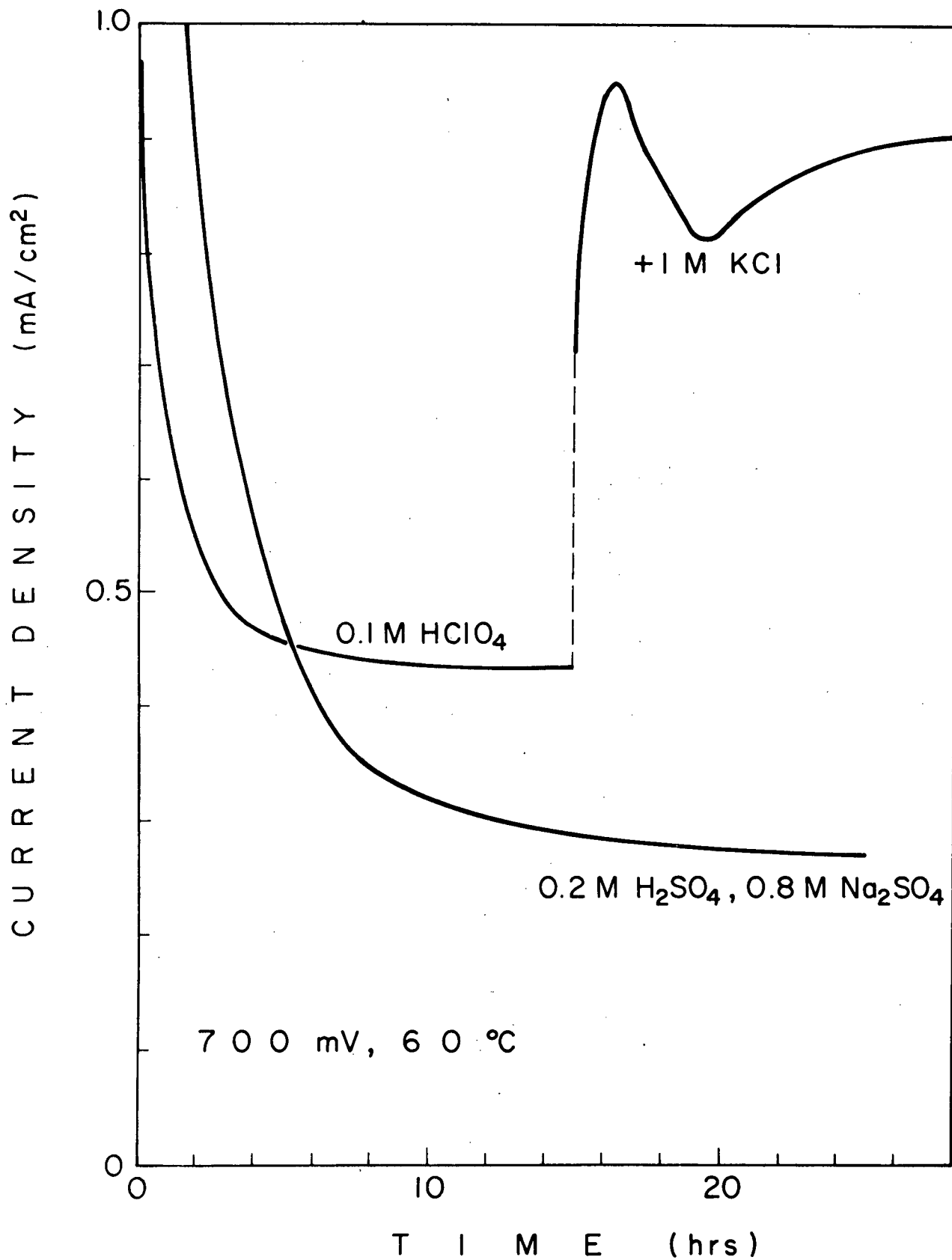


Fig. 45 Current decay at 700 mV, 60°C in various solutions.

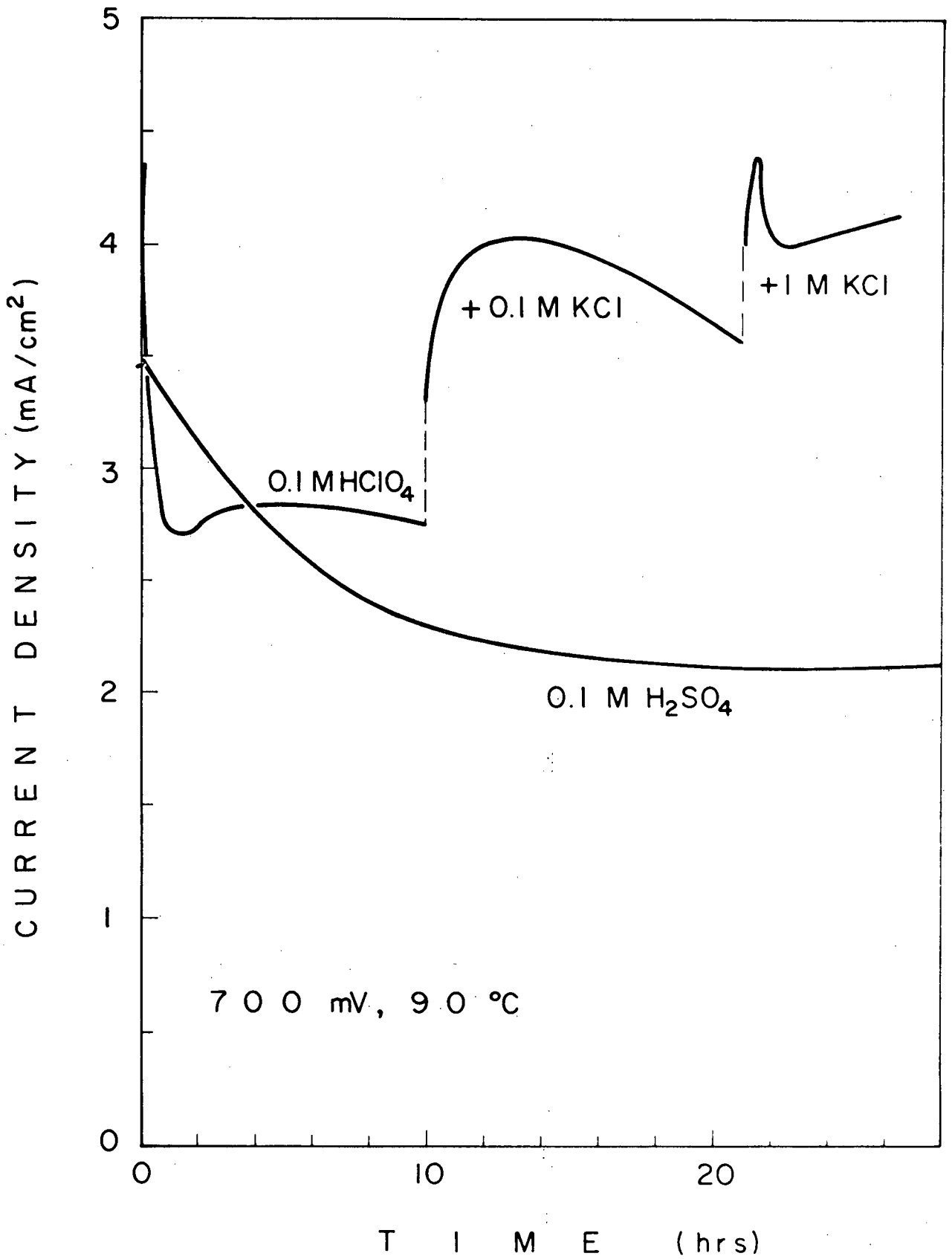


Fig. 46 Current decay at 700 mV, 90°C in various solutions.

TEMPERATURE (°C)

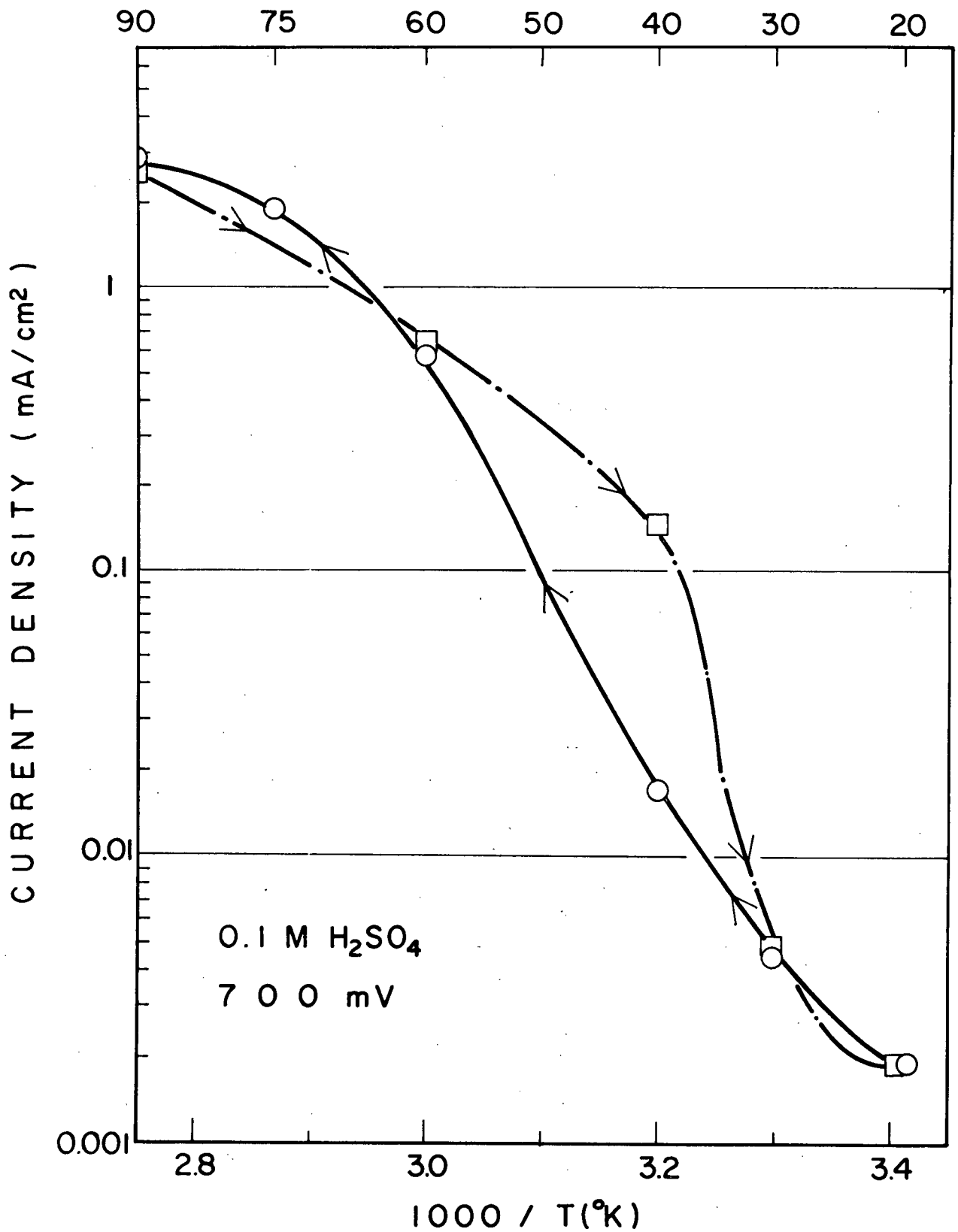


Fig. 47 Effect of temperature on current at 700 mV, in 0.1M H₂SO₄, showing hysteresis.

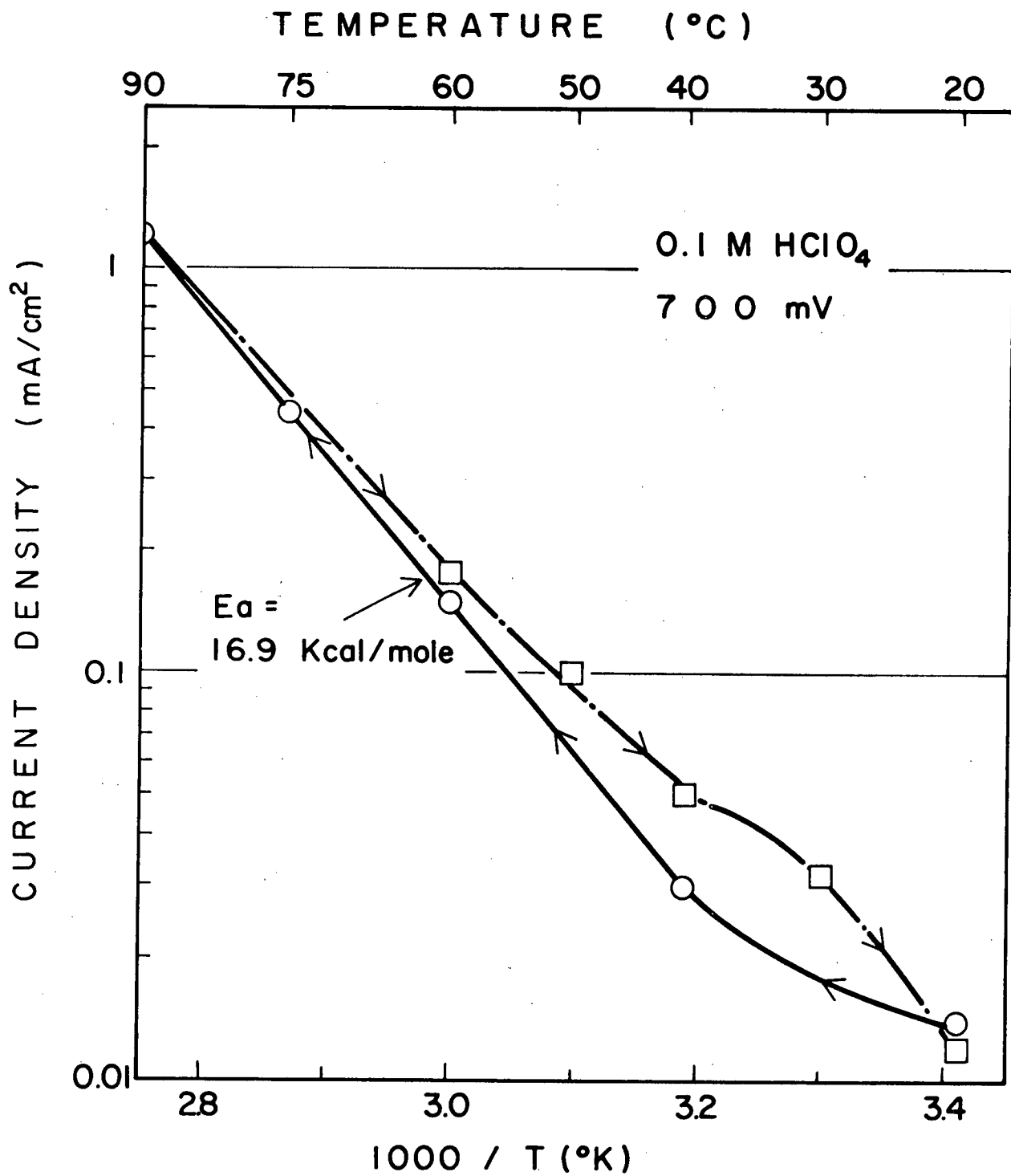


Fig. 48 Arrhenius diagram for current at 700 mV in 0.1M HClO₄.

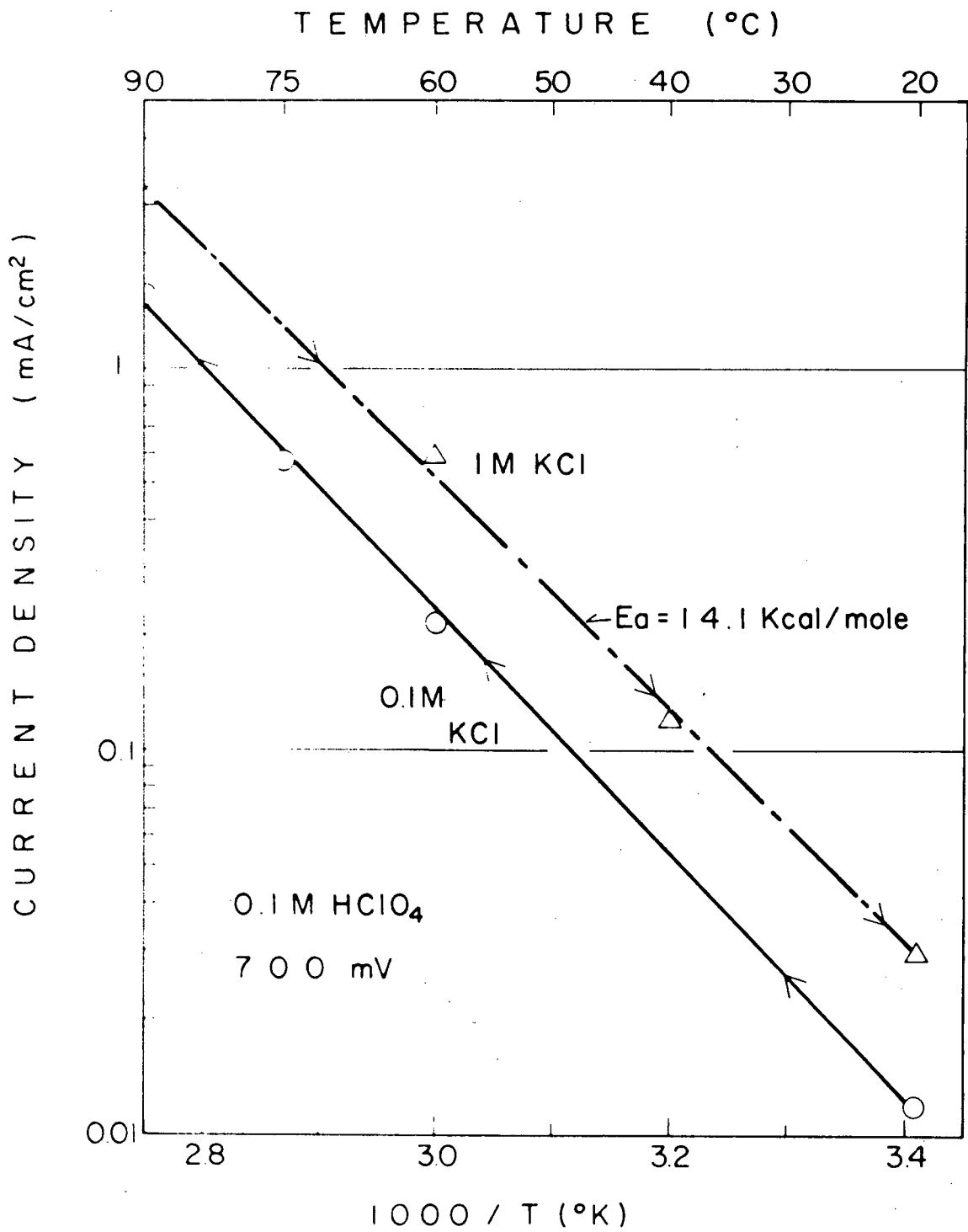
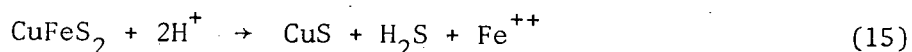


Fig. 49 Arrhenius diagram for current at 700 mV in 0.1M KCl and 1M KCl.

c) With Solution Analysis

In the preliminary experiments, Section I, the chemistry of dissolution in 0.1M HClO₄ and 0.1M H₂SO₄ was examined, primarily at high temperatures 125 → 175°C. It was found that the current efficiency for copper rarely rose above 32% and was less at low potentials. The extra current was used up in sulphur oxidation. However, the iron current efficiency was often improbably high, possibly due to the chemical dissolution of iron:



The object of the experiments in this section was to examine the chemistry of anodic dissolution, in particular in chloride and sulphate solutions at leaching temperatures (90°C). Considerable scatter was evident in some preliminary experiments, and it was evident that insufficient consideration had been given to the time dependence of the reaction. Therefore experiments are described herein which were carried out for extended periods of time, with frequent solution analysis. A new specimen was used for each experiment (at a given potential).

The meaning of the term current efficiency, as it is used in this work, has been defined in Section I. An exception to this definition is the current efficiency of iron.

To facilitate computations, the current efficiency of iron is calculated as though it were all Fe⁺⁺, and then the extra current efficiency of Fe⁺⁺⁺ present (if any) calculated at 1/3 of its actual value.

In this section sulphate produced during anodization was not determined directly, for the analytical method used in the previous section does not apply to strong chloride or sulphate solutions. Consequently total current efficiency, as used here, means total metal current efficiency:

$$\text{C.E. Total} = \text{C.E. Cu} + \text{C.E. Fe} + \text{C.E. Fe}^{3+}$$

but the real C.E. $_{Fe^{3+}}$ is three times that quoted.

The quantity $(100 - C.E._{Total})$ is a measure of C.E. $_{SO_4}$, as a first approximation.

(i) Dilute Chloride Solutions (90°C)

In Figure 50 is shown the results of anodizing separate specimens in

[0.2M HCl
0.3M NaCl] at 90°C at the following potentials:

535
635
735 mV vs. S.H.E.
935
1185

These conditions were chosen to approximate leaching in dilute chloride solutions.

The current density (C.D.) plot shows a marked increase of current with time, (for all except the lowest potential), and a steady increase of current with potential, up to 935 mV.

The current efficiency for copper (C.E. $_{Cu}$) for all potentials is 40 - 45%, after an initial period, in which it is generally lower, except for 535 mV. This plot illustrates the danger of taking only one solution analysis as was done in the preliminary experiments, for after ten hours the average C.E. $_{Cu}$ is only 30 - 35%.

For most potentials, iron current efficiencies are approximately the same as those of copper after 100 hours, (40 - 50%), but the trend is the down instead of up, and there is more scatter to the results. This plot partly explains the erratic C.E. $_{Fe}$ in Section I - iron dissolution rates are strongly time independent, in some cases.

The Fe/Cu ratio plot shows that preferential iron dissolution extends for about 50 hours, and then the ratio is close to unity; however, at 535 mV the ratio never reaches 1.0, probably because the dissolution rate is

so low, and iron current efficiencies are so high that chemical dissolution must be occurring.

The total current efficiency for all experiments is close to 90%, (after 30 hours) with the exception of the highest potential (1185), where it is 80%. Therefore sulphate production is certainly quite low, for 10% C.E. $\text{SO}_4^{=}$ requires only 3.3% sulphur oxidation.

Analysis for $[\text{Fe}^{+++}]$ or $[\text{Cu}^+]$ was not carried out in these experiments due to errors of both judgment and analysis. However, it is likely that this is not a serious omission as will be demonstrated.

(ii) Strong Chloride Solutions (90°C)

In Figure 51 are shown the results of anodizing separate specimens in $\begin{bmatrix} 3.0\text{M NaCl} \\ 0.2\text{M HCl} \end{bmatrix}$ at 90°C at the following potentials:

535 mV
635
735 (twice)
935
1085
1185

Current densities again increase markedly with potential (up to 935 mV), and time (after an initial decrease). Overall, the values are about double those obtained in dilute chloride, although the increase is greatest at lowest potential, 535 mV.

Copper current efficiencies are again in the 40 - 45% range (lower at the start) except for the 535 and 635 mV experiments, where it is 50 - 60%. $[\text{Cu}^+]$ analysis was carried out only on one experiment (P-36) at 535 mV, and a constant percentage 12.5% (+ 1.5%) of the total Cu was found to be Cu^+ . This, however, is only a small correction to the copper current efficiency, which is decreased from 61% to 57%. For higher potentials therefore, the formation of Cu as Cu^+ is likely to be negligible.

Iron current efficiencies were similarly 40 - 50%, except at low potentials; total current efficiencies were mostly near 90% , but rose to near 120% for 535 and 635 mV.

Fe/Cu ratios were close to 1.0 eventually, and again were higher at the beginning. $[\text{Fe}^{+++}]$ was determined for the high potential experiments, and found to be 10 - 20% of the total iron.

The high current efficiencies found at low potentials are probably caused by the chemical dissolution of iron (equation 15).

At high potentials, the electrodes developed a peculiar oscillating behaviour after a certain time (a couple of days). This is illustrated in Figure 52. It was found that this was quite reproducible; the height of the oscillations depended upon potential (935 mV being a threshold), whereas the frequency depended on temperature (80°C being a threshold).

This behaviour was not observed at the beginning of the experiment, however. Once established, though, it appeared to go on indefinitely, (for the life of the specimen).

No satisfactory explanation of this phenomenon can be advanced at this time; it seems appropriate nevertheless to record the observation in the hope that it may prove useful at some later date. It is possible, however, that sulphur chloride, S_2Cl_2 , is being formed under these conditions.

(iii) Sulphate Solutions (90°C)

The previous experiments in chloride solution were repeated with

[0.4M Na_2SO_4]
[0.1M H_2SO_4] :

535	mV
635	
735	(4 times)
935	
1185	

as shown in Figure 53.

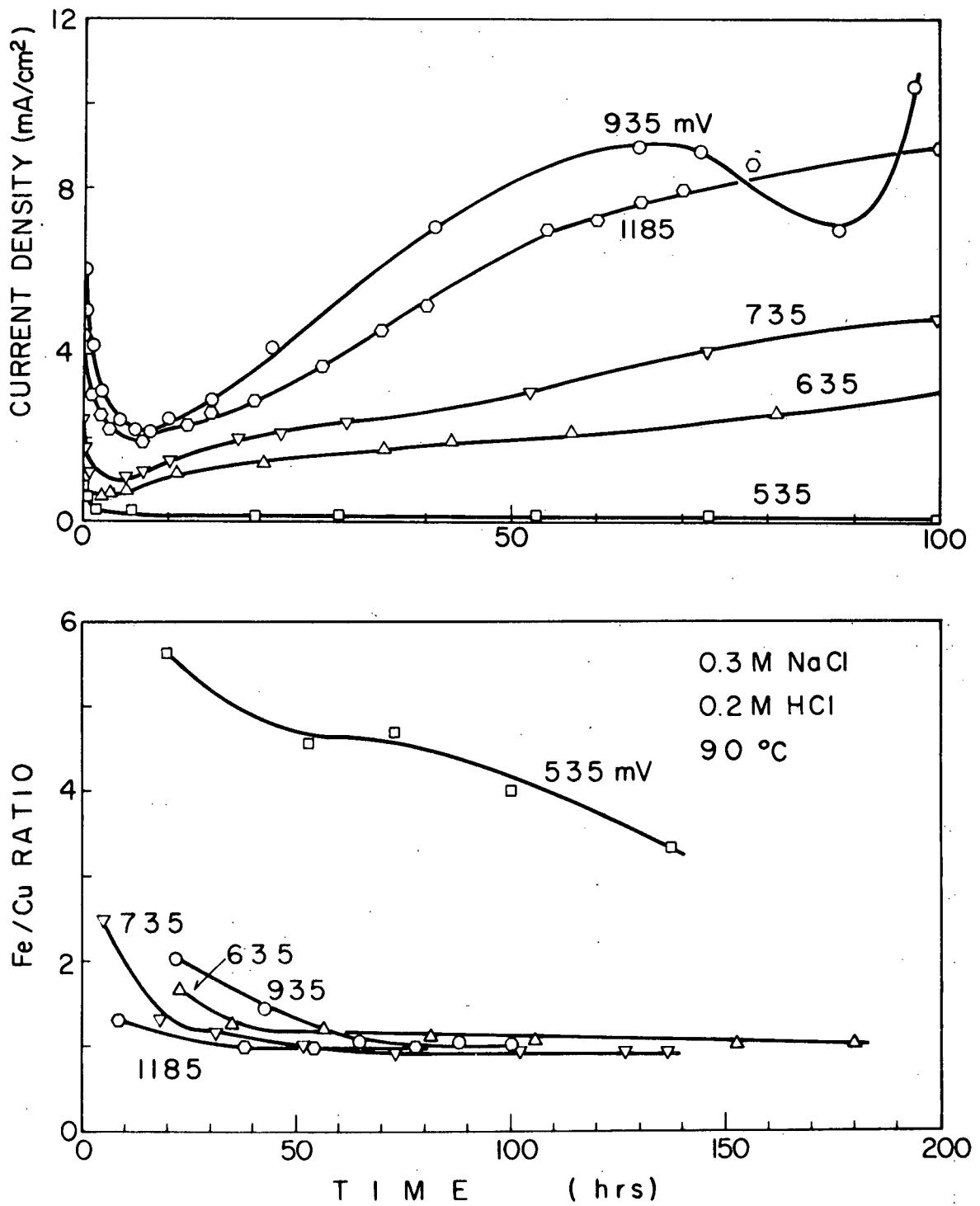


Fig. 50 Constant potential experiments in 0.3M NaCl, 0.2M HCl at 90°C, and various potentials.

(a),(b) Current density and Fe/Cu ratio.

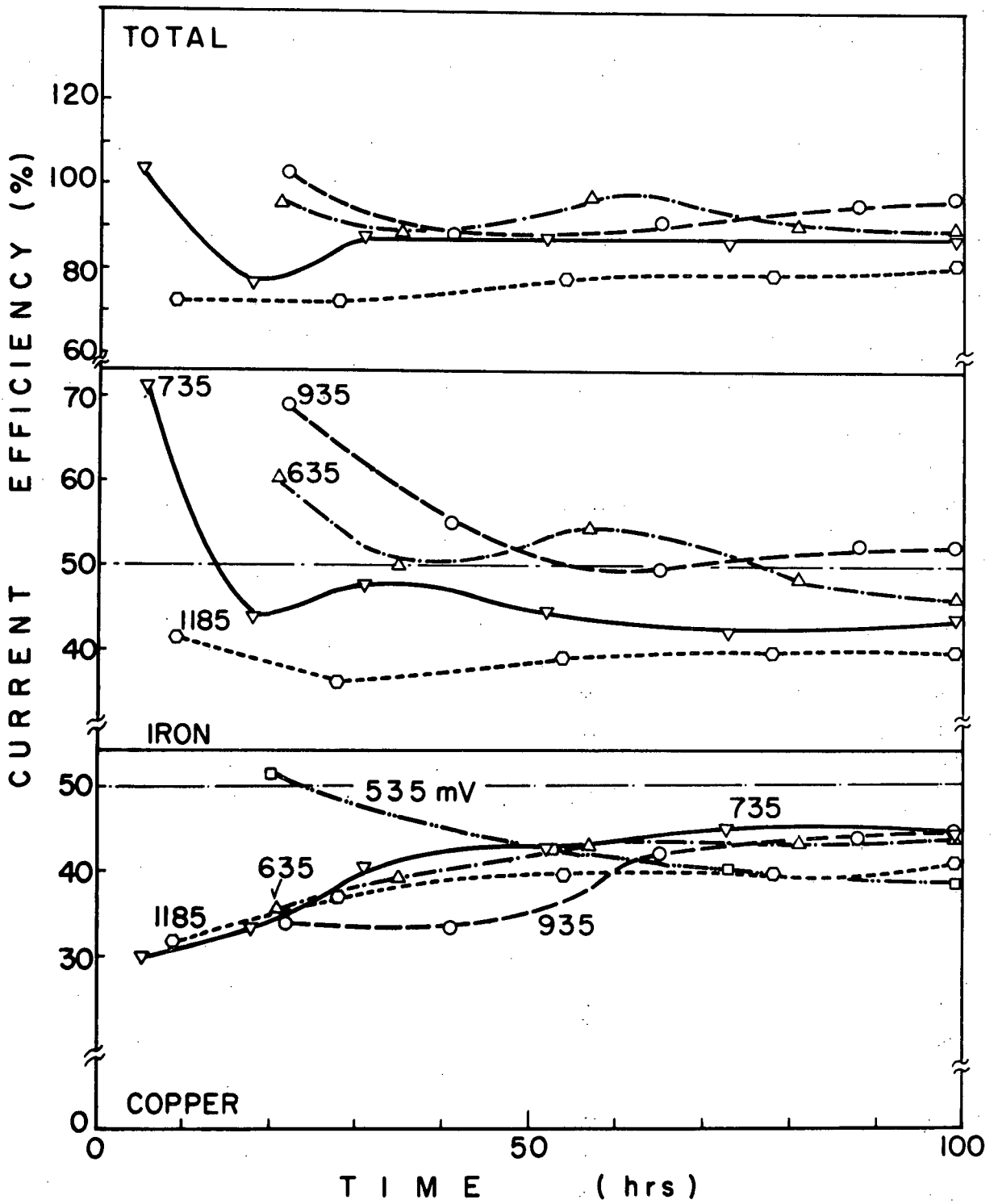


Fig. 50 (c), (d), (e) Current efficiency.

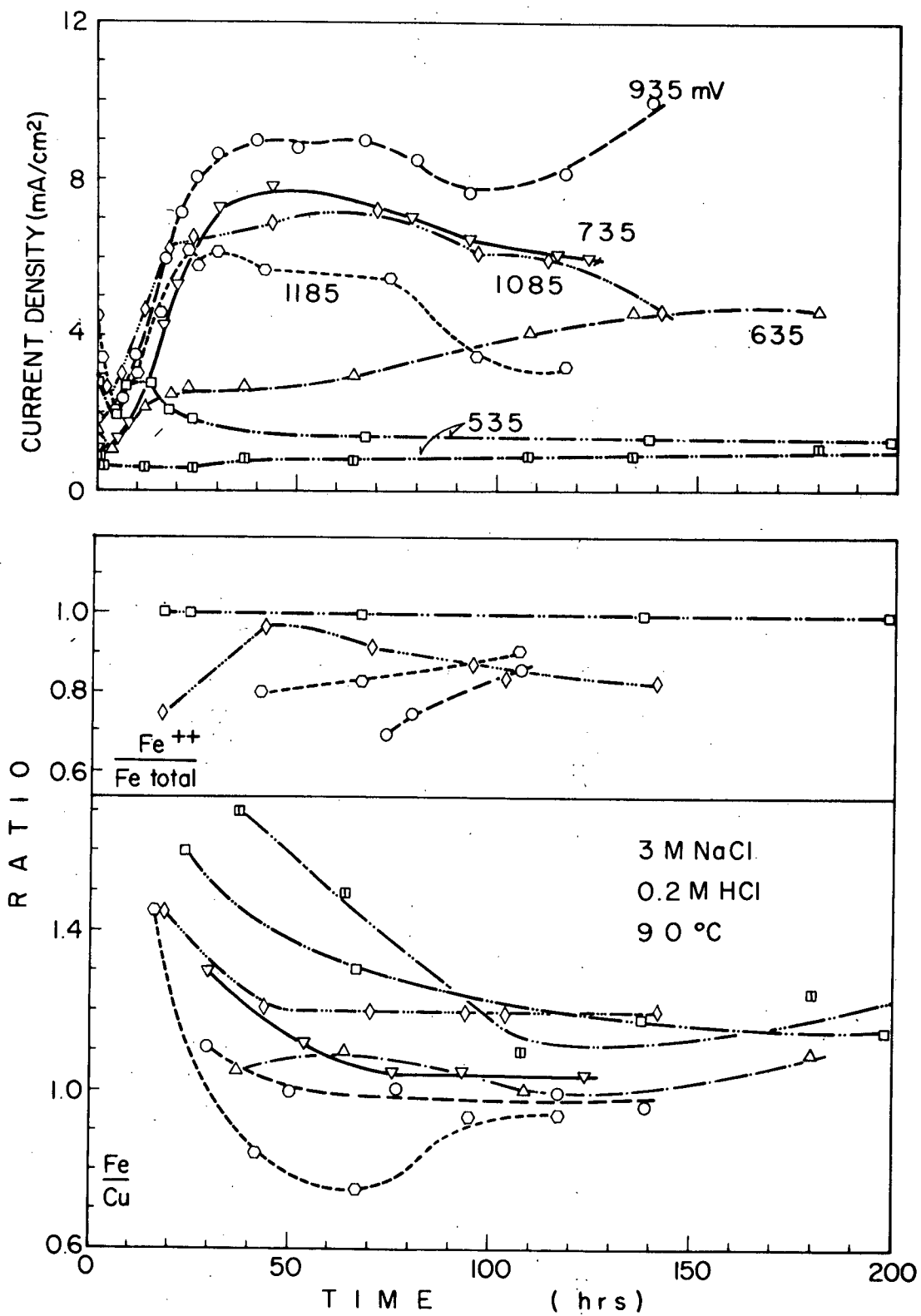


Fig. 51 Constant potential experiments in 3.0M NaCl, 0.2M HCl at 90°C, and various potentials.

(a),(b),(c) Current density and ratios.

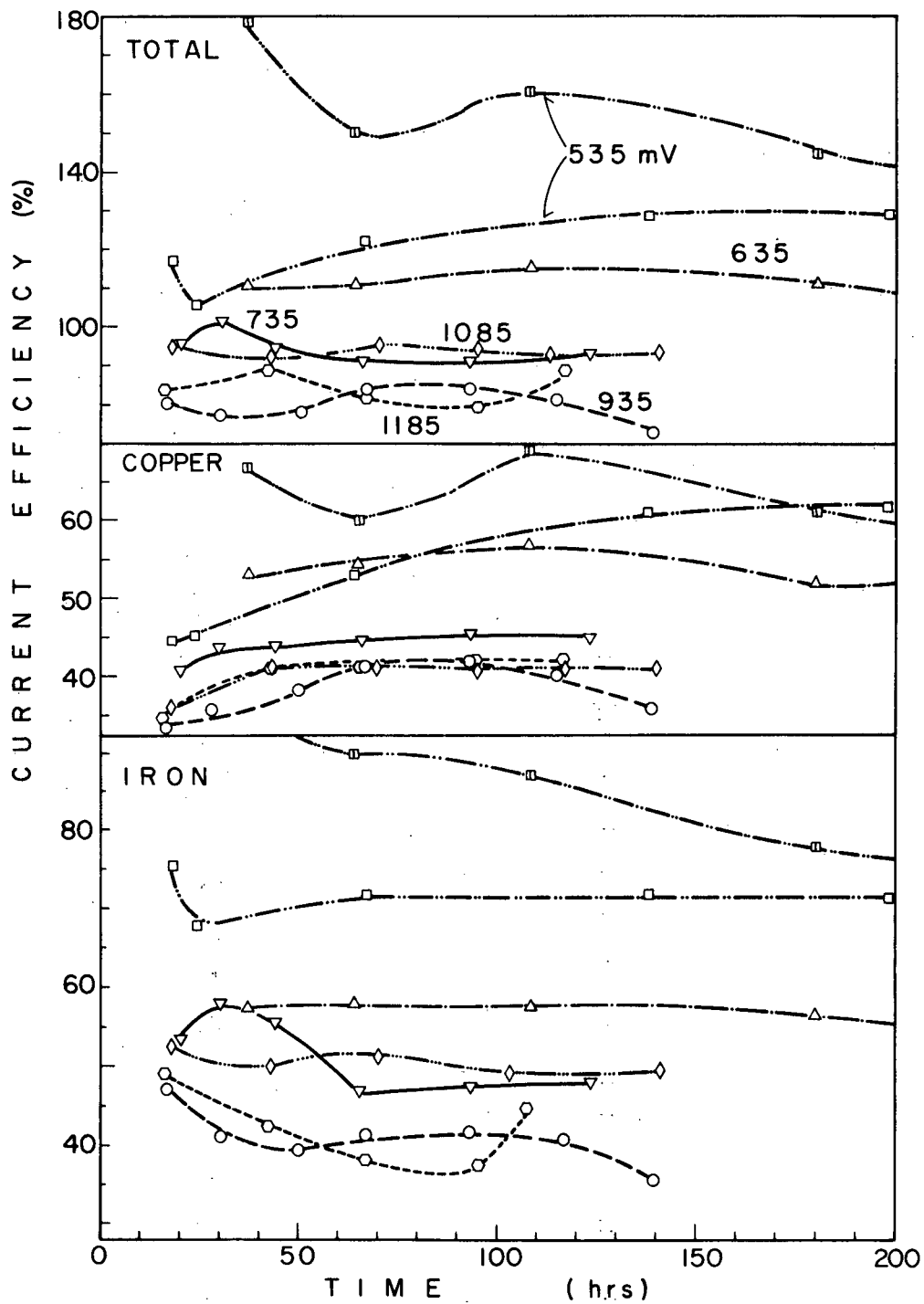


Fig. 51 (d), (e), (f) Current efficiency.

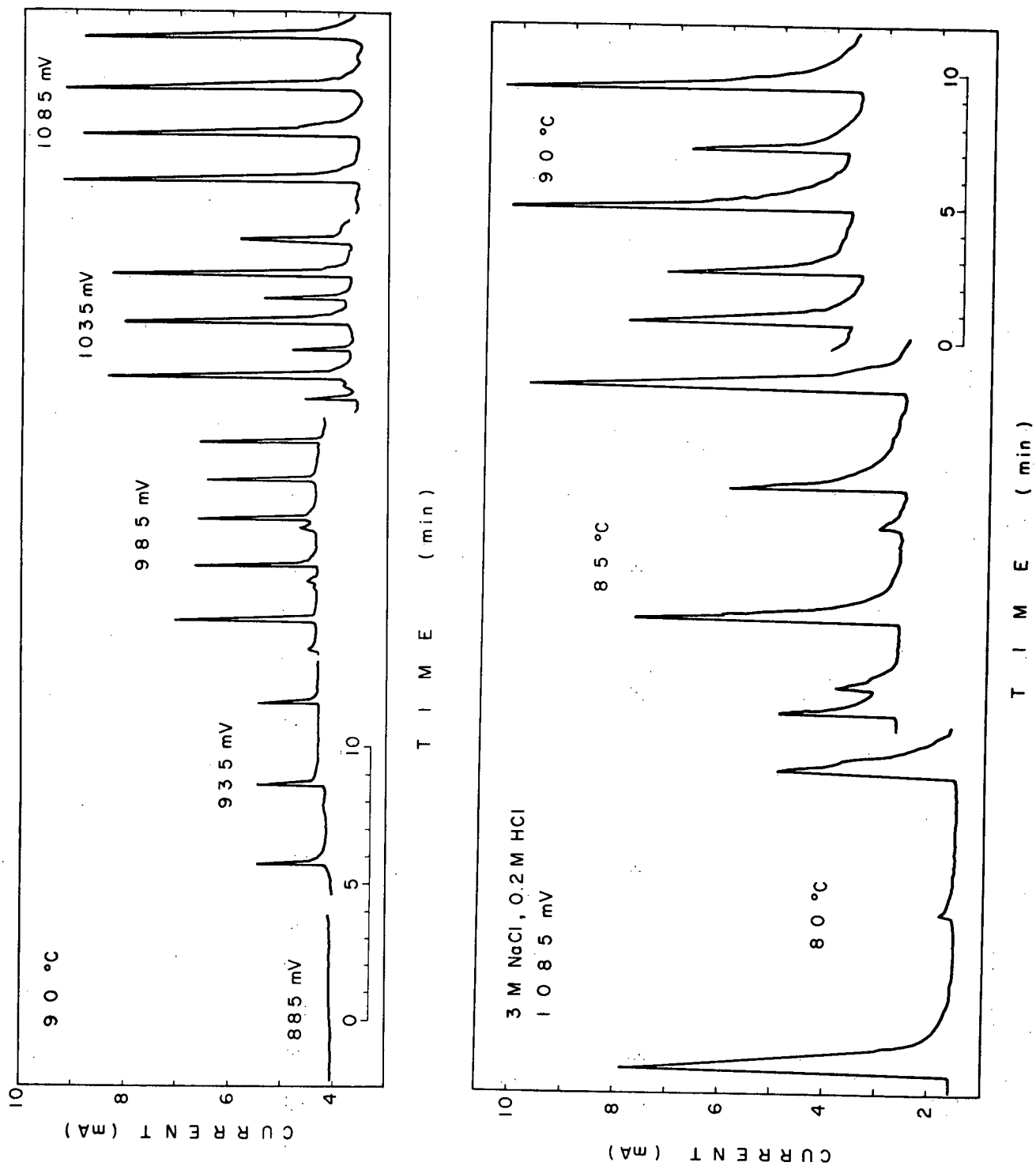


Fig. 52 Current oscillations produced after several hours at 900 mV, 90°C in 3M NaCl, 0.2M HCl. Effect of temperature and potential.

Current densities were generally lower than in chloride solutions, particularly at lower potentials, and decrease slightly with time. An exception to this rule was found in one experiment at 735 mV which increased with time. This was therefore repeated three times. The result was inconclusive - in two experiments (P 18, P30) the current went up, and in the other two (P 31, P 26) it went down (Figure 54).

735 mV appears to be a threshold value for the current density:

<u>mV</u>	<u>C.D.</u> (after 70 hours) (mA/cm ²)
535	0.2
635	0.4
735	0.4; 1.9; 1.8; 0.5
935	1.9
1185	4.5

In contrast, in chloride solution, the current increased steadily from 535 to 935, and then levelled off.

Copper current efficiencies were near 27% except for the lowest potentials:

<u>Potential</u>	<u>C.E.</u> _{Cu}
535 mV	11.5 %
635	19.5
735	29, 26, 27, 20
935	29
1185	26

These results confirm those in the preliminary experiments, Section I. The values are also relatively constant over the length of the experiment.

In contrast, the iron current efficiency showed a very strong time-dependence. This was shown to be partly due to chemical dissolution of

of iron, for 'blank' runs were carried out in some experiments, before the start, i.e. the specimens were held in the solution, with no applied potential, until iron dissolution stopped (usually about two days). This iron was then subtracted from the total in solution, and separately plotted. as "after subtracting blank".

This greatly reduced the time-dependence of $C.E._{Fe}$, which can be seen as about 25%.

The Fe/Cu ratio, greater than 1.0 at the start, declined steadily towards that value. After subtracting blank, values of about 0.8 were obtained.

Considerable Fe^{+++} dissolved, and Fe^{++}/Fe_T values were about 0.8. However, no Fe^{+++} dissolved in the blank runs, and initial Fe^{++}/Fe_T values after subtracting blank were often quite low: 0.1 → 0.4.

This means that 60 -90% of the iron dissolved, as Fe^{+++} , initially, e.g. P 21 Experiment (635 mV) averaged about 65% Fe as Fe^{+++} .

Total current efficiency plots, reflecting the complex iron behaviour, show considerable scatter; after 100 hours a mean value of about 70% is evident, except for low potentials where the amount of dissolution is still low. After subtracting the blank, 50 -60% total current efficiency is obtained near the start.

The 735 mV experiment was carried out four times, as mentioned, to determine the reproducibility, using a fresh specimen each time (Figure 54). The current densities, as noted, varied considerably as did the iron current efficiencies (16 - 36% after 150 hours); but the Cu and Fe^{3+} current efficiencies were quite reproducible (28% and 5% respectively). The Fe/Cu ratio was generally above 1.0, but fell below it after a sufficiently long time (100 - 200 hours) or after subtracting the blank.

The $\text{Fe}^{++}/\text{Fe}_T$ ratio varied greatly (0.5 - 0.85), but in any case showed that significant Fe^{+++} was produced. The total current efficiency showed an interesting correlation with current density and $\text{Fe}^{++}/\text{Fe}_T$:

Experiment	C.D.	C.E. Total	$\text{Fe}^{++}/\text{Fe}_T$
P18	1.6 → 3.1	90 → 72	.70 → .80
P30	1.3 → 2.4	110 → 87	.82 → .84
P31	0.4 → 0.7	78 → 53	.52 → .60
P26	0.6 → 0.5	80 → 50	.75 → .73
P26 (A.S.B.)		77 → 44	.10 → .65

Thus a high C.D. is associated with high C.E. and low fraction of Fe dissolved as Fe^{+++} .

(iv) Sulphate/Bisulphate Solutions (125°C)

The experiment described above viz. 735 mV, 90°C, $\begin{matrix} 0.4\text{M Na}_2\text{SO}_4 \\ 0.1\text{M H}_2\text{SO}_4 \end{matrix}$ were repeated three times at 125°C (P 22, 27, 28) in similar solutions. It was also repeated at 125°C in bisulphate, i.e. $\begin{matrix} 0.4\text{M NaHSO}_4 \\ 0.1\text{M H}_2\text{SO}_4 \end{matrix}$ (P 29); at the end of this experiment, the solution was changed, back to sulphate again (P 29A). The results are shown in Figure 55.

Again there is a fair range of current densities from one experiment to another. Of the three sulphate experiments, one increased sharply (100%), one decreased (35%) and the last stayed fairly level. On the average, the current density at 125°C (and 735 mV) was about double that at 90°C ($\sim 2.5 \text{ mA/cm}^2$ vs. $\sim 1.2 \text{ mA/cm}^2$).

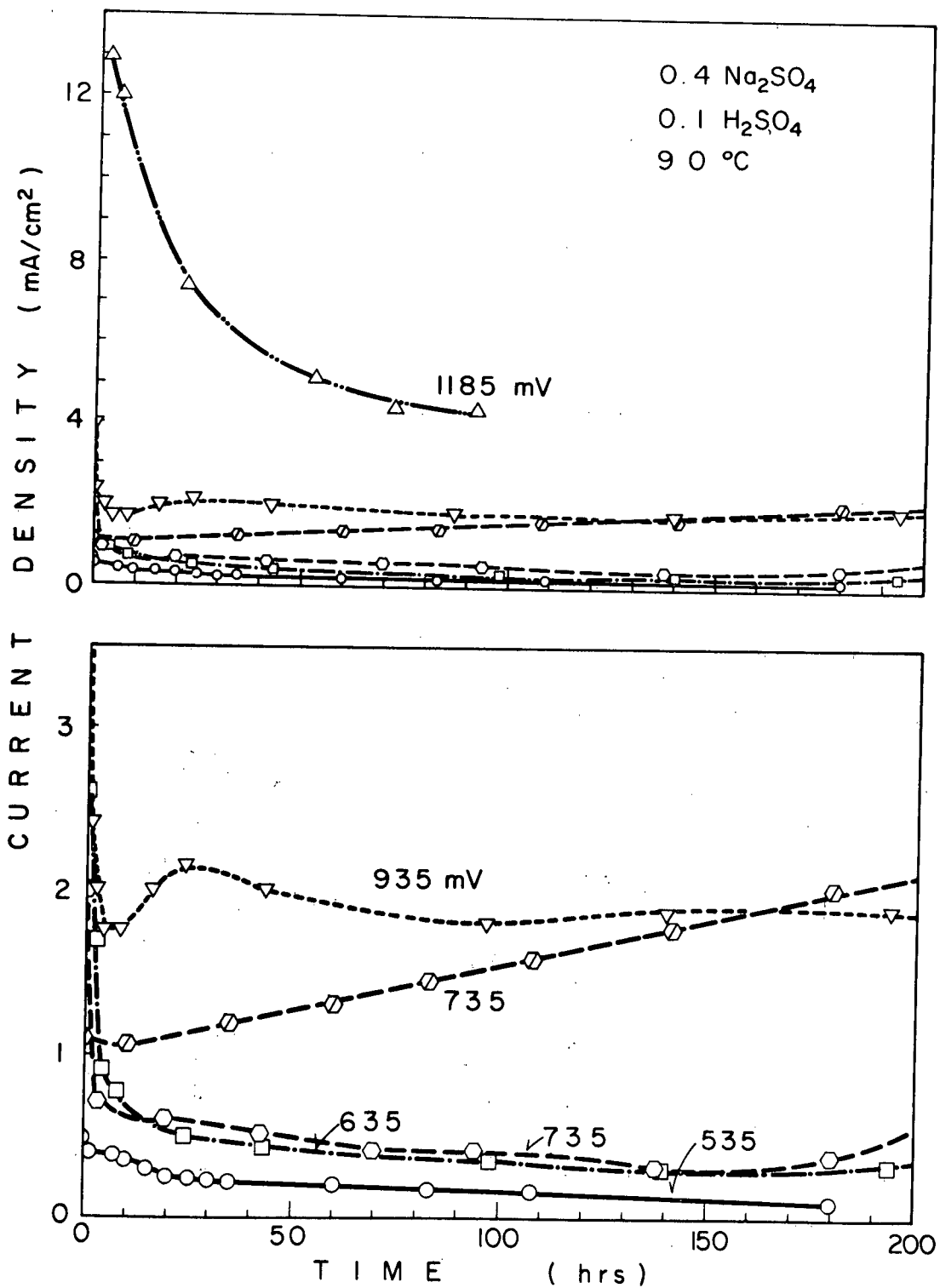


Fig. 53 Constant potential experiments in 0.4M Na₂SO₄, 0.1M H₂SO₄ at 90°C, and various potentials.
(a), (b) Current density.

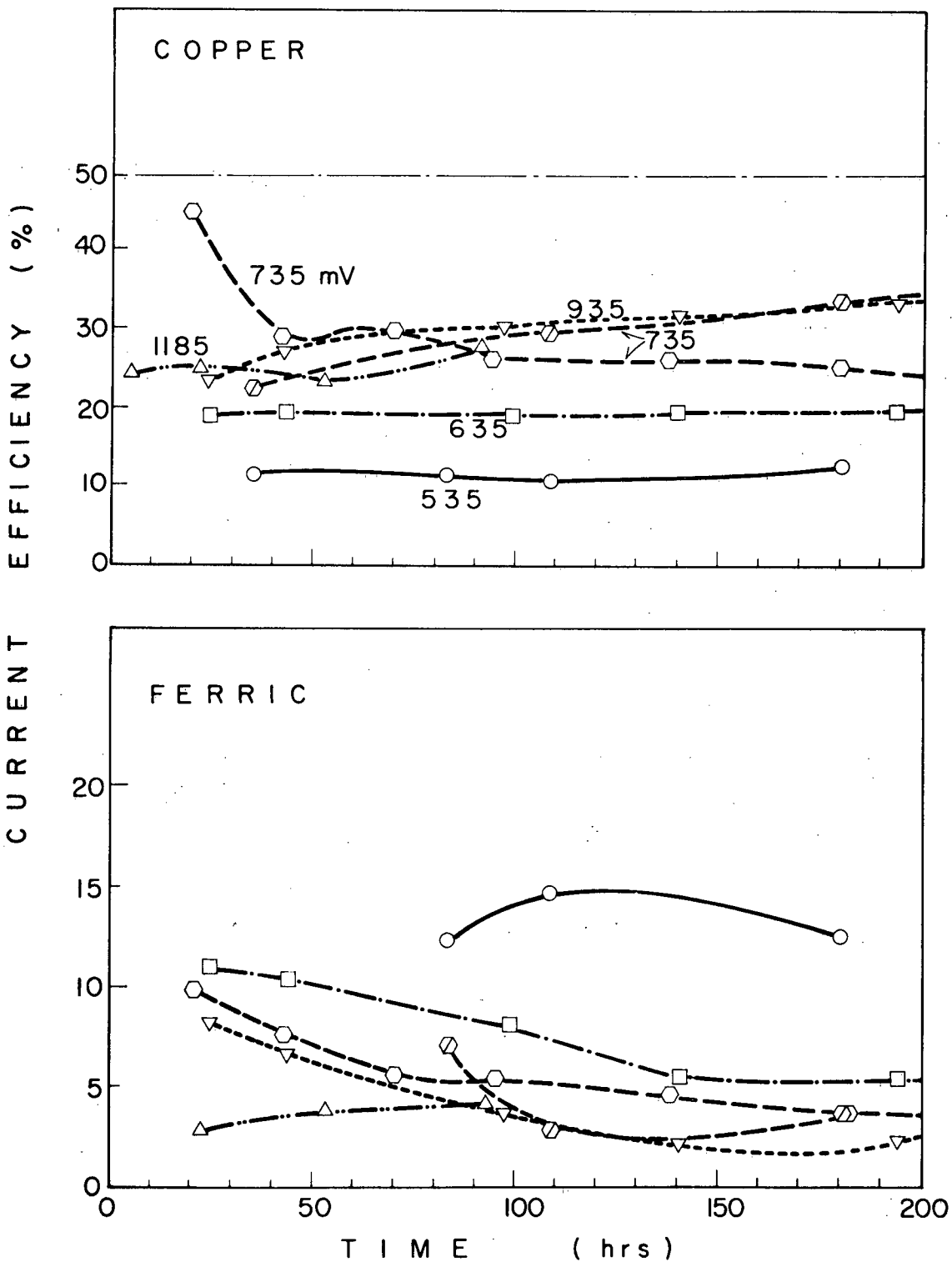


Fig. 53 (c) Copper current efficiency.
(d) Ferric ion current efficiency.

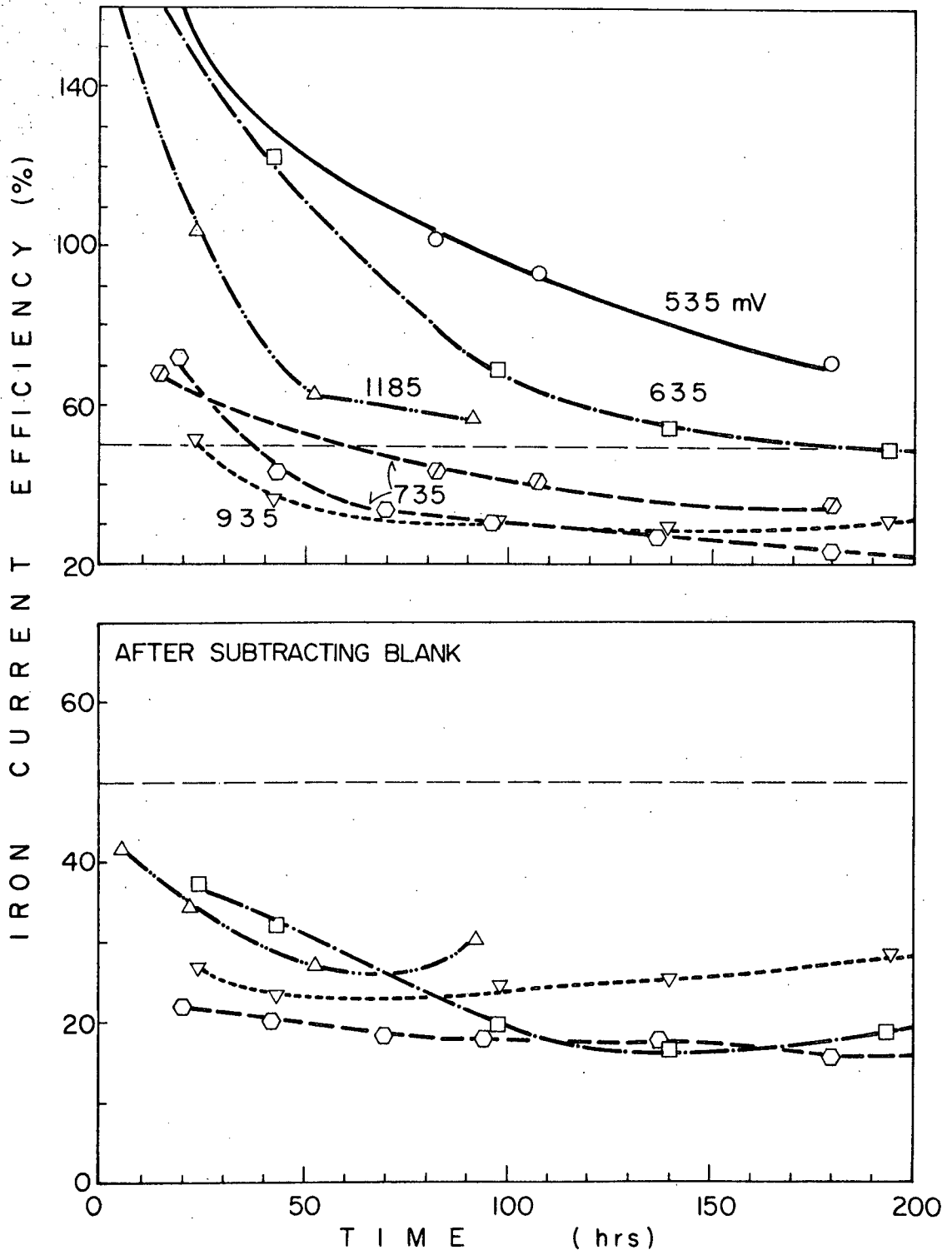


Fig. 53 (e) Iron current efficiency.
(f) Iron current efficiency after subtracting blank.

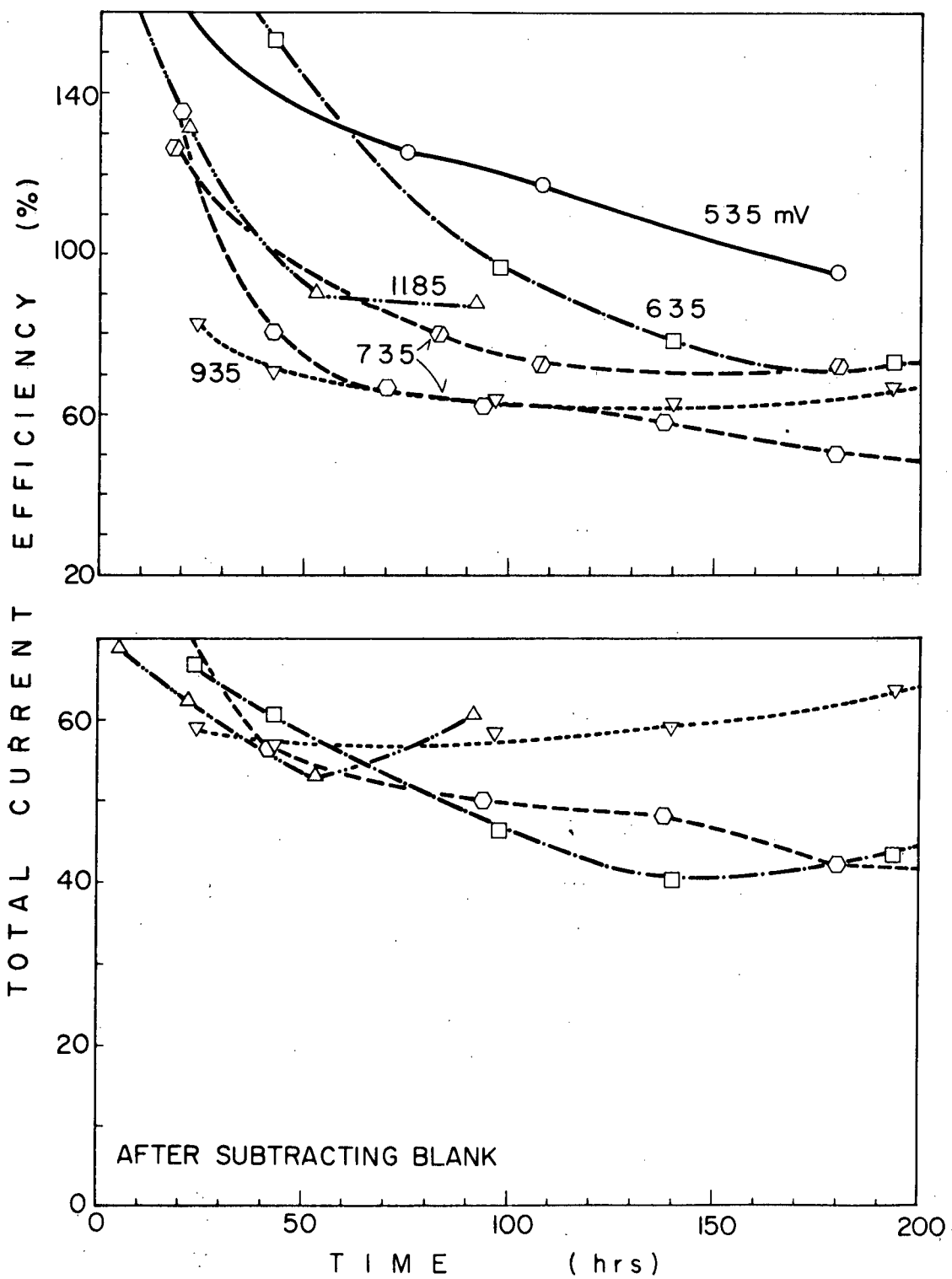


Fig. 53 (g) Total current efficiency.
(h) Total current efficiency after subtracting blank.

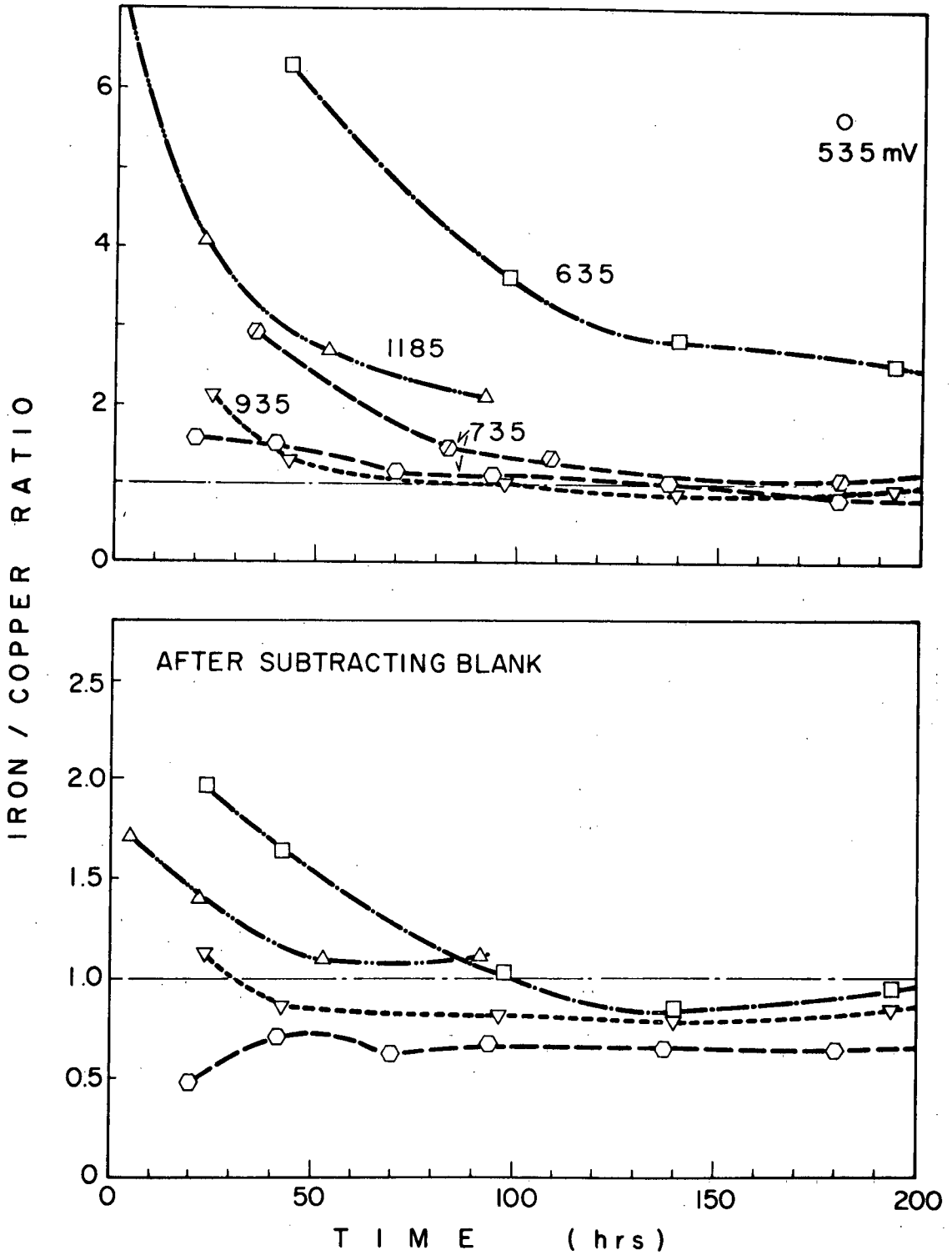


Fig. 53 (i) Fe/Cu ratio.
(j) Fe/Cu ratio after subtracting blank.

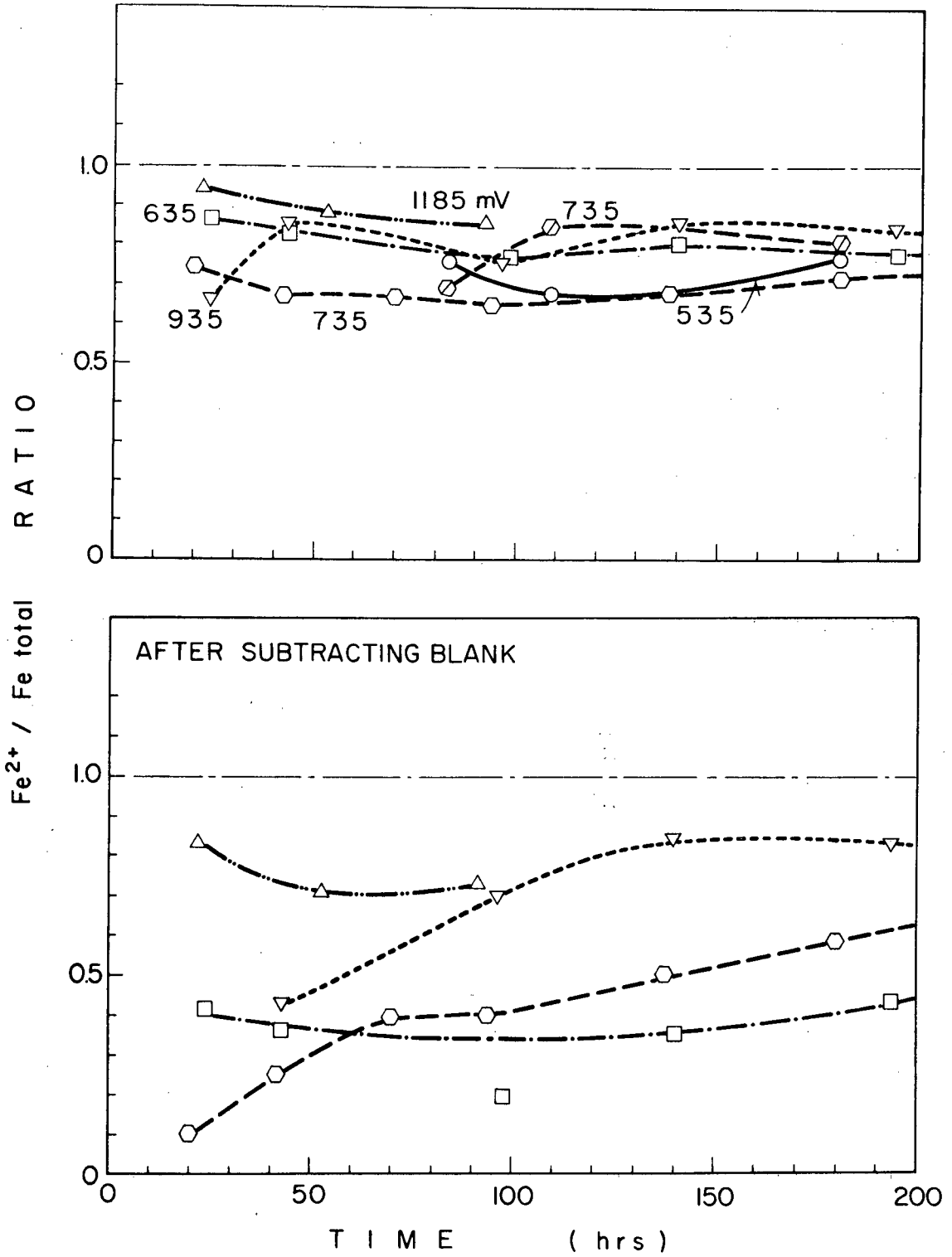


Fig. 53 (k) $\text{Fe}^{++} / \text{Fe}_{\text{Total}}$ ratio.
(l) $\text{Fe}^{++} / \text{Fe}_{\text{Total}}$ ratio after subtracting blank.

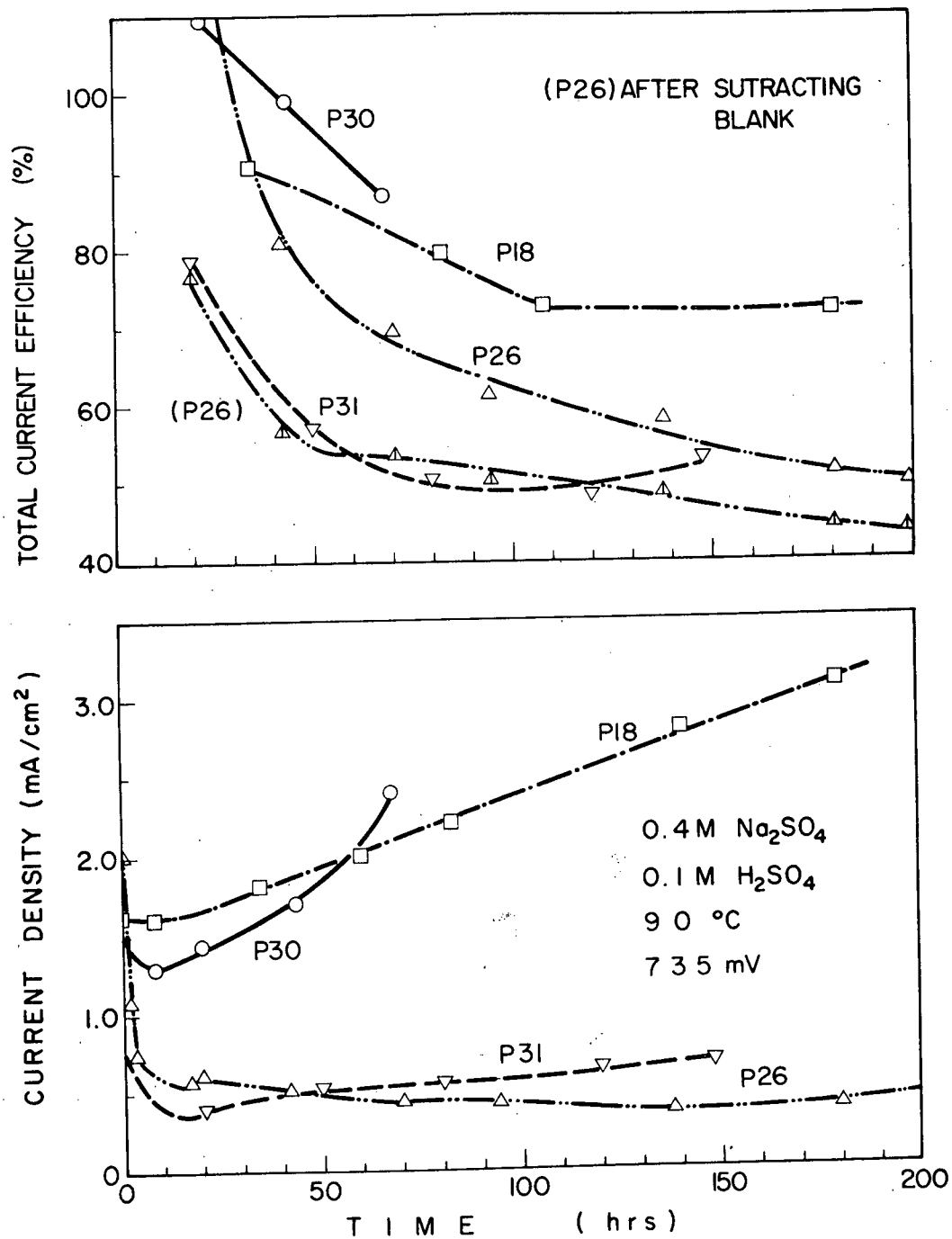


Fig. 54 Constant potential experiments in 0.3M Na₂SO₄, 0.2M H₂SO₄ at 90°C and 735 mV; various specimens.
(a) Current density.
(b) Total current efficiency.

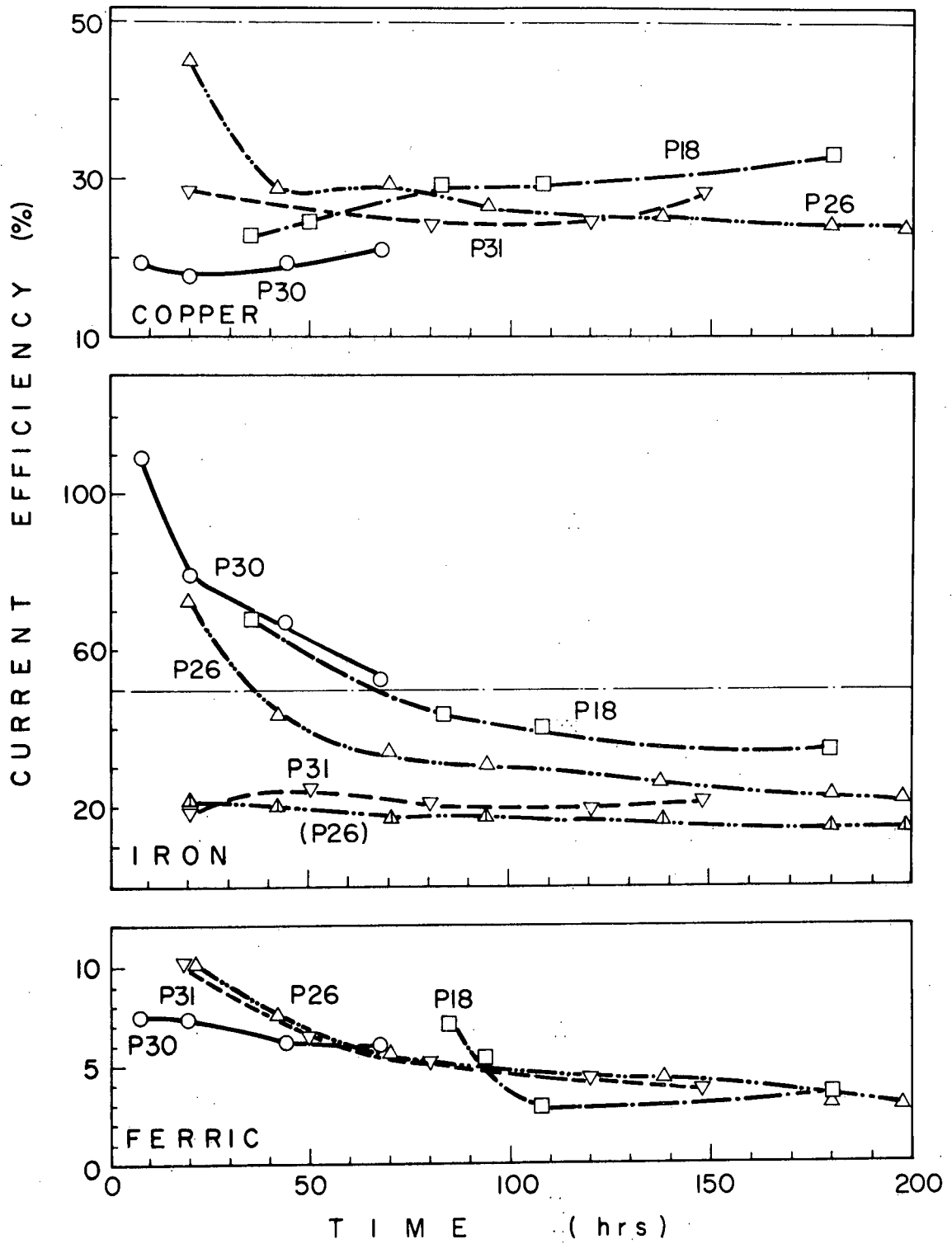


Fig. 54 (c) Copper current efficiency.
(d) Iron current efficiency.
(e) Ferric ion current efficiency.

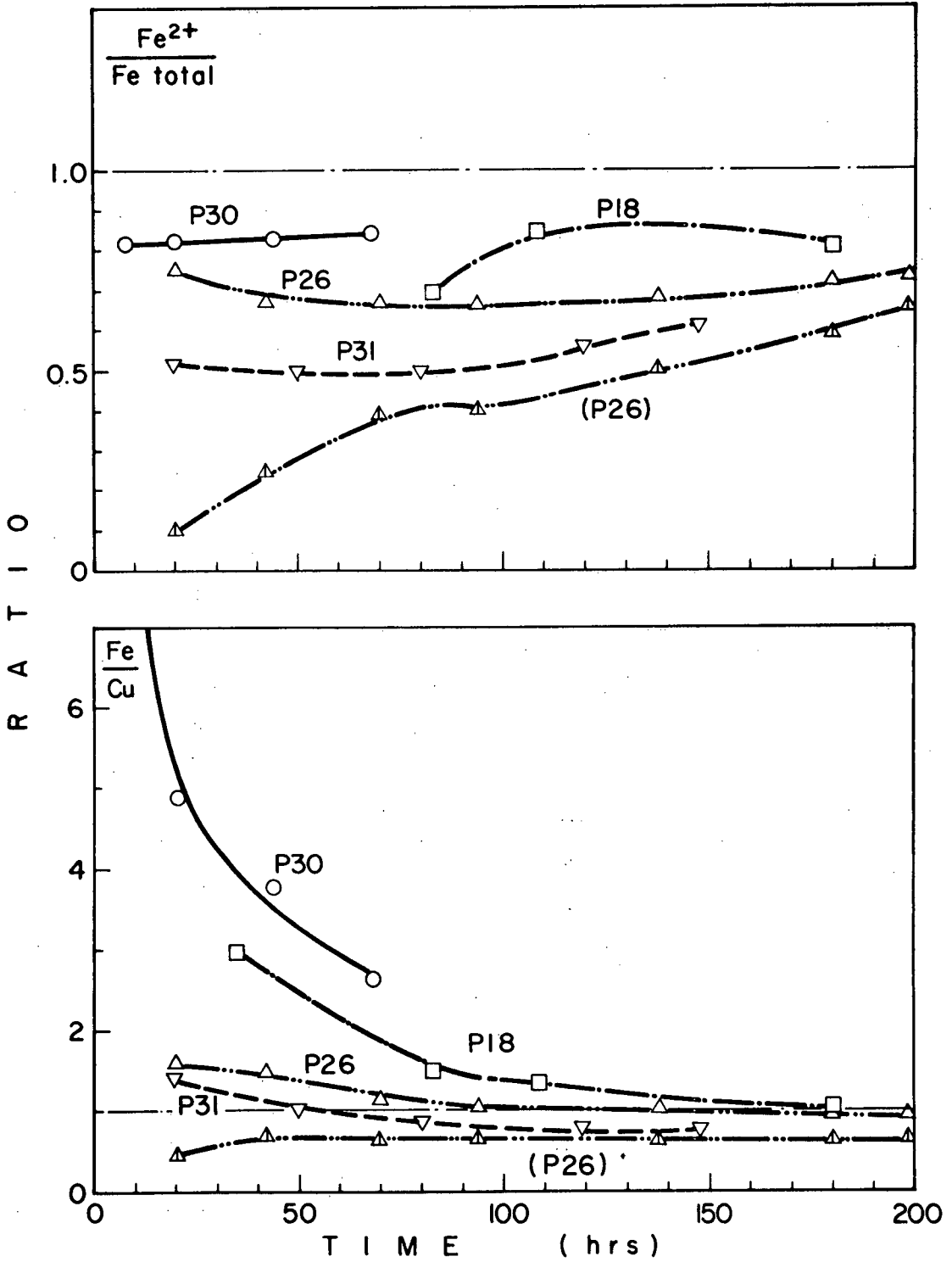


Fig. 54 (f) Fe^{++}/Fe_{Total} ratio.
(g) Fe/Cu ratio.

The current density in the bisulphate experiment was much lower (0.7 mA/cm^2), this being supported by P 29A (sulphate solution; 3.1 mA/cm^2). It would appear that current density rises with pH. Current efficiencies, however, declined with pH (based on one experiment).

Copper C.E. for sulphate solutions was about 22% (+4%), whereas in bisulphate it was 30% (+1.5%). Again P 29A supports this.

Iron and total C.E. show the same trend: after 50 hours the iron C.E. in sulphate solutions fell to about 18%, whereas in bisulphate, a constant 40% value was found. Total C.E. was about 35 - 50% (sulphate) after 50 hours, as against 75 - 67% (bisulphate).

Iron C.E. is probably lowered by hydrolysis in sulphate solutions at 125°C , if any Fe^{+++} ions are present. However the copper C.E. is not affected and it appears that increasing temperature and pH decreases total (metal) C.E. This implies increasing oxidation of sulphur.

(v) Bisulphate/Sulphate Solutions ($125^\circ\text{C} \rightarrow 175^\circ\text{C}$)

Specimen #P 32 was anodized successively (at 735 mV) at 125, 150 and 175°C in $\begin{pmatrix} 0.4\text{M NaHSO}_4 \\ 0.1\text{M H}_2\text{SO}_4 \end{pmatrix}$, then at 125 and 175°C in $\begin{pmatrix} 0.4\text{M Na}_2\text{SO}_4 \\ 0.1\text{M H}_2\text{SO}_4 \end{pmatrix}$ (Figure 56).

In bisulphate solution, the current density approximately trebled with each 25°C increment. Iron C.E. dropped somewhat (45, 38 and 34%) but copper C.E. dropped to near zero (27.5, 16.5 and 2.0%). Considering that these current efficiencies are cumulative, the incremental C.E. of the 175°C experiment is actually negative. (The same solution was kept in the cell). That is, the total copper in solution at the end of the 175°C experiment was less than 1/3 of that existing in solution at the start (i.e. after the 150°C experiment).

Blue CuS powder was scattered through the cell. Evidently some reducing agent had removed copper from solution, even more quickly than it was dissolved.

In sulphate solution, (at 125°C) the copper C.E. was nearly the same as in bisulphate (28%), but the iron was lower (23%). At 175°C very large currents were recorded, (52 mA/cm²), but this may have been due to a short circuit. The (cumulative) copper C.E. was reduced (10%) but not as severely as in the bisulphate case. The bisulphate experiment was repeated with a fresh electrode (P 33), at 150°C and 175°C (Figure 56). Current densities were 6 mA/cm² and 12 → 24 mA/cm² respectively, while copper C.E. was 13% (150°C) and 5% (175°C). Iron C.E. remained high at 62% and 52%, and total C.E. was 75% and 58%. These results confirmed that above 125°C, some reducing agent was produced, capable of precipitating copper from solution as CuS.

(vi) Chloride/Bisulphate Solutions - A Comparison

Electrode P 34 was anodized in (0.4M NaCl, successively (at 735 mV)
(0.1M HCl) at 175°C, 150°C and 125°C (Figure 57). Then a bisulphate solution

(0.4M NaHSO₄,
(0.1M H₂SO₄) was put in the cell and the experiment repeated, first at 125°C, then 175°C (Figure 28).

Very high current densities were recorded in chloride solutions; a plot of C.D. vs. Temperature is shown in Figure 59. An activation energy of 13.1 kcal/mole was calculated. Current efficiencies were also high.

CUMULATIVE C.E.

(Chloride)

Temp.	Cu	Fe	Total	(Fe ³⁺)
175°C	41.2	47.0	90.1	2.6
150°C	41.2	45.6	92.1	2.0
125°C	45.6	49.2	96.5	2.3

CUMULATIVE C.E.

(Bisulphate)

Temp.	Cu	Fe	Total	(Fe ³⁺)
125°C	29.9	46.0	77.1	1.2
175°C	1.3	27.4	29.3	0.5

This experiment demonstrates conclusively the difference between chloride and sulphate systems. In chloride solution virtually all the current may be accounted for by metal dissolution at each temperature; but in bisulphate solution approximately 1/2 the current is used up by sulphur oxidation at 125°C, and at higher temperatures some sulphur species actually reduces copper from solution.

In Figure 60 the difference between sulphate and chloride is again demonstrated. Specimen P 31 was first anodized at 90°C in (0.4M Na₂SO₄, 0.1M H₂SO₄) at 735 mV. Then the solution was changed to (0.4M NaCl, 0.1M HCl) and the experiment repeated.

	Current Density mA/cm ²	Current Density (%)			
		Cu	Fe	Fe ³⁺	Total
Sulphate	1.5	29	21	4	53
Chloride	3.8 → 5.8	43	54	2	97

(vii) Effect of Acid

The effect of acid strength on anodizing CuFeS₂ (at 90°C and 735 mV) in 0.5M Cl solution was examined in experiments P 3 and P 12.

P 3 0.3M NaCl
 0.2M HCl

P 12 0.46M NaCl
 0.04M HCl

In Figure 61, it can be seen that there is no appreciable difference to the current efficiencies, copper or iron, but the current density is about 50% higher in P 12.

In P 5 and P 16 a similar comparison was made, this time at 535 mV in 3M NaCl (90°C):

P 5 3M NaCl (pH = 3.5)

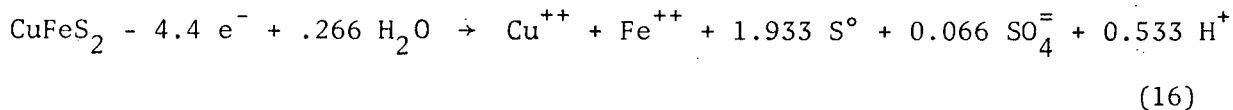
P 16 3M NaCl (pH = 0.5)
 0.2M HCl

In Figure 76, it is shown that without any added acid, the current steadily declined, instead of increasing, and the current efficiency for iron or copper was only 10 - 15% (instead of 80 and 60%).

The effect of electrode surface preparation was also examined, P 6, 7 and 11 were prepared by polishing whereas P 8, 9 and 13 were prepared by saw-cut. No systematic difference could be observed. All other electrodes were prepared by saw-cut.

(viii) Summary

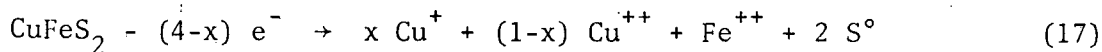
In dilute chloride solutions at 90°C, the probable anodic reaction for chalcopyrite is (in the potential range 535 - 1185 mV):



The above stoichiometry is reached only after considerable time (100 hours), before which iron is dissolved preferentially.

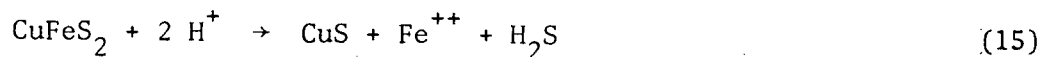
The current density increases with time, and potential up to 935 mV.

In strong chloride solutions at 90°C, the probable anodic reaction is similar to that found in dilute solution (equation 16). However, at low potentials (535 - 635 mV) some Cu^+ is produced:



where $x = 0.12$ at 535 mV and lower at 635 mV.

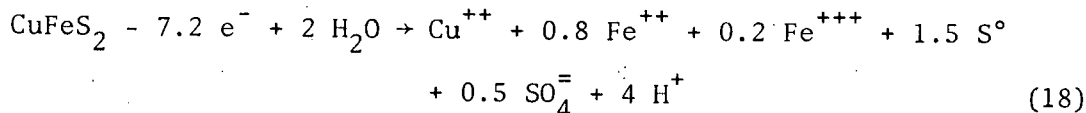
and considerable chemical dissolution of iron occurs:



The percentage of sulphur oxidized to sulphate, omitted in equation (17) for clarity, is small, as in dilute solutions, probably not exceeding 3%.

The situation is further complicated by the fact that at higher potentials (935-1185) approximately 10 - 20% of the iron dissolved appears in solution as Fe^{+++} . Anodic current densities in strong chloride solutions again increase with time, and potential, particularly at lower potentials.

The chemistry of the anodic dissolution of chalcopyrite in $\left(\begin{matrix} 0.4\text{M Na}_2\text{SO}_4 \\ 0.1\text{M H}_2\text{SO}_4 \end{matrix} \right)$ solutions at 90°C may be approximated:



This equation, which implies 27.8% current efficiency for copper, fits the data reasonably well in the potential range 735 - 1185 mV. At lower potentials, the current efficiency for copper is considerably reduced (to 10 - 20%), but the percentage of sulphur oxidized to sulphate continues to be about 25%.

The current densities in sulphate solution are much lower than in chloride, particularly at 735 mV or below. Furthermore, they usually decrease slowly with time, (as opposed to the increasing currents observed in chloride solutions).

CURRENT DENSITY AFTER 50 HOURS ANODIZING

Potential	0.5M [Cl]	3M [Cl]	0.5M [SO ₄]
535	0.1	0.8 - 1.4	0.2
635	2	2.8	0.4
735	2.5	7.8	0.5; 1.8
935	8.2	8.8	1.95
1085		7.0	
1185	6.6	5.6	5.3

The chemical dissolution of iron, which again complicates the stoichiometry of the anodic dissolution, occurs only as Fe^{++} dissolution.

The current density obtainable upon anodizing a given specimen varies widely from one specimen to another, but is related to 1) amount of iron dissolved chemically, and 2) the fraction of iron dissolved anodically as Fe^{++} .

At 125°C - 175°C , anodizations in chloride solutions are little different from those at 90°C , except for an increased current density. At 735 mV, an activation energy of 13.1 kcal/mole was determined for the current density.

In the sulphate system, however, raising the temperature changes the chemistry of anodic dissolution, as well as increasing the current density.

At 125°C in sulphate solutions $\left(\begin{array}{l} 0.4\text{M Na}_2\text{SO}_4 \\ 0.1\text{M H}_2\text{SO}_4 \end{array} \right)$ copper and iron current efficiencies fall to near 20%, indicating increasing oxidation of sulphur. However, in bisulphate $\left(\begin{array}{l} 0.4\text{M NaHSO}_4 \\ 0.1\text{M H}_2\text{SO}_4 \end{array} \right)$ current efficiencies remain nearly constant, at 27 - 30% (Cu) and $^{235}4$ - 40% (Fe).

Above 125°C , the current efficiency for copper falls even in bisulphate solutions, and at 175°C copper is actually removed from solution during anodization, indicating a negative current efficiency.

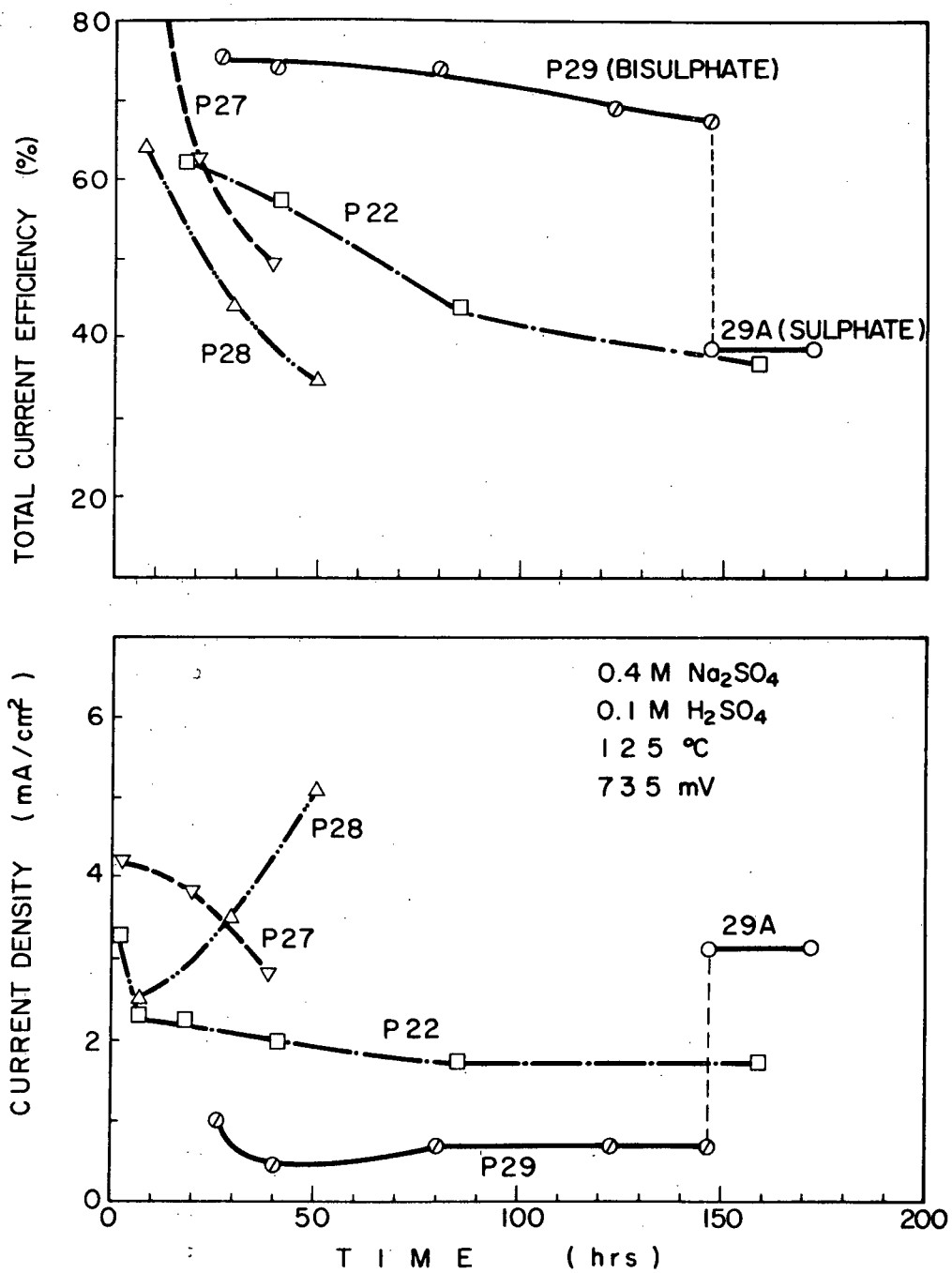


Fig. 55 Constant potential experiments in sulphate and bisulphate solutions at 125°C, 735 mV.
 (a) Current density.
 (b) Total current efficiency.

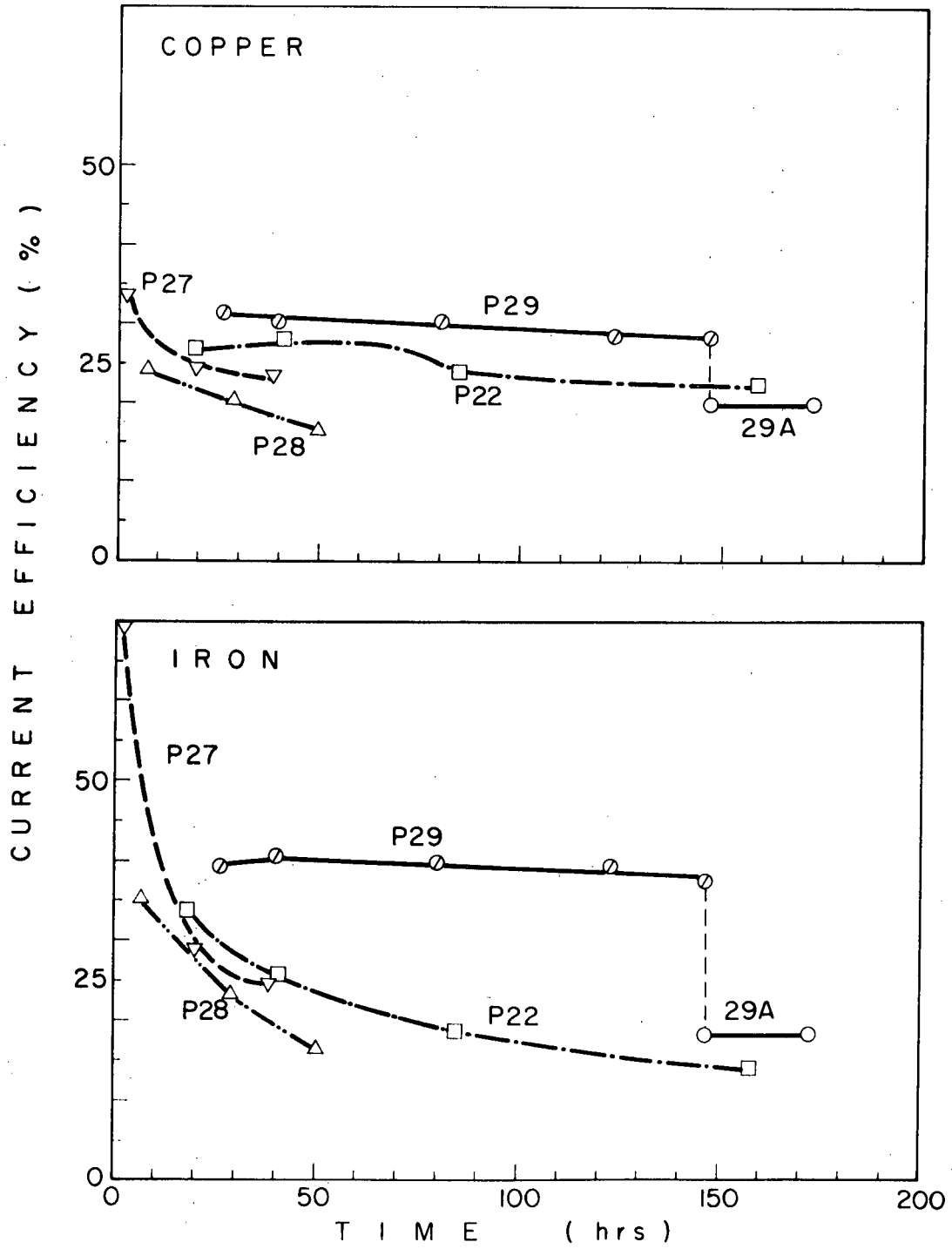


Fig. 55 (c) Copper current efficiency.
(d) Iron current efficiency.

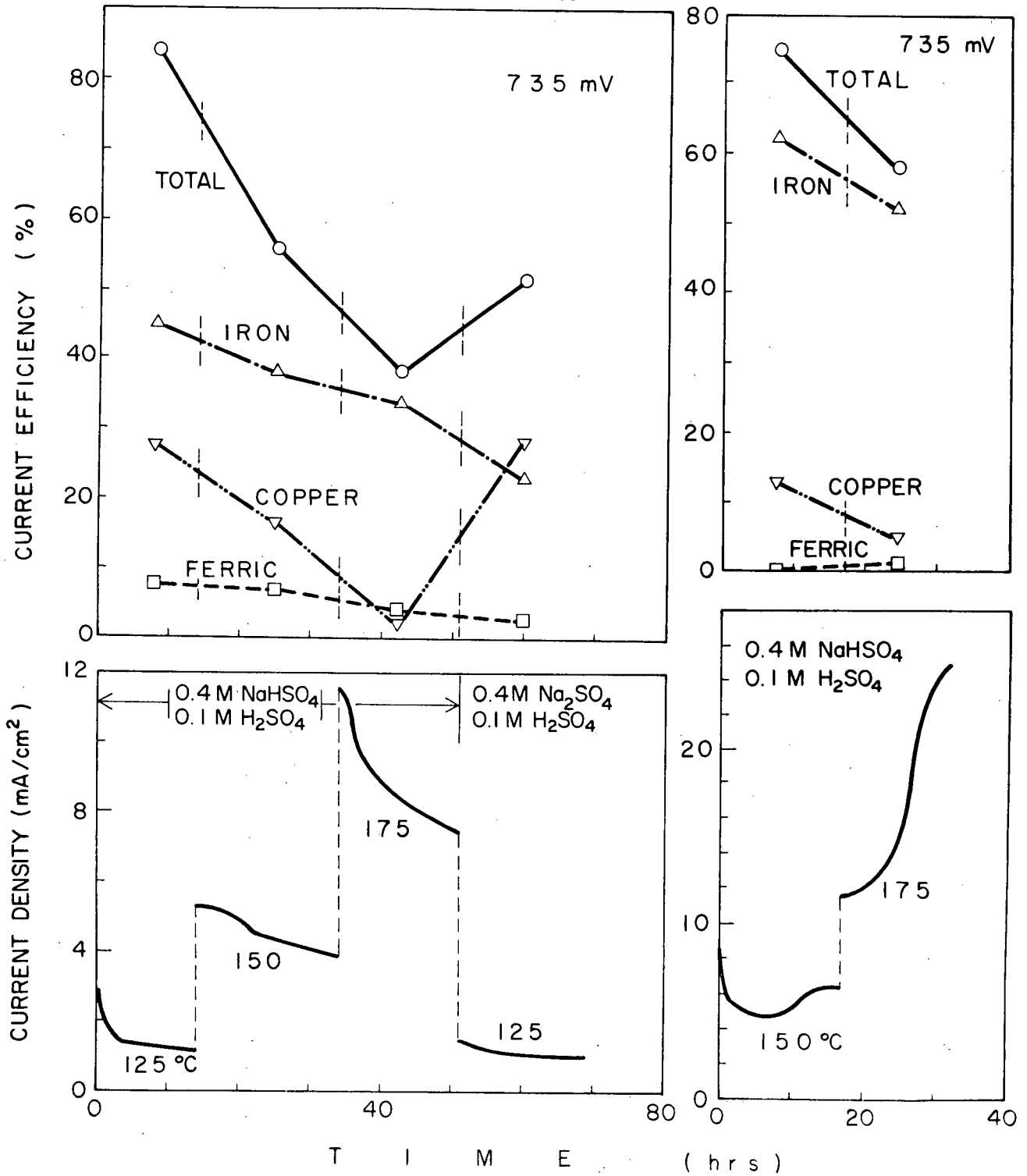


Fig. 56 Constant potential experiments in sulphate and bisulphate solutions at 125°C → 175°C, 735 mV.

Left: Successive experiments at 125°C, 150°C and 175°C in bisulphate; then at 125°C in sulphate solution.

Right: Successive experiments at 150°C and 175°C in bisulphate solution.

(Current efficiencies are cumulative for each bisulphate solution.)

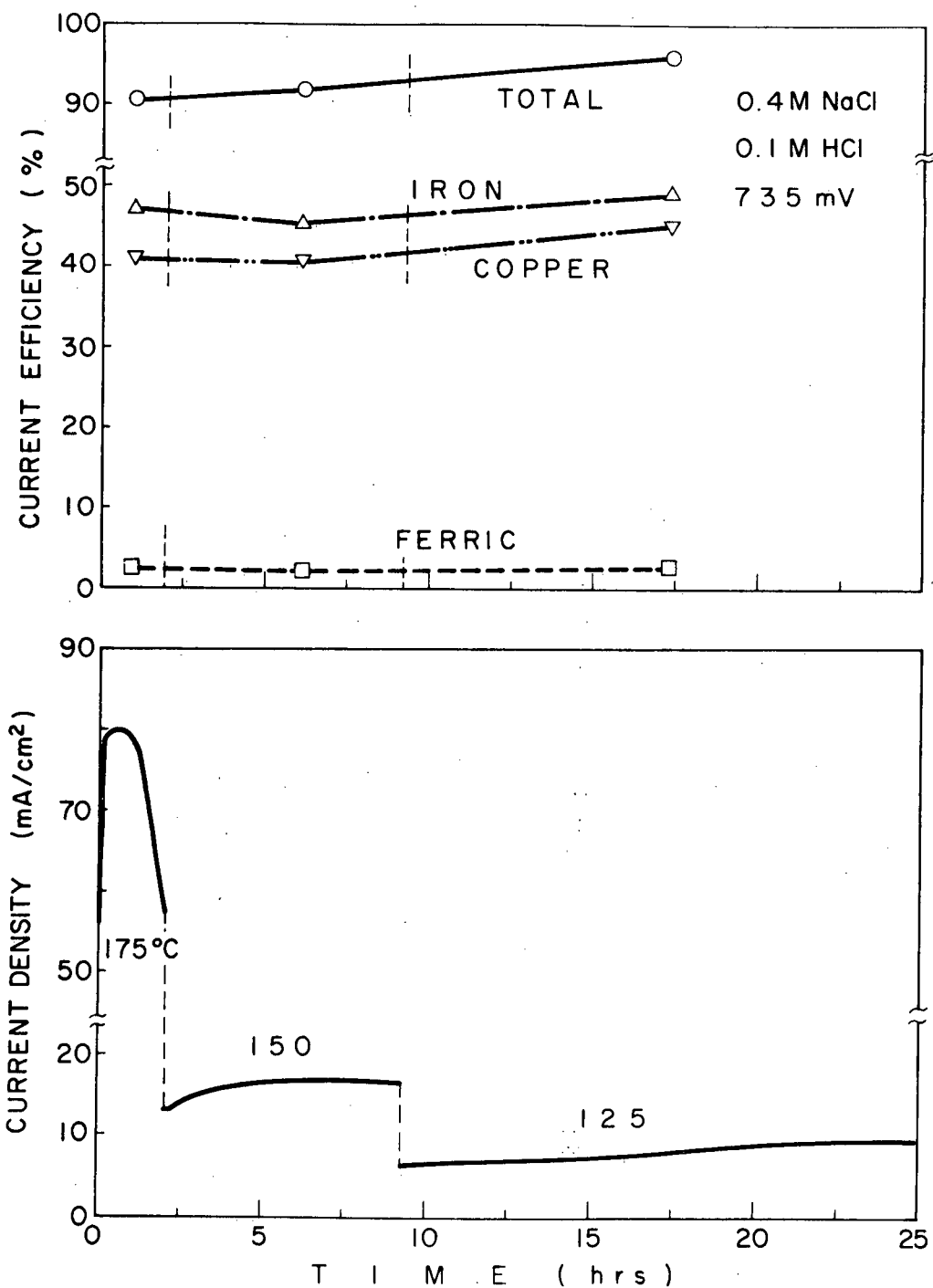


Fig. 57 Constant potential experiments at 735 mV in 0.4M NaCl, 0.1M HCl at 175°C, 150°C and 125°C.

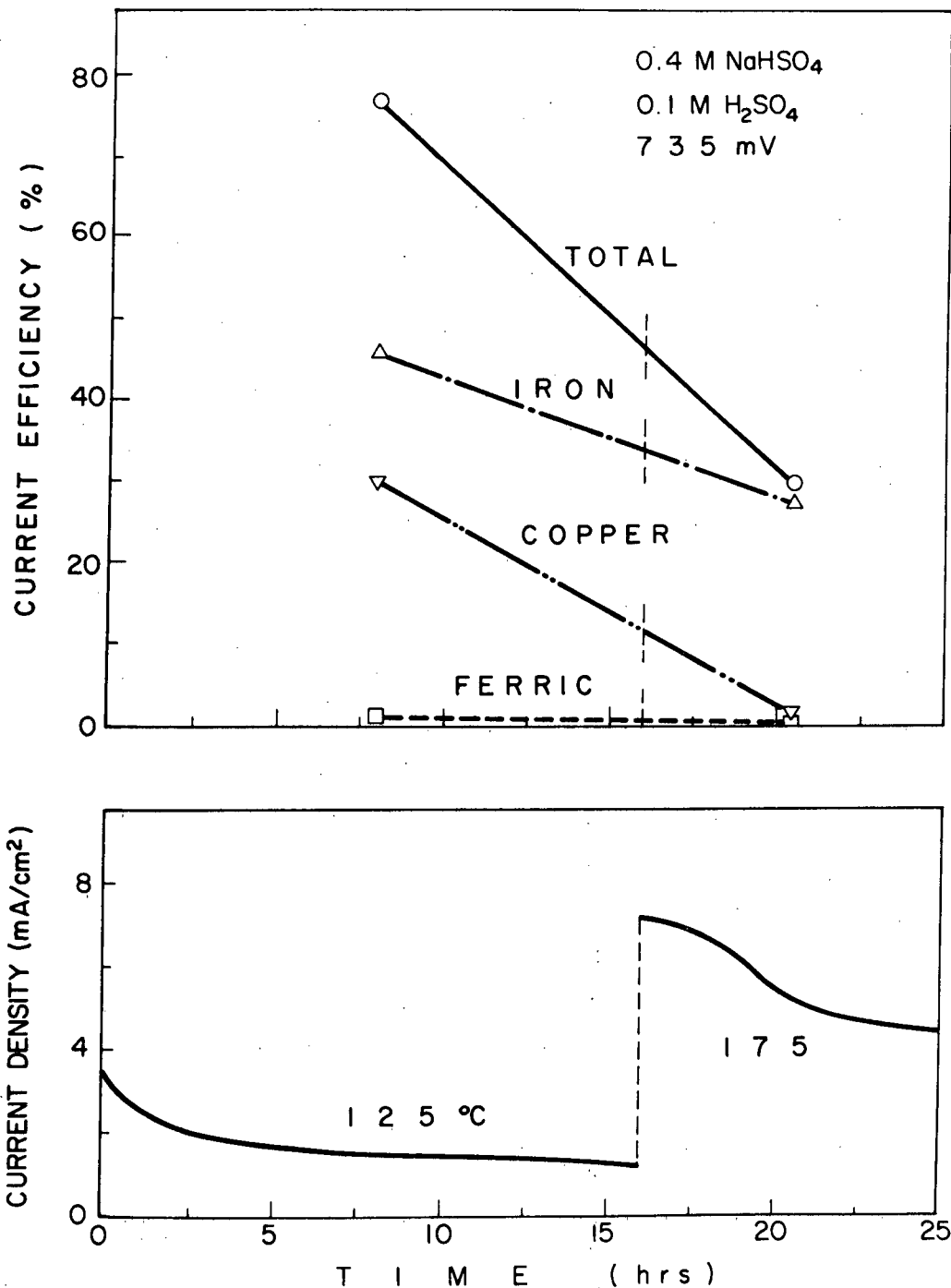


Fig. 58 Constant potential experiments at 735 mV in 0.4M NaHSO₄, 0.1M H₂SO₄ at 125°C and 175°C. Same specimen as used for last experiment (Fig. 57).

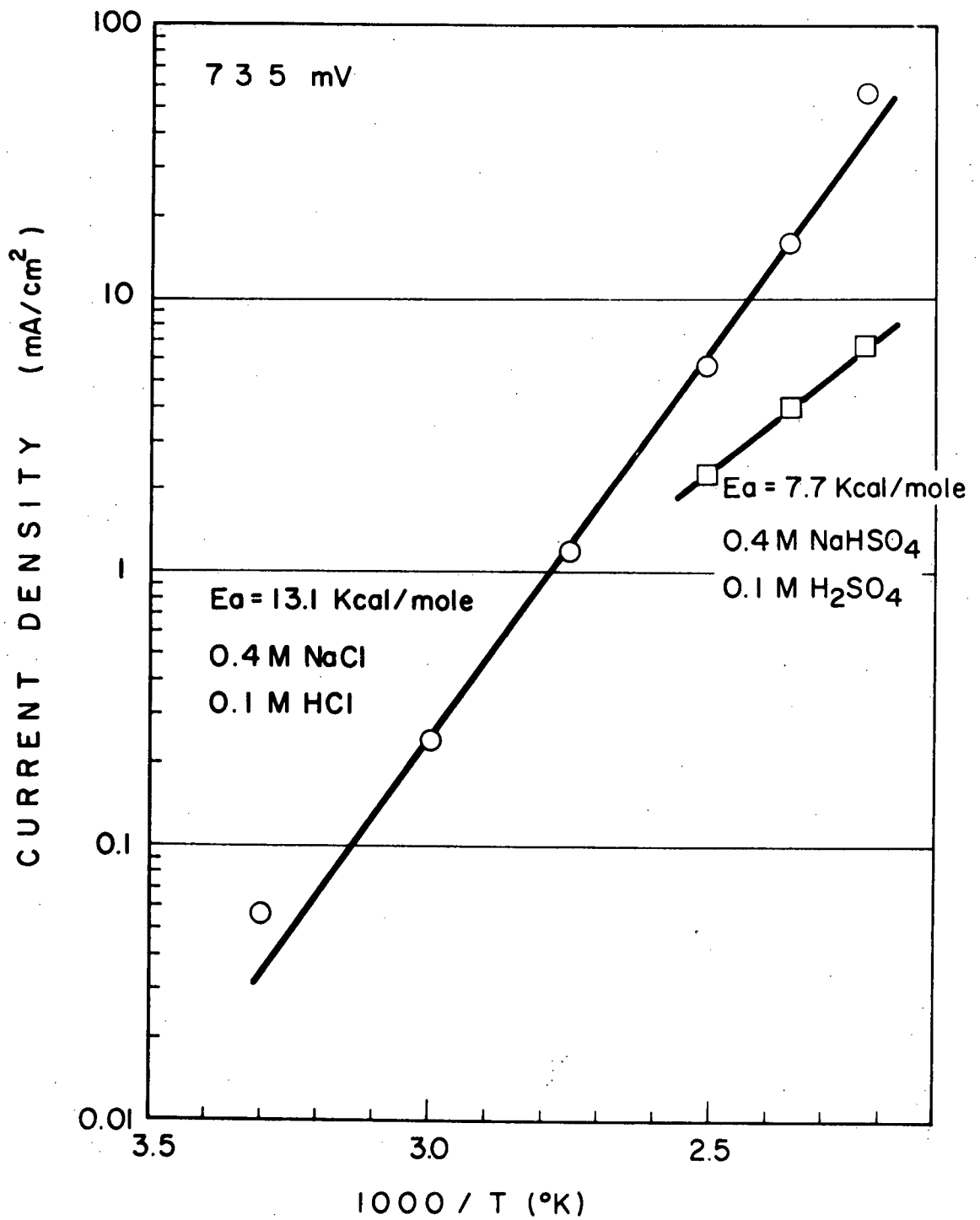


Fig. 59 Arrhenius diagram for current at 735 mV in 0.4M NaCl, 0.1M HCl.

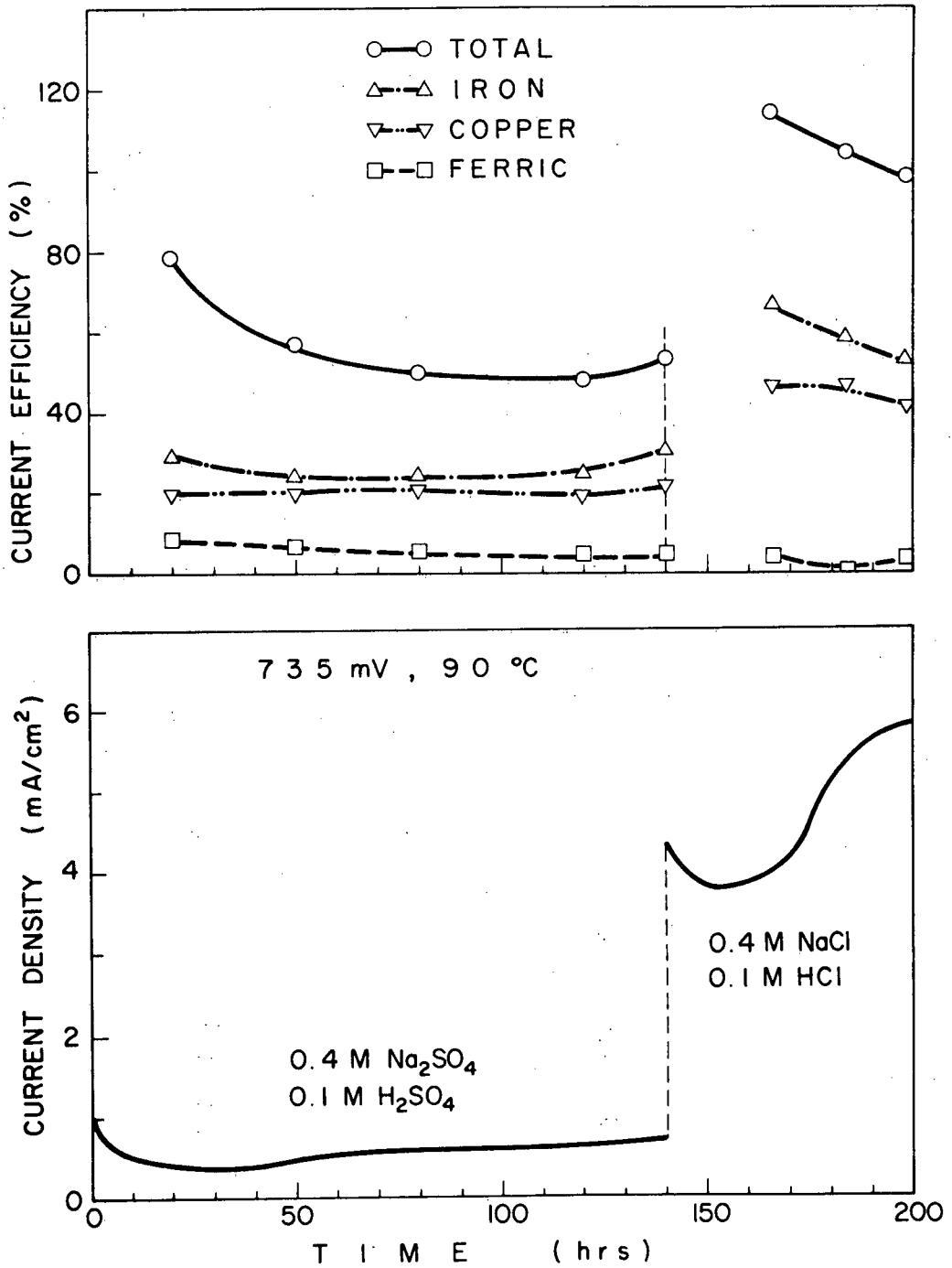


Fig. 60 Successive constant potential experiments at 90°C, 735 mV in bisulphate and chloride solutions.

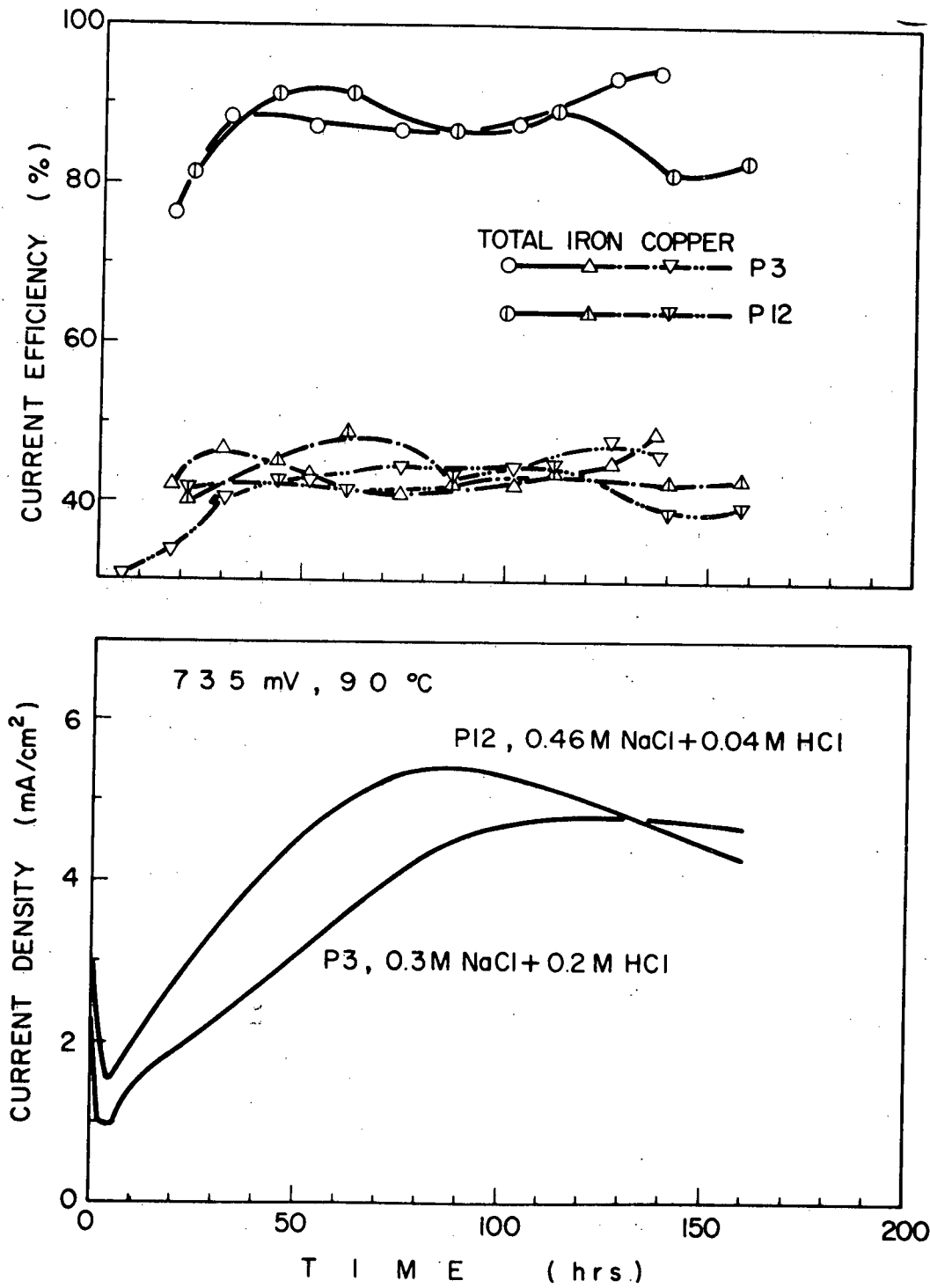


Fig. 61 Effect of decreased acid on constant potential experiment in dilute chloride solution at 735 mV, 90°C.

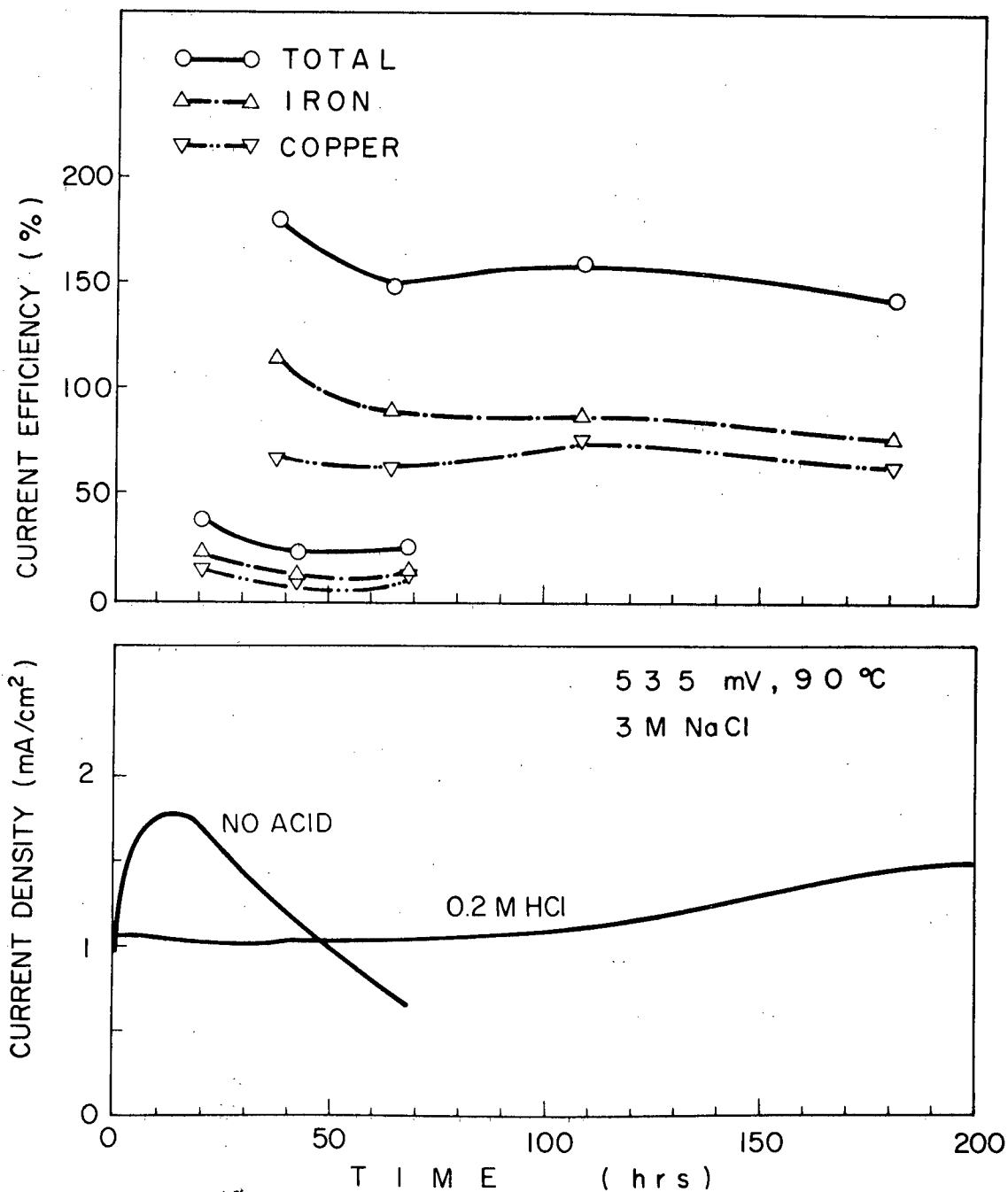


Fig. 62 Effect of no acid on constant potential experiment in strong chloride solution at 535 mV, 90°C.

IV Leaching

a) The Motive

The electrochemical experiments of the preceding sections showed that there is considerable difference in the anodic dissolution of chalcopyrite in chloride and sulphate. In particular, the dissolution rate is considerably faster at low potentials in chloride than in sulphate, and the oxidation of sulphur is significant (25%) in sulphate solutions but not in chloride.

The available data in the literature on the chemistry of leaching chalcopyrite are not very large, as outlined in the introduction, but they indicate little difference in the dissolution stoichiometry of ferric sulphate and ferric chloride leaching (130,131). All workers agree that ferric chloride leaching produces little or no sulphate, in agreement with the anodic dissolution in chloride solutions shown here.

However, Dutrizac (131) also claimed insignificant sulphate formation for ferric sulphate leaching, and this result has been frequently stated by other writers, reviewing hydrometallurgical processes for chalcopyrite concentrates (2,3,5,132).

The results of the electrochemical experiments described in this work do not appear to be compatible with Dutrizac's experiments, by reason of the sulphate formation observed here. This suggests that the electrochemical dissolution of chalcopyrite may have different stoichiometry than the chemical dissolution; such a result would place serious doubt on the postulate that chalcopyrite leaches electrochemically, and would materially reduce the value of these electrochemical experiments.

In order to resolve this problem, leaching experiments were undertaken, primarily to determine once more the chemistry of dissolution of chalco-

pyrite in ferric sulphate and ferric chloride.

b) Leaching Experiments on Massive CuFeS₂

(i) Preliminary experiments

Preliminary experiments were carried out using small pieces of CuFeS₂, placed in unstirred solutions for one day.

Specimen	Solution	Temp.	Atmosphere Control	Cu Dissolved	Equivalent Current Density (mA/cm ²)
				day-cm ² (mmoles)	
I-1	1M KCl	90°C	N ₂	0	0
O-1	1M KCl	90°C	Open Beaker	15	0.07
F-1	1M FeCl ₃ 0.2M HCl	85°C	Covered Beaker	100	0.43
F-2	0.5M FeCl ₃ 0.2M HCl	100°C	Narrow-necked flask with Condenser	130	0.60
F-3	0.5M FeCl ₃ 0.2M HCl	100°C		143	0.67
F-4	1M Fe(SO ₄) _{1.5} 0.2M H ₂ SO ₄	100°C		22	0.10

The equivalent current was calculated by assuming that the anodic dissolution produces only Cu⁺⁺ and Fe⁺⁺ (n = 4).

Then from Faraday's Laws: 1 mA = 213 μmole Cu/day

100 μmole Cu/day = 0.47 mA

It can be seen that no copper dissolves from chalcopyrite in a chloride solution, without an oxidizing agent, and that a small amount dissolves when there is free access to air. Ferric chloride dissolves far more copper than ferric sulphate (6 times) but the equivalent current densities are still quite low (see Figures 50, 53), and correspond to low applied potentials.

(ii) Morphology

Specimens were mounted in epoxy and fresh faces revealed by polishing. The leaching vessel was a round bottom flask fitted with a condenser and heated by a mantle; the specimen was placed in the bottom of the flask, face up, with no stirring.

In Figure 63 is shown scanning electron micrographs of specimens leached for five days at 95°C. In 1.0M ferric sulphate (F-6), attack appears to be primarily along fissures, as evidenced by sulphur deposits, whereas in 1M ferric chloride (F-5) there is overall attack.

Leaching for shorter periods in FeCl_3 still produces overall attack (Figure 64) (11 hours, 100°C, 1M FeCl_3).

A more detailed examination of the surface of chalcopyrite during ferric sulphate leaching showed progressive attack along grain boundaries. In Figure 65 is shown the surface of chalcopyrite after 11 hours leaching at 98°C in 1M $\text{Fe}(\text{SO}_4)_{1.5}$ (+ 0.2M H_2SO_4). The appearance of the surface is unchanged from the original, unleached condition, and polishing marks are clearly in evidence. In the same figure is shown the appearance of one small area, adjacent to a fissure, after 305 hours leaching. This illustrates what a leached surface can look like.

Three separate areas are shown, in Figure 66, as a function of leaching time. The area shown in Figure 66(a) is still apparently un-attacked after 305 hours, (at least according to the criteria of the polishing marks and the flattened, polished face). Figures 66(b) and (c) however, show substantial attack along fissures, (which were not visible on the specimen before leaching) after 71 hours. These fissures are widened after 135 hours, but still there is little or no attack on the original polished surface.

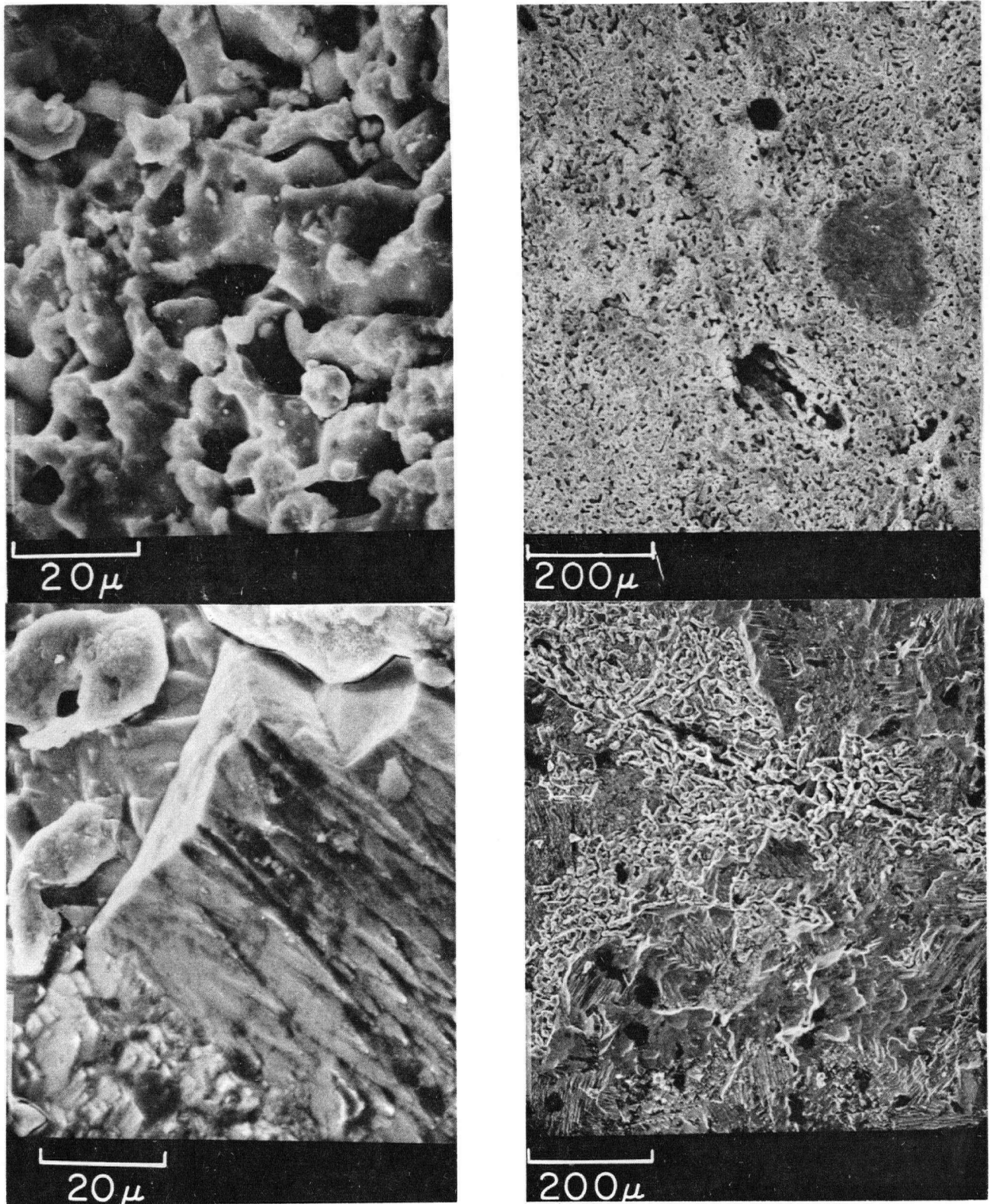


Fig. 63 Scanning electron micrographs of chalcopyrite after leaching (5 days, 95°C).

Top: 1M FeCl₃ The whole surface is covered with elemental sulphur.
Bottom: 1M Fe(SO₄)_{1.5} Chalcopyrite is largely unchanged. Sulphur is deposited along the grain boundaries (white).

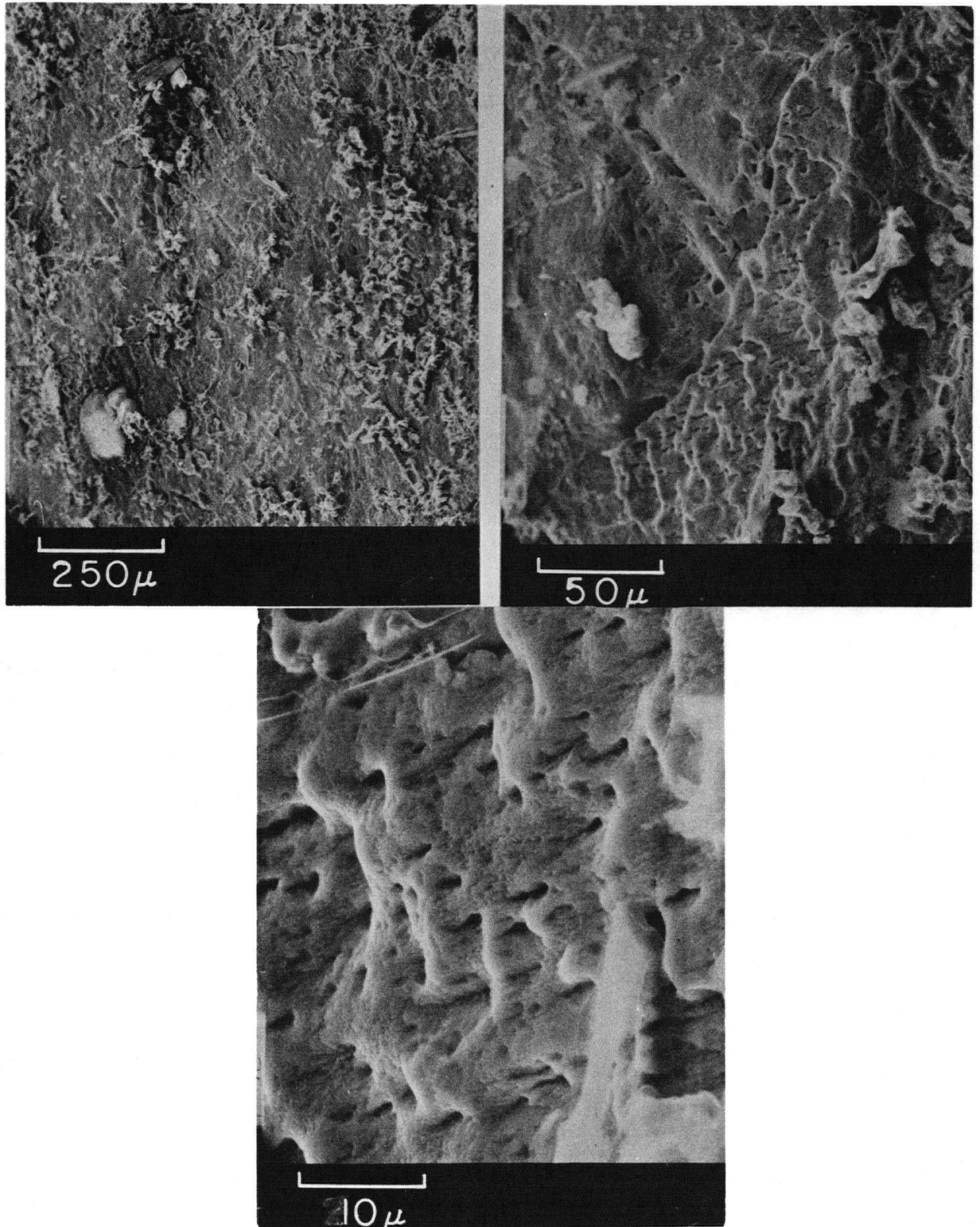


Fig. 64 Scanning electron micrographs of chalcopyrite after leaching (11 hours, 95°C, 1M FeCl₃).
The entire surface has the 'woolly' appearance of a sulphur coating.

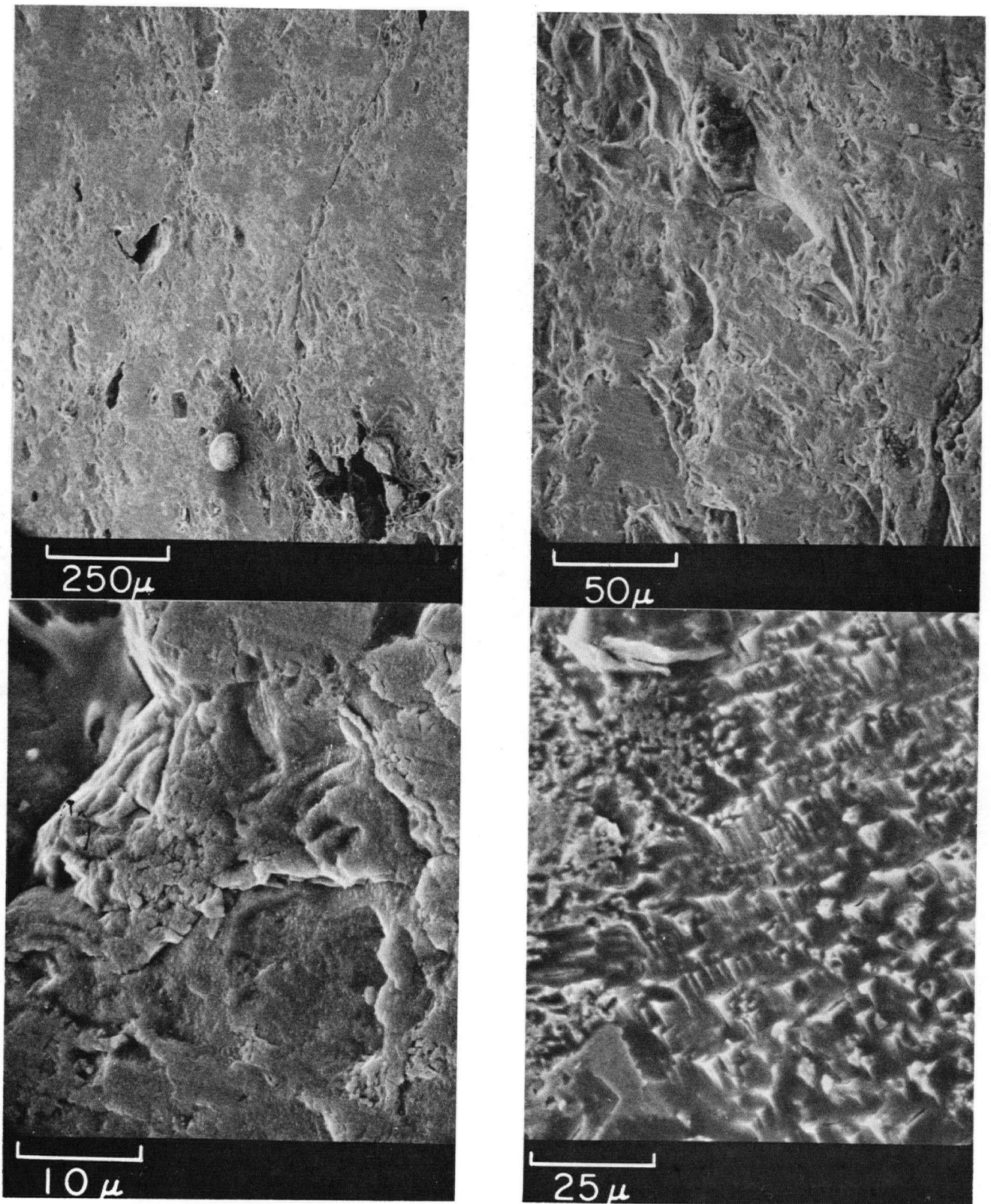


Fig. 65 Scanning electron micrograph of chalcopyrite after leaching in 1M $\text{Fe}(\text{SO}_4)_{1.5}$ at 95°C .

Top and bottom left: 11 hours leaching; surface still has the polished appearance.

Bottom right: 305 hours leaching. Area adjacent to fissure; fresh crystal facets of chalcopyrite visible.

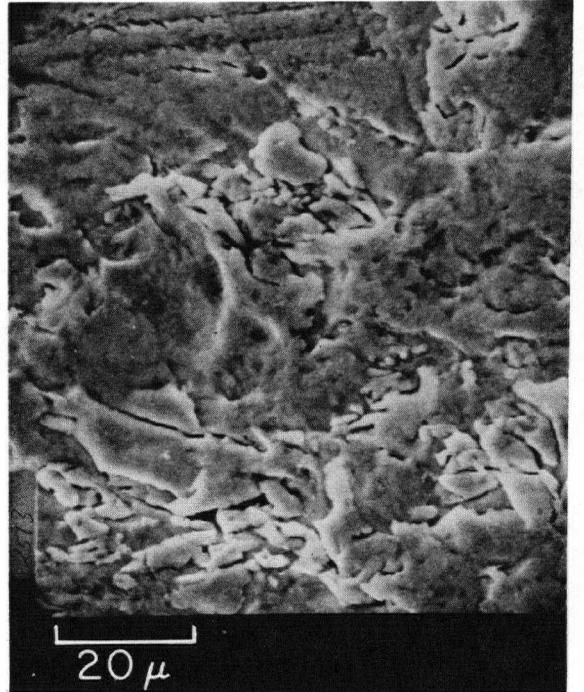
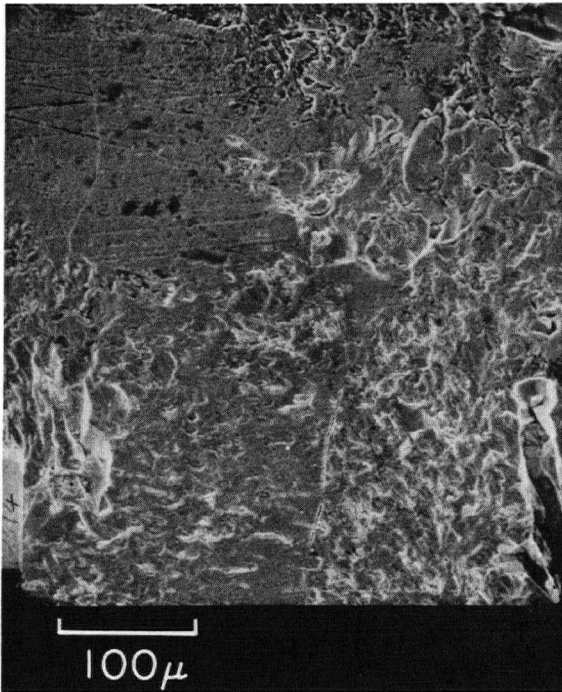
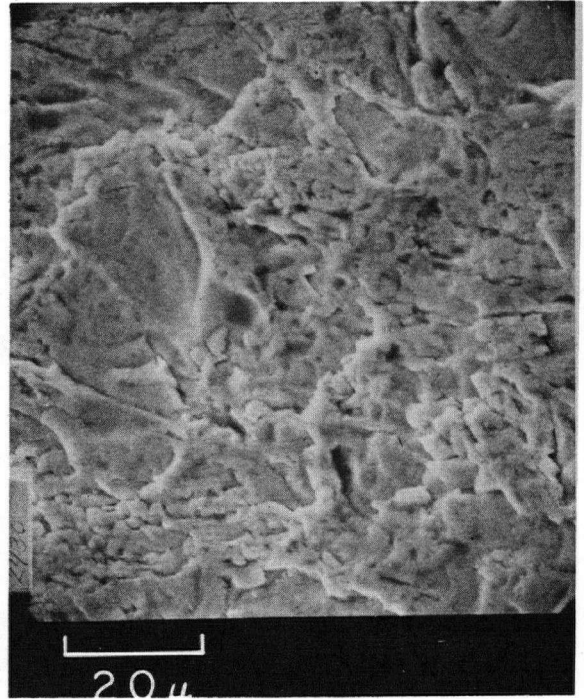
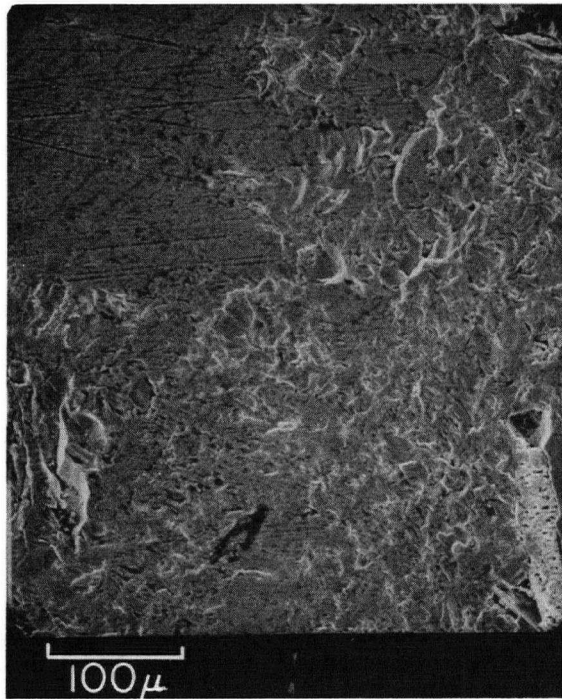


Fig. 66 Scanning electron micrographs of chalcopyrite after leaching with 1M $\text{Fe}(\text{SO}_4)_1.5$ at 95°C .

(a) Unattacked area.

Top : 71 hours
Bottom: 305 hours

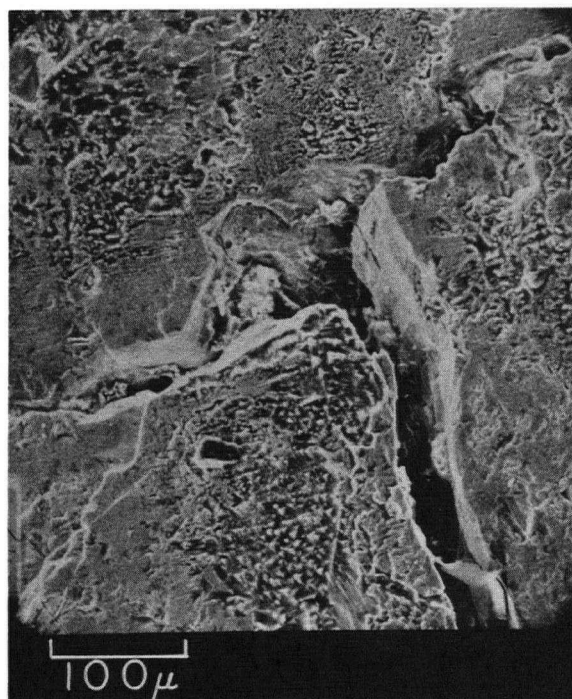
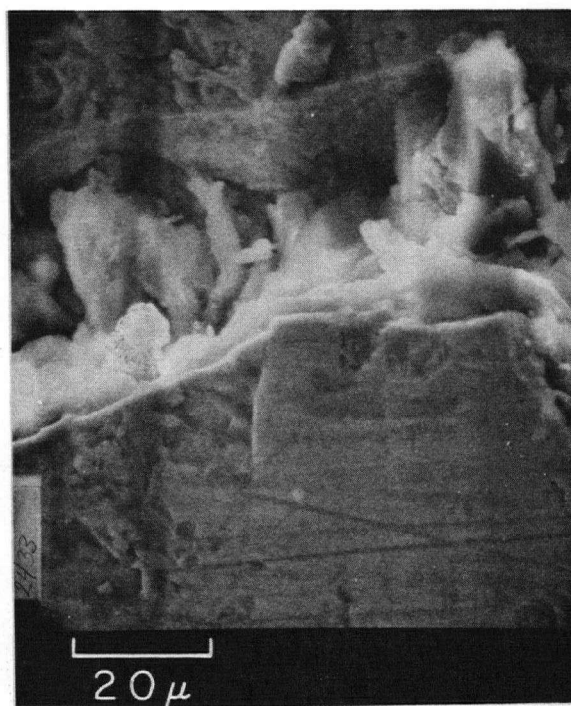
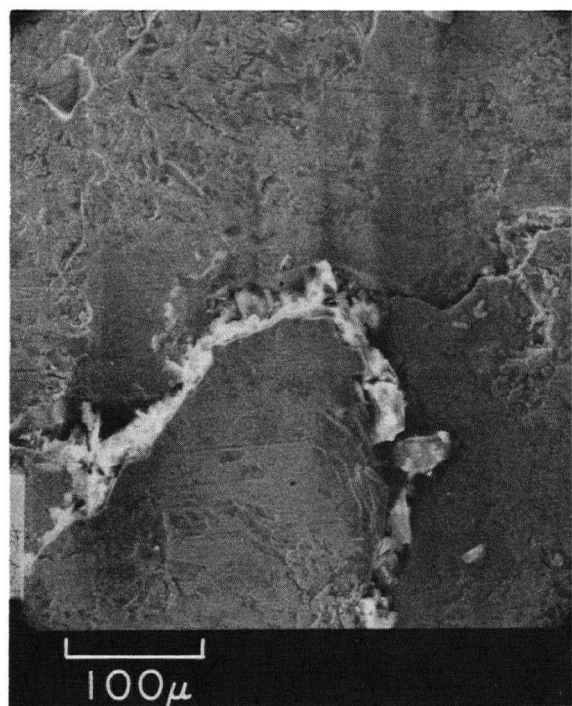


Fig. 66 (b) An area that has been attacked.

Top: 71 hours. Fissures formed with elemental sulphur deposit. No attack on surrounding area (polishing marks visible).
Bottom: 305 hours. Fissures largely unchanged, but surrounding area has been attacked; fresh crystal facets are visible.

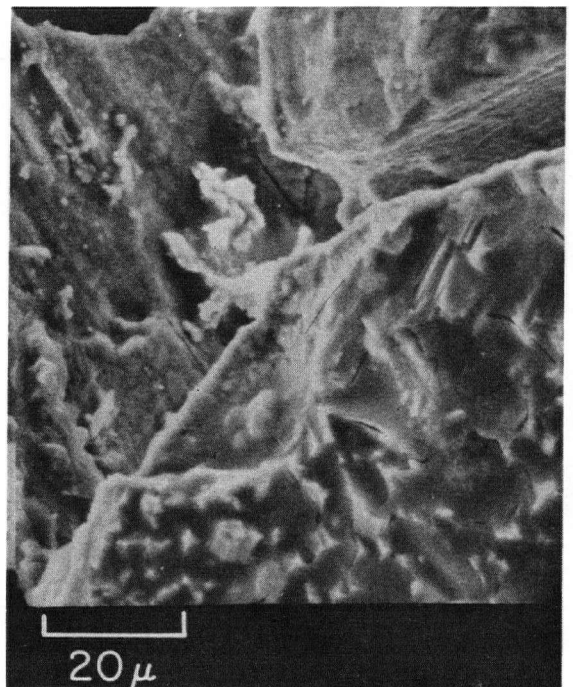
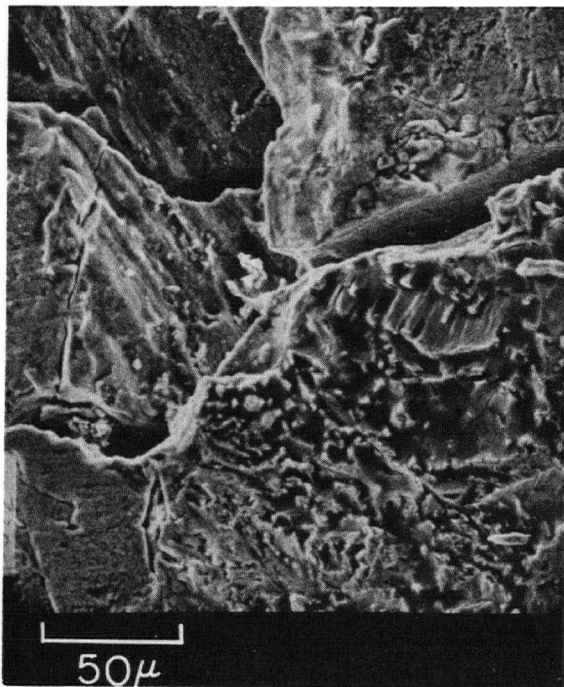
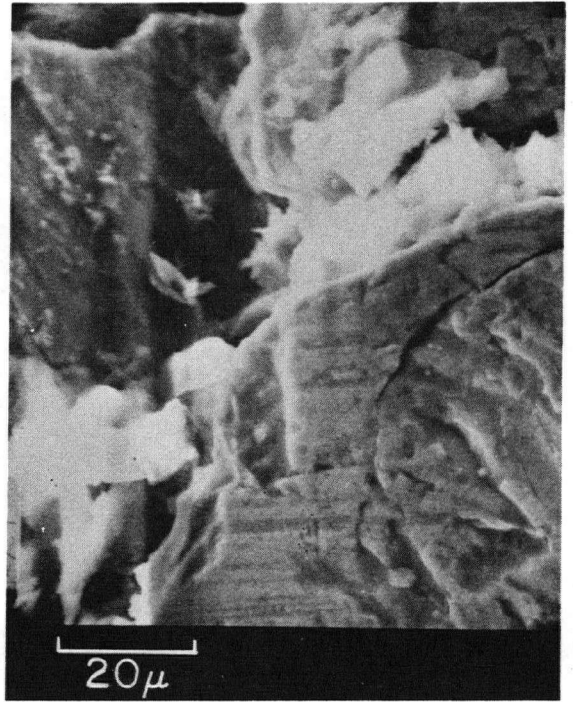
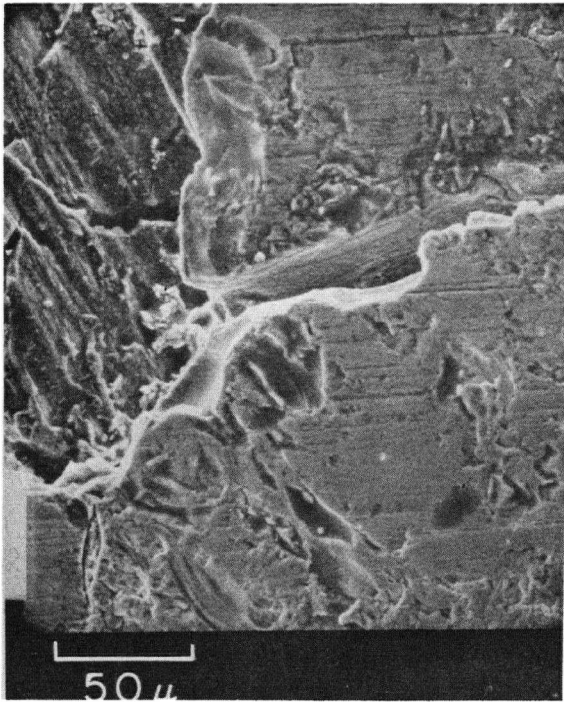


Fig. 66 (c) Another attacked area. Top : 71 hours
Bottom: 305 hours

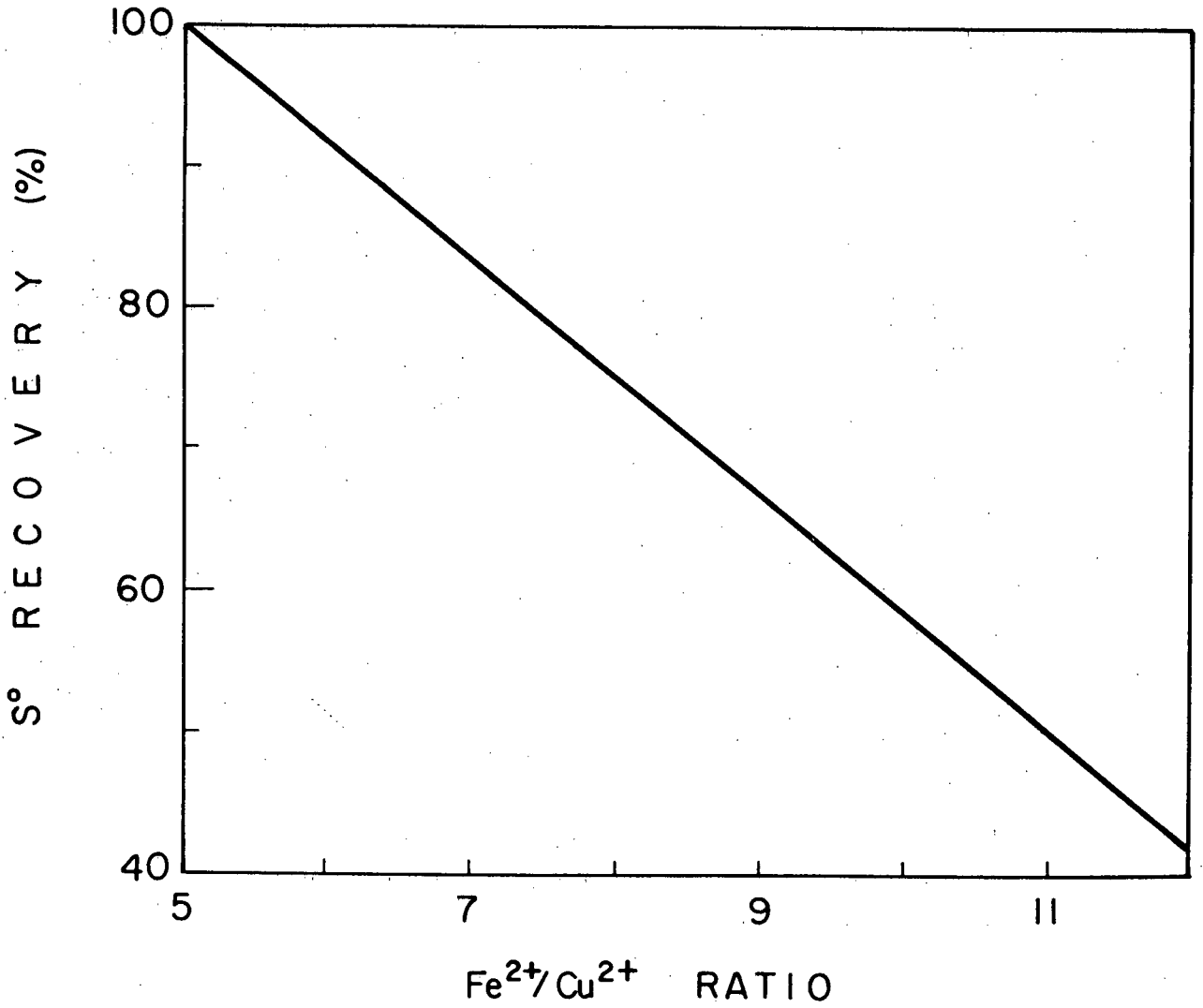


Fig. 67 Theoretical relationship between percent sulphur as S⁰ and Fe⁺⁺/Cu⁺⁺ ratio in equation (20).

After 305 hours the surface itself is attacked, and polishing marks are eliminated; fresh crystal facets are evident.

During this time copper dissolved at a fairly constant rate; quantitative data on this aspect is given in the next section.

(iii) A Comparison of Chemical and Electrochemical Dissolution

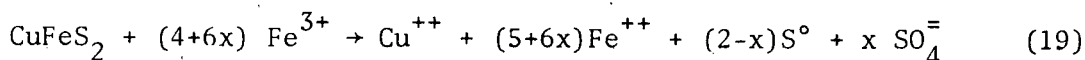
Specimens were mounted in epoxy as in the electrochemical experiments and the leaching carried out in an apparatus described in Figure 7, with nitrogen passing into the leaching vessel.

A typical leaching experiment in ferric sulphate (1.0M Fe(SO₄)_{1.5}, 0.2M H₂SO₄) gave the following result:

Temp.	Specimen Area (cm ²)	Time (days)	Dissolved Metals (mmoles)		Fe ⁺⁺ /Cu	S [°] (mmoles)	S [°] / 2 · Cu
			Cu	Fe ⁺⁺			
90°C	0.96	38	1.45	10.36	7.15	2.10	0.72

(S[°] analysis was by CS₂ extraction).

If the only products of CuFeS₂ leaching are Cu⁺⁺, Fe⁺⁺, S[°] and SO₄⁼, then the dissolution reaction may be written:



where x/2 = fraction of sulphur oxidized to sulphate.

Then the relationship between the percent sulphur as elemental sulphur (%S[°]) and Fe⁺⁺/Cu ratio is:

$$\%S^{\circ} = 100/12(17 - \text{Fe}^{++}/\text{Cu}^{++}) \quad (20)$$

$$\text{or } \text{Fe}^{++}/\text{Cu}^{++} = 17 - 12/100(\%S^{\circ}).$$

From this relationship (plotted in Figure 67) a Fe⁺⁺/Cu⁺⁺ ratio of 7.15 should correspond with 82% S[°]. The actual value of S[°] extracted is

72%.*

The rate of dissolution of Cu is 40.0 mmoles/day-cm². This may be translated into equivalent current density, by choosing a value for n, the number of electrons in the anodic reaction, which may be calculated from Fe⁺⁺/Cu⁺⁺ ratio:

$$n = \text{Fe}^{++}/\text{Cu}^{++} - 1 \quad (= 4+6x)$$

or from percent sulphur produced as S^o (%S^o):

$$n = 4 + 12/100(100-\%S^o)$$

In the above case:

$$n = 6.15 \text{ by Fe}^{++}/\text{Cu}^{++} \text{ produced.}$$

$$n = 7.35 \text{ by S}^o \text{ analysis.}$$

Then the equivalent current density is:

$$(n = 6.15) \quad 0.29 \text{ mA/cm}^2$$

$$(n = 7.35) \quad 0.345 \text{ mA/cm}^2$$

These currents correspond to an applied potential (Figure 53) of 635 - 735 mV, a reasonable value for ferric sulphate leaching (see Section V).

The current efficiency for copper in the anodic dissolution experiments (in sulphate) was typically 27%, although smaller at lower potentials. From the values for n, above, we may calculate current efficiency for copper, (C.E._{Cu}):

$$\begin{aligned} \text{C.E.}_{\text{Cu}} &= 100(2/n) = 32.6\% \text{ (by Fe}^{++}/\text{Cu}^{++}) \\ &27.2\% \text{ (by S}^o\text{).} \end{aligned}$$

There is reasonable agreement then between this leaching experiment in sulphate solution and electrochemical results, in two areas: the equivalent current density and the chemistry of dissolution.

* Only rhombic and monoclinic sulphur are soluble in CS₂, amorphous sulphur is not (196).

The results for a typical ferric chloride (1M FeCl₃, 0.2M HCl) leach at 90°C were:

Temp. (°C)	Time (Hrs.)	Dissolved Metals (mmoles/cm ²)		Fe ⁺⁺ /Cu ⁺⁺	$\frac{S^\circ}{2.Cu}$
		Cu ⁺⁺	Fe ⁺⁺		
90	140	2.97	14.9	5.02	.895
	212	3.75	18.2	4.83	

Thus the Fe⁺⁺/Cu⁺⁺ ratio was very close to 5.0, which corresponds to 100% elemental sulphur production; S[°] analysis by CS₂ extraction yielded 89.5% S[°]. The corresponding current efficiencies for copper are 50% and 39%, and the equivalent current densities (at 140 hours) 2.4 mA/cm² and 3.1 mA/cm².

Such current densities in strong chloride solutions (Figure 51) correspond to a potential of 635 mV; copper current efficiency at this potential was 55%.

There is then reasonable agreement between chemical and electrochemical experiments in chloride solutions as well as sulphate.

(iv) Chemistry of Dissolution (at 90°C) (using apparatus in Figure 7)

The results of ferric sulphate leaching are shown in Figures 68, 69. After an initial period, the rate of dissolution of copper was constant, even up to 57 days. When the solution was 1M in [Fe⁺⁺⁺], an induction period (100 hours) was noticeable, during which leaching rates were about one third of the later values. Aside from this phenomenon, similar leaching rates were observed in 1M and 0.1M Fe⁺⁺⁺. The ratio Fe⁺⁺/Cu⁺⁺ produced during leaching originally had high values (>10) at the beginning of a leach. This slowly declined to about 6.5 after about 10 days, and stabilized.

Leaching with ferric perchlorate gave similar dissolution rates, but the $\text{Fe}^{++}/\text{Cu}^{++}$ ratio declined steadily to very low values (<3) with no stable value. This was evidently due to oxidation of ferrous ions by perchlorate.

Leaching with ferric chloride resulted in greatly increased dissolution rates (Figure 70), which depended strongly on the $[\text{Fe}^{+++}]$.

The initial leaching period (50 hours) in dilute ferric chloride (0.1M) appeared to be influenced by the surface treatment of the mineral (Figure 71). Polishing or exposure to air for a few days, lowered the rate of dissolution of copper in this period, compared to a fresh saw-cut surface, by a factor of five or more. No such effect was found in either 1M FeCl_3 or ferric sulphate leaching.

After this initial period, approximately linear rates of dissolution were observed in dilute ferric chloride, which were approximately five times as high as in ferric sulphate.

In strong ferric chloride (Figure 70), leaching was very rapid for the first day or two, then levelled off.

$\text{Fe}^{++}/\text{Cu}^{++}$ ratios produced during ferric chloride leaching again started at high values (>10) but levelled off after two days (5M Fe^{+++}) or seven days (0.1M Fe^{+++}) at about 5.5.

c) Powder Leaching

In the previous section it was shown that the dissolution of massive specimens of chalcopyrite in ferric sulphate/chloride is in accord with the electrochemical results obtained earlier. However, the hydrometallurgical processing of chalcopyrite concentrates is unlikely to be carried out on

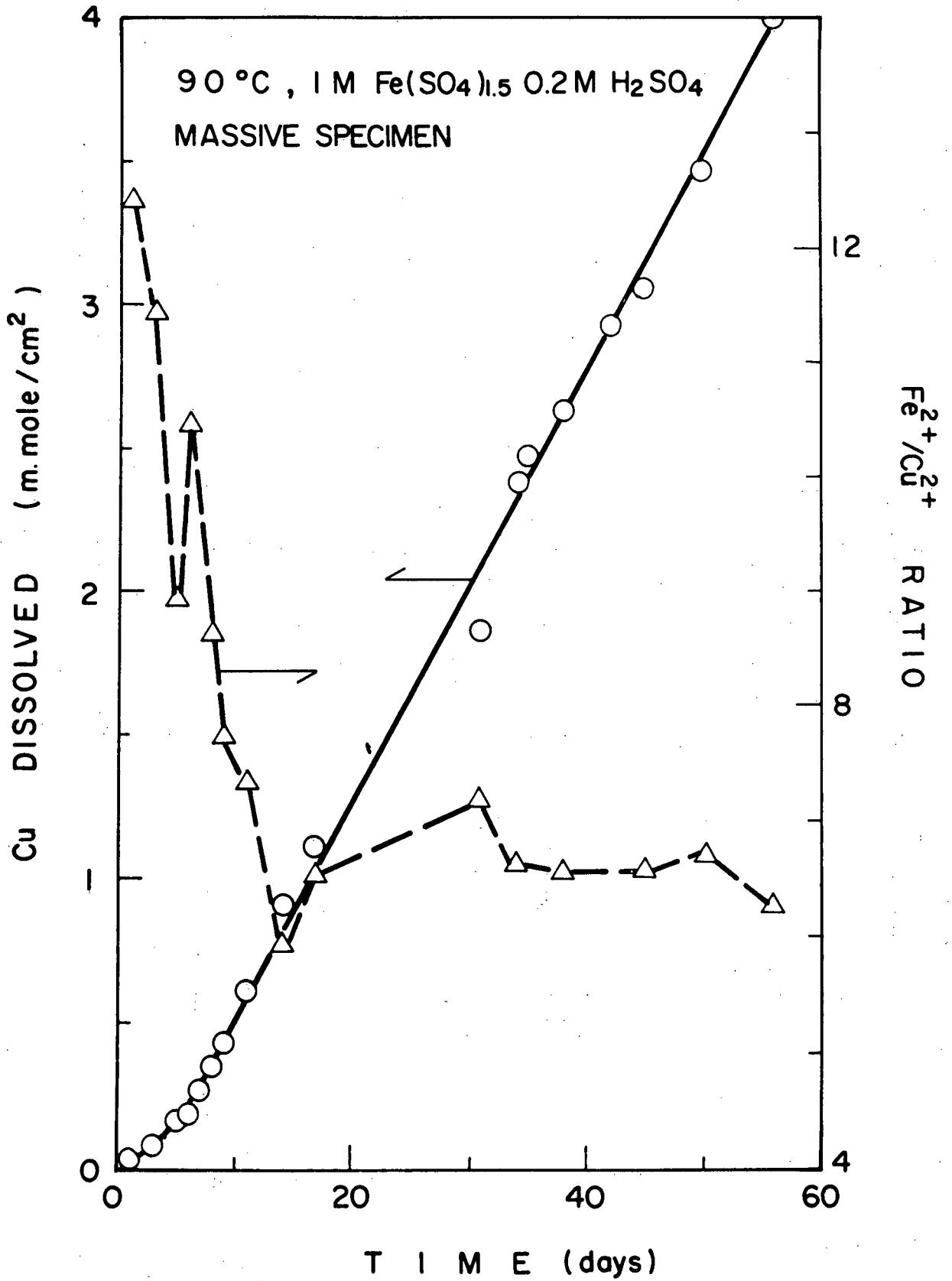


Fig. 68 Leaching of massive chalcopyrite in 1M Fe(SO₄)_{1.5}, 90°C.

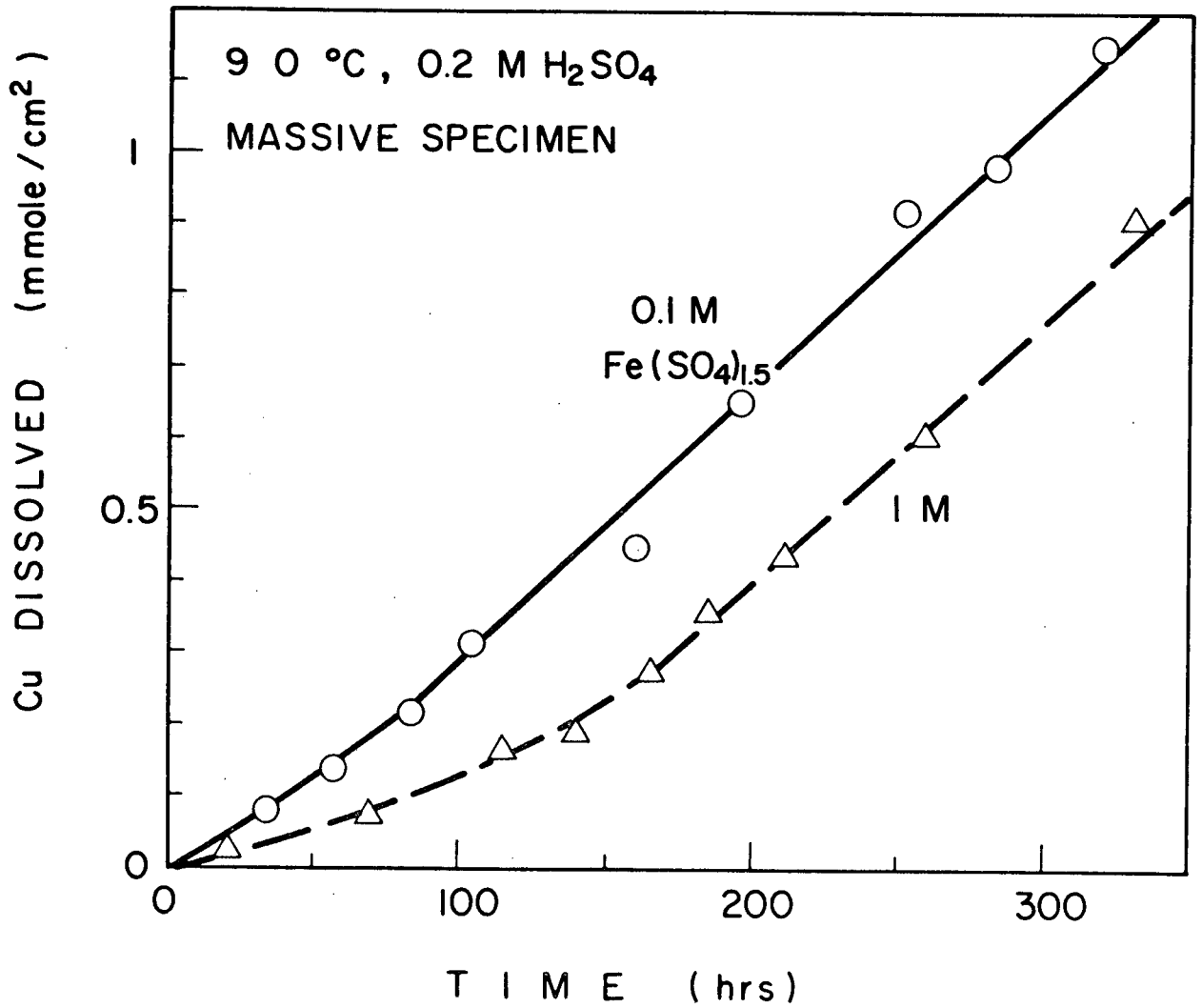


Fig. 69 Comparison of leaching in 0.1M and 1M Fe(SO₄)_{1.5}.

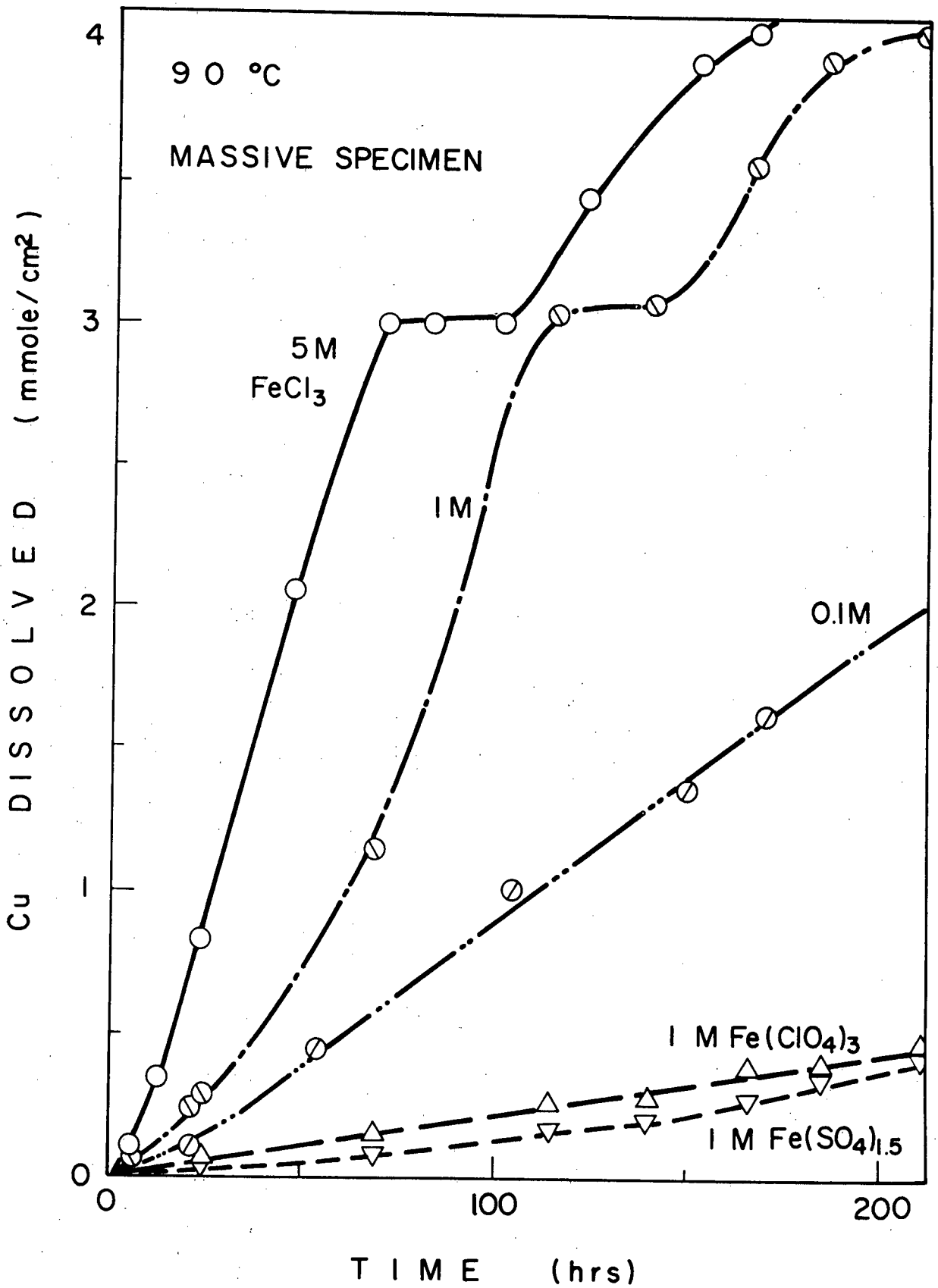


Fig. 70 Comparison of leaching in sulphate, perchlorate and chloride solutions.

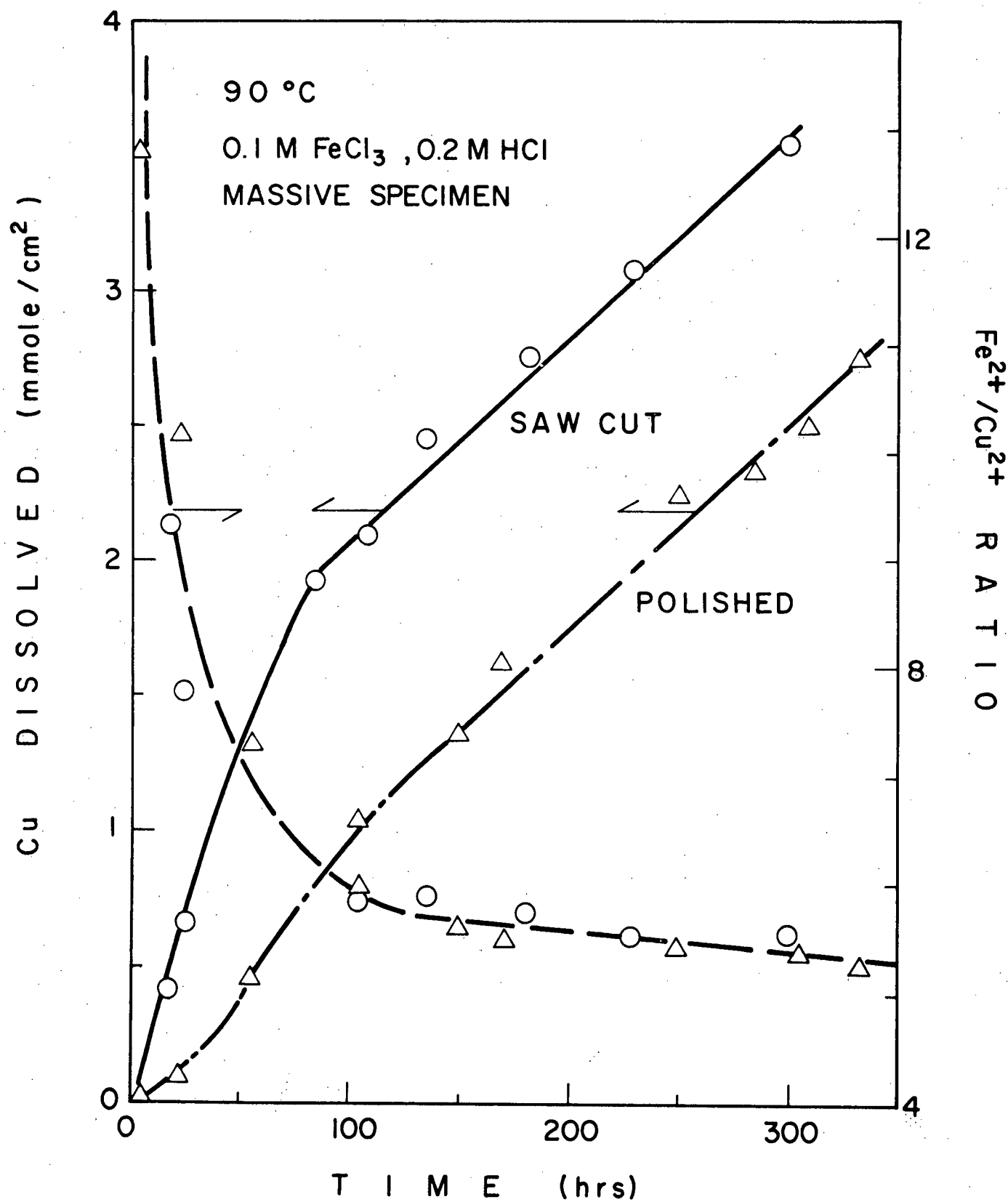


Fig. 71 Effect of surface preparation on FeCl₃ leaching.

massive specimens (except perhaps in heap or dump leaching) and given the peculiar morphology of leaching observed in Figures 63-66, it is quite possible that the leaching of finely ground material has entirely different characteristics. The factors affecting the dissolution of powdered material are the subject of study in this section.

Powdered material was obtained by crushing chalcopyrite (from the same source as before, a high grade lump of Craigmont ore); this was done with a mortar and pestle, in air. Chalcopyrite crushes very easily, and actually shatters on light impact; thus reasonably fine material was obtained without grinding.

Size reduction below about 200 mesh required grinding, however, which was undesirable due to the danger of oxidation. A significant fraction of shattered material was sufficiently fine, however, that grinding was not necessary unless a complete piece was to be reduced. The use of such a fraction assumes that it has the same properties as the rest of the material.

In order to conserve material, the purity of chalcopyrite used in this part of the work was not as high as it was earlier. Several analyses were carried out (using the method outlined in Scott (182), involving decomposition of the ore with Br_2/CCl_4 , followed by HNO_3) and an average purity of 93% was calculated. However, this will vary somewhat from one sample to another, owing to the desire not to homogenize the size distribution, as noted above.

(i) Shape of Leaching Curve

Sullivan (130) showed that in ferric sulphate leaching of powdered CuFeS_2 , the rate of extraction of copper fell off very rapidly; similarly, Dutrizac et al (131) reported that in ferric sulphate leaching of massive sintered disks of synthetic CuFeS_2 , a parabolic leaching curve was obtained. However, the results reported here clearly showed linear dissolution rates of massive, natural CuFeS_2 (even after 57 days), in accord with the anodic studies in sulphate solution.

The results of a typical leaching experiment in ferric sulphate are shown in Figure 72. A declining rate of dissolution is evident, as the reaction proceeds; plotting the extraction of copper vs. $\sqrt{\text{time}}$, gives a nearly linear relationship up to 60% extraction, but not beyond that (Figure 73).

If one assumes that the mineral particles are spheres, then the decline in available mineral surface area during a reaction may be corrected for by plotting $[1-(1-R)^{1/3}]$, (instead of % Cu extracted) where R = fraction of Cu extracted (199). Such a plot is also shown in Figure 73.

It can be seen that a nearly linear relationship exists up to a certain point (36% extraction).

The extraction of copper, as shown in this experiment, evidently stops at 70%; the reason is not apparent.

Other experiments, using 0.1M FeCl_3 , and a variety of particle sizes are shown in Figure 74, where $1-(1-R)^{1/3}$ is plotted. Linear relationships were also found.

(ii) Effect of Particle Size

As seen in Figure 74, increasing particle size decreases the rate of the Cu extraction in ferric chloride. The slopes of the leaching curves are

in the following ratios:

Size	Relative Slope	Approximate Mean Radius
-12+ 16	0.40	720 μ
-50+100	1.00	100 μ
-400	4.5	<17 μ

Since the area/gram of a mineral particle declines linearly with increasing values:

$$\frac{\text{Area}}{\text{gram}} \propto \frac{1}{r}$$

it can be seen that the rise in dissolution rates is not proportional to the rise in area for smaller particles. This assumes a constant roughness factor. However, the increase in rate is certainly substantial, and it indicates that the area of the particle exposed to the solution is an important factor. The actual size of the particles in the larger size ranges may have been reduced considerably by the magnetic stirring action (see below).

Not shown in Figure 74 is the fact that the leaching stops after 80 hours at 95% extraction (for -400 mesh particles), and 150 hours at 73% extraction (for -50+100 mesh particles).

In ferric sulphate particle size seems to be less important, Figure 75. Increasing dissolution rates are evident in going from (-12+16) to (-50+100), with no change thereafter, even at -400 mesh. Dissolution stopped at about 70% extraction. The reason for this phenomenon is not apparent.

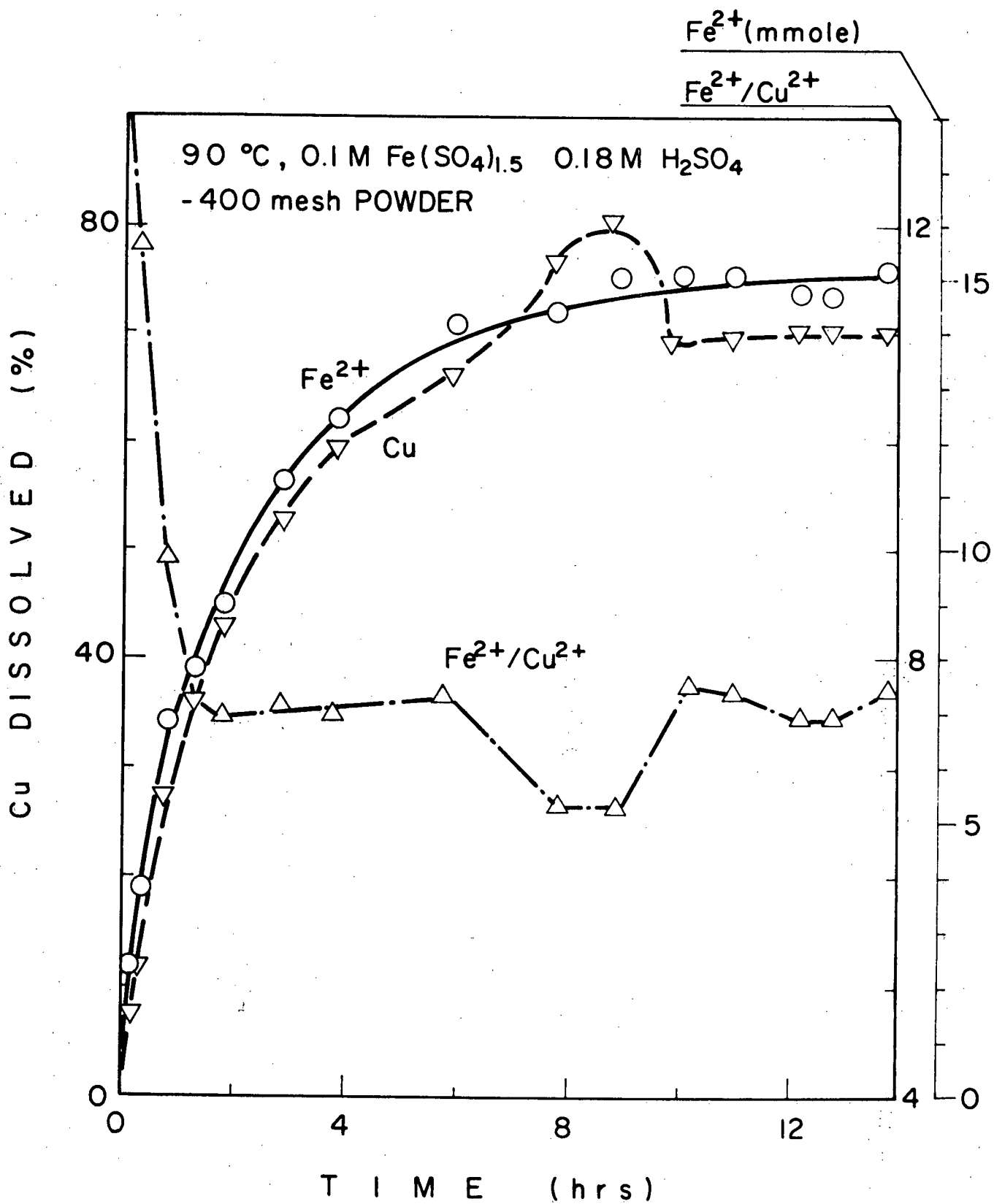


Fig. 72 The leaching of powdered chalcopyrite with ferric sulphate.

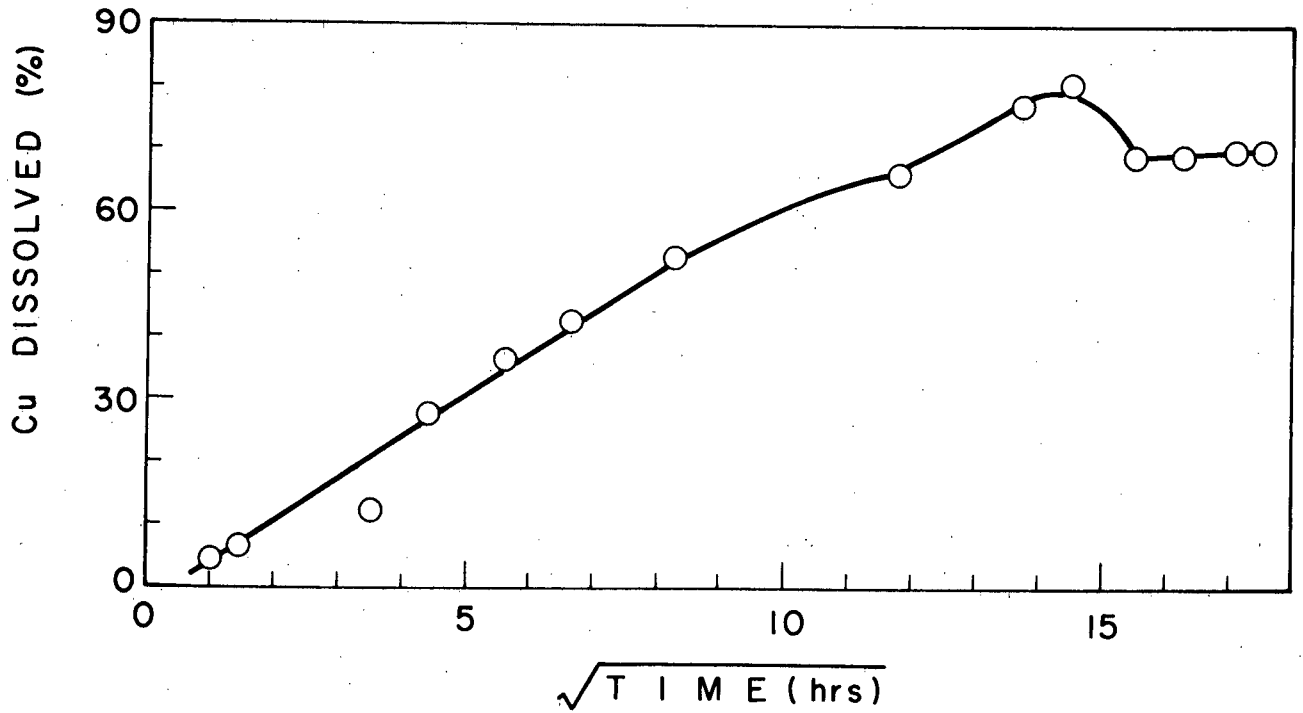
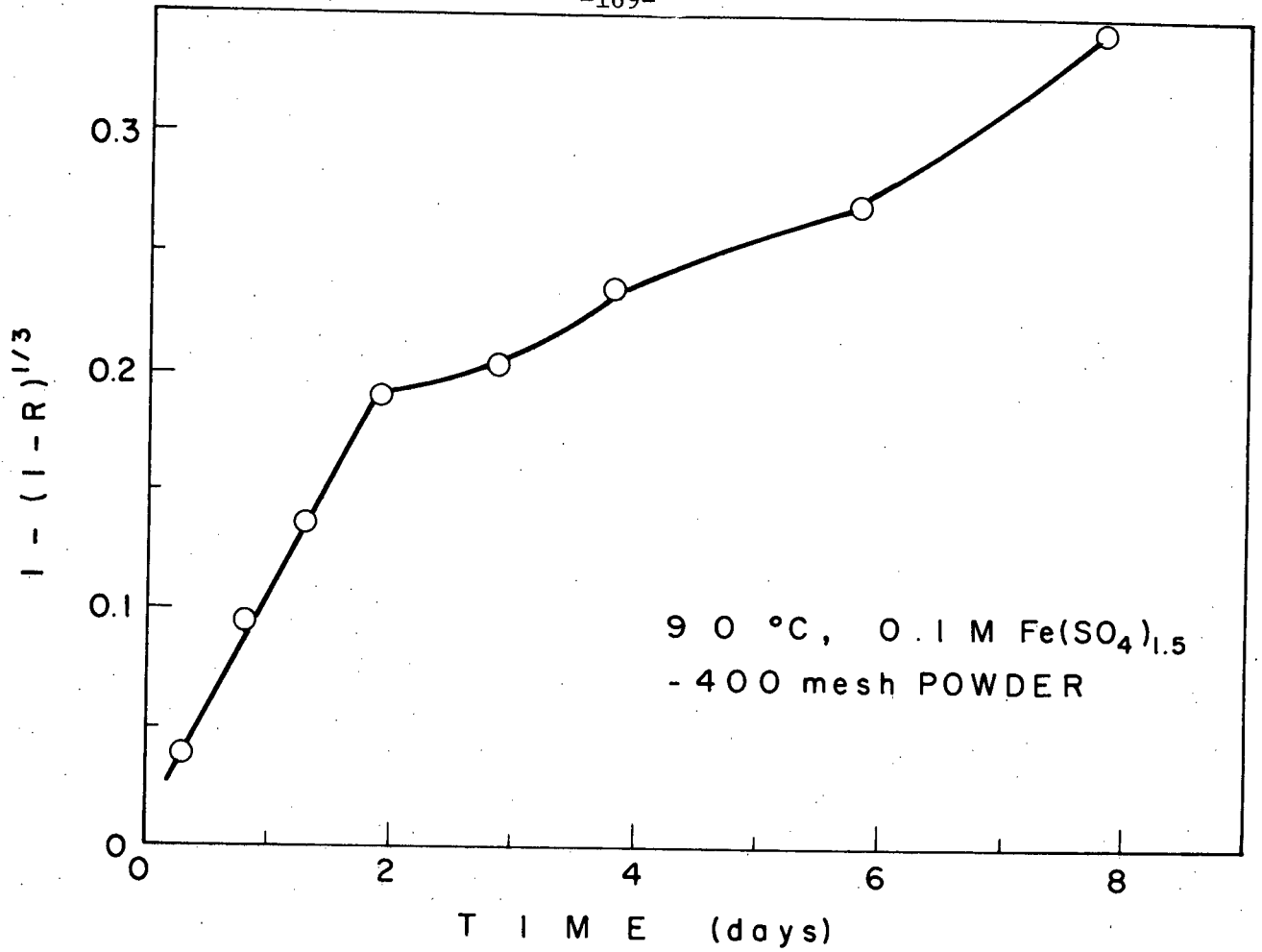


Fig. 73 Comparison of linear and parabolic kinetics in the leaching of powdered chalcopyrite with ferric sulphate.

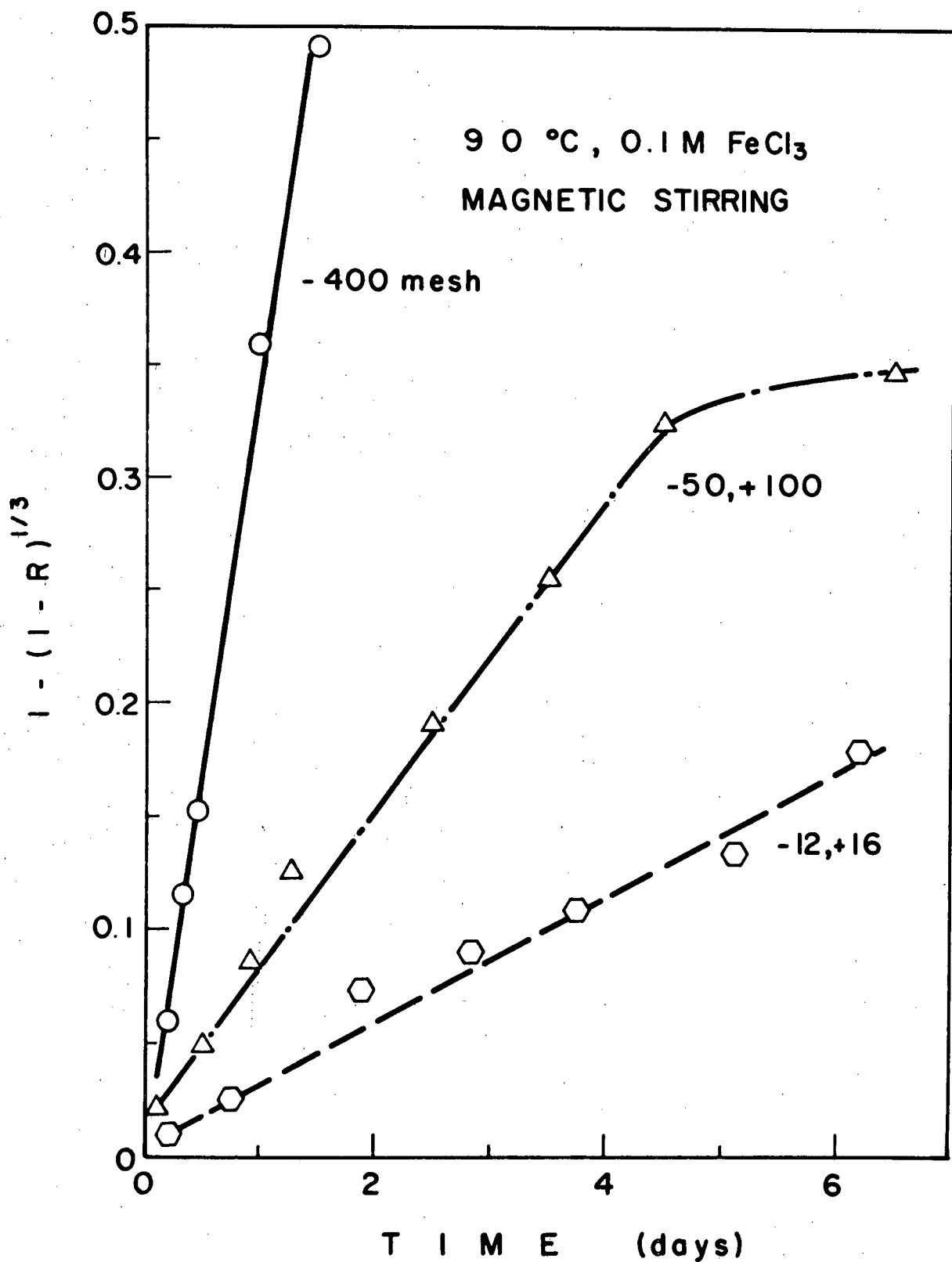


Fig. 74 Leaching of powdered chalcopyrite with ferric chloride.

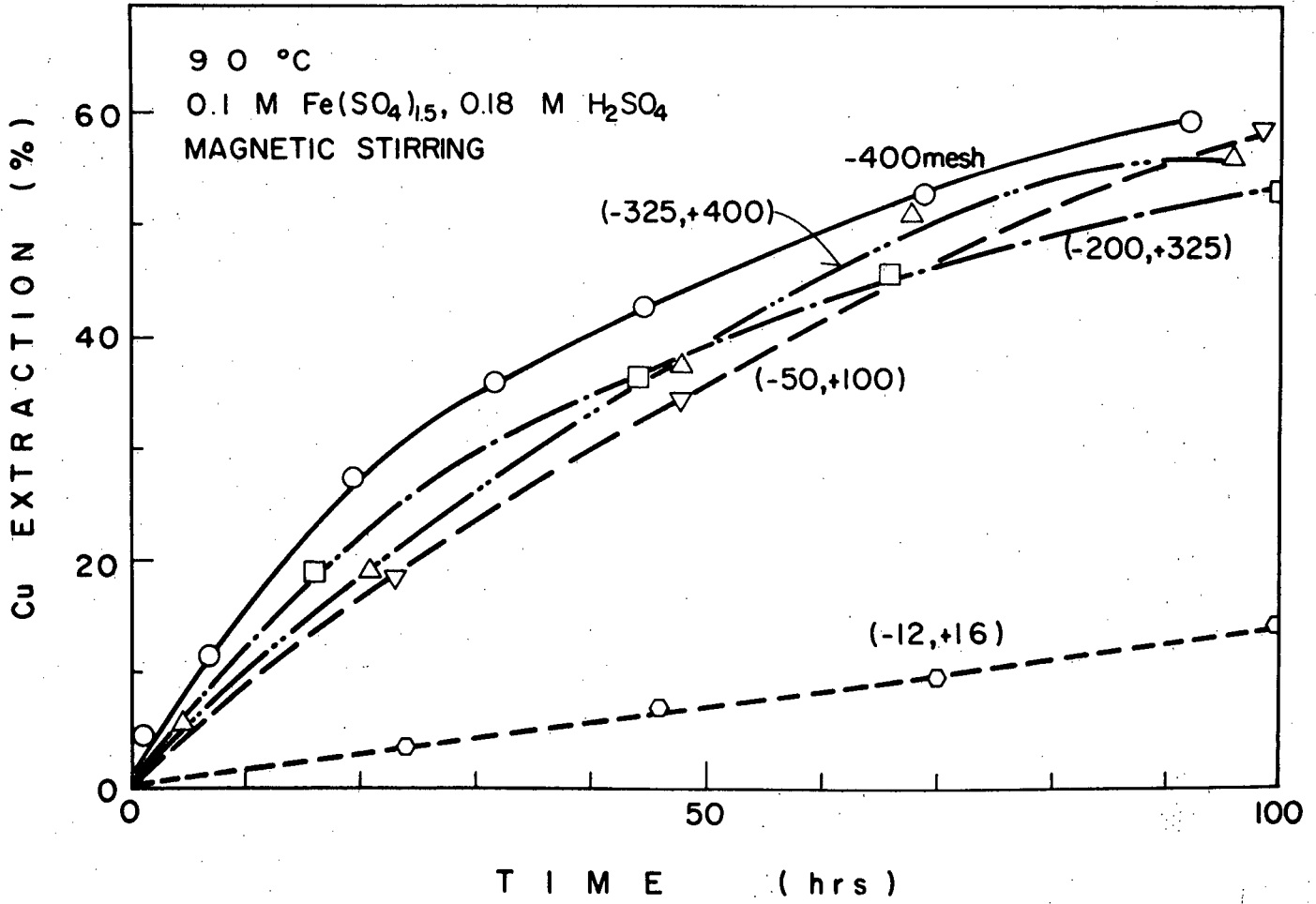


Fig. 75 Effect of particle size in ferric sulphate leaching.

(iii) Fe⁺⁺/Cu⁺⁺ Ratios Produced During Leaching

In Figure 68, an approximately constant ratio of 7.5 is established after the first day; the dip in the curve seems to be spurious. This experiment was done in ferric sulphate, and similar experiments produced Fe⁺⁺/Cu⁺⁺ ratios close to 7.5 (Figure 76).

In ferric chloride, ratios were close to 6.0 (Figure 77)

These values are approximately in agreement with those obtained in leaching of massive specimens, although somewhat higher in each case. The reason for this may be connected with the cessation of the reaction.

(iv) Effect of Ferric Concentration

In chloride solutions, increasing the [Fe⁺⁺⁺] increases the rate of extraction of copper (Figure 77). The increase, however, is by no means proportionate to [Fe⁺⁺⁺], as reported by Ermilov et al (140), on massive specimens.

In sulphate solutions, the dissolution rate does not improve for [Fe⁺⁺⁺] above 0.1M (Figure 76).

These results are again in agreement with earlier work here and in the literature (131), on massive specimens.

(v) Effect of Added Chloride

In 0.03M FeCl₃, the dissolution rate was increased 50% by adding 1M NaCl, but the effect was negligible in 0.1M FeCl₃.

(vi) Effect of [Fe⁺⁺]

In chloride solutions, addition of 0.1M [Fe⁺⁺] had no effect on the dissolution rate; however in sulphate solutions, a drastic reduction in rate was noted between 0.01M [Fe⁺⁺] and 0.1M [Fe⁺⁺] (Figure 78).

With 0.1M FeSO₄, leaching virtually stopped at 4% Cu extraction, whereas

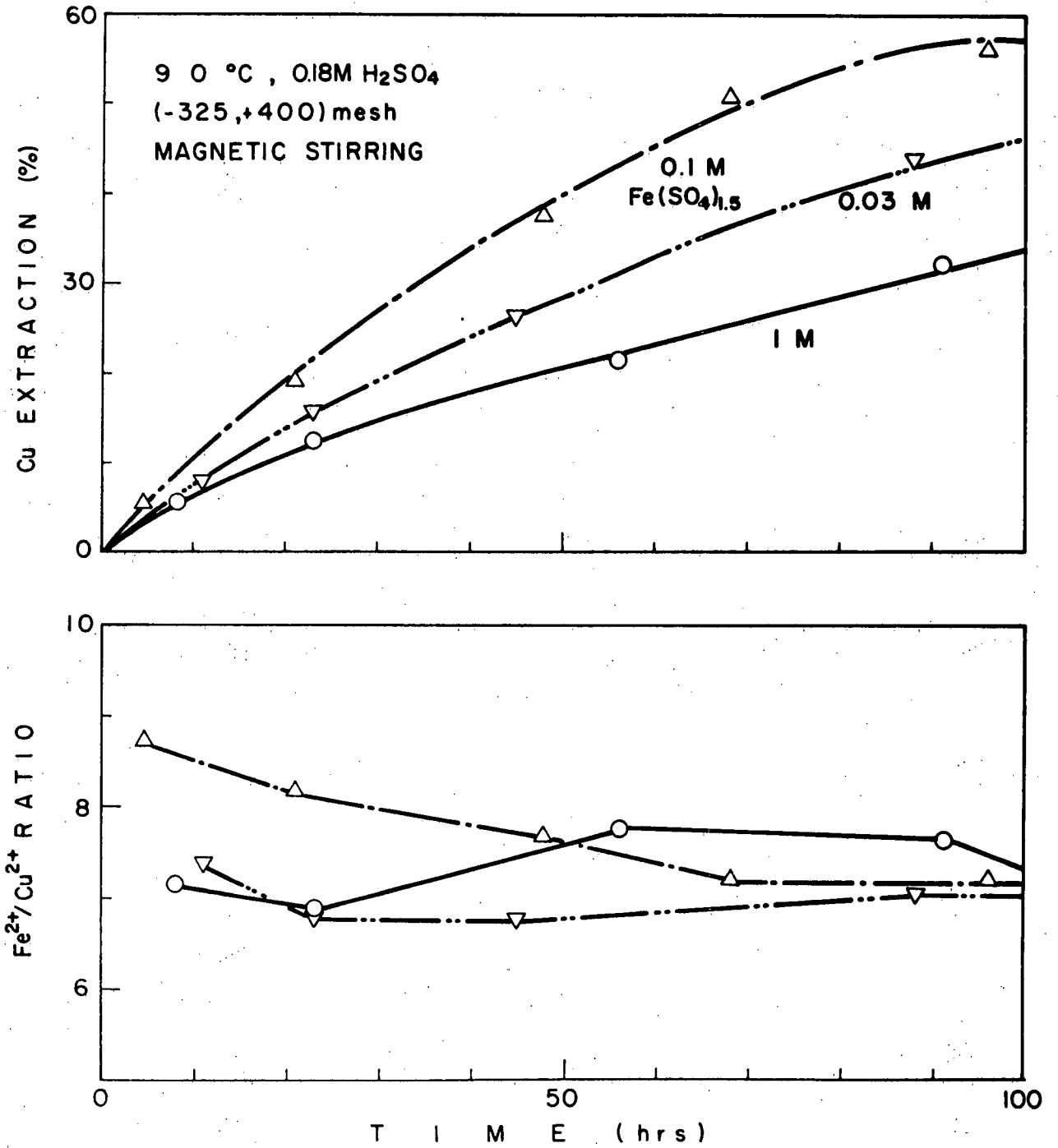


Fig. 76 Effect of [Fe⁺⁺⁺] in ferric sulphate leaching.

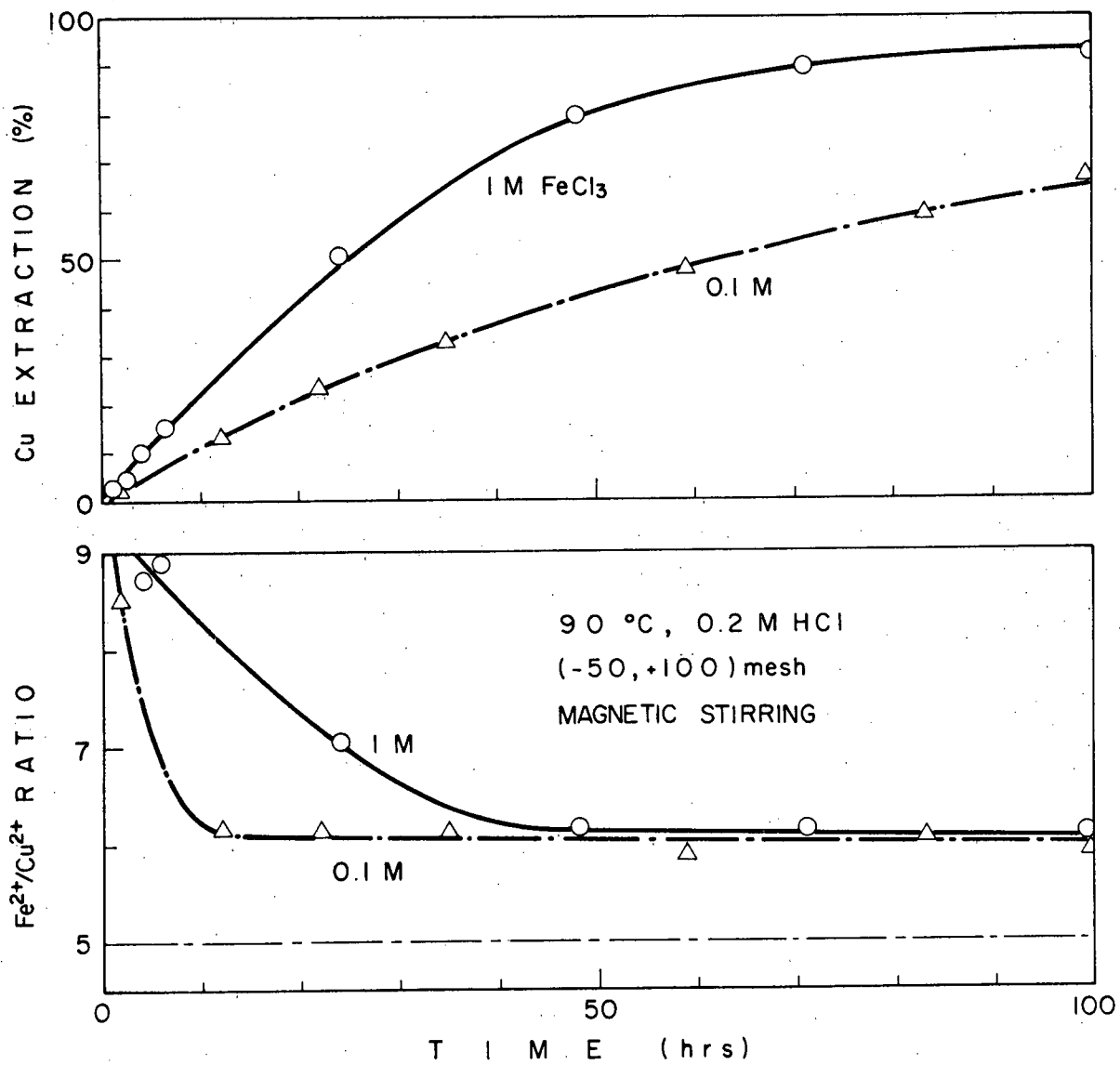


Fig. 77 Effect of $[Fe^{+++}]$ in ferric chloride leaching.

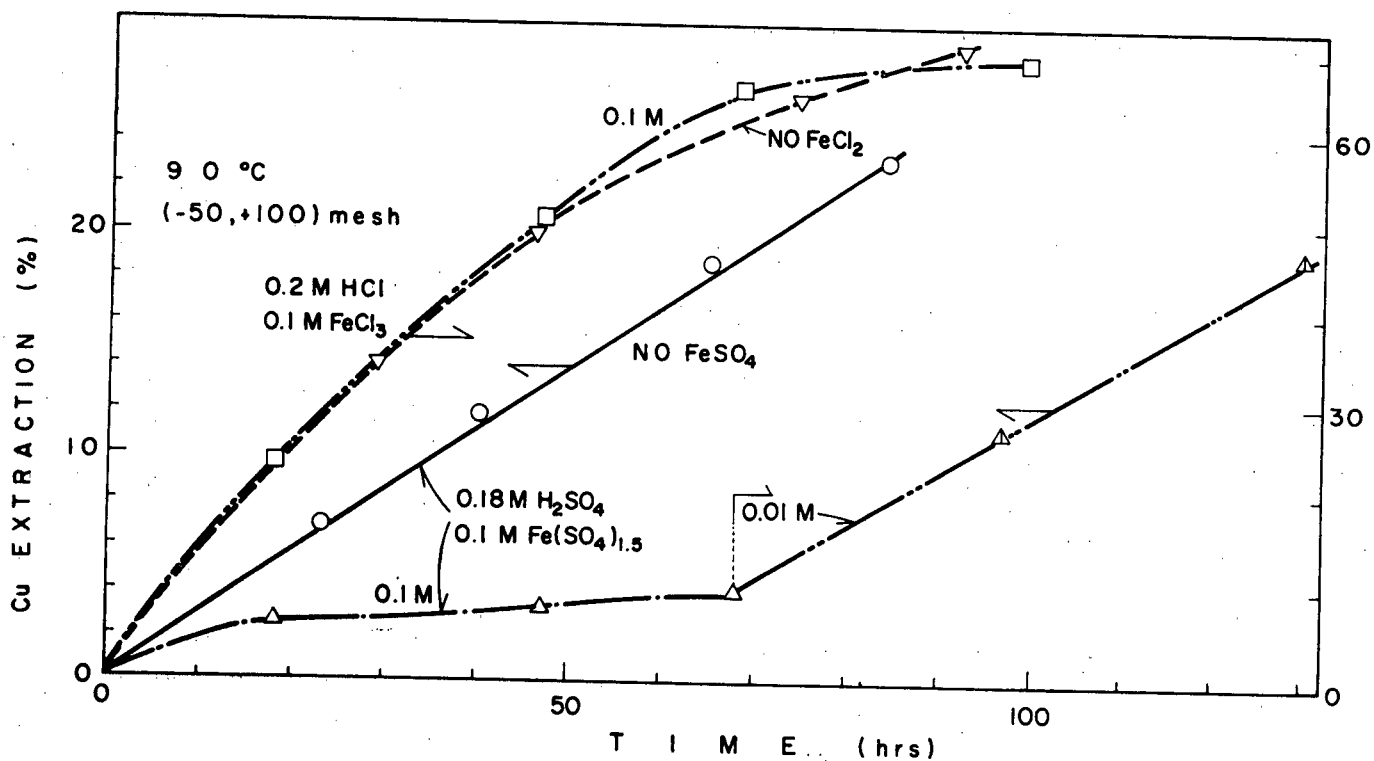


Fig. 78 Effect of $[Fe^{++}]$ in ferric sulphate and chloride leaching.

in 0.01M FeSO_4 the rate is the same as in a solution with no added FeSO_4 .

(vii) Effect of Acid

In chloride solutions, the dissolution rate appears to be at a minimum with 0.24M HCl with small increases observed at higher or lower pH.

In sulphate solutions, rates are similar in 0.018M and 0.18M H_2SO_4 .

(viii) Effect of Stirring Mode

Using (-50+100) mesh particles, a significant increase in rate of dissolution is realized by changing from mechanical to magnetic stirring, (Figure 79), in ferric chloride solution.

However, in ferric sulphate solution, a very much greater increase is realized (with magnetic stirring).

The reason for this increased rate is almost certainly the grinding action of the magnetic stirrer bar, which can cause size reduction of the particles or create some other beneficial effect, such as higher defect concentrations in the solid.

(ix) Effect of Temperature

The effect of temperature on leaching with 1M FeCl_3 is displayed in Figure 80. Using the amount of copper after 5 hours, an activation energy of 17.3 kcal/mole was calculated. This is somewhat higher than values calculated earlier for anodic dissolution (Figures 47-49, 59), but in agreement with values in the literature for ferric chloride (Ermilov (140) 12.3 kcal.) and ferric sulphate (Dutrizac (131), 17.3 kcal).

(x) Effect of Grain Size in Ferric Sulphate Leaching

Some single crystals of chalcopyrite, obtained from Ward's Museum, were verified by Laue photographs. Their size was approximately in the (-12+16) range.

It was of interest to study the leaching of this material because the earlier work (Section IV - (b)) had indicated that CuFeS_2 dissolved preferentially in ferric sulphate along fissures, which presumably were grain boundaries.

A comparison of the leaching of these single crystals with that of 'normal' (polycrystalline) CuFeS_2 is shown in Figure 81. Unfortunately the only data for polycrystalline material were obtained using magnetic stirring, whereas the single crystals were leached with a mechanical stirrer. However the rate is faster with the single crystals, even though the mechanical stirring produces slower extraction rates (see above).

This unexpected result seems to disprove the theory that ferric sulphate leaches primarily at grain boundaries. However, there is the possibility of sub-grain boundaries playing an important role.

Also the single crystals may be more reactive than the polycrystalline material by virtue of not having been ground or crushed in any way.

It may be significant that the $\text{Fe}^{++}/\text{Cu}^{++}$ ratio produced on leaching single crystals is abnormally high (Figure 81).

(xi) Summary: Comparison of Ferric Chloride and Ferric Sulphate Leaching

In Figure 79, the rate of dissolution of (-50+100) mesh CuFeS_2 is shown as being approximately equal in 0.1M FeCl_3 and 0.1M $\text{Fe}_2(\text{SO}_4)_3$, using magnetic stirring. These conditions are optimum for ferric sulphate leaching, for increasing $[\text{Fe}^{+++}]$, or finer particles do not increase the rate. However, FeCl_3 leaching is benefitted greatly by these two factors; furthermore high $[\text{Fe}^{++}]$ depresses the rate of ferric sulphate leaching, but not ferric chloride leaching.

Therefore it must be concluded that ferric chloride leaching is in general faster than ferric sulphate leaching, the difference depending on

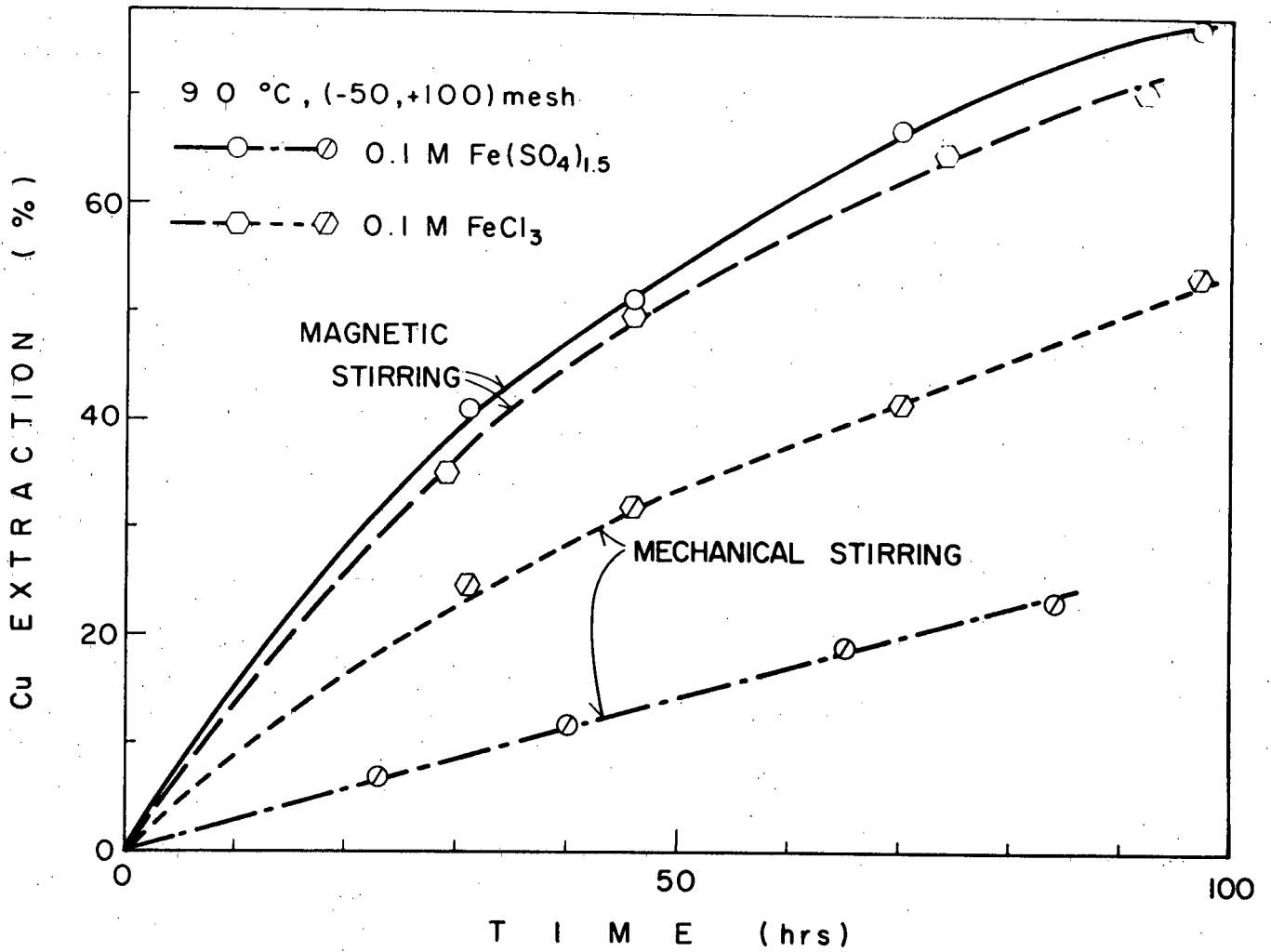


Fig. 79 Effect of stirring mode in ferric sulphate and chloride leaching.

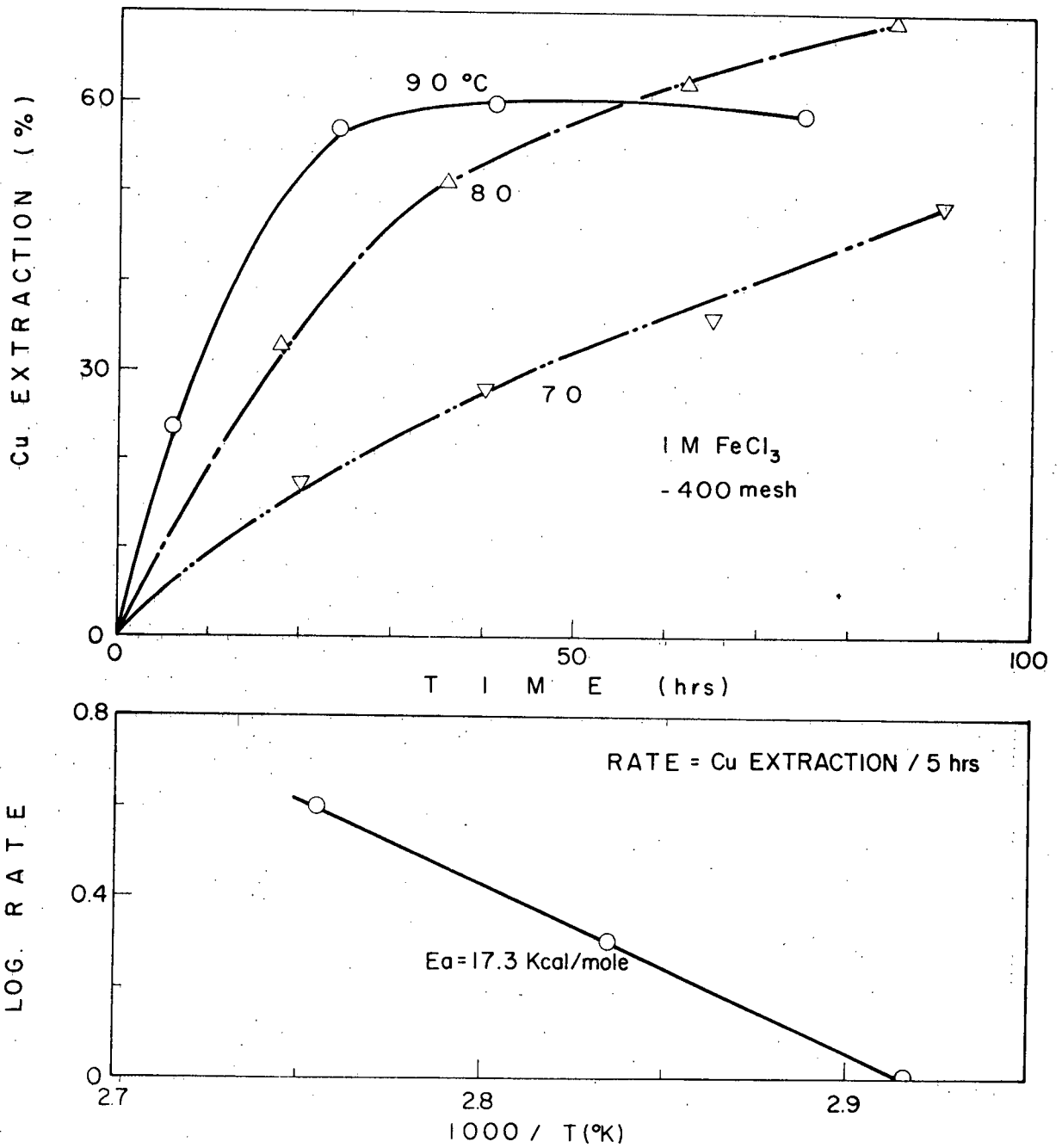
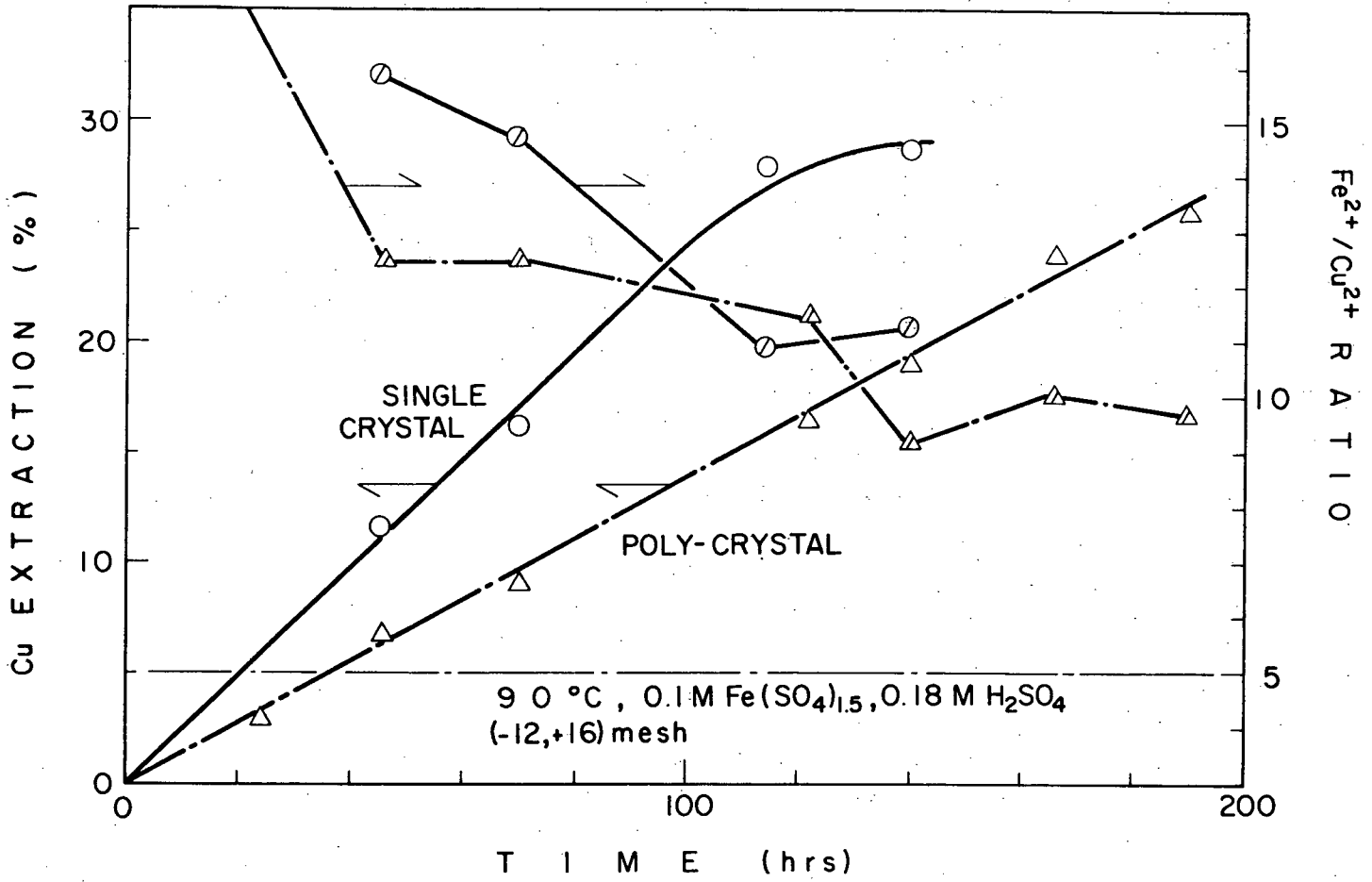


Fig. 80 Effect of temperature on ferric chloride leaching.

Fig. 81 Effect of grain size on ferric sulphate leaching.



[Fe⁺⁺⁺], [Fe⁺⁺] and the size of the particles.

d) Concentrate Leaching

In the experiments described in the previous section, it was demonstrated that chalcopyrite leaching in ferric solutions is facilitated by the following conditions:

- Chloride Solution
- High [Fe⁺⁺⁺]
- High Temperature
- Small Particle Size.

However, in all these experiments, extractions were slow compared to industrial requirements: e.g. 80 hours required to extract 90% of contained copper in 0.1M FeCl₃ from -400 mesh powder, 90°C.

It may be argued that raising the [Fe⁺⁺⁺] or temperature, or lowering the particle size will improve this extraction rate significantly, but it is difficult to visualize how 99% extractions could be obtained within an hour, as reported by Haver and Wong (137); e.g. in Figure 77 it is seen that only a 50% increase in rate is achieved in leaching (-50+100) material in 1M FeCl₃ rather than 0.1M.

The answer to this dilemma is to be found in the shape of the leaching curves, as mentioned in the introduction. This is demonstrated in this section, using actual concentrates from five separate mines:

Concentrate	% Cu	% Fe
Craigmont (B.C.)	26.0	52.5
Ruttan Lake (Man.)	31.9	31.9
Phoenix (B.C.)	27.5	31.5
Valley Copper (B.C.)	43.3	19.1
Granisle (B.C.)	39.1	20.0

(analysis carried out by author).

The first three concentrates were (supposedly) primarily chalcopyrite, but the last two contained some bornite (Cu_5FeS_4). The high iron content of the Craigmont concentrate may indicate the presence of some bornite also.

In Figure 82, the leaching of three of these concentrates in 1M FeCl_3 at 90°C is shown; a distinctly faster rate is evident at the start of each experiment, compared to that prevailing after the first three hours. In fact, the slow, second stage seemed to have a similar rate in all three experiments, and the distinguishing feature is the rate of the first stage.

Using Craigmont concentrate only, the same conclusion may be drawn about the effect of particle size or $[\text{Fe}^{+++}]$ (Figure 83), i.e. decreasing the particle size from 200 μ to 30 μ increases the rate of the first stage by 50% (0.1M FeCl_3) or nearly 100% (1M FeCl_3). Increasing the $[\text{Fe}^{+++}]$ from 0.1M to 1M increases the rate of the first stage by 60% (-400 mesh) or 45% ((-50+100) mesh). In all these cases, the second stage leaching rates were approximately equal.

This phenomenon has great importance in an industrial process, for leaching rates are not as important as extraction times. Due to the slow rate of the second stage, it is important to achieve the desired extraction within the first stage. Thus in Figure 83 (0.1M FeCl_3 leaching) only five hours are required to extract 36% of the copper in a (-400) mesh sample whereas 15 hours were required for a (-50+100) mesh sample. The extraction time (to 36%) was decreased by a factor of three; however the second stage leaching rate was hardly affected.

High extractions in short residence times are therefore consistent only with the persistence of stage 1 leaching essentially to completion; the effects of the above variables on stage 2 are so small that if the transition occurs before acceptable extraction, very long residence times

become mandatory.

The maximum extraction rates for the different concentrates was determined by leaching the finest fraction of each, in 4M FeCl₃ at reflux temperature, 109°C.

Concentrate	Finest Fraction	Max. Extraction Extent	Time	90% Extraction Time	Ratio
Craigmont	-400	100%	4 hrs.	2 hrs.	8
Ruttan	-325	86%	5	∞	∞
Phoenix	-270 +325	90%	3	3	12
Valley Copper	-400	100%	1	1/4	1
Granisle	-400	97%	2	1	4

These data are shown in Figure 84, where the very fast rate of dissolution of Valley Copper concentrate is evident, the rate in the first stage is 2 - 3 times as fast as it is for Craigmont, Phoenix, or Ruttan concentrates. The 90% extraction times are in the ratio 1:4:8:12:∞.

The difference between the various concentrates may be mineralogical or average particle size. It was difficult to reduce the Ruttan and Phoenix concentrates to -400 mesh, using a mortar and pestle - the brittleness that characterizes large pieces of chalcopyrite does not extend past about 200 mesh. Therefore each of the three less reactive concentrates was ground several hours in a small porcelain jar mill, and the -400 fraction leached as before, under optimum conditions.

The results of this extra grinding were not beneficial - in each case the extractions were slightly reduced.

The Fe⁺⁺/Cu⁺⁺ ratios produced during leaching were also determined (Figures 82, 84). For Craigmont concentrate values were close to 5.0

(1M Fe Cl₃ 90°C) or 4.5 (4M FeCl₃ 109°C). Values below 5.0 can be the result of bornite present in the sample, or prior oxidation. For the known bornite concentrates, Granisle and Valley Copper, values were near 3.2 (4M FeCl₃, 109°C); for Phoenix and Ruttan ratios were 5 - 5.5.

e) Summary

Leaching chalcopyrite with ferric chloride is much more effective than leaching with ferric sulphate. At 90°C, in dilute (ferric) solutions, the leaching rates are approximately equal, for particles larger than 100 mesh. However, in ferric chloride leaching, the reaction rate is greatly increased by using finer particles and higher [Fe⁺⁺⁺], these factors having negligible effect in ferric sulphate. Furthermore, in ferric sulphate, the leaching rate is severely depressed by high [Fe⁺⁺], whereas this has no effect in ferric chloride leaching.

The chemistry of the leaching reaction in ferric sulphate and ferric chloride is similar to that found in electrochemical experiments, i.e. there is a greater degree of sulphur oxidation in sulphate solutions than in chloride, (approximately 25%), and iron dissolves before copper does.

The observed leaching rate in ferric sulphate or ferric chloride also correlated with the anodic current densities obtained in the electrochemical experiments. Therefore the leaching of chalcopyrite appears to be an electrochemical reaction.

The morphology of leaching appears to be different in ferric sulphate from that in ferric chloride. In the former case, preferential attack along fissures was noted, whereas in the latter overall attack on the mineral surface was observed.

Similar dissolution chemistry was observed in the leaching of massive specimens and powdered material. Linear kinetics were observed with massive

specimens, but on powdered material a more complex behaviour was noted.

In ferric sulphate and under 'gentle' conditions in ferric chloride (i.e. large particles, low $[\text{Fe}^{+++}]$, low temperature) linear kinetics were observed up to a certain point (generally 50 -80% dissolution), and then the reaction slowed down and stopped. Under optimum conditions in ferric chloride (small particles, high $[\text{Fe}^{+++}]$, high temperature), a non-linear behaviour was evident; at the start of the reaction there was a very fast dissolution rate, whose extent depended on these same variables. After this stage, the second slow dissolution rate prevailed. This phenomenon leads to a drastic reduction in extraction times, which are no longer proportional to the (inverse of the) leaching rate, as in the linear case.

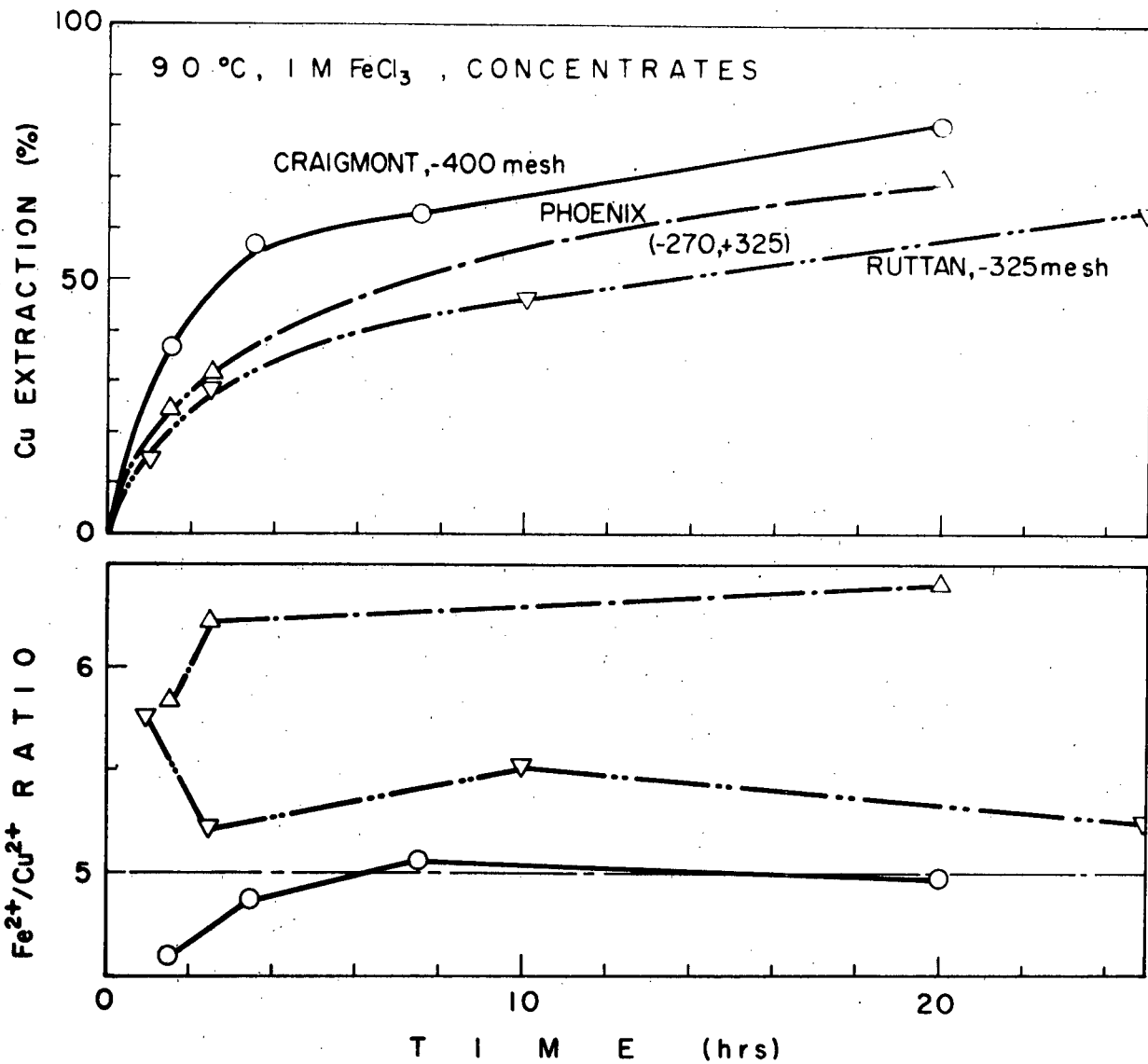


Fig. 82 Leaching of various concentrates with ferric chloride.

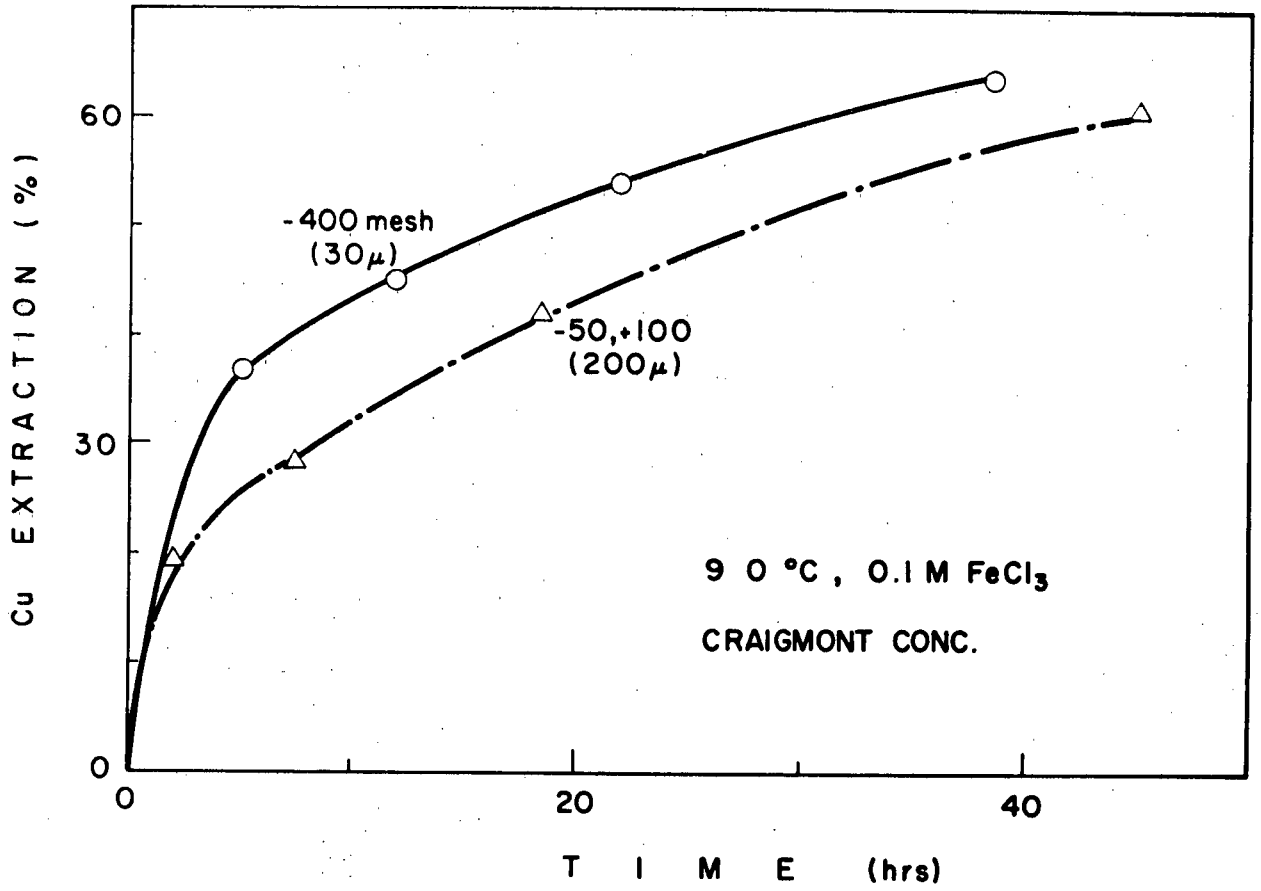


Fig. 83 Effect of particle size on concentrate leaching.

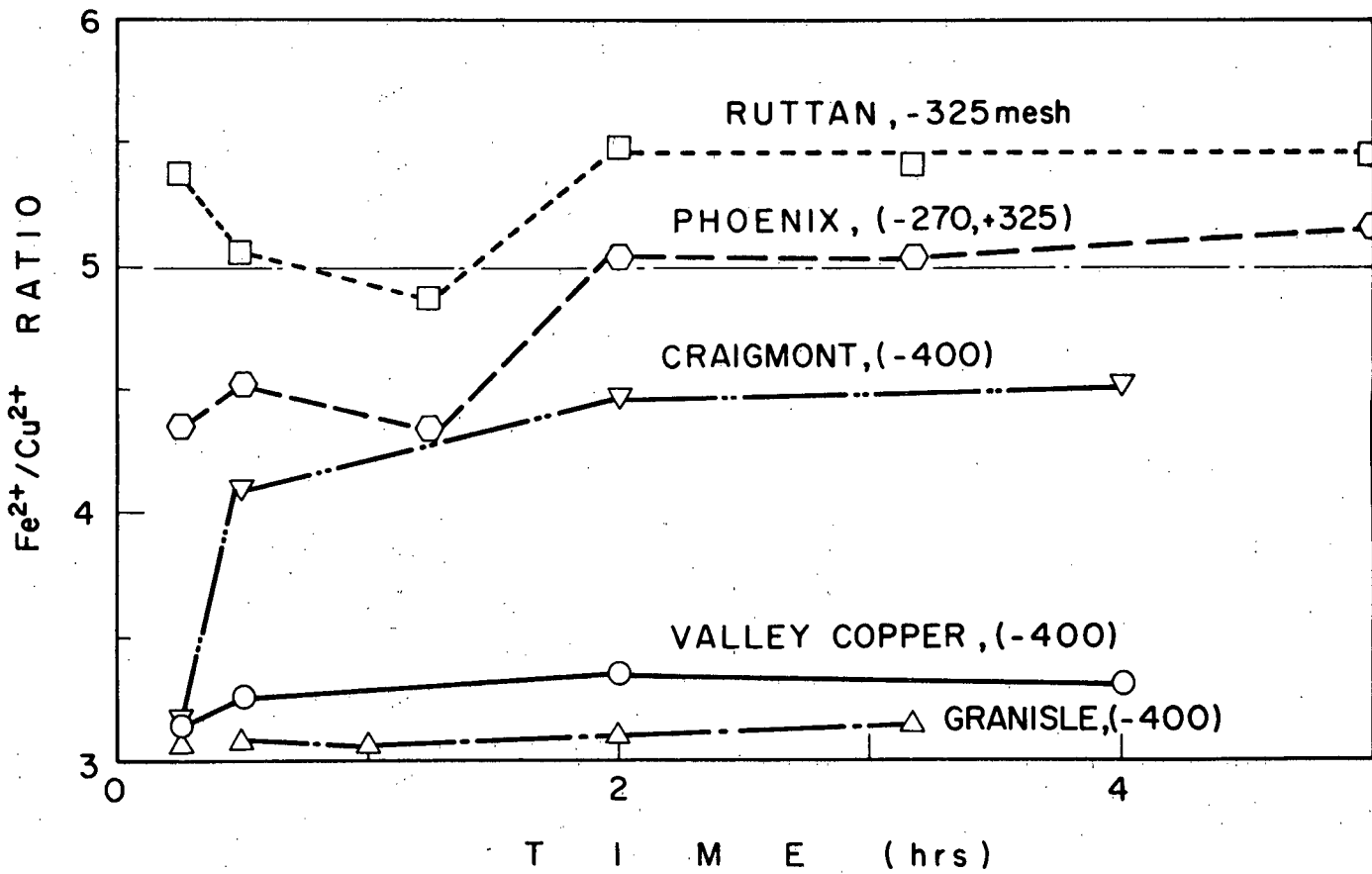
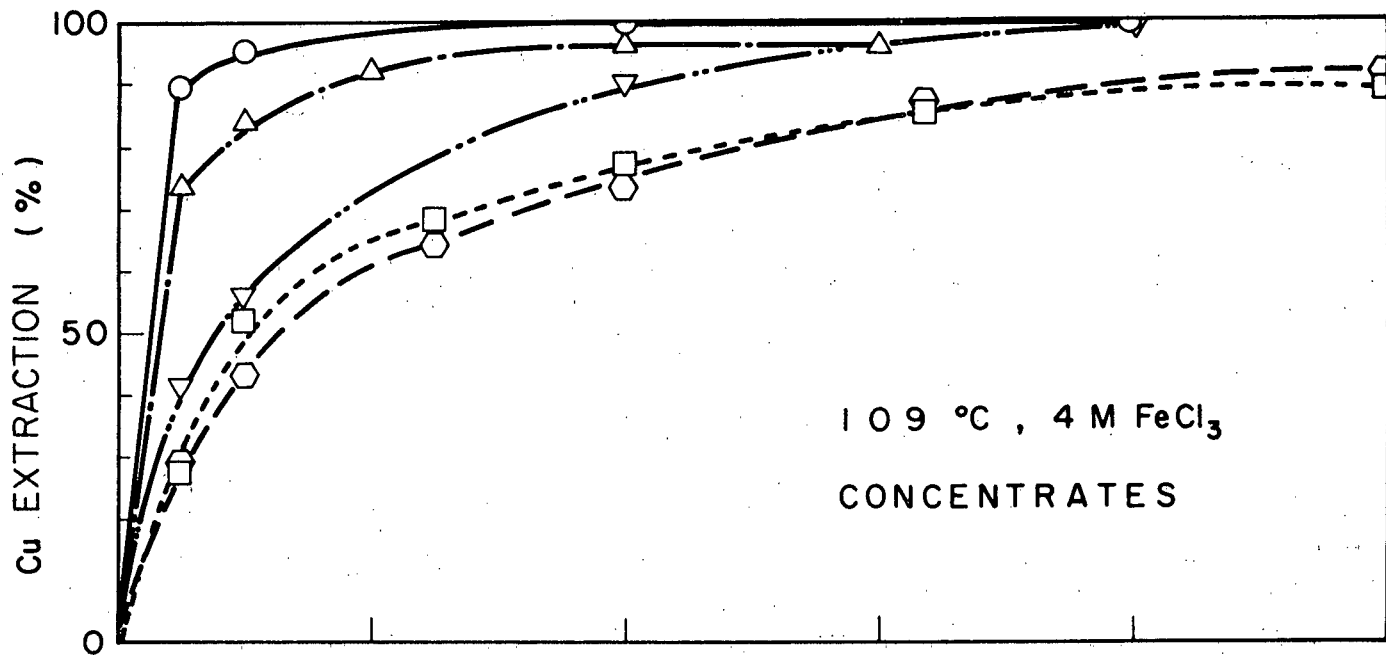


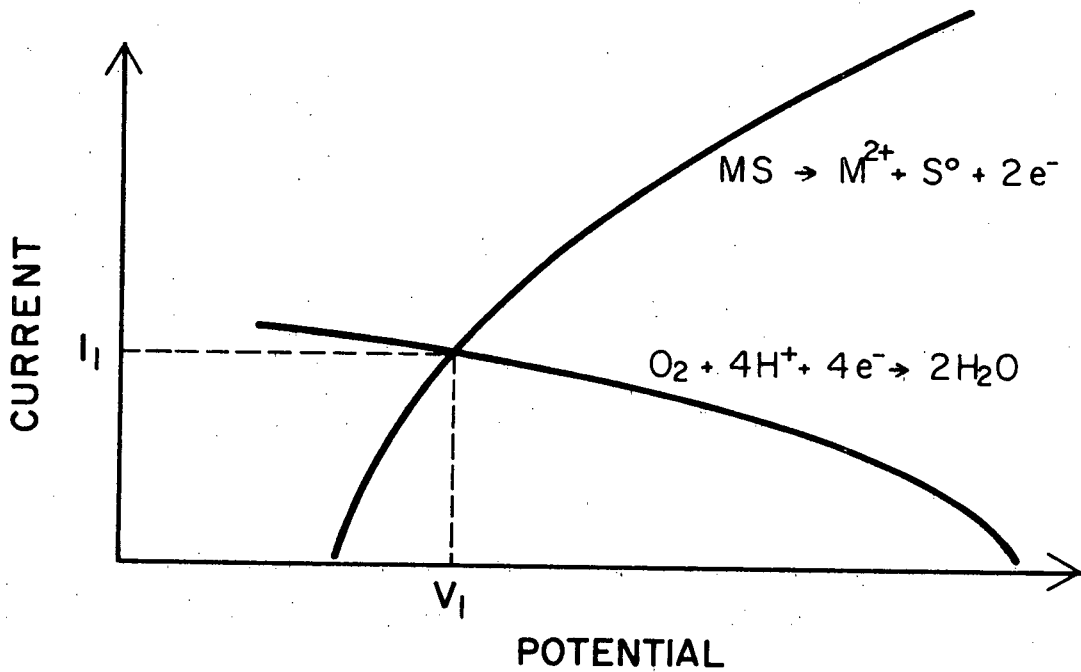
Fig. 84 Optimum leaching of various concentrates.

V Mixed Potential Measurements

a) Motive

The mixed potential of a mineral is that potential which results from the mineral being placed in a corroding environment. It differs from a true rest potential in that the combination of anodic and cathodic processes that take place in the mineral are no longer symmetrical, and a net corrosion current is present.

A typical mixed potential is obtained when a sulphide is placed in an oxygenated acid solution; here one cathodic process is the reduction of oxygen, probably strongly polarized, while the anodic process is the dissolution of the mineral:



In the figure V_1 is the mixed potential, and I_1 is the corrosion current, which is related to the leaching rate by the stoichiometry of the reaction.

The purpose of measuring mixed potentials in this work is two-fold:

- 1) To determine what typical values are
- 2) To determine how these values are affected by solution composition.

Mixed potentials provide a useful link between the chemical and electrochemical results; by knowing both the potential that a mineral assumes and the resulting current and chemistry associated with that potential, one may predict the leaching rates of the mineral, and compare these predictions with the observed chemical leaching results. If favourable, this comparison is substantial evidence for an electrochemical mechanism; it has been used successfully by Etienne (90) on copper sulphides, and Needes and Nicol (91) on uranium dioxide leaching.

b) Results

(i) Ferric Sulphate Leaching

Mixed potentials were measured using one-lead electrodes, against a Ag/AgCl electrode in 1M KCl, all at 90°C. This reference electrode was frequently checked, and when using a strong leaching solution, a 4M KCl solution was used in the Luggin capillary, although liquid-junction potentials appeared to be negligible. The apparatus was that shown in Figure 7, and all experiments were done at 90°C.

Duplicate electrodes were used in all the experiments to be described; they were freshly prepared by saw-cutting.

Starting with a solution $(0.2M H_2SO_4, 0.005M [Fe^{+++}])$ where Fe^{+++} is present as ferric sulphate, the $[Fe^{+++}]$ was increased in stages to 1.0M. Additions of

ferric sulphate were only made after a stable potential was reached; the total time required for this experiment (10 days) was 30 hours, including a 15 hour break. The results are shown in Figure 85.

As can be seen, a linear relationship of potential vs. $\log [\text{Fe}^{+++}]$ was obtained. The two electrodes were approximately 20 mV apart. The slope of the line is 62 mV. At $T = 90^\circ\text{C}$ (363°K), the coefficient in the Nernst equation is 72 mV:

$$\text{e.g. } \text{Fe}^{3+} + \text{e}^- \rightarrow \text{Fe}^{2+}$$

$$E = E^\circ - \frac{2.3RT}{nF} \log \frac{a_{\text{Fe}^{2+}}}{a_{\text{Fe}^{3+}}} = E^\circ - .072 \log \frac{a_{\text{Fe}^{2+}}}{a_{\text{Fe}^{3+}}}$$

where E is potential

E° is standard potential, and R, F have the usual meaning.

After completion of the experiment described above, successive additions of ferrous sulphate were made, (to the same solution) up to 0.5M (Figure 86). A total time of 24 hours was required for this experiment (5 additions).

Small additions, up to 0.05M $[\text{Fe}^{++}]$ had little effect, but thereafter a substantial drop in potential was observed. The electrodes were still ~ 20 mV apart. A total drop of 45 mV was obtained between $\left(\begin{array}{l} 1\text{M Fe}^{+++} \\ .001\text{M Fe}^{++} \end{array} \right)$ and $\left(\begin{array}{l} 1\text{M Fe}^{+++} \\ 0.5\text{M Fe}^{++} \end{array} \right)$.

This experiment was repeated on a dilute solution of ferric sulphate (0.1M) (Figure 87). Adding 0.1M $[\text{Fe}^{++}]$ raised one potential and dropped the other, adding 0.5M $[\text{Fe}^{++}]$ dropped both potentials by about 80 mV.

In every case after the perturbation caused by the addition of ferrous or ferric sulphate, the potential was slow to stabilize, about an hour being required. This phenomenon, and the persistent large difference between the two electrodes, indicates a significant degree of irreversibility of the reactions taking place on the chalcopyrite surface, during ferric sulphate

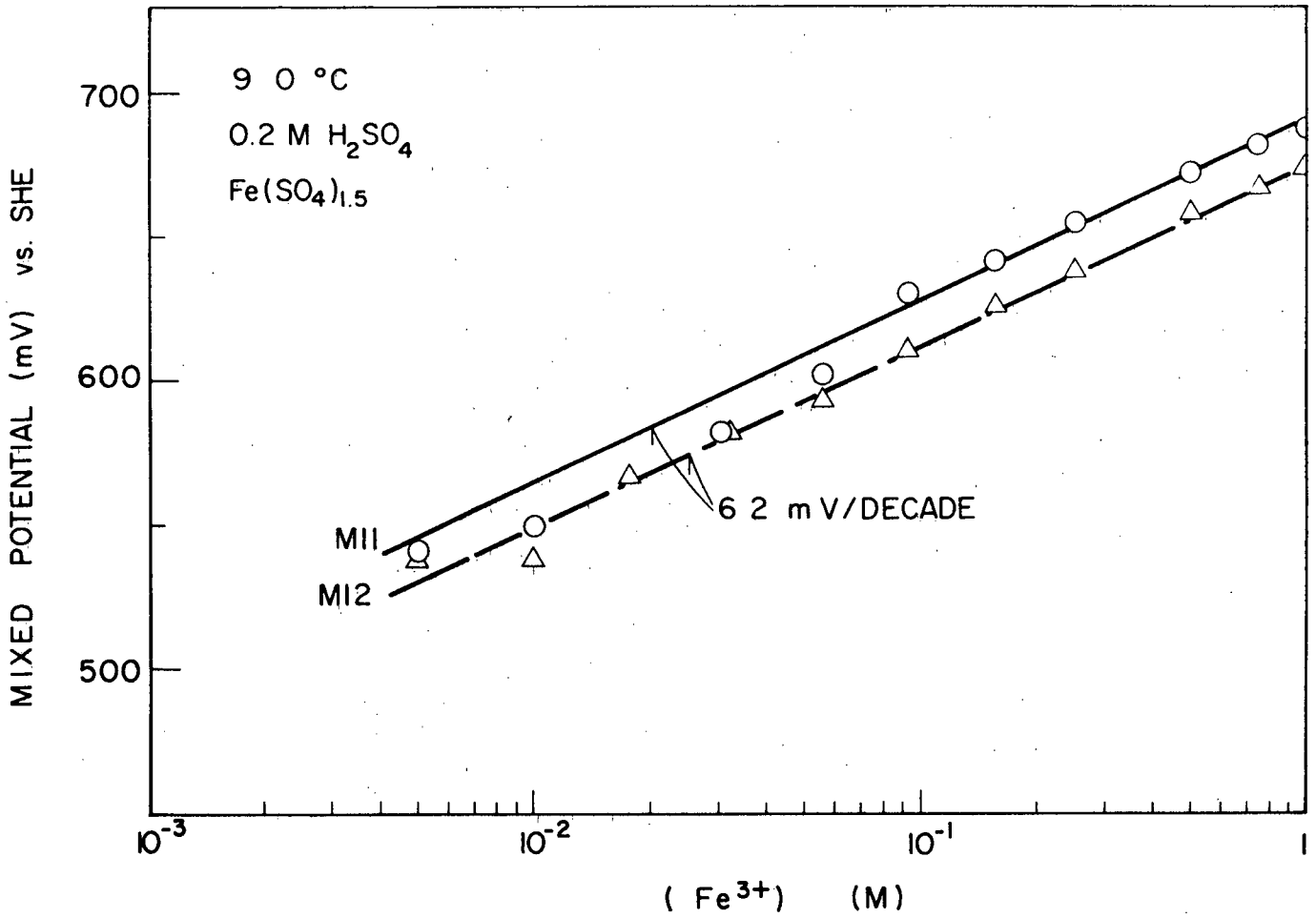


Fig. 85 Mixed potential of chalcopyrite in ferric sulphate.
Effect of [Fe⁺⁺⁺].

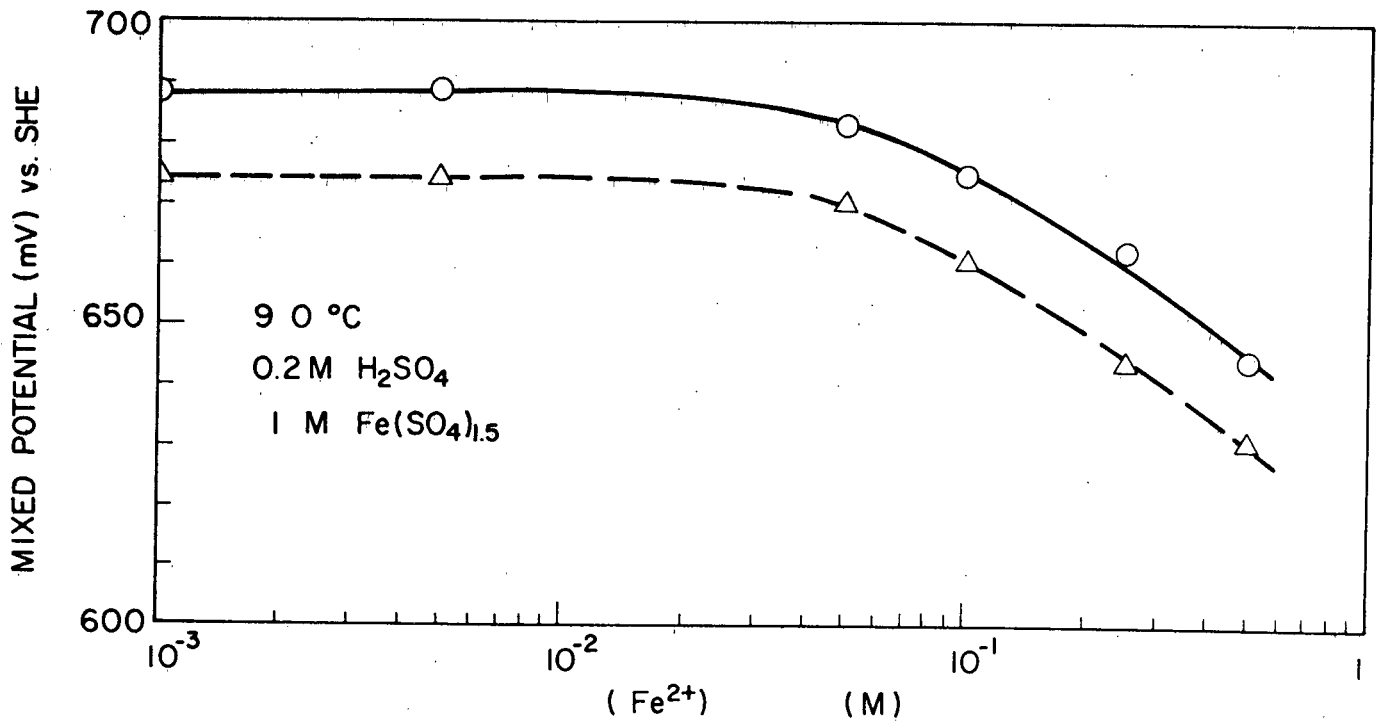


Fig. 86 Mixed potential of chalcopyrite in ferric sulphate.
Effect of [Fe⁺⁺].

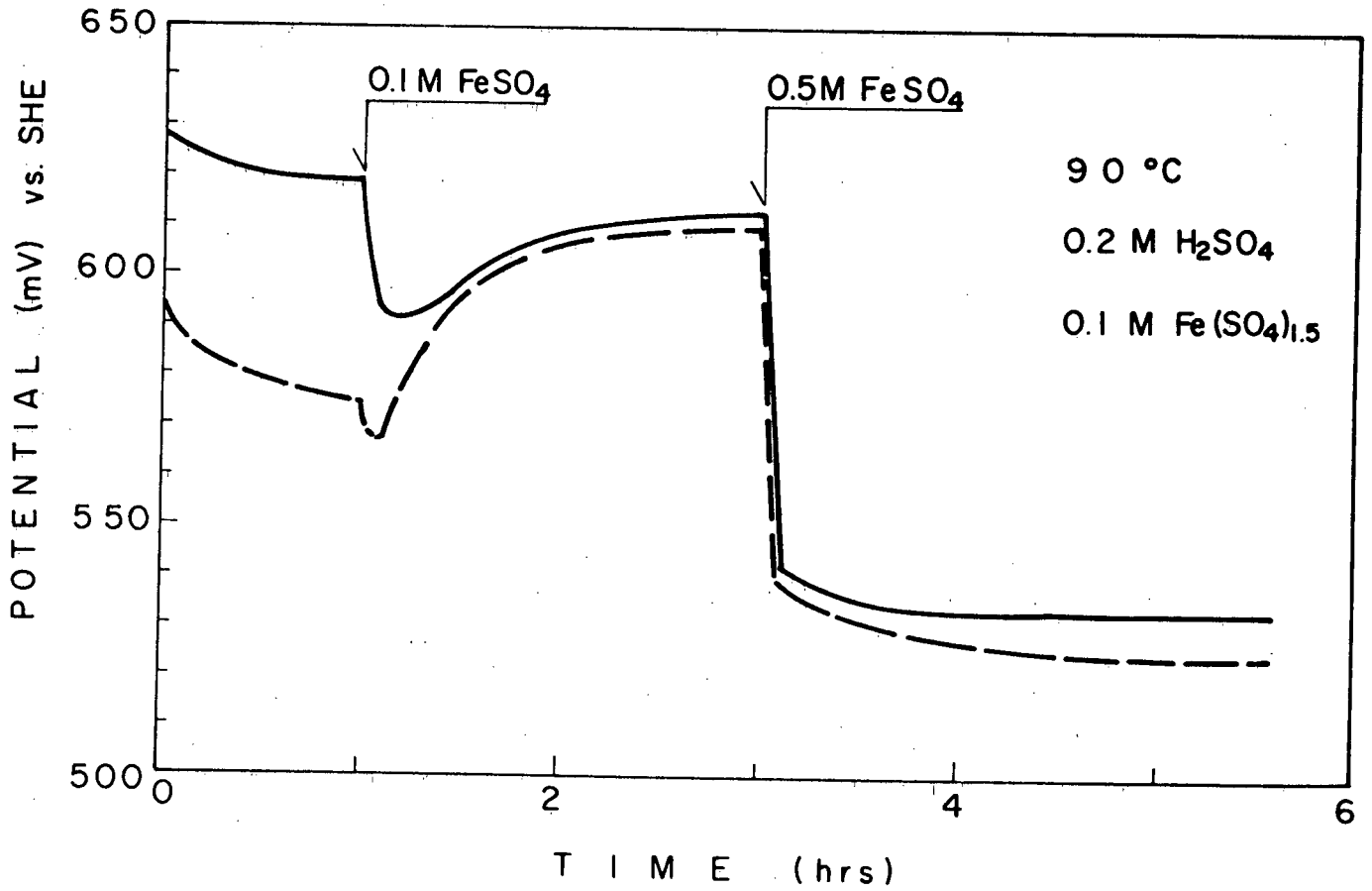


Fig. 87 Mixed potential of chalcopyrite in dilute ferric sulphate.
Effect of $[Fe^{++}]$.

leaching.

Typical mixed potentials to be expected during ferric sulphate leaching are about 610 mV ($[\text{Fe}^{3+}]/[\text{Fe}^{2+}] = 1$).

(ii) Cupric Chloride Leaching

Two new electrodes were prepared, and used for the balance of the experiments described.

Starting with a solution (3M NaCl, 0.2M HCl) (at 90°C) successive additions of CuCl_2 were made, from 0.005M - 1M (Figure 88). An excellent linear relationship with slope 55 mV was obtained, the two electrodes differing by a constant 5 mV.

A remarkable feature of this experiment was the rapidity with which the electrode re-equilibrated after each addition of CuCl_2 . The potential adjusted itself as quickly as the crystals dissolved, with no drifting whatever. This behaviour was in marked contrast to the previous experiment with ferric sulphate, where equilibration required about an hour, instead of a few seconds.

Adding CuCl to the solution obtained at the end of the last experiment, decreased the potential (Figure 89), with a slope of 65 mV. At the conclusion of this experiment, the solution contained 1M CuCl_2 , 1M CuCl , 3M NaCl and 0.2M HCl.

CaCl_2 was then added to this solution, up to 2M CaCl_2 (Figure 90). This had the effect of increasing the potential again, with a slope of 138 mV.

This experiment was repeated, using as starting solution

0.1M CuCl_2
0.1M CuCl
0.2M HCl
0.5M CaCl_2 .

The potential of the CuFeS_2 electrodes again displayed a linear relationship with $\log [\text{Cl}]$, slope 137 mV.

In each of these four experiments (Figures 87 - 90), the re-equilibration was very fast as noted above, and the potentials of the two electrodes were indistinguishable after the addition of 0.01M CuCl . This behaviour indicates that the reactions occurring on the chalcopyrite surface are substantially reversible, during CuCl_2 leaching.

The effect of $[\text{Cl}]$ on CuCl_2 potentials is diminished by low $[\text{Cu}^+]$ levels. Adding CaCl_2 to a solution containing no (added) Cu^+ , i.e. $\left(\begin{array}{l} 1.0 \text{ CuCl}_2 \\ 0.2\text{M HCl} \end{array} \right)$ increased the potential, as shown in Figure 91. The slope is reduced to 65 mV, from 137 mV ($\text{Cu}^{++}/\text{Cu}^+ = 1$). Similarly, adding $[\text{Cu}^+]$ on to solution already high in $[\text{Cl}]$, did not depress the potential as much as when $[\text{Cl}]$ is low (not shown).

(iii) Ferric Chloride Leaching

The effect of $[\text{Fe}^{+++}]$ on the mixed potentials in chloride solution is shown in Figure 92; the (positive) slope is 75 mV. The mixed potentials (1M FeCl_3) were 685/700 mV, compared with 674/688 mV (1M $[\text{Fe}^{+++}]$ as Ferric Sulphate) and 731/736 mV (1M CuCl_2).

The effect of FeCl_2 on the mixed potential of chalcopyrite in 1M FeCl_3 is negligible below 0.1M $[\text{Fe}^{++}]$, and only drops about 15 mV at 1M $[\text{Fe}^{++}]$ (Figure 93).

Even less effect is observed with 0.1M FeCl_3 (Figure 94).

Additions of CaCl_2 have no effect at all on the mixed potential in 0.15M FeCl_3 solution (Figure 95).

Additions of CuCl_2 , however, do have a significant positive effect, this being more evident in dilute FeCl_3 than concentrated (Figure 96).

The rapidity with which the CuFeS_2 electrodes re-equilibrated in FeCl_3

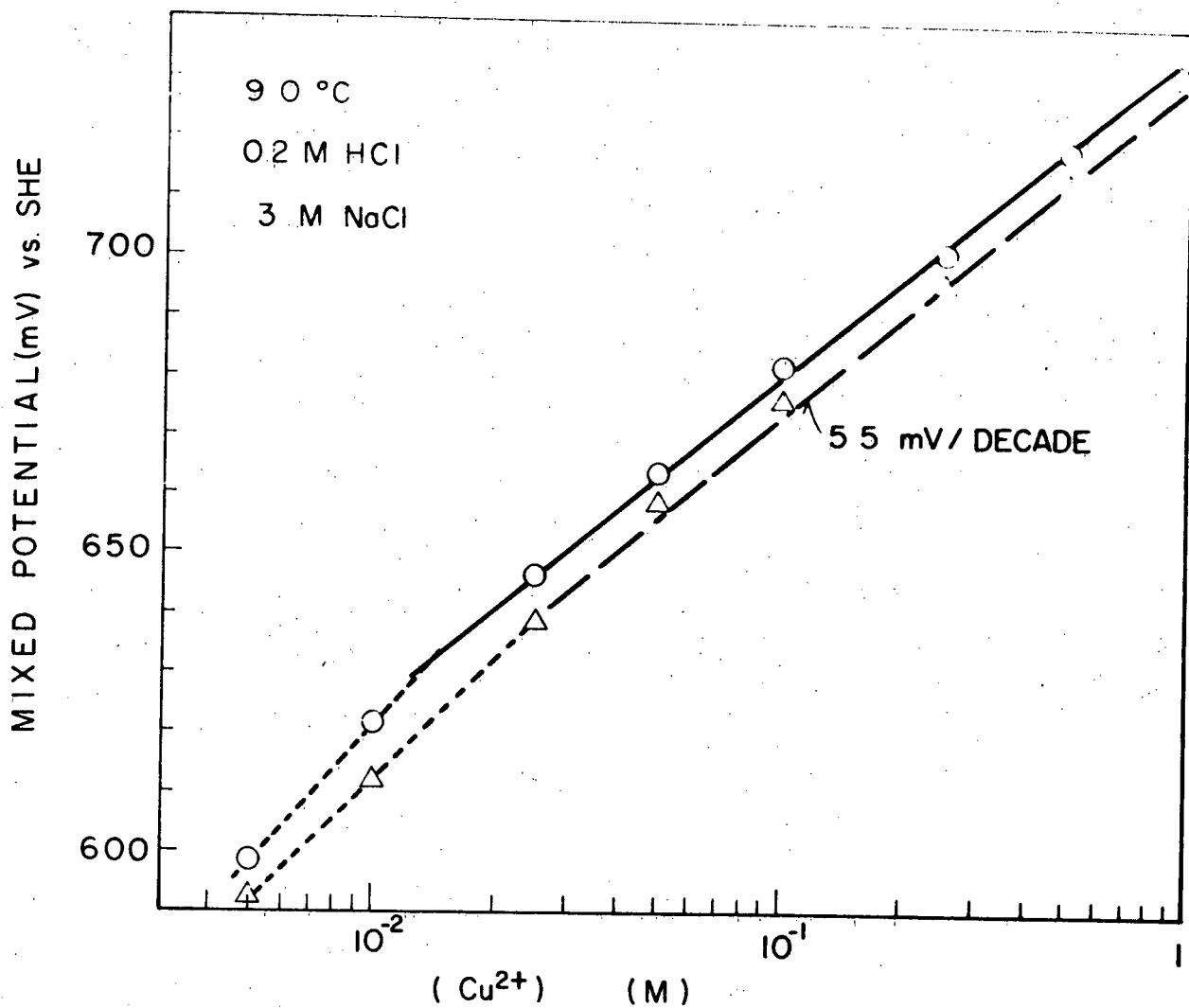


Fig. 88 Mixed potential of chalcopyrite in cupric chloride.
Effect of [Cu⁺⁺].

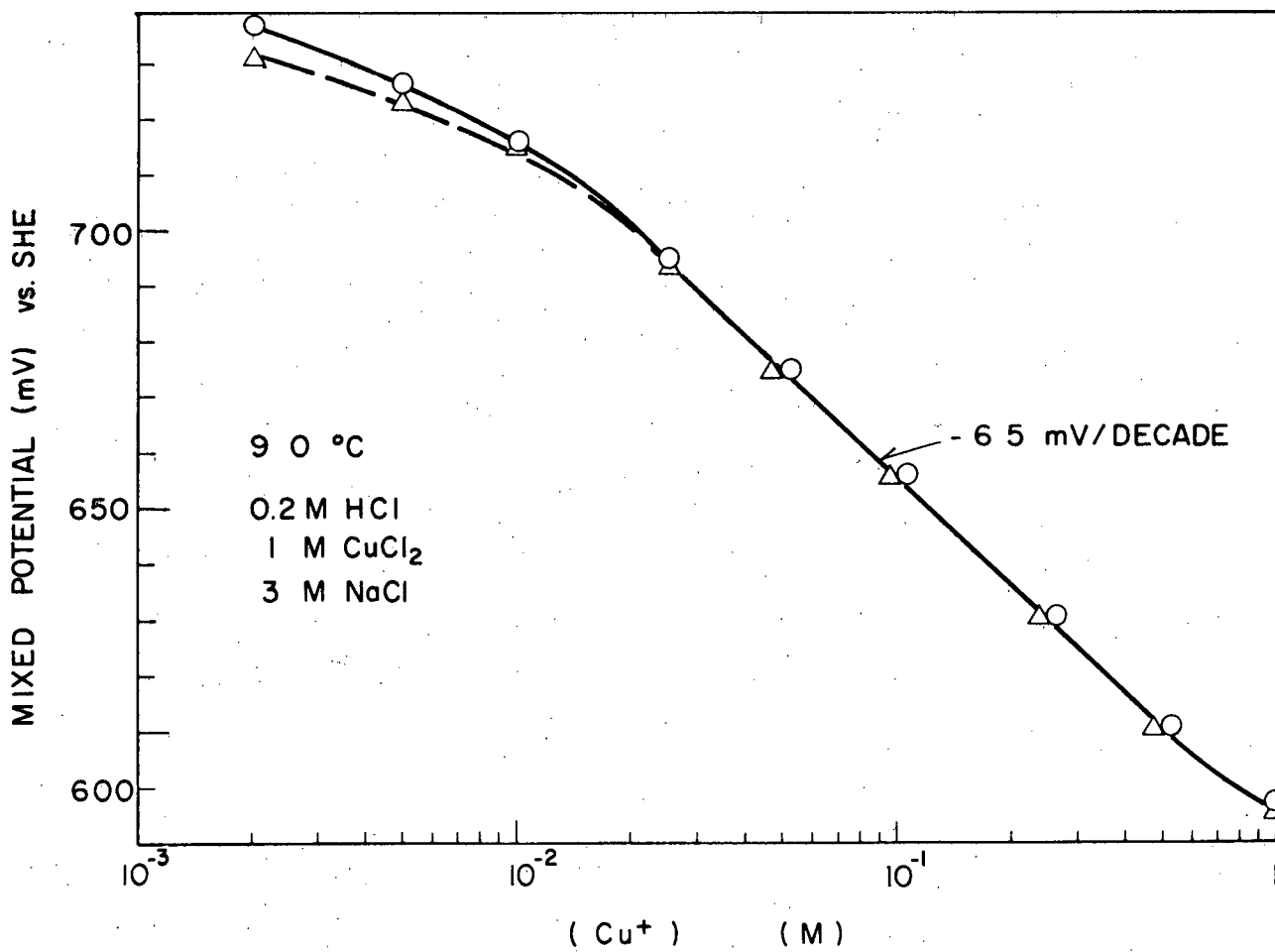


Fig. 89 Mixed potential of chalcopyrite in cupric chloride.
Effect of [Cu⁺].

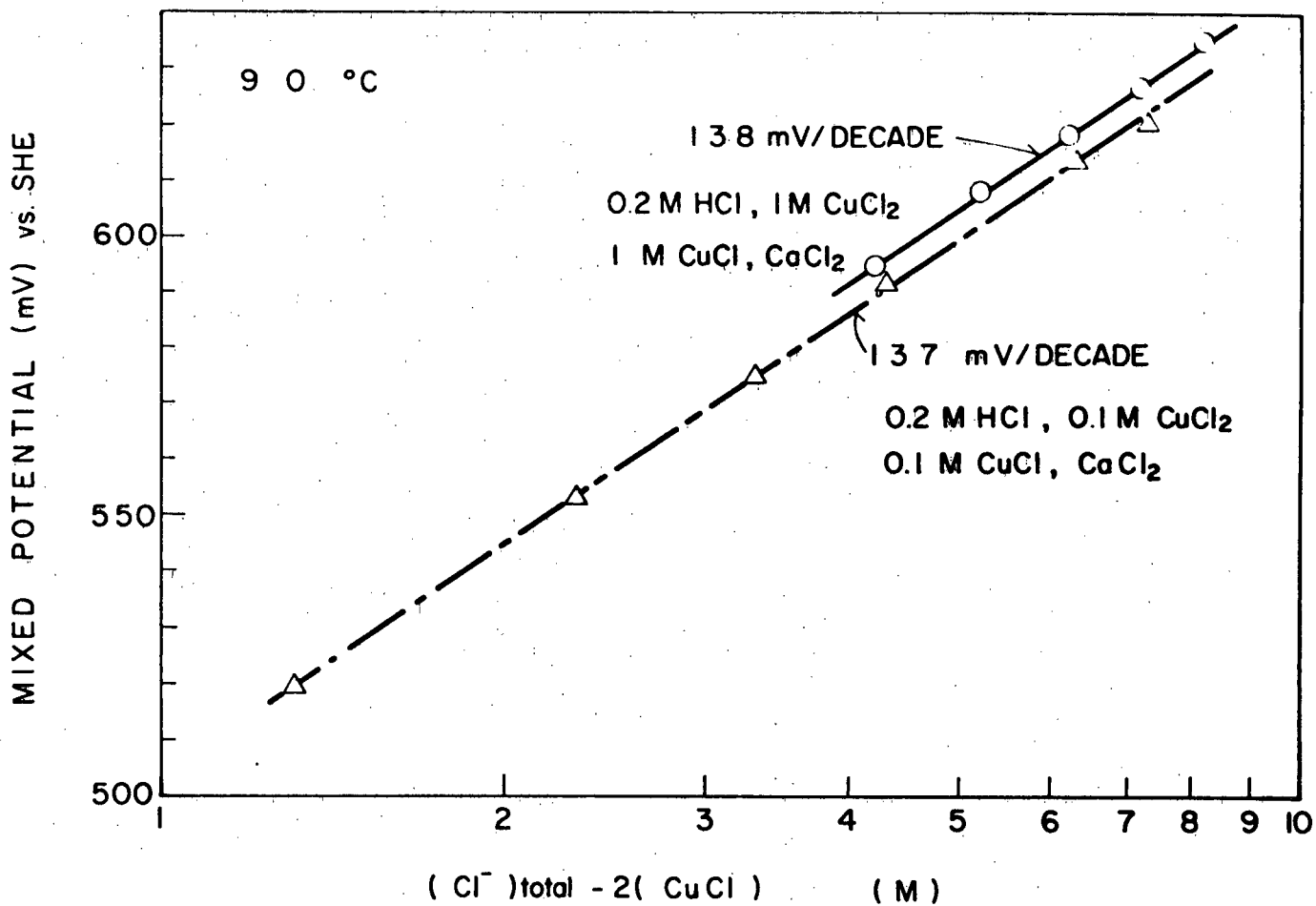


Fig. 90 Mixed potential of chalcopyrite in cupric chloride.
Effect of [Cl].

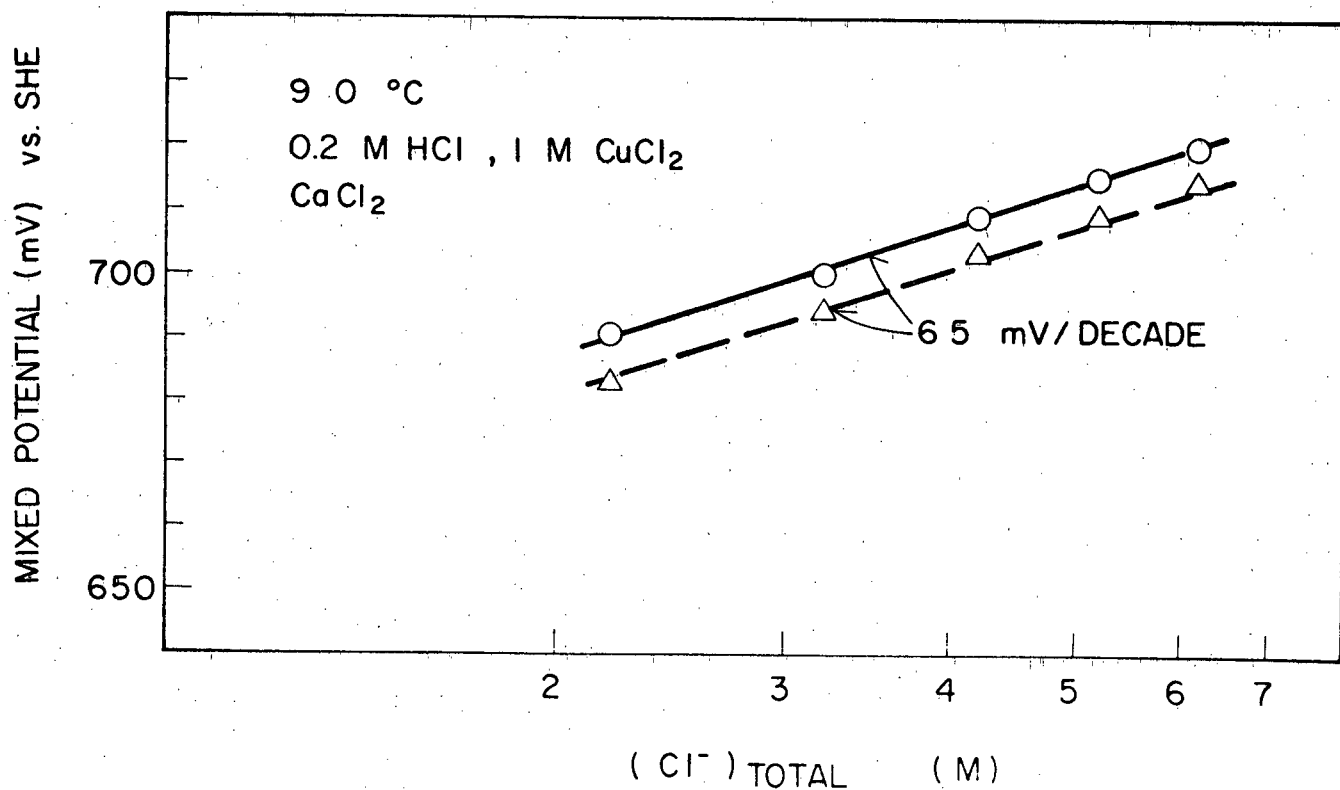


Fig. 91 Mixed potential of chalcopyrite in cupric chloride.
Effect of [Cl] in absence of cuprous chloride.

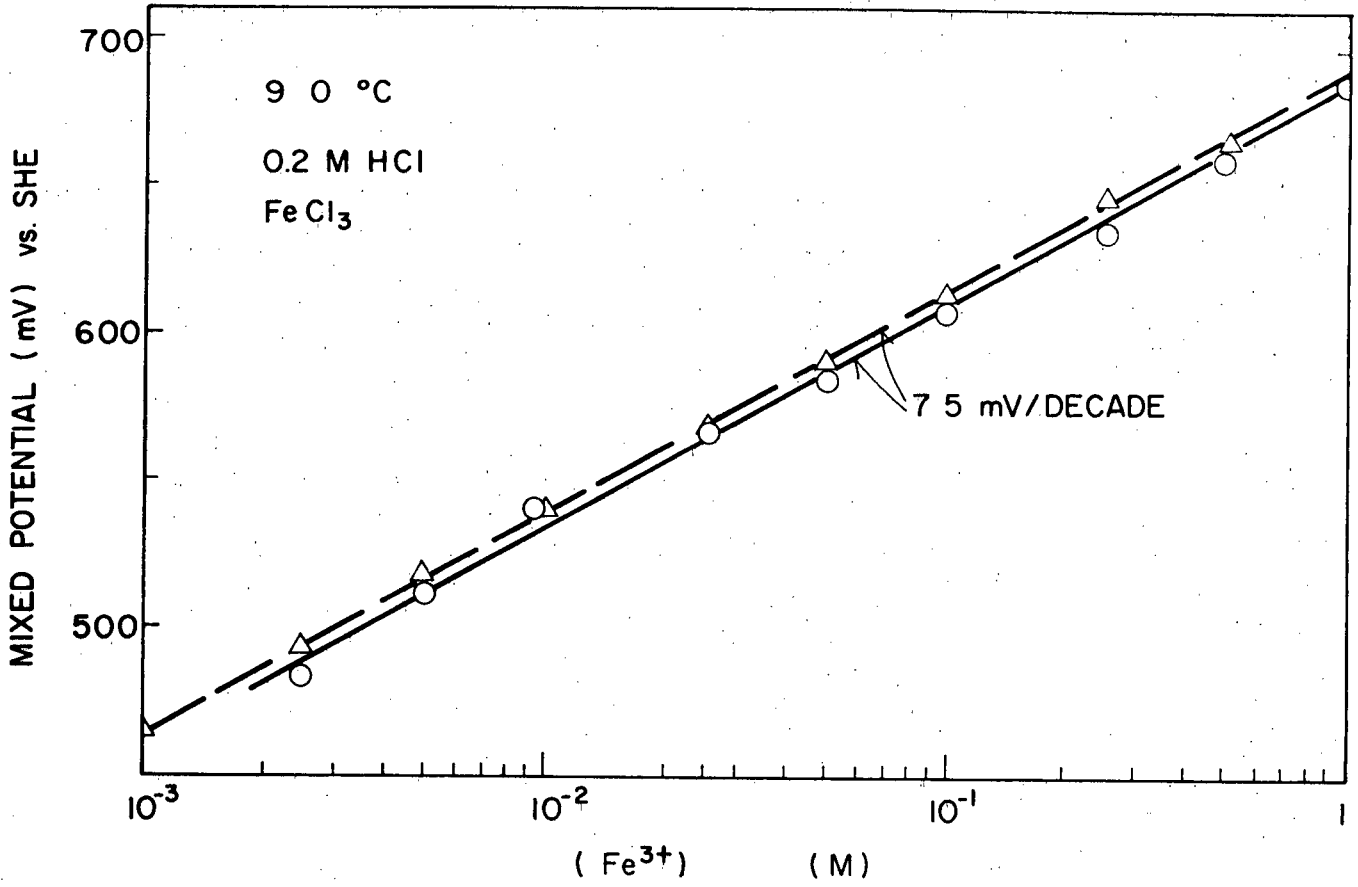
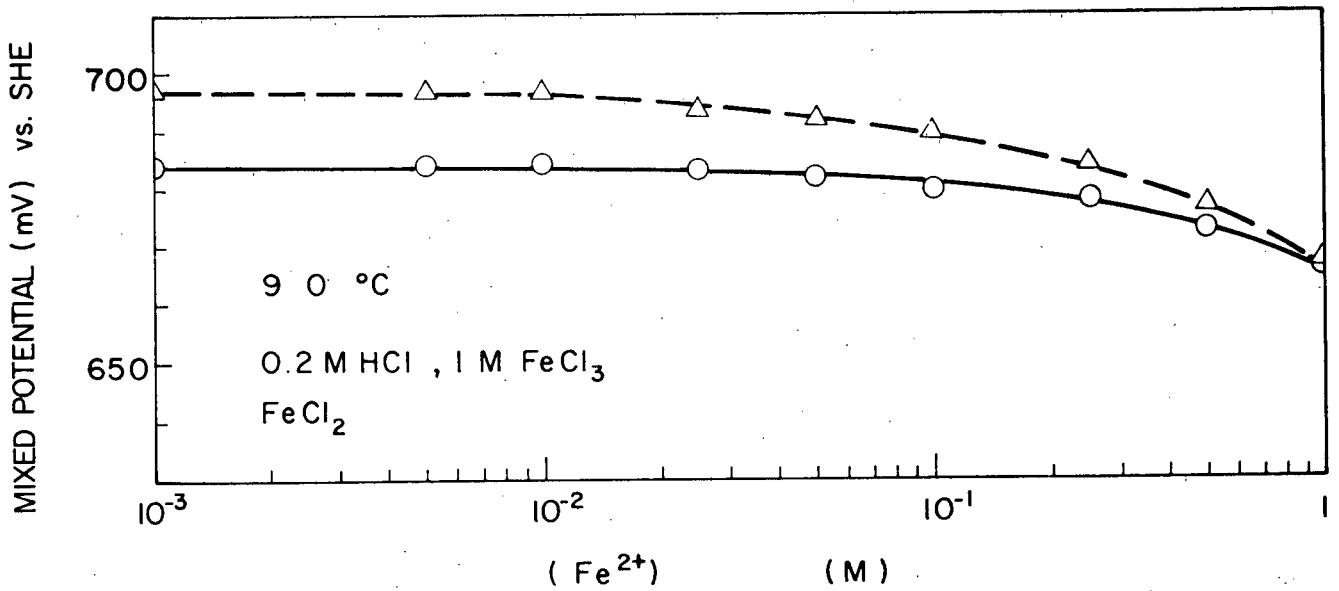
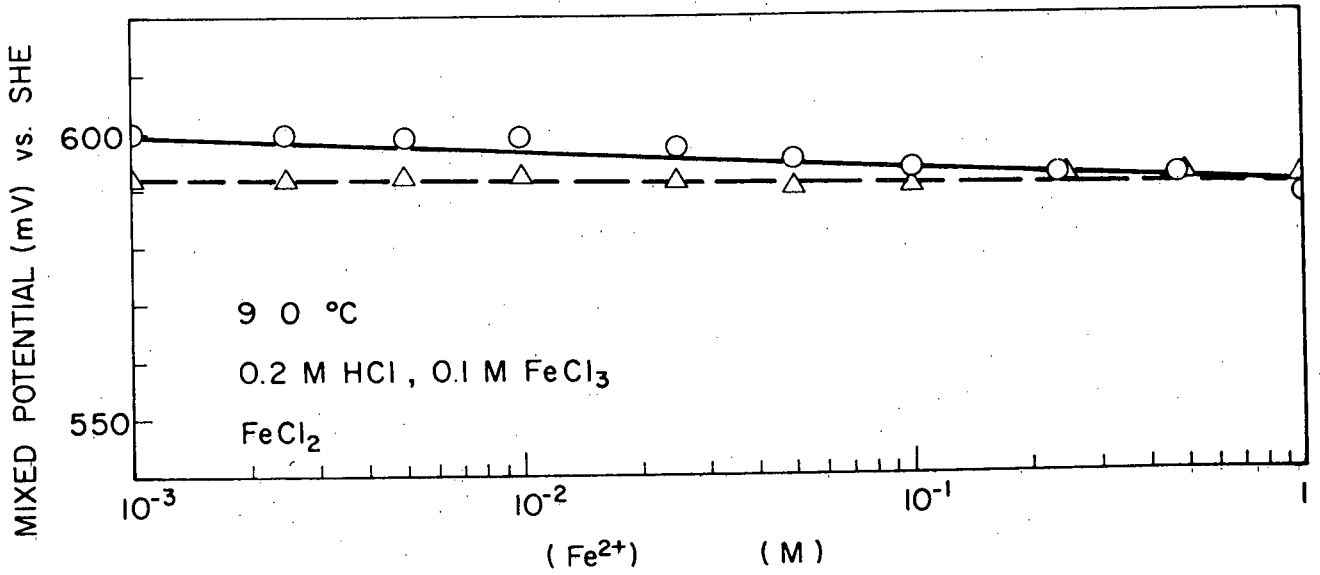


Fig. 92 Mixed potential of chalcopyrite in ferric chloride.
Effect of [Fe⁺⁺⁺].



Figs. 93, 94 Mixed potential of chalcopryrite in ferric chloride.
Effect of [Fe⁺⁺].

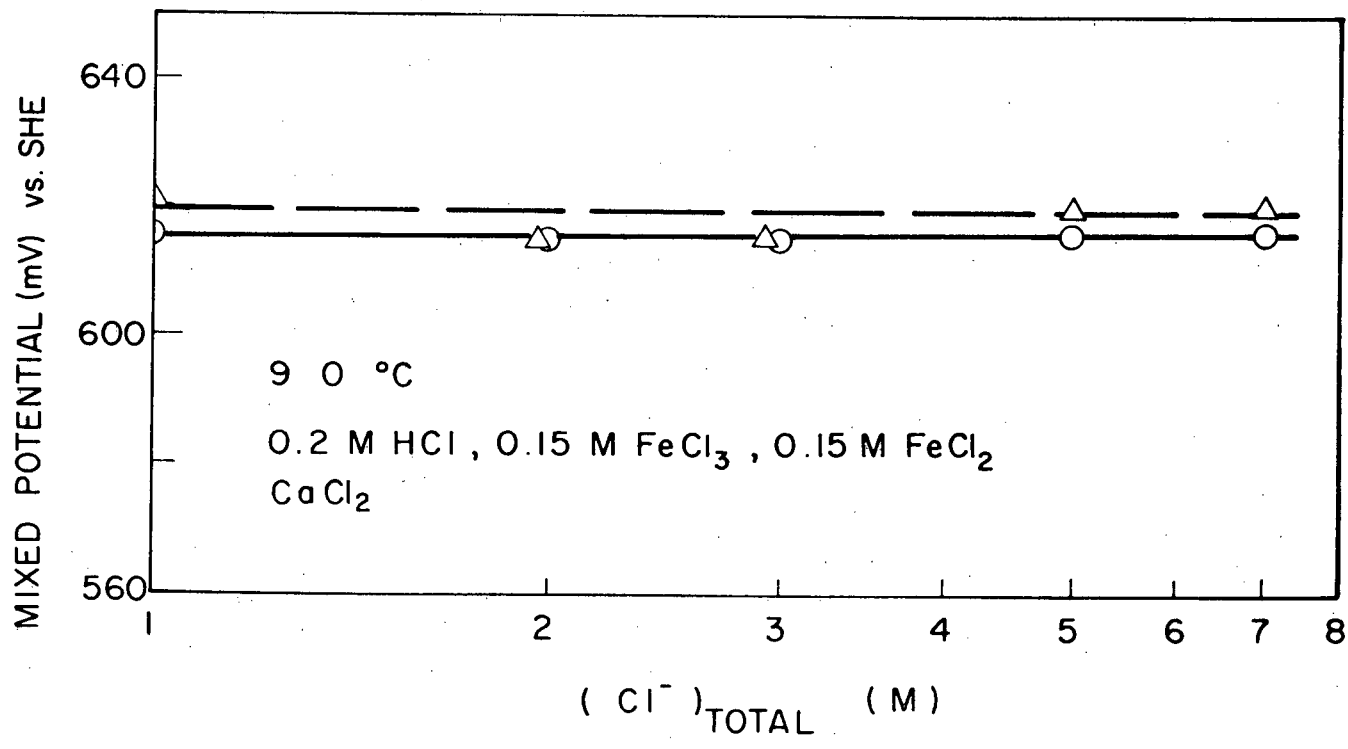


Fig. 95 Mixed potential of chalcopyrite in ferric chloride. Effect of [Cl⁻].

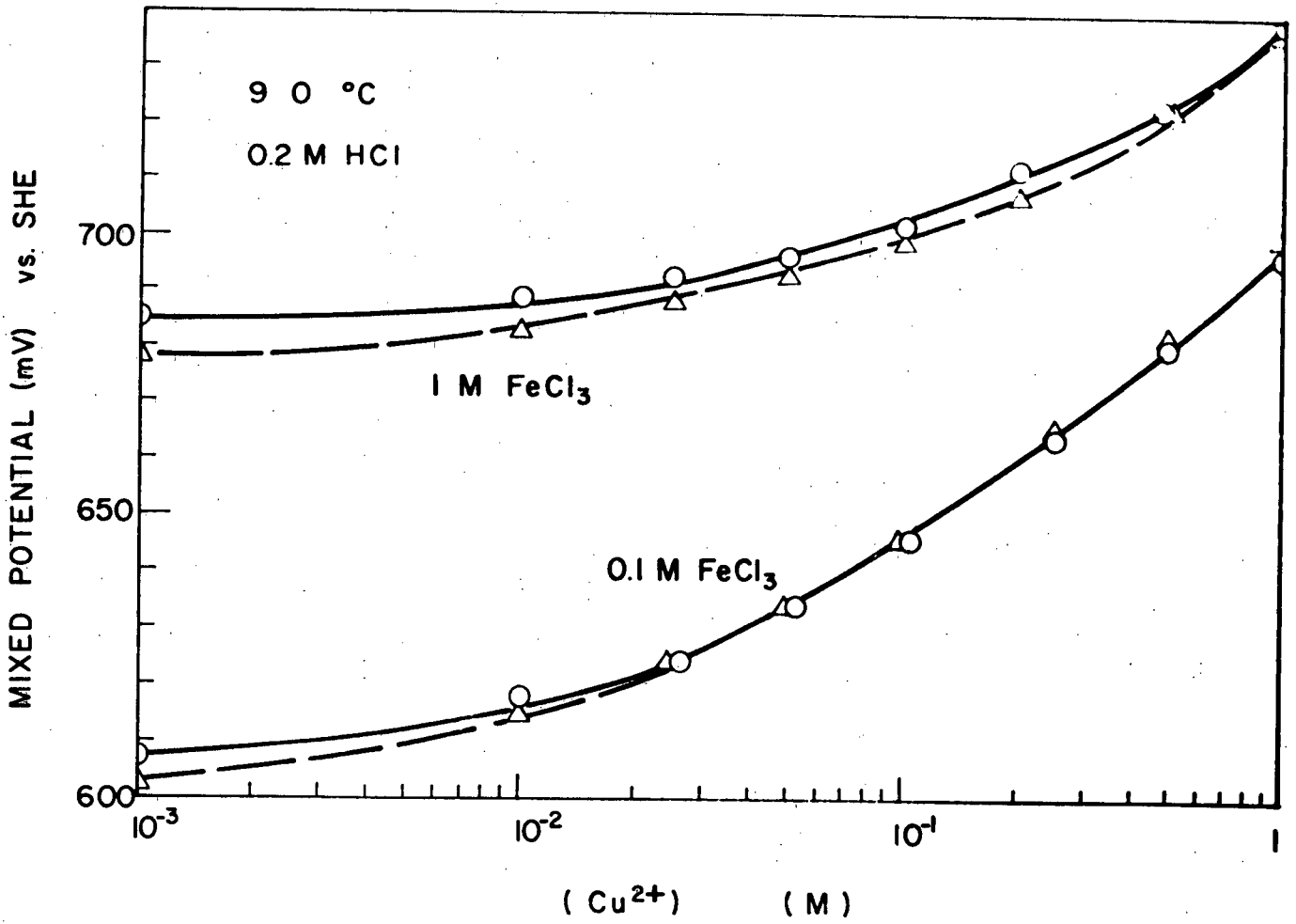


Fig. 96 Mixed potential of chalcopyrite in ferric chloride.
Effect of [Cu⁺⁺].

solutions was again noticeable, though not as much as in CuCl_2 leaching.

(iv) Summary

The mixed potential of chalcopyrite is responsive to $[\text{Fe}^{+++}]$ and $[\text{Fe}^{++}]$ in sulphate solutions, though the reactions appear to be irreversible. In ferric chloride solutions, the mixed potential is similarly responsive to $[\text{Fe}^{+++}]$, but not $[\text{Fe}^{++}]$.

In cupric chloride solutions, the mixed potentials respond immediately to changes in $[\text{Cu}^{++}]$ and $[\text{Cu}^+]$, and also $[\text{Cl}]$. The magnitude of the effects of $[\text{Cu}^+]$ and $[\text{Cl}]$ are interrelated viz. when $[\text{Cl}]$ is high, the effect of $[\text{Cu}^+]$ is reduced; and when $[\text{Cu}^+]$ is high, the effect of $[\text{Cl}]$ is increased.

In chloride solutions, both cupric and ferric, the reactions exhibit a high degree of reversibility.

Higher potentials can be achieved in 1M CuCl_2 solutions than in 1.0M FeCl_3 or 1.0M $\text{Fe}(\text{SO}_4)_{1.5}$ solutions, in which the mixed potentials are approximately equal.

c) Discussion

An electrochemical reaction may be said to be under anodic, cathodic or mixed control; this term refers to the relative degrees of polarization of the anodic and cathodic reactions. Thus in the figure on page 189 the cathodic reaction is highly polarized, and the overall reaction may be said to be under cathodic control.

The mixed potential of a mineral in a leaching environment may be used as an indicator of the control of the leaching reaction, if the Nernst potentials of the anodic and cathodic reactions can be calculated.

(i) Calculated Potentials

The standard potentials, E° , of the following half-cells at 298°K were calculated using the free-energy data given below:

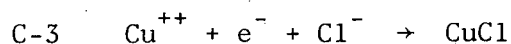
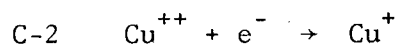
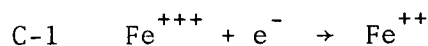
$$E^\circ = - \frac{\Delta F^\circ}{nF}$$

where ΔF° is the standard free energy change of the reaction

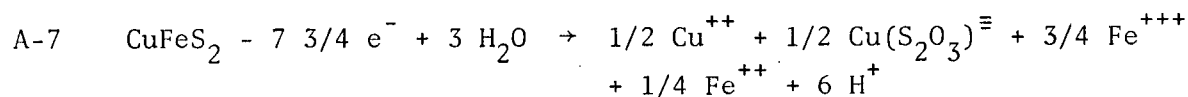
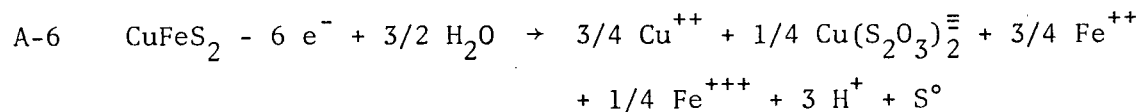
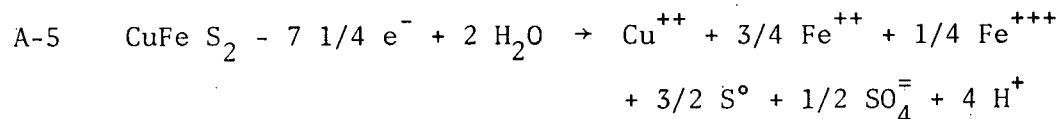
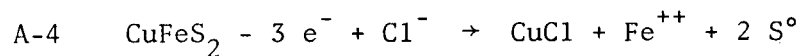
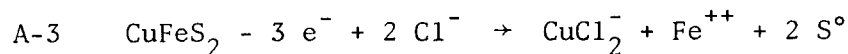
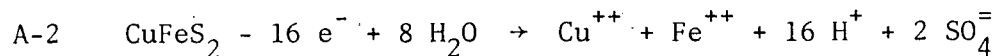
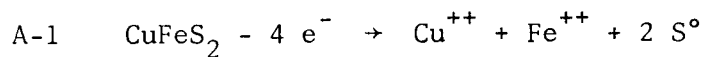
n is the number of electrons

F = Faraday = 23.06 kcal/volt

Cathodic Reactions



Anodic Reactions



Reaction	ΔF°_{298} kcal/mole	E° (mV)
C-1	- 17.78	770
C-2	- 3.53	153
C-3	- 12.38	536
A-1	40.78	442
A-2	139.62	379
A-3	30.05	435
A-4	28.40	411
A-5	69.94	419
A-6	63.60	460
A-7	82.35	461

	ΔF°_{298} kcal/mole	Reference
CuFeS ₂	- 45.55	63
CuS	- 11.7	187
Cu ⁺⁺	15.53	187
Cu ⁺	12.0	187
CuCl	- 28.2	187
CuCl ₂	- 57.9	187
Cu(S ₂ O ₃) ₂ ⁻	-250.3	This work
Fe ⁺⁺	- 20.30	187
Fe ⁺⁺⁺	- 2.53	187
Cl ⁻	- 31.35	187
SO ₄ ⁻	-177.34	187
H ₂ O	- 56.69	187

	ΔF°_{298} kcal/mole	Reference
$\text{SO}_3^=$	-116.1	187
$\text{S}_2\text{O}_3^=$	-124.0	187
$\text{S}_2\text{O}_6^=$	-231	187
$\text{S}_2\text{O}_4^=$	-143.4	187
$\text{S}_4\text{O}_6^=$	-244.3	187

The above data can only be applied to the present work with the following approximations in mind:

- 1) Free energy values are valid only at 25°C. The mixed potential and other experiments were largely carried out at 90°C.
- 2) The free energy values are mainly taken from an older reference (187).
- 3) Potential values for reaction C-1 in ferric chloride and sulphate are likely to be lower than 770 mV, due to complexing.
- 4) Potential values for reaction A-3 is likely to be lower at 90°C, due to increased stability of the CuCl_2^- complex at this temperature (188).
- 5) The free-energy value for CuFeS_2 as used here, has not been supported by published experimental evidence.
- 6) The free energy value for $\text{Cu}(\text{S}_2\text{O}_3)_2^=$ was calculated from Latimer's (187) data:

	ΔF_{298}°
$\text{Ag}(\text{S}_2\text{O}_3)_2^{\equiv}$	-247.6
$\text{Ag}(\text{CN})_2^-$	+ 72.05
$\text{Cu}(\text{CN})_2^-$	+ 69.3
$\therefore \text{Cu}(\text{S}_2\text{O}_3)_2^{\equiv}$	-250.3

Six possible anodic reactions have been written, but these fall within a range of only 81 mV (379 - 460 mV). The mixed potential experiments showed that electrode potentials during ferric and cupric leaching were generally 520 - 720 mV. Therefore none of these anodic reactions can be excluded on thermodynamic grounds.

The first two of these reactions represent 100% S° and 100% SO_4^{\equiv} formation respectively; the latter is actually favoured thermodynamically.

Reactions A-3, A-4 can be expected during chloride leaching (both are included, because the potential of A-3 seems unrealistically high). It can be seen that these reactions, which produce Cu^+ species, are only slightly favoured over A-1, which produces Cu^{++} (e.g. in sulphate solution).

Reactions A-5, A-6 are two possible reactions which can be postulated from data on sulphate solutions presented in Section III (ii). They incorporate a $\text{Fe}^{++}/\text{Fe}^{+++}$ ratio of 3.0, and a 25% oxidation of sulphur. The potential of reaction A-5 is very similar to that of A-4 (chloride solutions), whereas A-6 is 40 mV higher.

(ii) Ferric Sulphate Leaching

The above calculations indicate that the standard potential of the anodic dissolution of chalcopyrite in sulphate solutions is 420 mV \pm 40 mV

at 25°C. The actual mixed potential during ferric sulphate leaching is typically 200 mV higher than this (Figure 86); therefore there appears to be a significant degree of anodic polarization.

The $\text{Fe}^{3+}/\text{Fe}^{2+}$ couple has a standard potential of 770 mV, which increases with temperature; it has been found to react reasonably reversibly on a platinum surface, with a relatively small degree of activation polarization (189). Etienne utilized these data (90) to correlate electrochemical work on digenite with ferric sulphate leaching, with the implicit assumption that the charge transfer characteristics of the $\text{Fe}^{3+}/\text{Fe}^{2+}$ couple on digenite were similar to those on platinum. The correlation appeared to be reasonable.

However, the mixed potentials of chalcopyrite indicate that, in sulphate solutions at least, the $\text{Fe}^{3+}/\text{Fe}^{2+}$ couple is not reversible on the chalcopyrite surface. In a 0.1M Fe^{+++} , 0.1M Fe^{++} solution (Figure 87), a polarization of about 200 mV is apparent, since the mixed potential is near 600 mV, compared to a standard potential of 770 mV or higher.

With approximately equal amounts of cathodic and anodic polarization, the leaching of chalcopyrite in ferric sulphate solution may be said to be under mixed control.

This calculation may be refined by correction for (a) temperature and (b) complex formation. Using a method outlined below, the following corrections were calculated:

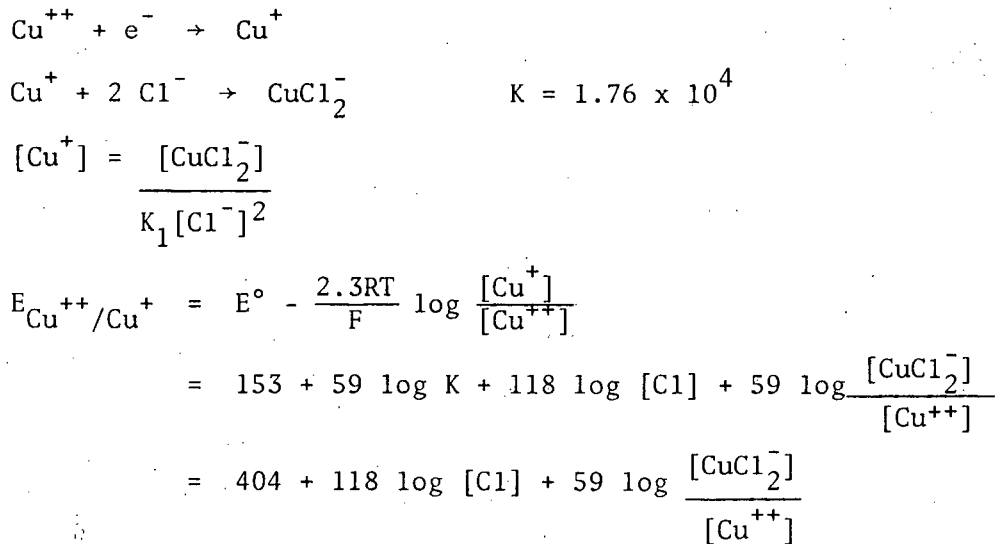
<u>Reaction</u>	<u>ΔE° (25 + 90°C)</u>
C-1	+ 77 mV
A-1	+ 8 mV
A-2	-121 mV

Furthermore, in sulphate solution, E° for the Fe^{3+}/Fe^{2+} couple (C-1) is reduced by 80 mV (1). Thus the overall effect of these corrections is negligible, (except to note that the sulphate reaction (A-2) becomes progressively more favourable with higher temperature); mixed control is still indicated.

(iii) Cupric Chloride Leaching

The standard potential of the anodic dissolution of chalcopyrite in chloride solutions was calculated (above) to be 411 mV. Actual mixed potentials were at least 200 mV above this; significant anodic polarization is again indicated.

The cathodic reaction may be written in more than one way, depending on the incorporation of chloride ions in the equation (C-2 or C-3).

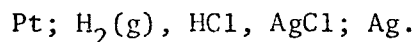


(at 25°C)

At 90°C, this equation changes significantly. In order to calculate the temperature coefficient of E° , it is necessary to use the van't Hoff Isochore (rather than the Criss and Cobble approach (200)). This choice*

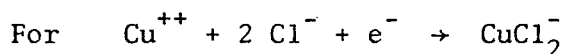
*A calculation based on the Criss and Cobble method yields a similar result in this case.

is dictated by the potential scale used in this work, which is based on the standard hydrogen electrode having a zero potential at each temperature, by definition. This follows from the use of Greeley's (178) values for the Ag°/AgCl reference electrode which were determined empirically from the cell:



Thus

$$\begin{aligned} \left(\frac{dE}{dt} \right)_{298} &= \frac{\Delta S^\circ_{298}}{nF} \\ &= \frac{\Delta H^\circ_{298} - \Delta F^\circ_{298}}{298 \cdot nF} \end{aligned}$$



$$\Delta H^\circ_{298} \quad 15.39 \quad -80.05 \quad \quad -66.1 \quad \rightarrow \quad -1.44$$

$$\Delta F^\circ_{298} \quad 15.53 \quad -62.7 \quad \quad -57.9 \quad \rightarrow \quad -10.73$$

Therefore

$$\left(\frac{dE}{dt} \right)_{298} = \frac{9290}{298 \times 23.06} = 1.352 \frac{\text{mV}}{^\circ\text{K}}$$

Assuming that this temperature coefficient remains constant up to 90°C

then $\Delta E_{363} = 88 \text{ mV}.$

Hence: $E_{\text{Cu}^{++}/\text{Cu}^+} (363^\circ\text{K}) = 492 \text{ mV} + 144 \log [\text{Cl}] + 72 \log \frac{[\text{CuCl}_2^-]}{[\text{Cu}^{++}]}$

In Figure 90, where the solution is $\left(\begin{array}{l} 0.1\text{M CuCl} \\ 0.1\text{M CuCl}_2 \\ 0.2\text{M HCl} \end{array} \right) + \text{CaCl}_2$, the mixed

potential of CuFeS_2 varies from 520 mV (0.5M CaCl_2) to 620 mV (3.5M CaCl_2) with a slope of 137 mV. As discussed below the [Cl] of the 0.5M CaCl_2 solution is considered to be 1.3M. Thus the calculated value is:

$$E_{\text{Cu}^{++}/\text{Cu}^+} = 492 + 144 \log (1.3) \\ = 508 \text{ mV (90}^\circ\text{C).}$$

This is very close to the experimental mixed potential of 520 mV (which was found for both electrodes). Therefore the degree of cathodic polarization must be quite small and the leaching of chalcopyrite in cupric chloride can be said to be under anodic control.

The dependence of the mixed potential upon $[\text{Cu}^{++}]$, (Cu^+) and $[\text{Cl}^-]$ is verification of this statement. The actual slopes observed for each variable:

$[\text{Cu}^{++}]$	+55 mV
$[\text{Cu}^+]$	-65 mV
$[\text{Cl}^-]$	+137 mV

are somewhat lower (72 or 144) than predicted by the Nernst equation, but this may be due to the use of concentrations instead of activities, or to a slight amount of cathodic polarization.

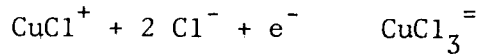
The dependence of [Cl] as shown in Figure 90 is plotted against $[\text{Cl}]^*$:

$$[\text{Cl}]^* = [\text{Cl}] - 2 [\text{CuCl}]$$

for it is assumed (187) that each Cu^+ ion is complexed as CuCl_2^- , and that therefore these Cl^- ions are no longer available. It is interesting that the slopes of the lines in Figure 90 only coincide when this definition is used. The variation between them is considerable (20% or more) if total [Cl] is used.

However, Helgeson (188) has calculated that in strong brines, the predominant Cu^+ species is CuCl_3^- , and the Cu^{++} ions are also complexed as

CuCl^+ . This would not change the expected slope of the line in Figure 90, viz.



Since two Cl^- ions are involved the slope should be 144 mV again, but the experimental slope, based on $[\text{Cl}^-]^*$ would change:

$$[\text{Cl}^-]^* = [\text{Cl}^-] - [\text{Cu}^{++}] - 3 [\text{Cu}^+].$$

The experimental slopes would now be 90 and 126 mV, in Figure 90. These values are obviously less satisfactory in the present context, but cannot be entirely discounted, without an evaluation of Helgeson's calculations.

If the anodic reaction is at all reversible, then its dependence on $[\text{Cl}]$ will tend to lower the mixed potential, thus providing a rationale for the reduced slope found experimentally.

The temperature dependence of the standard potential of the anodic reaction (A-3) was also calculated in the above manner. E° was found to decrease by 80 mV, from 25°C to 90°C. Thus the anodic polarization is even greater than indicated, reinforcing the concept of anodic control during cupric chloride leaching.

d) Ferric Chloride Leaching

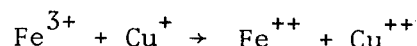
Similar mixed potentials are obtained in 1M FeCl_3 as in 1M $\text{Fe}(\text{SO}_4)_{1.5}$; therefore the conclusion may also be drawn that the reaction is similarly under mixed control. However, there are two important differences:

- 1) $[\text{Fe}^{++}]$ has little effect on the mixed potential in chloride solutions
- 2) The reaction appears far more reversible in chloride solutions.

The lack of effect of $[\text{Fe}^{++}]$ on the mixed potential can be explained by postulating that the active leaching agents in ferric chloride solutions are not Fe^{+++} ions but Cu^{++} ions. Since the $\text{Cu}^{++}/\text{Cu}^+$ couple has been

shown to be reversible on chalcopyrite, it is possible that this reaction will proceed much quicker than the $\text{Fe}^{3+}/\text{Fe}^{2+}$ couple.

The role of Fe^{3+} ions in ferric chloride leaching would then be to suppress the $[\text{Cu}^+]$, for the reaction:



$$K = 3.5 \times 10^8$$

tends strongly to the right.

$$[\text{Cu}^+] = \frac{[\text{Fe}^{2+}][\text{Cu}^{2+}]}{[\text{Fe}^{3+}]} \times 2.9 \times 10^{-9}$$

If this reaction was at equilibrium then the mixed potential should depend on $[\text{Fe}^{2+}]$. However, the important $[\text{Cu}^+]$ is that at the surface of the mineral, $[\text{Cu}^+]_s$, where it is being produced. The $[\text{Cu}^+]_s$ is probably limited by the speed with which the Fe^{3+} ions can diffuse from the bulk of the solution to the surface from which Cu^+ is introduced.

Since the $[\text{Cu}^+]$ will be very low in a strong Fe^{3+} solution, the complexing power of Cl^- ions, observed in cupric chloride leaching, will be unimportant; it is to be expected therefore that $[\text{Cl}^-]$ will not affect the mixed potential in ferric chloride leaching (Figure 95).

The effect of $[\text{Cu}^{2+}]$ in raising the mixed potential of chalcopyrite in ferric chloride solutions is supporting evidence for this theory. It is interesting to compare the potentials of the following solutions: (Figures 88, 96)

1M FeCl_3	678
	685
1M FeCl_3	738
1M CuCl_2	738
1M CuCl_2	731
3M NaCl	736

Thus 1M FeCl_3 has the same effect as 3M NaCl, when used with 1M CuCl_2 . Presumably, both the FeCl_3 and NaCl suppress the $[\text{Cu}^+]$, possibly in different ways.

e) Summary

Ferric sulphate leaching of chalcopyrite exhibits both anodic and cathodic polarization, and is under mixed control.

Cupric chloride leaching exhibits only anodic polarization and the reaction is therefore anodically controlled. The cathodic process is highly reversible.

Ferric chloride leaching appears to be cupric chloride leaching in reality, in which the $[\text{Cu}^+]$ is suppressed by the high $[\text{Fe}^{3+}]$. The reaction is therefore also under anodic control. However, simple ferric leaching, uncatalyzed by Cu^{++} , probably also occurs, though more slowly.

The actual mixed potential that chalcopyrite attains during ferric sulphate leaching is increased by high $[\text{Fe}^{+++}]$, but decreased by high $[\text{Fe}^{++}]$; typically it would be about 600 mV.

In ferric chloride leaching, the mixed potential depends only on $[\text{Fe}^{+++}]$, and (to a lesser extent) $[\text{Cu}^{++}]$. Typical mixed potentials should be in the range 680 - 720 mV in practical solutions.

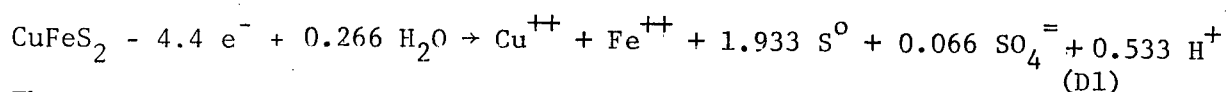
In cupric chloride leaching, the mixed potentials are increased by high $[\text{Cu}^{++}]$ and $[\text{Cl}]$ but decreased by Cu^+ ions. Actual potentials attained during a leach would decrease with time, as $[\text{Cu}^{++}]$ decreases and $[\text{Cu}^+]$ increases. In a strong chloride solution, the potential would probably start around 750 mV and finish at 600 mV, when the leaching becomes impractically slow.

D. DISCUSSION

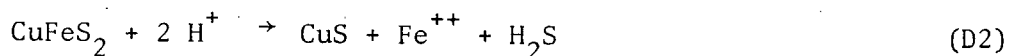
I The Chemistry of the Anodic Dissolution of Chalcopyrite

a) Chloride System

In chloride solutions the dissolution reaction appears to be quite straightforward:



The amount of sulphur oxidation is certainly small and of no great importance. However, at low potentials in strong chloride solution, much higher copper and iron current efficiencies (60 - 70%) are encountered than is allowed by this equation. Iron current efficiencies of greater than 50% may be achieved by chemical dissolution:



However, the corresponding process for copper was found not to occur to a detectable extent.

Copper current efficiencies of more than 50% are possible if the copper dissolves as cuprous, but even at the lowest potential only 12% of the copper was found as Cu^+ . Two explanations can be offered to resolve this problem:

- 1) Some of the Cu^+ was oxidized by atmospheric oxygen diffusing into the cell.
- 2) Some of the Cu^+ was oxidized by Fe^{3+} ions, simultaneously produced on anodizing.

The first possibility seems unlikely in view of the constant $\text{Cu}^+/\text{Cu}^{++}$ ratio with time.

The second possibility draws credence from the observation in sulphate solutions that an approximately constant proportion (1:4) of Fe^{+++} : Fe^{++} is dissolved at all potentials, and indeed at higher potentials in chloride solutions also.

If 20% of the iron then dissolves as Fe^{+++} it would likely react immediately with an equivalent quantity of Cu^+ , probably on or near the mineral surface. Thus the actual yield of Cu^+ would be 32% of the total Cu.



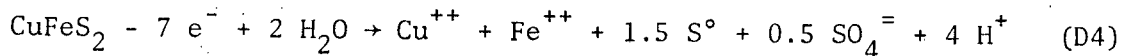
This would reduce the current efficiency for copper to 50%, (at 535 mV), and the extra current efficiency for iron can be accounted for by chemical dissolution, as stated.

b) Sulphate System (and Perchlorate)

In the sulphate system, the dissolution is not complicated by cuprous formation. but instead by sulphur oxidation. In the preliminary experiments it was shown that in 0.1M H_2SO_4 and 0.1M HClO_4 , current efficiencies of near 30% are obtained for copper and iron at all temperatures and potentials with two exceptions:

- 1) At low potentials (below 700 mV) less copper is dissolved
- 2) At high temperature (175°C), the chemical dissolution of iron becomes dominant.

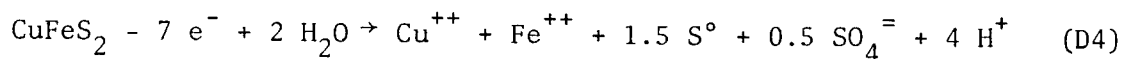
With these two exceptions in mind the dissolution reaction (in 0.1M H_2SO_4 and 0.1M HClO_4) is (ignoring Fe^{+++} formation for the moment):



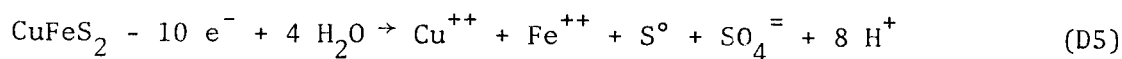
The predicted yield of sulphate (25% of the total sulphur) was actually found by spectrophotometric analysis in perchlorate solutions.

However, in later experiments (Section III (b)) the sulphate solutions used were 0.4M Na₂SO₄ and 0.1M H₂SO₄, and 0.4M NaHSO₄ and 0.1M H₂SO₄. At 90°C, the anodic dissolution reaction was similar to that in 0.1M H₂SO₄, based on copper and iron current efficiencies.

At 125°C, though, lower current efficiencies (20%) were observed in the sulphate solution, (but not in bisulphate). This indicates that an increased proportion of sulphur is oxidized under these conditions: (90°C):



(125°C; 0.4M Na₂SO₄ only):
0.1M H₂SO₄



At 150°C the copper current efficiency was also lower in bisulphate solution, and at 175°C it was negative.

This last result cannot be rationalized in terms of increased sulphur oxidation, and is indicative of a more complex process. It is rather surprising in view of the constant stoichiometry observed in 0.1M HClO₄, 0.1M H₂SO₄ and chloride solutions, at all temperatures as noted.

In oxygen pressure leaching of chalcopyrite (in sulphuric acid solutions) it has been observed (144) that the yield of elemental sulphur increases with [H⁺], the remainder of the sulphur being oxidized. At low pH, this oxidized sulphur is sulphate, whereas at higher pH (neutral or alkaline regions) intermediate sulphur species such as thiosulphate are found (146).

It is thus reasonable to suppose that in the anodic dissolution of chalcopyrite, the decreasing copper current efficiency can be attributed to increasing sulphur oxidation, which in turn can be attributed to

higher pH.

The pH of a 0.1M H₂SO₄ solution (and 0.1M HClO₄) will probably stay nearly constant over the range 25 - 175°C since the equilibrium



still has a positive log K value even at 300°C (188).

The pH of a 0.4M Na₂SO₄ solution rises with temperature due to the shift in the equilibrium² (188):



<u>Temp °C</u>	<u>log K</u>
25	-1.99
60	-2.40
100	-2.99
150	-3.74
200	-4.49

Thus the pH will probably rise from 1.25 (25°C, experimentally) to over 3 at 175°C, the increase being moderated by the equilibrium:



Values for the corresponding potassium salt are given by Helgeson (188):

<u>Temp °C</u>	<u>log K</u>
25	-0.84
60	-1.06
100	-1.30
150	-1.60
200	-1.94

In a bisulphate buffered solution on the other hand, the pH is less affected by the shift in the equilibrium of equation (D7). Experimental values of pH at 175°C were not obtained but the trend at 90°C can be expected to continue:

EXPERIMENTAL pH VALUES

	0.1M H ₂ SO ₄	0.4M NaHSO ₄ 0.1M H ₂ SO ₄	0.4M Na ₂ SO ₄ 0.1M H ₂ SO ₄
pH (20°C)	0.80	0.30	1.25
pH (90°C)	0.90	0.75	2.15

Therefore the results up to 150°C can be explained in terms of increased sulphur oxidation at higher temperatures, due to the rise in pH.

The details of the sulphur oxidation leave room for much speculation; the surface photomicrographs in Section I, obtained in 0.1M HClO₄ at 175°C, show that CuS crystals have been deposited from solution. Furthermore, the low current efficiencies found in bisulphate solutions at high temperatures also are associated with CuS deposition. Frequently, a thin film of CuS was deposited all over the epoxy mounting of the specimen, during a high temperature run.

Therefore, in postulating a mechanism for sulphur oxidation, the mass transfer of copper from the sulphide mineral to another site, via the solution, must be considered.

At least three mechanisms can be suggested:

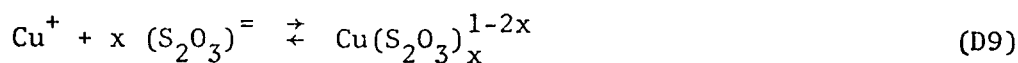
- i) Thiosulphate
- ii) Sulphur Disproportionation
- iii) Hydrogen Sulphide.

i) Thiosulphate Mechanism

It has been well established that thiosulphate is an important intermediate in the oxidation of sulphide minerals at neutral or higher pH (e.g. the ammonia leach of Sherritt-Gordon) (193). However, thiosulphate is known to be unstable at lower pH (approximately pH 5 (196)) particularly when the solution is hot and oxidizing, and its existence under these conditions is not usually considered.

Nevertheless, there is an extra complication in this situation, and that is the presence of copper in the solution.

Cuprous ions form a series of complexes with thiosulphate: (194)



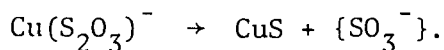
The analogous silver complex $\text{Ag}(\text{S}_2\text{O}_3)_2^=$ is listed by Latimer (187) as one of the strongest complexes known of that metal, being exceeded only by the cyanide.

COMPLEX	LOG K (25°C)	REFERENCE
AgCl_2^-	- 5.25	188
$\text{Ag}(\text{NH}_3)_2^+$	- 7.77	187
$\text{Ag}(\text{S}_2\text{O}_3)_2^=$	-13.78	187
$\text{Ag}(\text{CN})_2^-$	-18.75	187
$\text{Cu}(\text{CN})_2^-$	-16.00	187

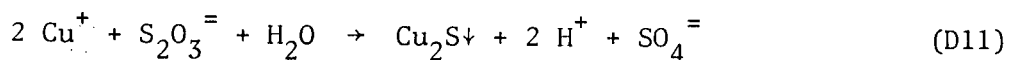
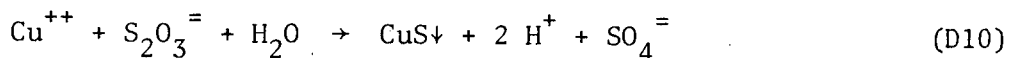
The strength of this cuprous thiosulphate complex stabilizes both cuprous and thiosulphate ions, the former being usually unstable in sulphate solutions (with respect to disproportionation: $2 \text{Cu}^+ \rightarrow \text{Cu}^0 + \text{Cu}^{++}$), and the latter being unstable in acid solutions (also with respect to disproportionation: $\text{S}_2\text{O}_3^{=} \rightarrow \text{S}^0 + \text{SO}_3^{=}$).

In fact, some brief experiments in this work indicated that some of the analytical techniques employed for copper analysis do not detect copper if it is present as the thiosulphate complex. For instance, the Cuproin method depends on the extraction of cuprous from the aqueous phase to an organic phase; if the cuprous is very strongly complexed in the aqueous phase, then it is possible that an unfavourable extraction ratio will be encountered.

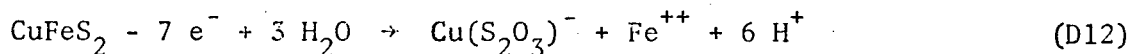
The strength of this complex notwithstanding however, its stability at elevated temperatures is limited by the reaction:



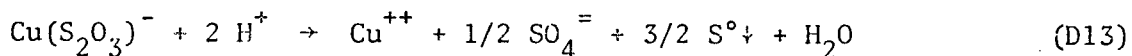
The exact stoichiometry of this reaction is uncertain, and probably varies with conditions, but it is certain that a copper sulphide (either CuS or Cu_2S) and an oxidized sulphur species are formed. This fact is used in Sherritt-Gordon's 'copper boil' step to remove copper from solution, after the leaching operation. The reactions have been written (191):



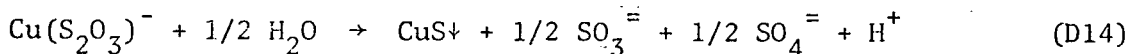
In this work we have clear evidence that copper has been transported via solution from one solid site to another. It is plausible therefore that at least some copper dissolves anodically as a cuprous thiosulphate complex which may either decompose to form soluble copper or a copper sulphide:



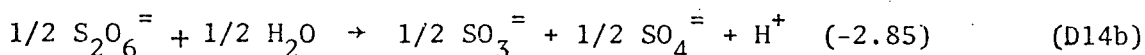
then



or:



This reaction may go through an intermediate step involving dithionate:



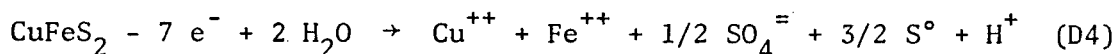
which is reported to decompose rapidly into $\text{SO}_3^{=}$ and $\text{SO}_4^{=}$ in acid solution (187).

The production of $\text{SO}_3^{=}$ allows more thiosulphate to be formed by reaction with elemental sulphur on the mineral surface:



and thereby permit more copper to be removed from solution, i.e. negative current efficiency.

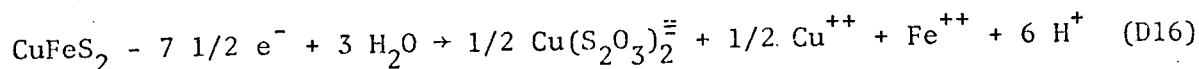
The sum of equations D12 and D13 is:



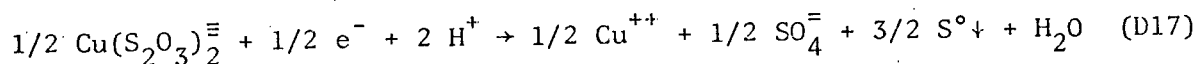
which is the observed stoichiometry of the anodic dissolution under most conditions in sulphate solutions. It is interesting that equation (D13), dissolution of copper, is favoured by acid solutions, whereas equation (D14), precipitation of copper, is not. This conforms to the observed pattern of lower copper current efficiencies at higher pH.

Alternatively, other equations may be written, particularly for the copper precipitation reaction, the details of which are not known, other than the fact that cupric sulphide is formed (195), (although some authors

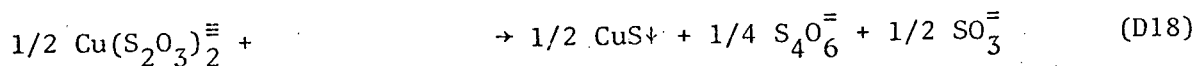
reported a mixture of cupric and cuprous sulphides). The dithiosulphate complex may be formed, e.g.



then either:



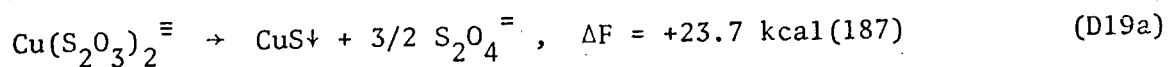
or:



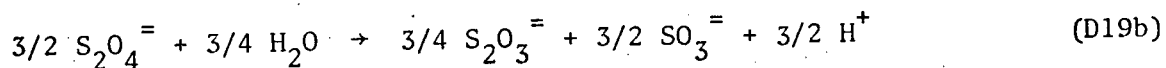
This last equation seems possible for tetrathionate, $\text{S}_4\text{O}_6^{\equiv}$, is a common oxidation product of thiosulphate, and also because the production of sulphite, SO_3^{\equiv} , allows more copper to be precipitated, as described above.

The reaction of sulphite, SO_3^{\equiv} , and elemental sulphur could well be favoured under conditions where the sulphur is in a metastable high energy form, as it may be after anodizing chalcopyrite.

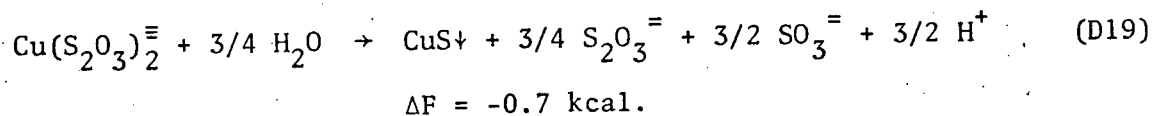
Still another decomposition reaction for the thiosulphate complex can be written, involving hyposulphite:



This reaction appears to be thermodynamically unfavourable. Hyposulphite however decomposes rapidly in acid solution to regenerate thiosulphate:



This reaction is favoured by 24.4 kcal (187). Thus the overall reaction is slightly favoured:



Again, the production of $\text{S}_2\text{O}_3^{\equiv}$ and SO_3^{\equiv} both permit the formation of more cuprous thiosulphate complexes, and hence a reduction in the level of copper in the solution, as noted above.

Hyposulphite can enter into several other reactions (192): copper dissolved as the sulphate reportedly is reduced to the reddish-brown hydride, CuH. This compound, which might easily be mistaken for hematite, Fe_2O_3 , readily decomposes to a sponge of metallic copper.

The various decomposition reactions described can be evaluated thermodynamically: *

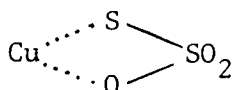
		ΔF_{298}° (kcal)	Expected Effect of Increased pH on Reaction
<u>DISSOLUTION OF COPPER</u>			
D13	(mono-complex)	- 3.8	Slower
<u>PRECIPITATION OF COPPER</u>			
(i) D14a	$S_2O_6^{=}$ formation	- 0.7	--
D14b	$SO_3^{=}/SO_4^{=}$ formation	- 2.88	Faster
D14	Overall	- 3.55	Faster
(ii) D18	$S_4O_6^{=}/SO_3^{=}$ formation	- 5.7	--
(iii) D19a	$S_2O_4^{=}$ formation	+23.7	--
D19b	$S_2O_3^{=}/SO_3^{=}$ formation	-24.4	Faster
D19	Overall	- 0.7	Faster

* The value of ΔF_{298}° used for $Cu(S_2O_3)_2^{=}$ is -250.3 kcal.; the derivation of this value is described in the last section. For $Cu(S_2O_3)^-$ a reasonable figure is arrived at simply by assuming that this complex is equally as stable as the di-complex. Then

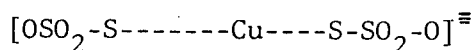
$$\Delta F_{298}^\circ = -126.3 \text{ kcal.}$$

It appears from the existing literature on this subject (194) that this is a reasonable approximation.

In evaluating these reactions, it must be recognized that paths (ii) and (iii) are derived from the di-complex, whereas (i) is derived from the mono-complex. The latter seems more likely, since there will not be an excess of thiosulphate in solution, and it apparently has a bridged structure (194):



as opposed to the linear structure of the di-complex:



One can visualize the formation of the bridged structure being favoured on a mineral surface.

Thermodynamically, the production of hyposulphite, $\text{S}_2\text{O}_4^{\equiv}$, seems unlikely at best although the overall reaction D19 is possible.

Reaction D18, producing tetrathionate cannot be ruled out on thermodynamic grounds, but it has three unfavourable characteristics:

- a) It is derived from the di-complex rather than the mono-thiosulphate
- b) It requires two new species to be nucleated
- c) It is not favoured by high pH.

Reaction D14 involving dithionate $\text{S}_2\text{O}_6^{\equiv}$, on the other hand, has none of these disadvantages, and appears to be the most likely reaction.

The competition between a solubilizing reaction D13 and D14 may simply boil down to a pH problem. The free energies are very similar (-3.8 vs. -3.55 kcal) but the pH dependence is opposite.

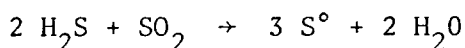
In summary, the thiosulphate mechanism postulates that copper dissolves as a cuprous thiosulphate complex which may either 1) decompose to give soluble copper, or 2) decompose to form a copper sulphide precipitate. The choice between these two paths is likely to be influenced by pH, with

the first being favoured at lower pH.

(ii) Sulphur Disproportionation Mechanism

The enhanced reactivity which elemental sulphur may have when produced under the non-equilibrium conditions existing on a chalcopyrite anode plays an important role in this mechanism.

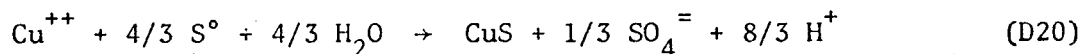
It is well known that at sufficiently high temperatures elemental sulphur can be made from H₂S gas (196):



However it is also possible for this reaction to be reversed, if

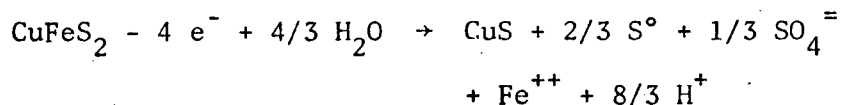
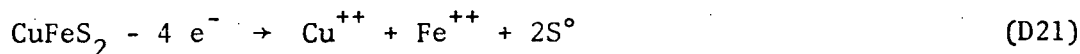
- 1) the activity of sulphur can be raised
- 2) the activity of H₂S can be depressed.

Under the conditions existing on a chalcopyrite anode, the freshly formed elemental sulphur will likely not be in its most stable form. Furthermore the activity of H₂S is depressed greatly by the copper content of the solution. Therefore the disproportionation reaction:



is possible (producing SO₄⁼ rather than SO₃⁼).

Combined with the 'normal' chalcopyrite dissolution:



This equation fits the data reasonably well, for it predicts a 16.7% sulphur oxidation, and a 33.2% current efficiency for copper, (presuming that the CuS is formed on the specimen, where it can be anodized:)



However, it would be expected that the disproportionation would increase with temperature, but this does not seem to be the case, generally.

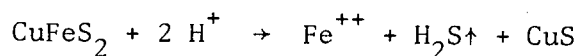
Alternatively, it can be postulated that the two reactions (D20, D21)

occur almost simultaneously, so that the copper never actually dissolves, (except as CuS). This idea is supported by the regular array of CuS crystals on the CuFeS₂ lattice in some cases (Figures 22-23). The CuS which has obviously precipitated from solution (Figure 21) may then be due to:

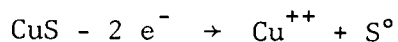
- 1) Actual separation of reactions as postulated initially, or
- 2) Some H₂S precipitation as discussed below.

(iii) Hydrogen Sulphide Mechanism

It is observed that some iron dissolves chemically from CuFeS₂ even at 90°C. Presumably the reaction is:



When combined with anodic dissolution, and H₂S precipitation:



it is possible that CuS could be transported 'through' the solution. This mechanism does not, however, predict sulphate formation nor does it agree with the temperature and pH data.

The limiting quantity would presumably be amount of H₂S evolved since there is an excess of copper in solution. This evolution will increase with temperature but not pH; in fact the CuS formation does not (always) increase with temperature but does increase with pH.

However, some H₂S evolution may occur, and cause some CuS precipitation, as a side reaction.

II The Anodic Polarization Curve of Chalcopyrite

Three main forms of polarization are commonly encountered in electrochemical processes: activation, concentration and ohmic. Each form affects the shape of the current/voltage (I/V) curve in a particular manner:

Activation: $I = ae^{bV}$ where a,b are constants

Concentration: Limiting Current (I independent of V)

Ohmic: $I = V/R$ where R is a resistance.

In order to gain an understanding of the anodic process on chalcopyrite, it may be necessary to consider forms of polarization which are peculiar to a compound semiconductor. A detailed analysis of such a system is beyond the scope of the present work, however, and only an outline can be attempted. Furthermore, where possible classical electrochemical concepts will be invoked, for in understanding new phenomena it is helpful to relate them to established concepts.

The anodic polarization curves of chalcopyrite as shown in Sections I and II contain two stages which differ principally in their time-dependence. The first stage is highly time dependent and the second is not; these have been labelled the diffusion region and the space charge region respectively.

An activation-controlled region must of course exist at the start of the polarization. In most cases, however, it has a very small range of potential.

In the diffusion region the current is nearly independent of potential; this region is clearly in evidence at low temperatures (20°C), for about 500 mV. However, the current in this region decays rapidly with time, and increases with temperature: it has an activation energy of 14 kcal. These observations suggest that a limiting current has been reached, which is

related to a diffusional process in the electrode.

In the space charge region the time-dependence of the current is much smaller, but the potential dependence is much greater, and is in fact linear:

$$I = V/R.$$

It is therefore postulated that at this stage there is a region within the semiconductor, across which there is a substantial drop in potential i.e. a space-charge region. Across this gap a significant electric field will exist, which can force the migrating cations out of the lattice. The flux of these cations will depend on the strength of the field, and will not decay with time.

The transition between the two regions is clearly marked on most occasions, and reproducible. There is a significant correlation (at a given temperature) between the size of the diffusion current and the potential of the transition point. For instance (at 20°C) in 1M HClO₄, the diffusion current is higher than in 0.1M HClO₄, but the transition potential is also higher. However, the slopes in the space-charge region are similar (Figure 34).

It appears then that the diffusion current is a leakage phenomenon, draining away the effect of increased potential so as to delay the start of the space-charge region. Therefore a higher leakage or diffusion current corresponds to a higher transition potential.

a) The Diffusional Process in Chalcopyrite

It has been well established by Wagner (201) and others that Cu⁺ ions have an unusually high ionic diffusivity, being exceeded in this respect only by Ag⁺. More highly charged species such as Cu⁺⁺, Fe⁺⁺, Fe⁺⁺⁺ are

more strongly held in the lattice, and anions such as sulphide, $S^{=}$, are considered virtually immobile in the temperatures range considered here.

The flux of ions across a charged interface may be expressed as the sum of a purely diffusional term and a potential-dependent term:

$$J = -D \frac{d[C]}{dx} - u[C] \frac{d\phi}{dx}$$

where J = flux of ions (mole/cm²-sec.)

D = diffusion coefficient (cm²/sec)

$[C]$ = concentration of ions (mole/cm³)

x = distance (cm)

u = mobility of ions

ϕ = potential (volts).

By the Nernst-Einstein equation:

$$u = \frac{D \cdot q}{KT}$$

where q = electron charge = 1.6×10^{-19} coulombs

K = Boltzmann's Constant = $1.38 \times 10^{-23} \frac{\text{Joule}}{\text{°K-molecule}}$

T = temperature °K

Therefore:

$$J = -D \left[\frac{d[C]}{dx} + \frac{q[C]}{KT} \frac{d\phi}{dx} \right] \quad (D22)$$

The concentration of Cu^{+} ions in chalcopyrite may be calculated from the cell dimensions (118) ($a = 5.24 \text{ \AA}$):

$$[C] = 2.5 \times 10^{-2} \frac{\text{mole}}{\text{cm}^3}$$

At 50°C:

$$\frac{q[C]}{KT} = 0.90 \frac{\text{coul-mole}}{\text{cm}^3\text{-joule}}$$

$$= 0.90 \frac{\text{mole-sec}}{\text{cm}^3\text{-coul-}\Omega}$$

$$= 0.90 \frac{\text{mole}}{\text{cm}^4} \cdot \frac{1}{\text{volt/cm}}$$

Therefore:

$$J = -D \left[\frac{d[C]}{dx} + 0.9 \frac{d\phi}{dx} \right] \quad (50^\circ \text{ C})$$

Therefore the current across an anode (which is related to the flux ∂ by the stoichiometry of the reaction) is dependent upon two terms. In order to evaluate the relative magnitudes of these terms, it is necessary to know the potential gradient and the concentration gradient. However, only very rough estimates of these quantities can be made:

The space-charge region on germanium is reported to be 10^{-4} cm. (198), while the available potential may be of the order of 200 mV. Therefore:

$$\frac{d\phi}{dx} = 2 \times 10^3 \text{ volt/cm.}$$

The maximum concentration difference is $[C] = 2.5 \times 10^{-2}$ mole/cm³, while the boundary layer for solid state diffusion of Cu⁺ ions might be guessed at 0.1μ (10^{-5} cm). Therefore:

$$\frac{d[C]}{dx} = 2.5 \times 10^{-3} \text{ mole/cm}^3$$

On the basis of these rough estimates, it appears that these terms have approximately equal magnitudes.

It follows then that the diffusion current dominates the low potential region, whilst the space-charge region takes over later.

Estimates of the diffusion coefficient, D , in chalcopyrite may be taken from the works of Etienne (90) and Cole (118), who studies the copper sulphides. As described in the Introduction, Frueh has pointed out that the structure of chalcopyrite is similar to that of digenite, $\text{Cu}_{1.8}\text{S}$, except

that the lattice is tighter (see p. 13). We may assume therefore that the diffusion coefficient of Cu^+ ions in digenite represents an upper bound for that in chalcopyrite.

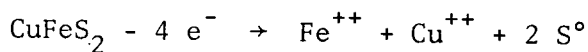
At 50°C , Etienne found $2.4 \times 10^{-10} \text{ cm}^2/\text{sec}$ and Cole $1.7 \times 10^{-7} \text{ cm}^2/\text{sec}$ (after extrapolation from 25°C , with an activation energy of 13 kcal).

Then the flux may be calculated:

$$J = 6.0 \times 10^{-13} \frac{\text{moles}}{\text{sec-cm}^2} \quad (\text{Etienne})$$

$$J = 4.2 \times 10^{-10} \frac{\text{moles}}{\text{sec-cm}^2} \quad (\text{Cole})$$

If the anodic reaction is (in chloride):



$$\text{Then } 1 \text{ mA/cm}^2 = \frac{2.5 \times 10^{-9} \text{ mole}}{\text{sec-cm}^2} (\text{Cu}^{++})$$

and the calculated current density that can be achieved is:

$$I = 2.4 \cdot 10^{-4} \text{ mA/cm}^2 \quad (\text{Etienne})$$

$$I = 1.7 \times 10^{-1} \text{ mA/cm}^2 \quad (\text{Cole}).$$

The actual current densities that are attained on anodizing chalcopyrite at 50°C (Figure 50) are about 0.50 mA/cm^2 (in chloride solution at 735 mV).

Thus the diffusion coefficient estimated using Cole's data, provides an approximately sufficient flux of Cu^+ ions, whilst Etienne's value is 1000 times too low.

However, Etienne also found that the anodic dissolution of digenite was too fast to be accounted for by her own experimental values for D; she therefore concluded that the actual diffusional process in that case was aqueous diffusion, in the shrinkage pores, rather than solid state diffusion.

In the present work such a conclusion is still possible. In fact, it is observed that iron dissolves out of chalcopyrite first, and therefore the matrix through the Cu^+ ions are diffusing may be very different from chalcopyrite. It may be a metastable iron-depleted lattice, or an actual CuS lattice. In any case, there is a strong possibility of (aqueous) pore diffusion.

It is interesting to note that the activation energies expected from equation (D22), are nearly independent of the relative magnitudes of the two terms (diffusional and potential-dependent), since the activation energy is associated with the common factor, the diffusion coefficient.

Thus activation energies can be determined over a temperature range which includes regions where either term is dominant.

Experimentally this is confirmed by the linearity of the Arrhenius plots. For instance, at 735 mV in chloride solutions the diffusion current is dominant at low temperatures (20°C) (Figure 33), but the space-charge current is dominant at 90°C (Figure 39). The Arrhenius plot is linear (Figure 63).

Furthermore the various activation energies are similar in different solutions (13.1 \rightarrow 14 kcal), and also similar to Etienne's: 12.1 kcal for digenite.

b) Effect of Solution

At 20°C , the diffusion region current is increased by increasing the strength of the solution, This can be rationalized by considering that the dissolution of the metal ions is aided, thus increasing the concentration gradient in equation (D22).

The space charge current, (at 20°C) in contrast, is almost unaffected

by the solution, and this also follows from equation (D22).

However, at 90°C, there is a great difference between chloride, perchlorate and sulphate solutions viz. the space-charge region starts around 500 mV in hydrochloric acid, 900 mV in perchloric acid and never in sulphuric acid.

Thus, in some manner, at 90°C, the onset of the space-charge region is affected by the solution. No really satisfactory explanation of this effect can be offered.

The 'passivity' of sulphuric acid may be due to the formation of a basic salt on the surface, but this seems unlikely in view of the fact that sodium sulphate solutions (at a higher pH) do not passivate the mineral to the same extent. The explanation may lie in the fact that the conductivity of a mineral specimen is rapidly decreased by anodizing in sulphuric acid. This loss in conductivity is apparently an inter-granular effect. This phenomenon correlates with the observation that in ferric sulphate leaching, dissolution occurs preferentially along fissures, which presumably are grain boundaries.

The positive effect of chloride ions of raising the space-charge current (and also lowering the transition potential) is hard to rationalize. It is possible that chloride ions catalyze the closing of the S_8 rings, a necessary step in the formation of elemental sulphur in its rhombic or monoclinic varieties. This postulate comes from the observation that chlorine reacts readily with sulphur at low temperatures to form S_2Cl_2 , and thus must be capable of opening the S_8 ring. It is therefore conceivable that a low energy transition state is formed with chloride ions that permits an easy transformation to or from an S_8 ring.

Another explanation for the beneficial effect of chloride ions lies in the shrinkage pore model of Etienne, described above. If it is true that the diffusional process takes place in an aqueous environment, then certainly increasing [Cl] will aid dissolution.

As a final speculation, it is worthwhile considering that space-charge currents are related to overall attack on the mineral (as evidenced by ferric chloride leaching), whereas diffusion currents are solely the product of grain-boundary attack (ferric sulphate leaching).

E. CONCLUSION

The leaching of chalcopyrite can be interpreted as an electro-chemical reaction. Ferric chloride leaching is faster than ferric sulphate leaching for four reasons:

- 1) In chloride solutions at typical leaching temperatures (90°C), the anodic current is potential dependent, whereas in sulphate solutions it is not.
- 2) The cathodic reduction of ferric sulphate is quite irreversible, and the reaction is under mixed control. Ferric chloride leaching actually proceeds via the cupric/cuprous couple which is highly reversible on chalcopyrite. The reaction is thus under anodic control.
- 3) Ferric sulphate attacks the mineral only along grain boundaries, whereas ferric chloride exhibits overall attack.
- 4) The current efficiency for copper in the anodic dissolution is near 45% in chloride solutions, but only 28% in sulphate solutions. The balance of the current is used up in sulphur oxidation.

REFERENCES

1. Handbook of Chemistry and Physics, C.R.L. Press, 53rd Edition, 1973, Ed. R.C. Weast, p. F-167.
2. K.N. Subramanian and P.H. Jennings, Can. Met. Quart., 11, 387 (1972).
3. R.J. Roman and B.R. Brenner, Mineral Science and Engineering, 5, 3 (1973).
4. (a) D.G. Treilhard, Eng. and Mining Journal, April (1973).
(b) J. Dasher, C.I.M. Bull., 48 (1973).
5. M.E. Wadsworth, Mineral Science and Engineering, 4, 36 (1972).
6. H.E. Merwin and R.H. Lombard, Econ. Geol., 32, 203 (1937).
7. J.E. Hiller and K. Probstain, Zeitschr. Kristallographie, 108, 108 (1956).
8. G. Donnay and G. Kullerud, Carn.Inst. Washington Year Book, 57, 246 (1958).
9. E.H. Roseboom and G. Kullerud, Carn.Inst. Washington Year Book, 57, 222 (1958).
10. R.A. Yund and G. Kullerud, J. Petrology, 7, 454 (1966).
11. G. Kullerud, R.A. Yund and G.H. Mah, Econ. Geol. Mon., 4, 323 (1969).
12. H. Mukaiyama and E. Izawa, in "Volcanism and Ore Genesis", T. Tatsumi ed., p. 339 (1970).
13. P.B. Barton, Jr., Econ. Geol., 68, 455 (1973).
14. Hiromi Shima, Ganseki Kobutso Kosho Gakkaishi, 47, 123-33 (1962).
15. P.B. Barton, Jr. and Priestley Toulomin, Econ. Geol., 54, 747 (1964).
16. M. Nambu and S. Kano, Gansehi Kobutso Kosho Gakkaishi, 60, 127 (1968).
17. R. Adams, R. Beaulieu, M. Vassiliadis and A. Wold, Mat. Res. Bull., 7, 87 (1972).
18. R. Adams, P. Russo, R. Arnott and A. Wold, Mat. Res. Bull, 7, 93 (1972).

19. J.H. Kim and T.R. Middleton, paper presented at AIME Annual Meeting, San Francisco (1972).
20. P.B. Barton and B.J. Skinner, in "Geochemistry of Hydrothermal Ore Deposits", ed. H.L. Barnes, p. 236 (1967).
21. L. Cabri, *Econ. Geol.*, 62, 910 (1967).
22. W.H. Maclean, L.J. Cabri and J.E. Gill, *Can. J. Earth Sci.*, 9, 1305 (1972).
23. S.R. Hall and E.J. Gabe, *Am. Mineralogist*, 57, 368 (1972).
24. A.H. Clark, *Econ. Geol.*, 65, 590 (1970).
25. L.J. Cabri and D.C. Harris, *Econ. Geol.*, 66, 673 (1971).
26. L.J. Cabri and S.R. Hall, *Am. Mineralogist*, 57, 689 (1972).
27. L.J. Cabri, *Econ. Geol.*, 68, 443 (1973).
28. S.R. Hall and J.F. Rowland, in preparation (1973)(ref. 27).
29. J.R. Rowland and S.R. Hall, in preparation (1973)(ref. 27).
30. N. Morimoto and K. Koto, *Am. Mineralogist*, 54, 1256 (1969).
31. N. Morimoto and K. Koto, *Am. Mineralogist*, 55, 106 (1970).
32. N. Morimoto and A. Gyobu, *Am. Mineralogist*, 56, 1889 (1971).
33. R.A. Munson, *Inorg. Chem.*, 5, 1296 (1966).
34. Y.Kajiwara, *Mineral. J. (Tokyo)*, 5, 399 (1969).
35. H. Shimazaki and L.A. Clark, *Can. Mineralogist*, 9, 648 (1970).
36. E.H. Roseboom, *Econ. Geol.*, 61, 641 (1966).
37. R.M. Garrels and C. Christ, "Solutions, Minerals and Equilibria", Harper and Row, New York (1965).
38. A. Golomzik, *Izv. Vysshikh. Ucheba. Zavedni. Tsveta. Met.*, 7, 2 (47).
39. K.K. Kelley, U.S. Bureau of Mines Bull. 406 (1937).
40. P. Bartholome, "On the Paragenesis of Copper Ores", *Studia Universitatis "Lovanium"* (1958) (Leopoldville, Belgian Congo).
41. J. Joly, *Phil. Mag.* 25, 856 (1913).
42. R. Townend, P.K. Schultz, H.W. Funder and P.A. Young, *Bull. Aust. Min. Dev. Lab.*, 2, 1-11, 76-77 (1966).

43. P.A. Young, Bull. Aust. Min. Dev. Lab., 3, 1-19 (1967).
44. H. McKinstry, Econ. Geol., 54, 975 (1959).
45. H. von Wartenberg, Z. Physik. Chem., 67, 446 (1909).
46. H. Zeumer and W.A. Roth, Z. Physik. Chem. A, 173, 365 (1935).
47. S.V. Lipin, V.S. Uskov and V.R. Klokman, Zhurnal Poikladavi Khimii, 15, 411 (1942).
48. L.H. Adami and E.G. King, U.S. Bureau of Mines, Rept. Invest. 6495 (1964).
49. J.C. Southard, Ind. and Eng. Chem., 32, 442 (1940).
50. K.K. Kelley, U.S. Bureau of Mines Bull., 592 (1961).
51. R.W. Millar, J. Am. Chem. Soc., 50, 1875 (1928).
52. C.T. Anderson, J. Am. Chem. Soc., 52, 2296 (1930).
53. C.T. Anderson, J. Am. Chem. Soc., 53, 476 (1931).
54. C.T. Anderson, J. Am. Chem. Soc., 54, 107 (1932).
55. C.T. Anderson, J. Am. Chem. Soc., 59, 486 (1937).
56. J-H. Hu and H.L. Johnson, J. Am. Chem. Soc., 75, 2471 (1953).
57. E.F. Westrum, Jr., J.B. Hatcher and D.W. Osborne, J. Chem. Phys., 21, 419 (1953).
58. F. Gronvold, E.F. Westrum, Jr. and Chien Chou, J. Chem. Phys., 30, 528 (1959).
59. E.F. Westrum, Jr. and A.F. Beale, Jr., J. Phys. Chem., 65, 353 (1961).
60. E.G. King and W.W. Weller, U.S. Bureau of Mines, R.I. 5590 (1959).
61. W.W. Weller, U.S. Bureau of Mines, R.I. 6669 (1965).
62. L.B. Pankratz and E.G. King, U.S. Bureau of Mines, R.I. 7435 (1970).
63. "Thermodynamic Properties of Copper and its Compounds", I.N.C.R.A. Monograph II, ed. E.B. King, Mah, L.B. Pankratz, International Copper Research Association, Cambridge, Mass. (1973).
64. T. Rosenquist, Metals Trans., 185, 451 (1949).
65. A.A. Brooks, J. Am. Chem. Soc., 75, 2464 (1953).

66. F.D. Richardson and J.E. Antill, *Trans. Farad. Soc.*, 51, 22 (1955).
67. H.H. Kellogg, *Can. Met. Quart.*, 8, 3 (1969).
68. W.A. Krivsky and R. Schumann, Jr., *Metals Trans. AIME*, 982 (1957).
69. J.R. Craig and W.R. Lees, *Econ. Geol.*, 67, 373 (1972).
70. L. Pauling and C.O. Brockway, *Zeits. Krist.*, 82, 188 (1932).
71. "Crystal Structures of Minerals", L. Bragg, G.F. Claringbull and W.H. Taylor, Bell and Sons, Ltd., London (1965).
72. "Structural Inorganic Chemistry", A.F. Wells, Clarendon Press, Oxford (1960).
73. G. Donnay, L.M. Carliss, J.D.H. Donnay, N. Elliott and J.M. Hastings, *Phys. Rev.*, 112, 1917-1923 (1958).
74. D.J. Vaughan, Ph.D. Thesis, Oxford (1971).
75. S.J. Pickart, *Mineral. Soc. Amer. Spec. Pap.*, 3, 145 (1970).
76. A.S. Marfunia and A.R. Mkrtychan, *Geokhimiya*, 10, 1094 (1968).
77. B.V. Borshagorskii, A.S. Marfunia, A.R. Mkrtychan, R.A. Stukan and G.N. Nadzharyan, *Izv. Akad. Nauk., U.S.S.R., Ser. Khim.* 1968 (6) 1267.
78. N.N. Greenwood and H.J. Whitfield, *J. Chem. Soc. A*, 1697 (1968).
79. J. Piekoszewski, J. Suwalski and S. Ligenza, *Phys. Status. Solidi*, K99 (1969).
80. L.J. Cabri and R.H. Goodman, *Geokhimiya* 636 (1969).
81. F. Aramu, T. Bressani and P. Manca, *Nuovo Cimento*, B51, 370 (1967).
82. C.L. Herzenberg, *Nuovo Cimento*, 53, 516 (1968).
83. E. Frank, *Nuovo Cimento*, 58, 407 (1968).
84. A.J. Frueh, *Geochimica et Cosmochimica Acta.*, 6, 79 (1954).
85. A.J. Frueh, *Zeit. Krist.*, 106, 299 (1955).
86. A.J. Frueh, *Am. Mineral.*, 44, 1010 (1959).
87. G.F. Karavaev, A.S. Poplavnoi and V.G. Tyuterev, *Izv. Vyssh. Ucheb. Zaved. Fiz.*, 13, 42 (1970).
88. M. Telkes, *Am. Mineralogist*, 25, 536 (1950).

89. E.N. Zevgolis, Ph.D. Thesis, Univ. Minnesota (1971).
90. A. Etienne, Ph.D. Thesis, Univ. Brit. Col. (1970).
91. C.R.S. Needes, M.J. Nicol, Nat. Inst. Met. (Johannesburg) Report #1380 (1972).
92. J.T. Woodcock, Proc. Aust. Inst. Min. Met., No. 198, 47 (1961).
93. R.J. Cornelius and J.T. Woodcock, Proc. Aust. Inst. Min. Met., No. 185, 65 (1958).
94. I.H. Warren, Aust. J. App. Sci., 7, 346 (1956).
95. T.R. Scott and N.F. Dyson, Trans. Am. Inst. Min. Engrs., 242, 1815 (1968).
96. E. Peters and H. Majima, Can. Met. Quart., 7, 111 (1968).
97. J. Wright, Amdel Bull. #12, 47 (1971).
#13, 27 (1972).
98. R. Woods, Proc. Aust. Inst. Min. Met., #241, 53 (1972).
99. A.P. Prosser, IX Commonwealth Mining and Metallurgical Congress, London, 1969, Vol. 3.
100. M. Majima and E. Peters, VIII Int. Min. Proc. Cong., Leningrad, E1 (1968).
101. F. Habashi, Min. Sci. Eng., 3, 3 (1971).
102. J. Sullivan, U.S. Bureau Mines, Tech. Pap., 473 (1930).
103. G. Thomas, T.R. Ingraham and R.J.L. MacDonald, Can. Met. Quart., 6, 281 (1967).
104. J.A. King, Ph.D. Thesis, Univ. London (1966).
105. A.R. Burkin, Min. Sci. Eng., 1, 4 (1969).
106. J. Sullivan, U.S. Bureau Mines, Tech. Paper, 487 (1930).
107. G. Thomas and T.R. Ingraham, Can. Met. Quart., 6, 153 (1967).
108. K.J. Jackson and J.D.H. Strickland, Trans. Met. Soc. AIME, 212, 373 (1958).
109. I.H. Warren, Aust. J. App. Sci., 9, 36 (1956).
110. F. Loewen, M.A. Sc. Thesis, Univ. Brit. Col. (1967).

111. J. Dahms, J. Gerlach and F. Pawlek, *Erzmetall.* 20, 203 (1967).
112. O.B. Tkachenko and A.L. Tseft, *Tr. Inst. Met. Obogaskeh. Akad. Nauk. Kaz. S.S.S.R.*, 30, 15 (1969).
113. K. Wrabetz and W. Noddack, *Z. Elektrochem.*, 59, 96 (1955).
59, 752 (1955).
60, 722 (1956).
114. B.Z. Ustinskii and D.M. Chizikov, *Zh. Prikl. Khimii.*, 22, 1249 (1949).
115. M. Sato, *Econ. Geol.*, 55, 1202 (1960).
116. V. Kuxmann and H. Biallass, *Enzmetall*, 22, 53 (1969).
117. H.J. Matheu and H. Rickert, *Zeit. Phys. Chem. Neue Folge Bd.* 79, S315 (1972).
118. S. Cole, Ph.D. Thesis, Univ. Columbia (1972).
119. P. Brennet, S. Jafferalli, J.M. Vanseveren, J. Verecken and R. Winrad, *Met. Trans. AIME*, 5, 127 (1974).
120. S. Venkatachalam, R. Mallikarjunan, *Inst. Min. Met. Trans.*, 77, 45 (1968).
121. A.G. Losharev, A.F. Vozinar, *Zh. Prikl. Khimii*, 26, 49 (1953).
122. D.M. Chizikov and B.Z. Ustinskii, *Izvest. Akad. Nauk. S.S.S.R., Otdel Tekh. Nauk.*, 229 (1948).
123. L.S. Renzoni, R.C. McQuire and W.V. Barker, *J. Metals*, 10, 414 (1958).
124. F. Habashi and N. Torres-Acuna, *Tr. AIME*, 242, 780 (1968).
125. T. Kato and T. Oki, *Denki Kagaku*, 40, 670 (1972).
126. T. Kato and T. Oki, *Japan Inst. Metals. Journal*, 36, 947 (1972).
127. J.D. Sullivan, U.S. Bureau of Mines, *Tech. Pap.*, 486 (1930).
128. J.E. Dutrizac, R.J.C. MacDonald and T.R. Ingraham, *Met. Trans.*, 1, 225 (1970).
129. J.E. Dutrizac, R.J.C. MacDonald and T.R. Ingraham, *Met. Trans.*, 1, 3083 (1970).
130. J.D. Sullivan, *Trans. AIME*, 106, 515 (1933).
131. J.E. Dutrizac, R.J.C. MacDonald and T.R. Ingraham, *Trans. Met. Soc. AIME*, 245, 955 (1969).

132. E. Peters, "The Physical Chemistry of Hydrometallurgy", AIME Int. Symposium on Hydrometallurgy, Chicago (1973).
133. J.E. Dutrizac, R.J.C. MacDonald, Can. Met. Quart., 12, 409 (1973).
134. F. Lowe, Ph.D. Thesis, Univ. of Arizona (1970).
135. F.A. Forward and I.H. Warren, Metall. Rev., 5, 137 (1960).
136. R.O. Pike, G.H. West, L.V. Steck, R. Cummings and B.P. Little, Trans. AIME, 90, 311 (1930).
137. F.P. Haver and M.M. Wong, U.S. Bureau of Mines, R.I. 7474 (1971).
138. P.A. Pazdnikov and Yu-M. Potashnikov, Sb Nauch-Tekh. Tr. Trudov Nauch. Issled. Inst. Metall. Chelyb. Sovet. Narod. Khoz., #2, 121 (1960).
139. W. Mulak and J. Niemec, Roczn. Chemii, 42, 775 (1968).
140. V.V. Ermilov, O.B. Tkachenko and A.L. Tseft, Tr. Inst. Met. Obogasch., Akad. Nauk. Kaz. S.S.S.R., 30, 3 (1969).
141. V.E. Klets and A.P. Serikov, Tr. Irtutsk. Politekh. Inst., 18, 31 (1963).
142. Can. Patent #938793, Cominco Ltd. (1973).
143. U.S. Patent #3,785,944, Duval Corp. (1974).
144. A.I. Vizsolyi, J. Metals, 19, 52 (1967).
145. P.H. Yu, Ph.D. Thesis, Univ. of Utah (1972).
146. F. Forward, J. Metals, 7, 457 (1955).
147. M. Kuhn, paper presented at 3rd C.I.M. Hydrometallurgy Conference, Edmonton (1973).
148. J.D. Porter, P.B. Queneau and T.J. Hudson, paper presented at AIME Annual Meeting, San Francisco (1972).
149. F. Habashi, Trans. S.M.E.-AIME, 254, 224 (1973).
150. G. Bjorling and G.A. Kolta, Proc. Intern. Mineral Processing Cong. 7th, New York (1965).
151. G. Springer, Trans. Inst. Min. Met., C11 (1970).
152. W.H. Brattain and C.G.B. Garrett, Bell System Techn. Journal, 34, 129 (1955).
153. K. Jibiki, M.Sc. Thesis, U.B.C. (1971).

154. T. Oki and S. Ono, Japan Inst. Min. Met. Journal, 83, 1159 (1967).
155. H. Sawamoto, T. Oki and A. Nishina, Nagoya Univ., Fac. Eng. Memoirs, 14, 197 (1962).
156. Internat. Symp. on High Temperature Electrochemistry, Guildford, U.K. (1973).
157. D. de G. Jones and H.G. Masterson, "Techniques for the Measurement of Electrode Processes at Temperatures above 100°C", in Adv. Corros. Science and Tech., ed. M.G. Fontana and R.W. Staehle, Vol. I (1970).
158. W.C. Waggener and A.M. Tripp, Rev. Sci. Instr., 30, 677 (1959).
159. R.H. Krenz, A.S.T.M., Spec. Tech. Pub., 368 (1963).
160. M.H. Lietzke, R.S. Greeley, W.T. Smith and R.W. Stoughton, J. Phys. Chem., 64, 652 (1960).
161. E.V. Franck, J.E. Savolainen and W.L. Marshall, Rev. Sci. Instr., 33, 115 (1962).
162. A.J. Ellis, J. Chem. Soc., 2299, 4300 (1963).
163. G. Kennedy, Econ. Geology, 45, 629 (1960).
164. A.L. Bacarella and A.L. Sutton, J. Electrochem. Soc., 112, 546 (1965).
165. M.W. Connell, U.S. Patent #2,625,573 (1953).
166. P.W. Bridgeman, "The Physics of High Pressure", Bell and Sons (1949).
167. A. Disteche, Rev. Sci. Instr., 30, 474 (1959).
168. V.V. Gerasimov, Corrosion of Reactor Materials, A Collection of Articles, A.E.C. Transl. 5219, p.13 (1962).
169. J. Giner, J. Electrochem. Soc., 111, 376 (1966).
170. S. Stene, Rec. Trans. Chim. Pays-Bas, 49, 1133 (1930).
171. M.H. Lietzke and R.W. Stoughton, in "Encyclopaedia of Electrochemistry", C.A. Hampel, Ed. Reinhold, N.Y., p. 505 (1964).
172. M.H. Lietzke and R.W. Stoughton, J. Phys. Chem., 67, 2573 (1963).
173. G. Kortum and W. Hausserman, Ber. Bunsenges. Physikchem., 69, 594 (1965).
174. R.W. Lietzke and R.W. Stoughton, J. Phys. Chem., 68, 3043 (1964).
175. M.H. Lietzke and R.W. Stoughton, J. Am. Chem. Soc., 75, 5226 (1953).

176. M.H. Lietzke and J.V. Vaughan, *J. Am. Chem. Soc.*, 77, 876 (1954).
177. D.G. Ives and G.J. Janz, "Reference Electrodes", Academic Press, N.Y. (1961).
178. R. Greeley, Ph.D. Thesis, Univ. of Tennessee (1960).
179. E.B. Sandell, "Colorimetric Determination of Trace Amounts of Metals", Interscience Publishers, New York, 3rd Ed. (1959).
180. R.J. Bertolacini and J.E. Barney II, *Anal. Chem.*, 30, 202 (1958).
181. J. Agterdenbos and N. Martinus, *Talanta*, 11, 875 (1964).
182. "Standard Methods of Chemical Analysis", N.H. Furman ed., Vol. I, p. 544, Sixth edition, D. Van Nostrand Co., Inc., Princeton, N.J. (1962).
183. L.S. Renzoni, R.C. McQuire and W.V. Barker, *J. of Metals*, 10, 414 (1958).
184. Symposium on the Thompson Operation, *C.I.M. Bullentin*, 57, 1181 (1964).
185. J. Gerlach, H. Hähne and F. Pawlek, *Z. Erzbergan Metallhüttenw.*, 19 (2) 66 (1966).
186. H. Majima and E. Peters, VIII Internat. Mineral Processing Congress, Leningrad, EI (1968).
187. W. Latimer, "Oxidation Potentials", 2nd edition, Prentice-Hall, N.J. (1950).
188. H. Helgeson, "The Thermodynamics of Hydrothermal Systems at Elevated Temperatures and Pressures", *Amer. J. Science*, 247, 729 (summer 1969).
189. K.J. Vetter, *Electrochemical Kinetics, Theoretical and Experimental Aspects*, Academic Press, N.J. (1967).
190. E. Devuyt, Ph.D. Thesis, Univ. of B.C. (1973).
191. "The Winning of Nickel", J.R. Boldt and P. Queneau, Longmans, Toronto, p. 306 (1967).
192. T. Ngoi and E. Peters, Private communication.
193. F.A. Forward and V.N. Mackiw, *J. Metals*, 461 (1965).
194. D.I. Ryabchikov and V.G. Sil'nichenko (Moscow Regional Ped. Inst.) *Bull. acad. sci. U.R.S.S., Classe sci. chim.* 19-26 (1947).

195. "A Comprehensive Treatise on Inorganic and Theoretical Chemistry", J.W. Mellor, Wiley (N.Y.) (1922).
196. "Mellor's Modern Inorganic Chemistry", Rev. Ed., G.D. Partees, Longmans, London (1967).
197. V.F. Toropova, I.A. Sirotina and T.I. Lisova, Uchenye Zapiski Kazan. Gosudarst. Univ. im. V. I. Ul'yanova-Lenina, Khim. 115, No. 3, 43-52 (1955).
198. S.M. Ahmed and D. Maksimov, Mines Branch Research Report, R196, Ottawa (1968).
199. R. McElroy, Ph.D. Thesis, U.B.C. (1972).
200. C.M. Criss and J.W. Cobble, J. Amer. Chem. Soc., 86, 5385 (1964).
201. C. Wagner, "Conduction and Diffusion in Ionic Crystals", in "The Molecular Designing of Materials and Devices", ed. A. Von Hippel, MIT Press (1965).

APPENDIX A

A THERMOCHEMICAL STUDY OF THE Cu-Fe-S MINERALS*

Introduction

The Cu-Fe-S system has been extensively investigated by Yund and Kullerud¹ at temperatures as low as 200°C and their interpretation of the stable assemblages at this temperature is given in Figure 1. It can be seen that, in addition to the usual binary sulphides, there are four stable ternary sulphides:

Chalcopyrite	CuFeS_2	(cp)
Bornite	Cu_5FeS_4	(bn)
Cubanite	CuFe_2S_3	(cb)
Kdaite	$\text{Cu}_{5.5}\text{FeS}_{6.5}$	(id)

Of these, the first two minerals are very commonly encountered in nature, and are the major sources of copper in Canada, whilst cubanite is comparatively uncommon and idaite is rarely reported. However, in contrast to the reliable thermochemical data available on the binary sulphides^{2,3} few such studies are reported on the ternary sulphides and Young⁴ has summarized the work to date (1967).

'Maier'⁵ using a value of 743°C (?) for the decomposition temperature of CuFeS_2 arrives at the values:

$$\Delta H_{298}^{\circ} = -41.59$$

$$\Delta G_{298}^{\circ} = -41.33 \text{ Kcal/mole}$$

Bartholome⁶ using the assemblages shown in Figure 2, and available data on equilibrium partial pressures of sulphur over these

*Taken from report submitted for INCRA Grant #160, by D. Jones and E. Peters (1970).

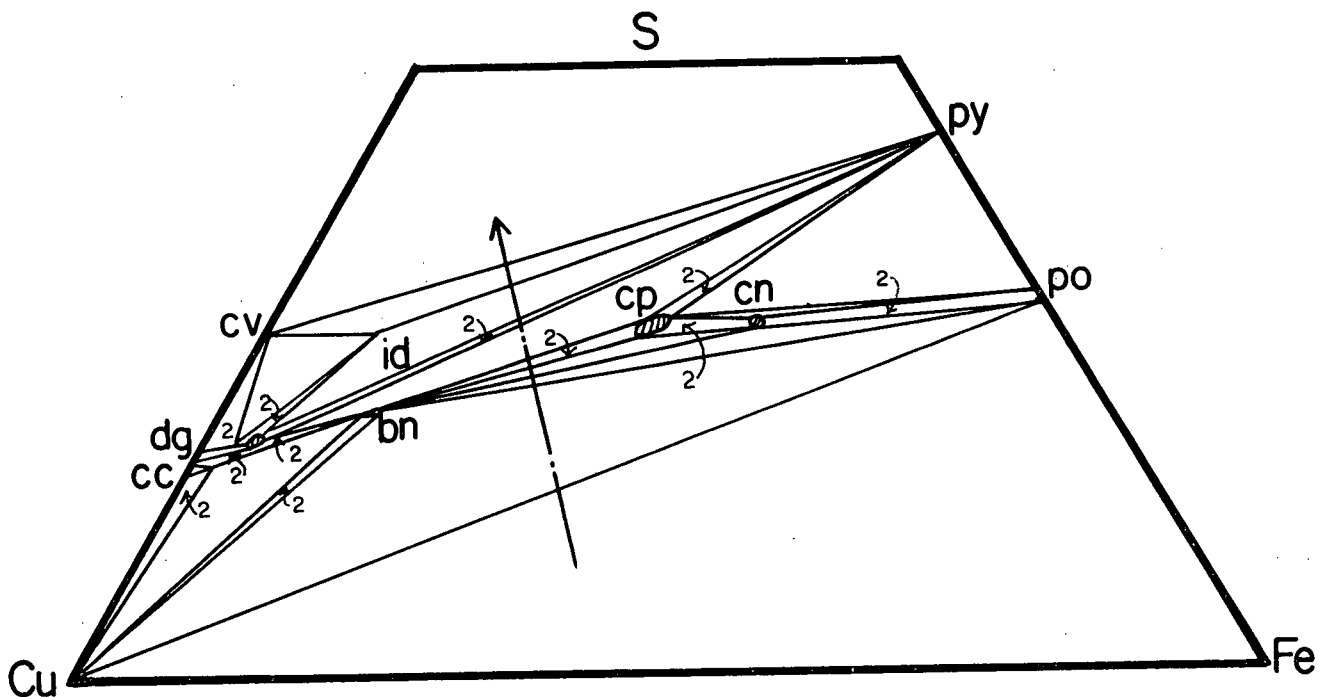


Fig.1 Cu-Fe-S system at 200°C.
(Yund & Kullerud)

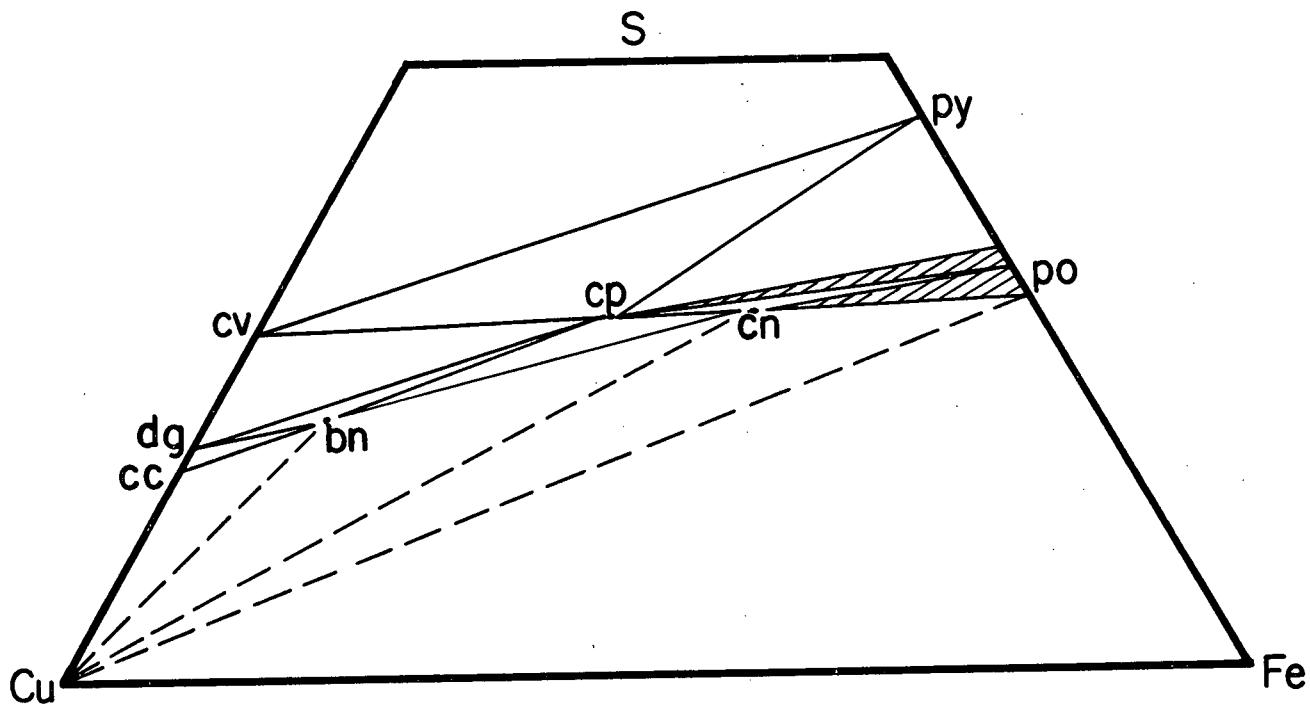


Fig.2 Cu-Fe-S system at 25°C.
(Bartholomé)

assemblages (at 25°C) deduces:

	$-\Delta G^\circ_{298}$
CuFeS_2	-45.0 ± 3.5 kcal/mole
Cu_5FeS_4	-89.0 ± 6.0
CuFe_2S_3	-69.0 ± 3.0

His work suffers from the fact that his ternary diagram is probably not correct¹ and the large error limits imposed by the lack of data.

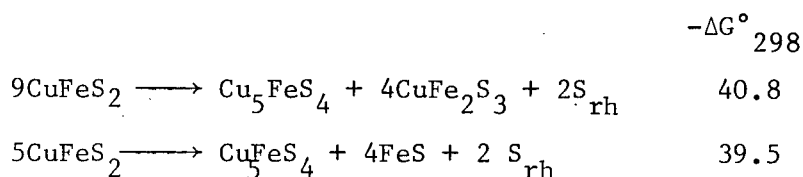
Golomzik⁷ reports some sulphur pressures at 500, 600 and 700°C over chalcopyrite, quoted from a source so obscure as to be suspicious, and calculates:

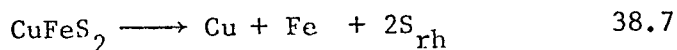
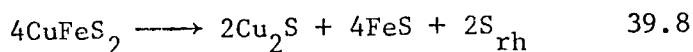
$$\Delta G^\circ_{298} (\text{CuFeS}_2) = -51.49 \text{ Kcal/Mole}$$

This calculation is subject to serious errors due to the heat of transformation, specific heat changes and presence in the sulphur vapor of species other than diatomic.

Young⁴ similarly made some calculations, utilizing the sulphur vapor pressures for each mineral tabulated by Merwin and Lombard⁸; to do this, as in the above calculations, it was necessary to assume what the decomposition products are, and this is never an unambiguous choice.

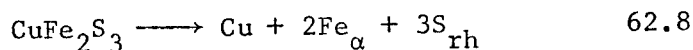
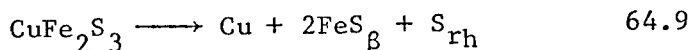
Thus, for example, one may write four different reactions for CuFeS_2 :



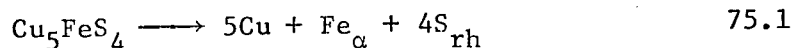
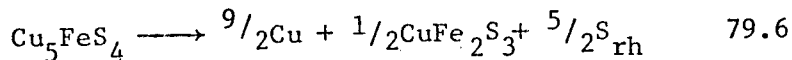


Similarly for CuFe_2S_3 :

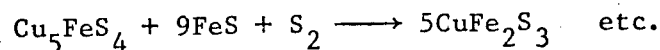
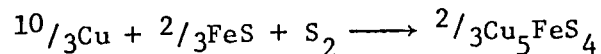
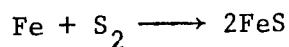
$-\Delta G_{298}^\circ$



and Cu_5FeS_4 :



Young considers these values to be rough estimates at best. He also does some separate calculations based on mineral assemblages alone. Following the arrow in Fig.1, he writes the set of reactions as each tie-line is crossed:



(Each reaction is written with one mole S_2)

Then, using the fact that the free energy change for each successive reaction is smaller (i.e. less negative) than the one preceding it, he writes the appropriate set of inequalities.

$$\frac{2}{3} \Delta G^\circ(\text{FeS}) - \frac{2}{3} \Delta G^\circ(\text{Cu}_5\text{FeS}_4) \leq -2 \Delta G^\circ(\text{FeS})$$

$$\Delta G^\circ(\text{Cu}_5\text{FeS}_4) + 9\Delta G^\circ(\text{FeS}) - 5\Delta G^\circ(\text{CuFe}_2\text{S}_3) \leq \frac{2}{3} \Delta G^\circ(\text{FeS}) - \frac{2}{3}\Delta G^\circ(\text{Cu}_5\text{FeS}_4)$$

etc.

Then, knowing $\Delta G^\circ(\text{FeS})$, the inequalities may be solved, giving lower limits for the free energies of each mineral. So far the calculation appears acceptable, but then the author goes on to obtain upper limits by using Bartholome's estimate for digenite;

$$\Delta G^\circ(\text{Cu}_9\text{S}_5) = -101.0 \pm 8.0 \text{ Kcal/mole}$$

and putting the values for the lower limits back into the inequalities. Firstly, we now have a very reliable digenite value from Etienne's work²

$$\Delta G_{298}^\circ(\text{Cu}_9\text{S}_5) = -90.7 \pm 3.0 \text{ Kcal/mole}$$

and secondly, the algebra of this step appears to be incorrect. Upper limits may be obtained, but they do not approach the lower limits as closely as Young suggested. However, they are still useful and together with the previous results are given in Table 1.

Table 1. Calculated Free Energies of Minerals: ΔG°_{298} (Kcal./mole)

Mineral	1)	2)	3)	4)	5)
CuFeS_2	45.3 ± 0.2	43.5 ± 2.1	45.0 ± 4.5	40.8	38.7
CuFe_2S_3	68.2 ± 0.2	66.2 ± 2.2	69.0 ± 4.5	64.9	62.8
Cu_5FeS_4	85.9 ± 6.1	84.9 ± 5.2	89.0 ± 8.0	79.4	75.1
Cu_5FeS_6	100.8 ± 3.8	102.3 ± 2.4	-	97.5	-

- 1) Young's calculations from mineral assemblages.
- 2) Our modification of 1) as outlined above.
- 3) Bartholomé calculations from sulphur pressures.
- 4) Young's calculations based on Merwin and Lombard's decomposition pressures and Bartholomé (low-T) assemblages.
- 5) Repeat of 4) with Kullerud's (high-T) assemblages.

The formula for idaite used in all these efforts is Cu_5FeS_6 ; according to Kullerud¹, the correct one is $\text{Cu}_{5.5}\text{FeS}_{6.5}$.

Combustion Experiments

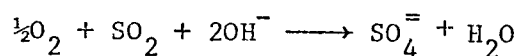
The principle of bomb calorimetry is that the heat of formation, ΔH° of a substance may be determined from its combustion to a product of known heat content. For organic materials this is very convenient because most of them are very easily ignited, under high oxygen pressure, to what is essentially water and carbon dioxide. However, for inorganic substances, combustion is not so simple, for a variety of products are possible and often their heat content is unknown.

Previous combustion work on sulphides goes back a long way, but appears to have gone out of fashion for some time now, in favor of other techniques such as measuring the equilibrium gas pressures and composition as a function of temperature. The reason for this decline in interest appears to be two-fold: Firstly, values of ΔH° obtained from combustion are often caught in an 'error-limits squeeze' i.e. a small difference between two large numbers, such that a small error in the heat of combustion results in a large error in the heat of formation. Secondly, the exact nature of the product of combustion is not easily determined, and a 95% combustion is not good enough.

For this reason, it was intended that the product of a combustion of CuFeS_2 and Cu_5FeS_4 should be converted to a soluble form, which presumably would be a known species.

Experimental Results

Using a Parr adiabatic bomb calorimeter with 30 atm. O₂, CuFeS₂ samples could be ignited to form SO₂ and a solid oxide product. Several attempts were made to quantitatively convert the SO₂ to SO₃ and dissolve the gas in a basic solution within the bomb; however, there is difficulty in oxidizing the SO₂ completely, and since this overall reaction:



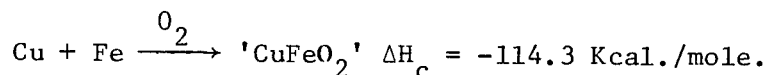
is strongly exothermic, a large error is introduced by any unoxidized SO₂. Therefore it appeared more accurate to leave the sulphur in its SO₂ form and keep SO₃ formation to a minimum; this necessitated using a dry bomb. Any SO₃ present can easily be detected by its fuming in air.

The nature of the solid oxide product constituted the most difficult problem; it was extremely insoluble in cold acid, and only dissolved slowly in boiling sulphuric - far slower than the stainless steel capsule. Evidently there was no ordinary solution which could dissolve the oxide in a reasonable length of time (say one hour) without attacking the bomb itself.

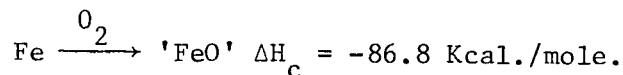
Experiments were conducted to see if the oxide could be reduced by a zinc amalgam covered dilute sulphuric acid. This was partially successful, but the reaction was far too slow and by no means complete. Other amalgams were tried with similar results.

Another approach that was tried was igniting CuFeS₂ with NH₄Cl and/or NH₄ClO₄, in the hope a soluble salt would be formed. Again there was partial success, but never 100% conversion, due to the incomplete combustion.

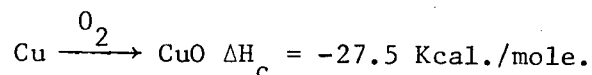
Therefore it was decided to abandon all attempts to solubilize the oxide product, and instead to determine its heat content indirectly. No ΔH values for 'CuFeO₂' could be found in the literature, and so this had to be determined experimentally. A one-to-one mixture of copper and iron powder can be ignited to give a heat of combustion ΔH_c of 114.3 kcal./mole



Iron powder alone can be ignited, but copper powder can not.



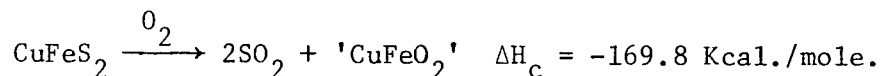
However, assuming that CuO and 'FeO' mix with no significant interactions one obtains:



This assumption, which gives a value for CuO that is 10 Kcal. lower than the literature value, nevertheless gave some apparently consistent results, as follows;

CuS, Cu₂S, FeS, and FeS₂ were all ignited, and literature values of ΔH° of these substances were only obtained by using the values of ΔH_c of CuO and FeO, determined experimentally. Thus it appeared that the ΔH_c value for single 'CuFeO' was a useful one.

The ignition of CuFeS₂ gave however a very low value:

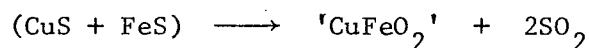


Using the literature value for SO_2 ($\Delta H_f^\circ = -71.0$ Kcal./mole) and the experimental value for CuFeO_2 of -114.3, we obtain:

$$\Delta H_f^\circ(\text{CuFeS}_2) = -86.5 \text{ Kcal./mole}$$

This is an impossibly large figure, and would imply several unknown reactions and mineral associations. Estimates based on mineral associations and gas pressures are about half this value.

However, combustion of a (CuS and FeS) mixture gave identical results which was extremely puzzling.



$$\Delta H_c = - 221.8 \text{ Kcal/mole}$$

$$\text{This leads to: } \Delta H_f(\text{CuFeS}_2) = -86.9 \text{ Kcal./mole}$$

Therefore the results were internally self-consistent, but wrong! The way out of the dilemma was finally found however, by re-investigating the combustion of CuS. In order to get more accurate data larger samples were ignited and it was found that the heat of combustion was dependent upon the size of the sample.

	Weight of sample (g)	ΔH_c (CuS) (Kcal./mole)
Earlier results	0.91	84.0
	0.96	84.1
	1.52	89.8
	2.13	86.2
	2.38	88.2
	3.28	94.1
	6.30	98.4
Theoretical result:	96.0 \pm 1.3	

Evidently, the original value $\Delta H_f(\text{CuO})$ of -27.5 kcal. was incorrect, and applied only to samples in a narrow size range. With smaller samples too much heat is lost to the surroundings and the sample is never totally combusted. Similar but more dramatic results were found for (CuS and FeS) mixture:

Weight of sample (g)	$-\Delta H_c(\text{CuS} + \text{FeS})$ (Kcal/mole)
1.08	221.8
3.04	135.2
5.06	120

The low heat of combustion CuFeS_2 was finally made clear when the combustion products were examined upon the microprobe. This instrument showed that while the combustion product of CuS and FeS (separately) contained no sulphur, the CuFeS_2 combustion product certainly did. DTA work on the later substance indicated the presence of copper ferrite CuFe_2O_4 .

Owing to the unsatisfactory nature of these experiments, corresponding work on bornite was not advanced beyond the preliminary stage.

CONCLUSIONS

Combustion experiments upon CuFeS_2 with pure O_2 gave a mixed product containing some residual sulphur, whose heat content was not known.

Attempts to solubilize this product failed and so did efforts to determine its heat content experimentally.

Experiments designed to oxidize CuFeS_2 with other oxidants which would give a soluble product were also unsuccessful.

Combustion of simple copper and iron sulphides gives a heat of combustion which is dependent upon the size of the sample.

Corrections to Young's calculations

- 1) The 'descending' column in Table 4 has the inequality sign backwards; therefore these are lower limits.
- 2) The value for digenite (from Bartholome) 101.8 kcal. (w.r.t. S_{rh}) can be replaced by Etienne's value of 90.7 ± 3.0 .
- 3) Upper limits cannot be obtained in any way by using the lower limits (shown in table 4).
- 4) Upper limits may be obtained by introducing values for (dg) and (py) (as well as (po)) into inequalities (28), (29), (30) and (32) (not 27, 28, 29, 31, as suggested). These may be reduced to:

$$cn \leq po + cp \quad (28)$$

$$2bn \leq dg + cn \quad (29)$$

$$7cp + 2dg \leq 5bn + 2py \quad (30)$$

$$4id \leq dg + 4py + 11cv \quad (32)$$

Substituting (28) and (29) into (30) gives a value for (cp), which may then be used in (28) to obtain (cn), etc.

5) Known values used were:

$$(dg) = -90.7$$

$$(py) = -42.0$$

$$(po) = -37.37$$

$$(cv) = -22.5$$

References

1. R.A. Yund and G. Kullerud, J. Petrol., 7, 454, (1966).
2. A. Etienne, Ph.D. Thesis, U.B.C., 1970.
3. K.K. Kelly, U.S. Bureau of Mines Bull., 584, 592.
4. P.A. Young, AMDEL Bulletin, April 1967.
5. Maier, quoted in K.K. Kelly, U.S. Bur. Min. Bull., 406
6. P. Bartholomé, Studia Univ. Lovan. Faculté des Sciences.
(Leopoldville) 4, 1, (1958)
7. A. Golomzik, Izv. Vysshikh. Uchebn. Zavednii, Tsvetn. Met. 7(2) 47(1964)
8. M.E. Merwin and R.H. Lombard, Econ. Geol., (1937) 32, 203.
9. D.W. McGlashan, A.D. Rovig, and D.M. Podbnik, Trans. S.M.E.,
244, 446, (1969).
10. S. Venkatachalan and R. Mallikarjunan, Trans. Inst. Min. Metal.,
C, 181, (1970).
11. P. Ruetschi and R.F. Amlie, J. Electrochem. Soc., 112, 665 (1965).
12. K. Jibiki, M.Sc. Thesis, U.B.C., 1971.
13. E. Peters, and H. Majima, Can. Met. Quart., 7, 111, (1968).
14. G.M. Swinkels and A.L. Mular, AIME Meeting, Denver, 1970.
15. Brodie, M.Sc. Thesis, U.B.C., 1969.
16. G. Thomas and T.R. Ingraham, Can. Met. Quart., 6, 153 (1967).
16. G. Thomas and T.R. Ingraham, Can. Met. Quart., 6, 153, (1967).
17. G. Thomas, T.R. Ingraham, and R.J.C. MacDonald, Can. Met. Quart.,
6, 281, (1967).
18. J.E. Dutrizac, R.J.C. MacDonald, and T.R. Ingraham, Trans. TMS-AIME,
245, 995 (1969).
19. J.E. Dutrizac, R.J.C. MacDonald, and T.R. Ingraham., Met. Trans.
1 225, (1970).

APPENDIX B

The data from some of the constant-potential experiments (Figs. 50, 51) in Section III(b) are included here for greater clarity. The later experiments in sulphate solutions are more adequately represented in the figures.

Potential	Dilute Chloride Solution	Strong Chloride Solution
535 (SHE)	p.2, p.3	p.5, p.16
635	p.1	p.17
735	p.12, p.14	p.4
935	p.7, p.8	p.6, p.9
1085		p.15
1185	p.10	p.11, p.13

SUMMARY OF P1

Potential = 450 mV (AgCl) = 635 mV (S.H.E.)
 Temperature = 90°C
 Saw Cut Electrode

Electrode Area = 0.64 cm²
 Solution: 0.3M NaCl
 0.2M HCl

Time (Hr.)	Current (mA)	C.D. ₂ (mA/cm ²)	Cu (mmoles)	Fe _T (mmoles)	Fe/Cu Ratio	Current Efficiency %			Coulombs
						Cu	Fe	Total	
.25	.38	.59							
2.00	.39	.61							
3.00	.41	.64							
5.00	.50	.78							
11.00	.79	1.23	.0335			34			19
21.00	.91	1.41	.089	.150	1.69	35.7	60.3	96.0	48.1
35.00	1.12	1.75	.190	.244	1.28	39.1	50.0	89.1	94.0
43.00	1.2	1.97							
57.0	1.44	2.25	.453	.573	1.265	43.1	54.6	97.8	203.1
81.00	1.65	2.58	.748	.84	1.12	43.1	48.4	91.5	335
106.00	1.87	2.92	1.10	1.19	1.08	42.6	46.1	88.7	499.3
136.00	1.87								
153.00		2.81	1.994	2.145	1.075	47.5	51	98.5	810.7
180.00	1.90	2.97	2.17	2.38	1.10	43.3	47.5	90.8	968

SUMMARY OF P2

Potential = 350 mV (AgCl) = 535 mV (S.H.E.)
 Temperature = 90°C
 Saw Cut Electrode

Electrode Area = 1.2 cm²
 Solution: 0.3M NaCl
 0.2M HCl

Time (Hr.)	Current (mA)	C.D. ₂ (mA/cm ²)	Cu (mmoles)	Fe _T (mmoles)	Fe/Cu Ratio	Current Efficiency %			Coulombs
						Cu	Fe	Total	
.08	.84	.69							
.50	.50	.42							
1.50	.35	.29							
5.50	.25	.21							
20	.175	.15	.0374	.210	5.62	51.1	288	340	14.1
30	.175	.15							
53	.165	.14	.0772	.352	4.55	42.8	195	238	34.8
73	.14	.12	.0942	.370	4.70	39.4	154	194	46.2
100	.12	.10	.1142	.457	4.00	38.5	154	193	57.3
126	.075	.063							
137	.078	.065	.149	.4945	3.32	40.1	133	173.1	71.7

SUMMARY OF P3

Potential = 350 mV (AgCl) = 535 mV (S.H.E.)
 Temperature = 90°C
 Saw Cut Electrode

Electrode Area = 1.25 cm²
 Solution: 0.3M NaCl
 0.2M HCl

Time (Hr.)	Current (mA)	C.D. ₂ (mA/cm ²)	Cu (mmoles)	Fe _T (mmoles)	Fe/Cu Ratio	Current Efficiency %			Coulombs
						Cu	Fe	Total	
.08	2.3	1.8							
.50	1.5	1.2							
1.50	1.25	1							
5.50	1.35	1.08	.04	.10	2.5	30.0	74	10.4	26
7.25	1.52	1.21							
10	1.75	1.40							
18	2.4	1.91	.193	.251	1.3	33.3	43.3	76.6	112
23	2.7	2.15							
31	3.0	2.4	.490	.58	1.182	40.6	48.0	88.6	233
52	3.9	3.1	1.10	1.15	1.045	42.7	44.6	87.3	498
73	5.15	4.1	1.93	1.81	.937	44.9	42.1	87.0	830
126	6.0	4.8	4.82	4.56	.945	48.1	45.5	93.6	1935
137	6.0	4.8	5.07	5.50	.922	45.3	49.1	94.4	2160

SUMMARY OF P4

Potential = 550 mV (AgCl) = 735 mV (S.H.E.)
 Temperature = 90°C
 Saw Cut Electrode

Electrode Area = 0.60 cm²
 Solution: 3M NaCl
 0.2M HCl

Time (Hr.)	Current (mA)	C.D. ₂ (mA/cm ²)	Cu (mmoles)	Fe _T (mmoles)	Fe/Cu Ratio	Current Efficiency %			Coulombs
						Cu	Fe	Total	
.08	0.9	1.5							
.50	0.65	1.1							
1	0.63	1.05							
3.50	0.71	1.2							
5	0.80	1.35							
8	1.05	1.7							
12	1.65	2.75							
17	2.6	4.3							
20	3.2	5.3	.193	.250	1.30	41.4	53.6	95.0	90
30	4.4	7.3	.520	.690	1.32	43.6	58.0	101.6	230
44	4.7	7.8	1.042	1.215	1.16	43.5	50.7	94.2	463
53	4.7	7.8							
66	4.4	7.3	1.878	1.975	1.05	44.4	46.7	91.1	817
79	4.2	7.0							
93	3.9	6.5	2.90	3.02	1.05	45.4	47.2	92.6	1235
114	3.7	6.16							
123	3.6	6.0	3.80	4.07	1.07	45.1	48.2	93.3	1627

SUMMARY OF P5

Potential = 350 mV (AgCl) = 535 mV (S.H.E.)
 Temperature = 90°C
 Saw Cut Electrode

Electrode Area = 1.3 cm²
 Solution: 3M NaCl
 No Acid

Time (Hr.)	Current (mA)	C.D. (mA/cm ²)	Cu (mmoles)	Fe _T (mmoles)	Fe/Cu Ratio	Current Efficiency %			Coulombs
						Cu	Fe	Total	
.08	1	.77							
1.00	1	.77							
2	1.15	.89							
4	1.50	1.15							
6.50	1.9	1.46	.03	.074	2.20				
12	1.9	1.46							
20	1.72	1.32	.091	.144	1.58	14.1	22.3	36.4	124.7
30	1.55	1.19							
41.5	1.17	0.90	.123	.130	1.06	10.3	10.9	21.2	231
54.5	.65	0.50							
68	.45	0.35	.173	.191	1.11	11.4	12.6	24.0	293

SUMMARY OF P6

Potential = 750 mV (AgCl) = 935 mV (S.H.E.)
 Temperature = 90°C
 Polished Electrode

Electrode Area = 0.71 cm²
 Solution: 3M NaCl
 0.2M HCl

Time (Hr.)	Current (mA)	C.D. (mA/cm ²)	Cu (mmoles)	Fe _T (mmoles)	Fe/Cu Ratio	Current Efficiency %			Coulombs
						Cu	Fe	Total	
.08	2.2	3.1							
.25	2.1	2.95							
2.50	2.0	2.80							
4	2.05	2.90							
6	2.35	3.3							
8	3.0	4.2							
10	3.9	5.5							
18.50	8.6	12.1	.501	.728	1.45	34.2	49.6	83.8	283
28	10.0	14.1	1.10	1.63	1.48	35.4	52.4	87.8	601
35	10.0	14.1							
40	9.5	13.4							
48	8.9	12.5	2.77	3.29	1.18	40.9	48.5	89.4	1309
54	8.75	12.3							
78	7.4	10.4							
94	7.7	10.8	5.93	6.41	1.08	44.2	47.9	92.1	2586

SUMMARY OF P7

Potential = 750 mV (AgCl) = 935 mV (S.H.E.)
 Temperature = 90°C
 Polished Electrode

Electrode Area = 1.3 cm²
 Solution: 0.3M NaCl
 0.2M HCl

Time (Hr.)	Current (mA)	C.D. ₂ (mA/cm ²)	Cu (mmoles)	Fe _T (mmoles)	Fe/Cu Ratio	Current Efficiency %			Coulombs
						Cu	Fe	Total	
.17	2.6	2.05							
.42	2.4	1.90							
1.00	1.9	1.50							
2.00	1.5	1.18							
4	1.0	.79							
10	1.0	.79							
17	1.12	.88							
19	1.27	1.00	.318	.210	.66	81.9	54	136	75
24	1.47	1.16							
30	1.65	1.30							
37	2.1	1.60	.379	.405	1.07	41.8	44.7	86.5	175

SUMMARY OF P8

Potential = 750 mV (AgCl) = 935 mV (S.H.E.)
 Temperature = 90°C
 Saw Cut Electrode

Electrode Area = 0.70 cm²
 Solution: 0.3M NaCl
 0.2M HCl

Time (Hr.)	Current (mA)	C.D. (mA/cm ²)	Cu (mmoles)	Fe _T (mmoles)	Fe/Cu Ratio	Current Efficiency %			Coulombs
						Cu	Fe	Total	
.10	4.2	6.0							
.66	3.6	5.1							
1.17	2.95	4.2							
2	2.2	3.15							
6	1.63	2.33							
10	1.75	2.50							
15	2.03	2.90							
22	2.95	4.2	.286	.582	2.04	34.1	69.3	103.4	162
41	4.95	7.1	.843	1.245	1.48	33.5	55.1	88.6	436
65	6.3	9.0	2.05	2.40	1.17	42.0	49.25	91.25	942
72	6.2	8.9							
88	4.8	6.9	3.23	3.86	1.195	43.9	52.5	96.4	1420
97	7.3	10.5							
100	11.5	16.5	3.86	4.52	1.17	44.9	52.6	97.5	1660

SUMMARY OF P9

Potential = 750 mV (AgCl) = 935 mV (S.H.E.)
 Temperature = 90°C
 Saw Cut Electrode

Electrode Area = 0.92 cm²
 Solution: 3M NaCl
 0.2M HCl

Time (Hr.)	Current (mA)	Cu (mmoles)	Fe _T (mmoles)	Fe/Cu Ratio	Fe ⁺⁺ (mmoles)	Current Efficiency %			Coulombs
						Cu	Fe	Fe ⁺⁺⁺	
.08	2.4								
.34	1.95								
1	1.62								
3	1.65								
6	2.25								
9	3.20								
15	5.10								
17	5.5	.337	.474	1.40		33.4	46.9	80.3	195
21	6.65								
25	7.5								
29.5	8.0	.875	1.010	1.15		35.6	41.1	76.7	474
40	8.4								
50	8.1	2.13	2.20	1.03		38.3	39.5	77.8	1075
67	8.25	3.45	3.60	1.04	2.70	40.7	42.5	83.2	1635
80	7.8								
93	7.1	5.15	5.08	.99	4.15	42.4	41.8	84.2	2342
117	7.6	6.25	6.28	1.005	5.88	40.7	40.9	81.6	2965

SUMMARY OF P10

Potential = 1000 mV (AgCl) = 1185 mV (S.H.E.)
 Temperature = 90°C
 Saw Cut Electrode

Electrode Area = 1.06 cm²
 Solution: 0.3M NaCl
 0.2M HCl

Time (Hr.)	Current (mA)	Cu (mmoles)	Fe _T (mmoles)	Fe/Cu Ratio	Fe ⁺⁺ (mmoles)	Current Efficiency %			Coulombs
						Cu	Fe	Total	
.17	4.7								
.50	3.6								
1	3.3								
3	2.4								
7	2.2								
9	2.3	.139	.182	1.31		31.9	41.8	73.7	84
12	2.5								
15	2.75								
20	3.1								
28	3.9	.556	.545	0.98	.542	37.1	36.3	73.4	290
35	4.9								
40	5.5								
54	7.4	1.665	1.665	1.00	1.665	39.1	39.1	78.2	823
60	7.8								
65	8.25								
70	8.5								
78	9.1	3.05	3.05	1.00	3.05	39.4	39.4	78.8	1535

SUMMARY OF P11

Potential = 1000 mV (AgCl) = 1185 mV (S.H.E.)
 Temperature = 90°C
 Saw Cut Electrode

Electrode Area = 1.00 cm²
 Solution: 3M NaCl
 0.2M HCl

Time (Hr.)	Current (mA)	Cu (mmoles)	Fe _T (mmoles)	Fe/Cu Ratio	Fe ⁺⁺ (mmoles)	Current Efficiency %				Coulombs
						Cu	Fe	Fe ⁺⁺⁺	Total	
.08	3.7									
1.00	2.9									
5	2.35									
10	3.2									
20	5.0									
26	5.3	.633	.810	1.28	.421	36.2	46.2	11.1	93.5	338
30	5.2	Beginning to oscillate								
35	5.2	Oscillating strongly								
40	6.0									
45	5.7	1.60	1.725	1.075	1.34	42.5	45.8	5.0	93.3	728

SUMMARY OF P12

Potential = 550 mV (AgCl) = 735 mV (S.H.E.)
 Temperature = 90°C
 Saw Cut Electrode

Electrode Area = 1.00 cm²
 Solution: 0.46M NaCl
 0.04M HCl

Time (Hr.)	Current (mA)	Cu (mmoles)	Fe _T (mmoles)	Fe ⁺⁺ (mmoles)	Current Efficiency %				Coulombs
					Cu	Fe	Fe ⁺⁺⁺	Total	
.107	3.0								
.08	1.6								
1.00	1.35								
3	1.45								
10	2.00								
22	2.95	.34	.358	.350	40.3	41.5		81.8	163
43.5	4.1	1.01	.93	1.05	44.8	46.6		91.4	435
61	4.95	1.595	1.52	1.82	42.8	48.9		91.7	720
75	5.3								
87	5.5	2.75	2.56	2.73	43.7	43.3		87.0	1215
112	5.1	3.89	3.43	3.92	44.5	44.9		89.4	1685
140	4.5	4.36	4.86	4.77	38.9	43.2	.4	82.5	2170
159	4.3	5.03	5.50	5.36	39.3	43.2	.6	83.1	2472

SUMMARY OF P13

Potential = 1000 mV (AgCl) = 1185 mV (S.H.E.)
 Temperature = 90°C
 Saw Cut Electrode

Electrode Area = 1.50 cm²
 Solution: 3M NaCl
 0.2M HCl

Time (Hr.)	Current (mA)	Cu (mmoles)	Fe _T (mmoles)	Fe/Cu Ratio	Fe ⁺⁺ (mmoles)	Current Efficiency %				Coulombs
						Cu	Fe	Fe ⁺⁺⁺	Total	
.08	4.5									
1	2.7									
3	1.9									
5	2.05									
8	2.5									
12	3.5									
16	4.6	.292	.415	1.43	.42	34.2	49		83.2	163
		Oscillating								
23	6.2									
25	5.8									
		Oscillating strongly								
30	6.2									
42	5.7	1.53	1.58	0.83	1.26	41.1	42.4	4.3	88.8	720
67	5.5	2.60	2.440	0.78	2.03	40.6	38.2	3.2	82.0	1235
95	3.5	3.75	3.33	0.95	3.57	42.1	37.4		79.5	1720
117	3.2	4.45	4.66	0.96	4.27	42.4	44.4	1.9	88.7	2027

SUMMARY OF P14

Potential = 550 mV (AgCl) = 735 mV (S.H.E.)
 Temperature = 90°C
 Saw Cut Electrode

Electrode Area = 0.78 cm²
 Solution: 0.5M HCl

Time (Hr.)	Current (mA)	Cu (mmoles)	Fe _T (mmoles)	Fe/Cu Ratio	Fe ⁺⁺ (mmoles)	Current Efficiency %				Coulombs
						Cu	Fe	Fe ⁺⁺⁺	Total	
.17	0.90									
4	.70									
19	1.22									54
24	1.90									
25	1.57	.165	.25	1.51		39.4	59.6		99.0	81
43	2.1	.4.6	.556	1.33	.42	40.1	53.6	6.5	100.2	200
50	2.2									
70	3.1	.957	1.072	1.12	.84	42.0	47.1	5.0	94.1	440
95	3.75	1.650	1.78	1.08	1.40	42.8	46.1	4.9	93.8	745
113	4.0	2.075	2.37	1.14	1.82	40.5	46.2	5.4	92.1	990
141	4.5	3.09	3.40	1.10	3.325	42.4	46.6	0.5	89.5	1408
165	5.05	3.99	4.25	1.07	3.76	42.7	45.6	2.6	90.9	1792

SUMMARY OF P15

Potential = 900 mV (AgCl) = 1085 mV (S.H.E.)
 Temperature = 90°C
 Saw Cut Electrode

Electrode Area = 0.80 cm²
 Solution: 3M NaCl
 0.2M HCl

Time (Hr.)	Current (mA)	Cu (mmoles)	Fe _T (mmoles)	Fe/Cu Ratio	Fe ⁺⁺ (mmoles)	Current Efficiency %				Coulombs
						Cu	Fe	Fe ⁺⁺⁺	Total	
.17	2.7									
2	2.15									
4	2.05									
9	3.0									75
		Oscillations begin								
12	3.8									110
		Oscillating strongly								
18	5.0	.393	.5705	1.45	.42	36.1	52.5	6.9	95.5	210
24	5.2									
43	5.5	1.537	1.882	1.225	1.815	41.0	50.2	.9	92.1	724
70	5.8	2.66	3.30	1.237	3.05	41.2	51.1	2.6	94.0	1270
95	4.9	3.66	4.55	1.242	4.00	40.6	50.5	3.0	94.1	1775
113	4.9	4.26	5.27	1.235	4.38	39.8	49.2	4.1	93.1	2130
141	3.7	5.36	6.44	1.202	5.37	41.3	49.6	4.0	93.9	2580

SUMMARY OF P16

Potential = 350 mV (AgCl) = 535 mV (S.H.E.)
 Temperature = 90°C
 Saw Cut Electrode

Electrode Area = 0.94 cm²
 Solution: 3M NaCl
 0.2M HCl

Time (Hr.)	Current (mA)	Cu (mmoles)	Fe _T (mmoles)	Fe/Cu Ratio	Fe ⁺⁺ (mmoles)	Current Efficiency %				Coulombs
						Cu	Fe	Fe ⁺⁺⁺	Total	
.17	0.78									
.50	0.61									
12	0.61									
24	0.57									
37	0.58	.271	.462	1.70		66.6	114		180.6	78.5
64	0.75	.471	.705	1.50		60.1	89.8		149.9	151.4
108	0.65	1.00	1.189	1.12		73.5	87.3		160.8	263.8
134	0.71									
180	0.75	1.50	1.88	1.25	1.625	62.0	77.5	5.4	144.9	468
230	0.65	1.98	2.36	1.19	2.11	63.5	75.7	4.0	143.2	601
256	0.65	2.20	2.60	1.18	2.19	63.5	75.0	5.8	144.3	670

SUMMARY OF P17

Potential = 450 mV (AgCl) = 635 mV (S.H.E.)
 Temperature = 90°C
 Saw Cut Electrode

Electrode Area = 0.65 cm²
 Solution: 3M NaCl
 0.2M HCl

Time (Hr.)	Current (mA)	Cu (mmoles)	Fe _T (mmoles)	Fe/Cu Ratio	Fe ⁺⁺ (mmoles)	Current Efficiency %				Coulombs
						Cu	Fe	Fe ⁺⁺⁺	Total	
.17	1.05									
1	.75									
12	1.45									
23	1.78									
37	1.8	.532	.580	1.09		52.8	57.6		110.4	194.5
64	2.0	.964	1.060	1.10		52.7	58.0		110.7	353
108	2.7	2.005	2.02	1.01		57.4	57.8		115.2	675
134	3.0									
180	3.0	3.4	3.75	1.10	3.40	51.4	56.6	2.6	110.6	1278
230	2.5	4.25	4.68	1.10	4.15	52.8	55.9	3.3	112.0	1615
256	2.45	4.62	5.19	1.12	4.50	49.9	56.0	3.7	109.6	1787

SUMMARY OF P18

Potential = 550 mV (AgCl) = 735 mV (S.H.E.)
 Temperature = 90°C
 Saw Cut Electrode

Electrode Area = 1.50 cm²
 Solution: 0.4M Na₂SO₄
 0.1M H₂SO₄

Time (Hr.)	Current (mA)	Cu (mmoles)	Fe _T (mmoles)	Fe/Cu Ratio	Fe ⁺⁺ (mmoles)	Current Efficiency %				Coulombs
						Cu	Fe	Fe ⁺⁺⁺	Total	
.17	1.65									
10	1.60									
35	1.80	.251	.738	2.94		22.9	68.1		90.9	212
60	2.0									
83	2.2	.850	1.27	1.49	.876	29.5	44.1	7.0	80.6	555
108	2.45	1.145	1.555	1.36	1.325	29.7	40.4	2.8	72.9	754
141	2.8									
180	3.1	2.60	2.76	1.06	2.08	33.4	35.5	3.5	72.4	1500

SUMMARY OF P19

Potential = 350 mV (AgCl) = 535 mV (S.H.E.)
 Temperature = 90°C
 Saw Cut Electrode

Electrode Area = 1.62 cm²
 Solution: 0.4M Na₂SO₄
 0.1M H₂SO₄

Time (Hr.)	Current (mA)	Cu (mmoles)	Fe _T (mmoles)	Fe/Cu Ratio	Fe ⁺⁺ (mmoles)	Current Efficiency %				Coulombs
						Cu	Fe	Fe ⁺⁺⁺	Total	
.17	0.80									
1	0.65									
6	0.65									
7	0.64									
10	0.60									
15	0.52									
20	0.47									
25	0.44									
30	0.41									
35	0.38	.0394	.565	14.3		11.7	170		182	64
60	0.35									
83	0.32	.0742	.65	8.75	.495	11.7	102	12.3	126	122.6
108	0.29	.0813	.702	8.64	.48	10.5	93.5	14.7	118.7	144.8
180	0.19	.145	.825	5.69	.638	12.5	71.1	12.4	96.0	218